Doctorate of Philosophy

Schrödinger's Catwalk

Brian Flynn

University of Bristol

January, 2021

CONTENTS

LIST OF TABLES

LIST OF FIGURES

LISTINGS

ACRONYMS

^{13}C	carbon-13
^{14}N	nitrogen-14
AI	artificial intelligence
AIC	Akaike information criterion
AICC	Akaike information criterion corrected
BF	Bayes factor
BFEER	Bayes factor enhanced Elo ratings
BIC	Bayesian information criterion
CLE	classicallikelihood estimation
CPU	central processing unit
DAG	directed acyclic graph
EDH	experiment design heuristic
ES	exploration strategy
ET	exploration tree
FH	Fermi-Hubbard
FN	false negatives
FP	false positives
GA	genetic algorithm
GES	genetic exploration strategy
GPU	graphics processing unit
HPD	high particle density
IQLE	interactive quantumlikelihood estimation
JWT	Jordan Wigner transformation
LE	Loschmidt echo

LTL log total likelihood

ML machine learning

MVEE minimum volume enclosing ellipsoid
MW microwave

NN neural network
NV nitrogen-vacancy
NVC nitrogen-vacancy centre

OF objective function

PBS portable batch system
PGH particle guess heuristic
PL photoluminescence

QC quantum computer
QHL quantum Hamiltonian learning
QL quadratic loss
QLE quantumlikelihood estimation
QM quantum mechanics
QML quantum machine learning
QMLA Quantum Model Learning Agent

SMC sequential monte carlo
SVM support vector machine

TLTL total log total likelihood
TN true negatives
TP true positives

VQE variational quantum eigensolver

GLOSSARY

Q	Quantum system which is the target of Quantum Model Learning Agent, i.e. the system to be characterised
champion model	The model deemed by QMLA as the most suitable for describing the target system
chromosome	A single candidate, in the space of valid solutions to the posed problem in a genetic algorithm
expectation value	Average outcome expected by measuring an observable of a quantum system many times, Section 1.2.1
gene	Individual element within a chromosome
hyperparameter	Variable within an algorithm that determines how the algorithm itself proceeds
instance	A single implementation of the QMLA algorithm, resulting in a nominated champion model
likelihood	Value that represents how likely a hypothesis is
model	The mathematical description of some quantum system, Section 4.1
model space	Abstract space containing all descriptions (within defined constraints such as dimension) of the system as models
probe	Input probe state, $\|\psi\rangle$, which the target system is initialised to, before unitary evolution
results directory	Directory to which the data and analysis for a given run of QMLA are stored
run	Collection of QMLA instances, usually targeting the same system with the same initial conditions
spawn	Process by which new models are generated, ususally by combining previously considered models

success rate Fraction of instances within a run where QMLA nominates the true model as champion

term Individual constituent of a model, e.g. a single operator within a sum of operators, which in total describe a Hamiltonian.

volume Volume of a parameter distribution's credible region,

win rate For a given candidate model, the fraction of instances within a run which nominated it as champion

Part I

CONTEXTUAL REVIEW

1

QUANTUM THEORY

Quantum mechanics (QM) – the study of nature's fundamental processes, manifest in its smallest particles – has been at the forefront of physics since the early 20th century [**?**]. Advances in theoretical understanding of quantum mechanical systems in the first half of the century [**?**, **?**, **?**, **?**, **?**] which came to underpin all modern information and communications technologies [**?**, **?**]. The 21st century, on the other hand, is poised to see the development of technologies which *deliberately* exploit the most intricate quantum processes in order to yield some non-classical advantage. This thesis focuses on the application of machine learning to the characterisation of quantum mechanical systems through use of quantum simulators, so it is pertinent first to introduce the vocabulary of QM.

QM is central to the topics described in this thesis, however it is impossible to succinctly capture the entire discipline; in this chapter we will only introduce concepts utilised throughout. For completeness, we elucidate some fundamental topics of linear algebra and quantum theory in Appendix B, but consider them too cumbersome to include in the main text. For a more complete and general introduction to QM, the reader is referred to [**?**, **?**]. Likewise, in this chapter we quickly summarise the key aspects of quantum computation, but for further details, we recommend unfamiliar readers to consult [**?**], while a more complete discussion is presented in [**?**].

1.1 QUANTUM MECHANICS

At any time, a quantum system, Q, can be described by its *wavefunction*, $\Psi(t)$, which contains all information about Q. In analogy with Newton's second law of motion, which allows for the determination of a particle's position at any time, $\vec{r}(t)$, given its conditions such as mass and acceleration as well as its initial position, $\vec{r}(t_0)$, quantum *equations of motion* can describe the evolution of Q through its wavefunction [**?**]. One proposal[1] for the equation of motion to describe the evolution of the wavefunction under known conditions, i.e. determining $\Psi(t)$ from $\Psi(t_0)\ \forall t > t_0$, is *Schrödinger 's equation* [**?**, **?**, **?**].

Although the Schrödinger equation is a *postulate* of QM (see Appendix B.2), let us introduce it in reverse order to elucidate its meaning, following [**?**]. We have yet to describe the structure of the wavefunction, which we will do in Section 1.2, but here we will represent wavefunctions using *Dirac notation* (Appendix B.6), and can think of them generically as vectors, i.e. $\Psi(t) \to |\psi(t)\rangle$. Suppose we have two such wavefunctions, $|\phi(t)\rangle, |\psi(t)\rangle$ which are functions of time $t > t_0$.

0 Colloquially referred to as *Quantum 1.0*.

1 The most noteworthy alternative formalism, due to Heisenberg [**?**], was shown equivalent to the Schrödinger picture described here.

We start with the assumption that *similarity* is conserved between two wavefunctions, if they undergo the same transformation (Susskind's *minus first* law of classical mehcanics [**?**])

$$\langle \phi(t)|\psi(t)\rangle = \langle \phi(t_0)|\psi(t_0)\rangle \tag{1.1}$$

Then, assuming some equations of motion capture the dynamics of Q, there exists some evolution operator, $\hat{U}(t)$, which deterministically maps $|\psi(t_o)\rangle$ to $|\psi(t)\rangle$.

$$|\psi(t)\rangle = \hat{U}(t)\,|\psi(t_0)\rangle\,, \tag{1.2}$$

where we have not yet imposed any restrictions on $\hat{U}$. Combining Eqs. (1.1) to (1.2),

$$\begin{aligned} \langle \phi(t)|\psi(t)\rangle &= \langle \phi(t_0)|\hat{U}^\dagger\hat{U}|\psi(t_o)\rangle \\ \Rightarrow \langle \phi(t_0)|\hat{U}^\dagger(t)\hat{U}(t)|\psi(t_o)\rangle &= \langle \phi(t_0)|\psi(t_0)\rangle \\ \Rightarrow \hat{U}^\dagger(t)\hat{U}(t) &= \hat{\mathbb{1}} \quad \forall t, \end{aligned} \tag{1.3}$$

where the result $\hat{U}^\dagger(t)\hat{U}(t) = \hat{\mathbb{1}}$ is the condition for *unitarity* (Appendix B.5), so we can claim the quantum wavefunction evolves unitarily.

By construction, we require that after zero time, i.e. $t = t_0$, the wavefunction has not changed:

$$\begin{aligned} |\psi(t = t_0)\rangle = \hat{U}(t = t_0)\,|\psi(t_0)\rangle = |\psi(t_0)\rangle \\ \Rightarrow \hat{U}(t = t_0) = \hat{\mathbb{1}}. \end{aligned} \tag{1.4}$$

Without loss of generality we can set $t_0 = 0$, giving $\hat{U}(0) = \hat{\mathbb{1}}$. Then, let us consider an infintesimally small time increment $t_0 + \epsilon$: again, take $t_0 = 0$ so $t = \epsilon$, where $\epsilon \gg \epsilon^2$.

We can say

$$\hat{U}(\epsilon) = \hat{\mathbb{1}} + \mathcal{O}(\epsilon), \tag{1.5}$$

which merely suggests that the time evolution operator at very small time is very close to the identity, with some small displacement proportional to the time, which must be an operator to act on the wavefunction (vector). We suppose the form of the offset, so we can write

$$\hat{U}(\epsilon) = \hat{\mathbb{1}} - \epsilon\left(\frac{i}{\hbar}\hat{H}_0\right), \tag{1.6}$$

where the inclusion of the phase $-i$ is arbitrary, and we have named as $\hat{H}_0/\hbar$ the operator by which the time evolution differs from the identity. In other words, the operator $\hat{H}_0$ is generically the generator of the evolution/dynamics of Q: any difference between $|\psi(t_0)\rangle$ and $|\psi(t)\rangle$ arises

solely due to $\hat{H}_0$. So far there is no restriction on $\hat{H}_0$, except that it must be of the same dimension as the Hilbert space in question. Recalling the unitarity condition, however:

$$\begin{aligned} \hat{U}^\dagger(\epsilon)\hat{U}(\epsilon) &= \hat{\mathbb{1}} \\ \Rightarrow \left(\hat{\mathbb{1}} + \frac{i}{\hbar}\epsilon\hat{H}_0^\dagger\right)\left(\hat{\mathbb{1}} - \frac{i}{\hbar}\epsilon\hat{H}_0,\right) &= \hat{\mathbb{1}} \\ \Rightarrow \hat{\mathbb{1}} + \frac{i}{\hbar}\epsilon(\hat{H}_0^\dagger - \hat{H}_0) + \mathcal{O}(\epsilon^2) &= \hat{\mathbb{1}} \\ \Rightarrow (\hat{H}_0^\dagger - \hat{H}_0) &= 0 \\ \Rightarrow \hat{H}_0^\dagger &= \hat{H}_0. \end{aligned} \tag{1.7}$$

Eq. (1.7) results in the condition for *Hermiticity*, meaning that $\hat{H}_0$ is an observable of Q. In fact, this is the *Hamiltonian* of the system, described in the next section.

We can also use the infintesimal evolution to see

$$\begin{aligned} |\psi(t)\rangle &= \hat{U}(t)\,|\psi(t_0)\rangle \\ \Rightarrow |\psi(\epsilon)\rangle &= \hat{U}(\epsilon)\,|\psi(t_0)\rangle \\ \Rightarrow |\psi(\epsilon)\rangle &= \left(\hat{\mathbb{1}} - \epsilon\frac{i}{\hbar}\hat{H}_0\right)|\psi(t_0)\rangle \\ \Rightarrow |\psi(\epsilon)\rangle &= |\psi(t_0)\rangle - \epsilon\frac{i}{\hbar}\hat{H}_0\,|\psi(t_0)\rangle \\ \Rightarrow \frac{|\psi(\epsilon)\rangle - |\psi(t_0)\rangle}{\epsilon} &= -\frac{i}{\hbar}\hat{H}_0\,|\psi(t_0)\rangle \end{aligned} \tag{1.8}$$

Taking the limit as $\epsilon \to 0$, the left hand side of the final line of Eq. (1.8) is the definition of the derivative of the wavefunction, $\frac{d|\psi(t)\rangle}{dt}$. Taken together, we have

$$\frac{d}{dt}\,|\psi(t)\rangle = \frac{-i}{\hbar}\hat{H}_0\,|\psi(t_0)\rangle\,, \tag{1.9}$$

where $|\psi(t)\rangle$ is the wavefunction at time t, $|\psi(t_0)\rangle$ is the wavefunction at t_0, such that $t > t_0$, $\hbar = 1.054 \times 10^{-34}$ is the reduced Planck constant and $\hat{H}_0$ is the *Hamiltonian* of Q. For brevity we generally refer to $t_0 = 0$, and absorb $\hbar$ into $\hat{H}_0$, which will later manifest in the Hamiltonian scalar parameters. Eq. (1.9) is the most general form of *Schrödinger equation*, otherwise known as the *time-dependent* Schrödinger equation; we include it as Postulate 6 when describing the fundamentals of QM (Appendix B.2), since it can be seen as an irreducible equation of motion which is essential to the description of quantum systems.

As mentioned, we presented this argument in a nonstandard order: we started with Eq. (1.2), which we can now consider the *solution* to the Schrödinger , specifically

$$\begin{aligned} |\psi(t)\rangle &= \hat{U}(t)\,|\psi(0)\rangle \\ \hat{U}(t) &= e^{-i\hat{H}_0 t} \end{aligned} \tag{1.10}$$

which describes the unitary evolution of the state according to the unitary evolution operator, $\hat{U}(t)$.

1.1.1 *Hamiltonians*

In the previous section we introduced the Hamiltonian[2] of Q as the generator of its time evolution dynamics; Hamiltonians are of primary importance in this thesis, so it is worth pausing to consider their physical meaning. We saw in Eq. (1.7) that $\hat{H}_0$ is Hermitian, meaning that the operator is physically observable according to Postulates 2 to 3 of quantum mechanics (Appendix B.2). The Hamiltonian operator captures the energy of Q: the eigenvalues of the observable $\hat{H}_0$ are the permitted energy levels of the system.

The quantum Hamiltonian, $\hat{H}_0$, is analogous to the classical Hamiltonian, insofar as it captures all the interactions of a given system which contribute to its time evolution. Knowing the classical Hamiltonian and the initial conditions – position and momentum – Hamilton's equations of motion allow for the calcaultion of those quantities for the particle in question an infintesimal time later [**?**]. Likewise, knowledge of the initial wavefunction, $|\psi(t_0)\rangle$, and the system's quantum Hamiltonian, $\hat{H}_0$, the quantum equations of motion – Schrödinger 's equation, Eq. (1.9) – permits the calculation of the wavefunction at later times. As such the Hamiltonian must consist of all processes which influence the evolution of Q; we will later break the Hamiltonian into independent *terms* which each correspond to unique physical interactions Q is subject to, Section 4.1. We can think that each process/interaction Q undergoes contributes to its total energy, giving intuition as to why its eigenvalues are the energy levels.

Hamiltonians describe *closed* quantum systems, i.e. where *all* processes and interactions which influence Q are accounted for. Realistic quantum systems are influenced by a myriad of proximal systems, and it is therefore infeasible to analytically account for them all. Instead, *open* quantum systems' dynamics are described by Lindbladian operators, which encompass the Hamiltonian form. The Lindblad master equation is a generalisation of the Schrödinger equation, providing the equation of motion for open quantum systems [**?**, **?**]. In this thesis we only consider closed models for quantum systems; for meaningful impact of the techniques presented here, it will be necessary to expand them to account for the open system dynamics of realistic experiments. We do, however, show initial progress towards this endeavour by modelling a physical system through a closed Hamiltonian, Chapter 9.

1.2 QUANTUM INFORMATION

We have not yet described the structure of the wavefunction, instead performing the previous analysis with respect to some arbitrary objects. The wavefunction for a physical system, Q, is

2 Aside: the author shares a hometown with the mathematician for whom it is named, William Rowan Hamilton. It is hoped that, after another 150 years, the next physicist from Trim, Co. Meath, Ireland might profitably use knowledge of Hamiltonians on a quantum computer (QC).

also known as its *state*, a complete mathematical description of the system [**?**]. States are vectors[3], $|\psi\rangle \in \mathbb{C}$; the valid state space for Q is its *Hilbert space*, $\mathcal{H}$, which is a generalisation of Euclidean vector space, i.e. $|\psi\rangle \in \mathcal{H}$. The Hilbert space defines the overlap between any two vectors as the *inner product*, $\langle\psi|\phi\rangle$ (Appendix B.1). In general[4], a state can be seen as a *superposition* across its eigenstates, $\{|v_i\rangle\}$.

$$|\psi\rangle = \sum_i \alpha_i |v_i\rangle \tag{1.11a}$$

$$\text{subject to} \quad \sum_i |\alpha_i|^2 = 1, \quad \alpha_i \in \mathbb{C}. \tag{1.11b}$$

The cornerstone of QM is the effect of *measurement* on quantum systems: in general Q can be seen as occupying a multitude of eigenstates as in Eq. (1.11a); observing the system forces $|\psi\rangle$ into a definite occupation of a single eigenstate, where the *probability* that it is measured in each eigenstate $|v_i\rangle$ is given by $|\alpha_i|^2$, according to Born's rule [**?**]. α_i are hence named *probability amplitudes* since they inform the probability of measuring the corresponding eigenstate.

For an ideal[5] single particle, when the state, Eq. (1.11a), has two available eigenstates, e.g. the horizontal (H) and vertical (V) polarisation of a single photon, we can designate Q as a two-level computational platform, called a *qubit*, analogous to the workhorse of classical computation, the bit. A qubit's state vector can then be written as a sum over the two available eigenstates, where we assign vectors to the eigenstates as $\{|H\rangle = |v_1\rangle, |V\rangle = |v_2\rangle\}$.

$$|\psi\rangle = \alpha_1 |v_1\rangle + \alpha_2 |v_c\rangle, \tag{1.12}$$

where $\alpha_i \in \mathbb{C}$ and $|\alpha_1|^2 + |\alpha_2|^2 = 1$.

In general, a qubit requires two orthogonal state vectors to define a *basis*; we list a number of the usual special cases:

$$X\text{-basis} = \begin{cases} |+\rangle = \dfrac{1}{\sqrt{2}}(|0\rangle + |1\rangle) \\ |-\rangle = \dfrac{1}{\sqrt{2}}(|0\rangle - |1\rangle) \end{cases} \tag{1.13a}$$

$$Y\text{-basis} = \begin{cases} |i\rangle = \dfrac{1}{\sqrt{2}}(|0\rangle + i|1\rangle) \\ |-i\rangle = \dfrac{1}{\sqrt{2}}(|0\rangle - i|1\rangle) \end{cases} \tag{1.13b}$$

3 We immediately use Dirac notation to represent the state; it is defined in Appendix B.6.

4 We expand on this brief description in Appendix B.3.

5 Here we restrict to the space of ideal, *logical* qubits. In reality, physical qubits are beset by errors, demanding error correction routines such that multiple particles are needed attain a single logical qubit.

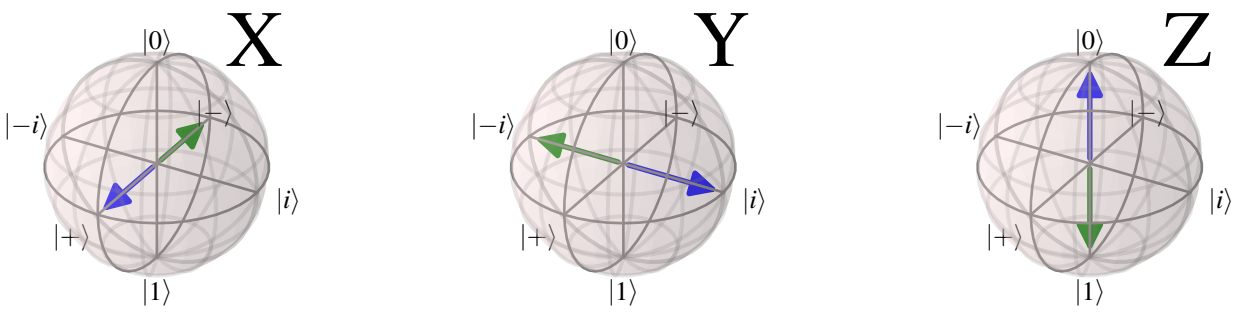

Figure 1.1: Bloch sphere representation of bases, where each pair of basis states are shown by blue and green vectors. The X-basis has basis vectors $\{|+\rangle, |-\rangle\}$; Y-basis has $\{|i\rangle, |-i\rangle\}$ and Z-basis has $\{|0\rangle, |1\rangle\}$.

$$Z\text{-basis} = \begin{cases} |0\rangle \\ |1\rangle \end{cases} \tag{1.13c}$$

A visual tool for representing qubits is the *Bloch sphere*, which presents orthogonal basis states as parallel unit vectors of opposite direction: we show each of the bases of Eq. (1.13) in Fig. 1.1.

We can make two remarks about basis states for a single qubit:

- Basis states from one basis can be seen as superpositions with respect to alternative bases
  - e.g. in the X-basis, $|+\rangle$ is a basis vector, but in the Z-basis, $|+\rangle = \frac{|0\rangle+|1\rangle}{\sqrt{2}}$ is a superposition over basis vectors.
- Bases are local rotations of each other
  - rotating the X-basis through an angle $\pi/2$ about the Y-axis results in the Z-axis.

As we alluded to in Section 1.1: by imposing mathematical structure on quantum systems' states, i.e. representing Q as a state vector at any time, then operations which alter the state of the system must be matrices, which we will call *operators*. In general an n-dimensional vector is rotated by an $n \times n$ matrix; therefore to rotate the one-qubit state, given by a two-dimensional vector, we require a 2×2 operator. One-qubit operators have the effect of rotating the state vector, which we can again visualise on the Bloch sphere. By thinking of qubits generically with respect to any basis, we can encode information in the qubit's amplitudes, by performing operations (or *gates*) upon the qubit, we change the information, i.e. we can design information processing techniques leveraging the infrastructure – states, operators and measurement – of QM.

We introduce a set of speical one-qubit operators, the *Pauli matrices*,

$$\hat{\sigma}_x = \begin{pmatrix} 0 & 1 \\ 1 & 0 \end{pmatrix} \tag{1.14a}$$

$$\hat{\sigma}_y = \begin{pmatrix} 0 & -i \\ i & 0 \end{pmatrix} \tag{1.14b}$$

$$\hat{\sigma}_z = \begin{pmatrix} 1 & 0 \\ 0 & -1 \end{pmatrix} \tag{1.14c}$$

The Pauli matrices are used to define rotation operators about their respective axes, and hence are very useful: we can break *any* rotation of a qubit into rotations of various angles, θ, about the three axes of the Bloch sphere. Any single qubit operation can therefore be expressed as a product of the *rotation operators*, $\hat{R}_x, \hat{R}_y, \hat{R}_z$, exemplified in Fig. 1.2 and defined for $w \in \{x, y, z\}$ as

$$\hat{R}_w(\theta) = e^{-i\frac{\theta}{2}\hat{\sigma}_w} = \cos(\theta/2)\,\hat{\mathbb{1}} - i\sin(\theta/2)\,\hat{\sigma}_w. \tag{1.15}$$

The Pauli matrices are Hermitian, meaning they are observable. We can see that the eigenstates of $\hat{\sigma}_z$ are the Z-basis states: $\hat{\sigma}_z|0\rangle = |0\rangle\,; \hat{\sigma}_z|1\rangle = -|1\rangle$. Recalling the earlier claim that the two-level quantum system (e.g. H and V polarisation of a photon) can be mapped to eigenvectors[6] of an obserable operator to form a qubit, we term the Z-basis the *computational* basis. By defining the computational basis, we ground abstract computational reasoning in the physical realisation: anywhere throughout this thesis where the basis states $|0\rangle, |1\rangle$ are referenced, we mean the eigenstates of the physical axis which is defined as the Z-axis for the system in question. In the computational basis, then, a qubit can be specified as

$$|\psi\rangle = \alpha_0|0\rangle + \alpha_1|1\rangle. \tag{1.16}$$

The concepts of qubits representing quantum systems, as well as operators altering their states and measurement collapsing those states, extend straightforwardly to multipartite systems, by merging Hilbert spaces through tensor products, as we show in Appendix B.3.1. The cases where this is a simple mathematical exercise represent *pure* states; of course this leads to the more intricate topic of *mixed* states and entanglement, briefly described in Appendix B.4. In this thesis, however, we are concerned only with pure states, i.e. separable qubits. While single qubit states are spanned by the Pauli opeartors, multi-qubit states are spanned by the Pauli group, $\mathbb{G}$: n-qubit states are spanned by $\mathbb{G}_n = \left(\mathbb{C}^2\right)^{\otimes n}$.

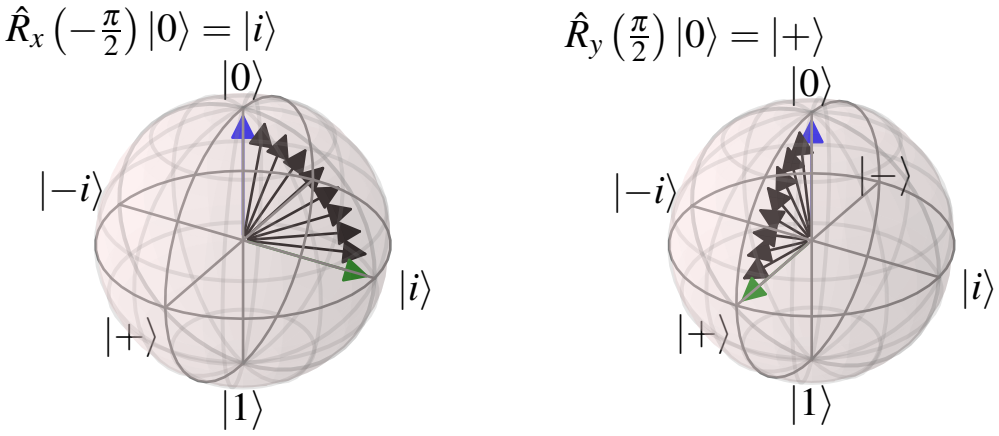

Figure 1.2: Rotations on Bloch sphere. The initial and final state are shown in blue and green respectively, while intermediate states are shown in black. **Left**, The Z-basis unit vector, $|0\rangle$, is rotated about the X-axis, resulting in the unit vector along the Y-axis. **Right**, The Z-basis unit vector, $|0\rangle$, is rotated about the Y-axis, resulting in the unit vector along the X-axis.

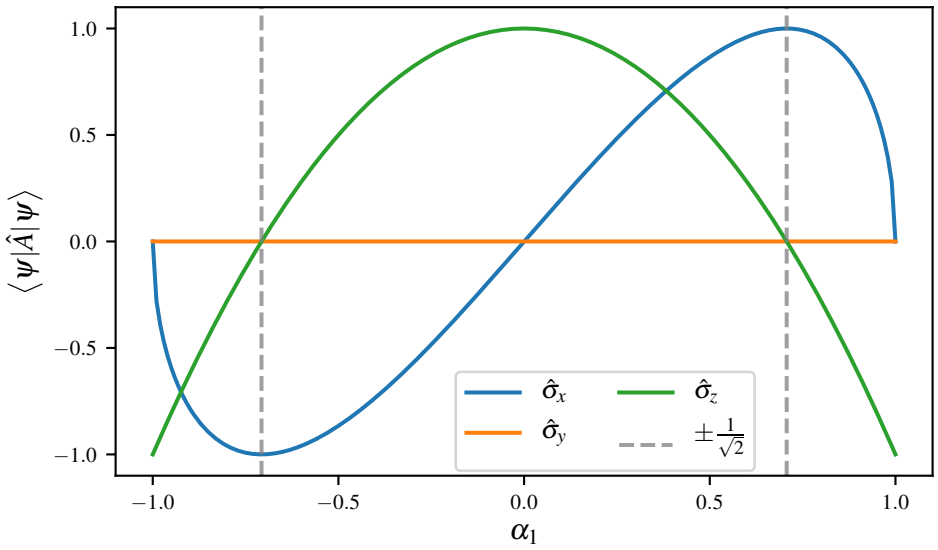

Figure 1.3: Expectation values of the observable $\hat{A}$ – here the Pauli matrices – for $|\psi\rangle = \alpha_0|0\rangle + \alpha_1|1\rangle$. Coefficients are real, varying $\alpha_1 \in (-1, 1)$, such that $\alpha_0 = \sqrt{1-\alpha_1^2}$.

1.2.1 *Expectation value*

Upon measurement, the state vector of Q has amplitude associated with only one eigenvector. On average, however, the eigenvector to which it would collapse encodes statistical insight on the state prior to measurement. In other words, if we prepared $|\psi\rangle$ and measured it – via some observable, $\hat{A}$ – and repeat the procedure N times, then as $N \to \infty$, the average outcome is the *expecatation value* for the system is given by

$$\langle \hat{A} \rangle = \langle \psi | \hat{A} | \psi \rangle = \sum_i \alpha_i \langle v_i | \hat{A} | v_i \rangle \,, \tag{1.17}$$

where $\langle \hat{A} \rangle$ is the expectation value (average) for the observable, $\hat{A}$; $|v_i\rangle$ are the eigenvectors of $\hat{A}$, and $\alpha_i \in \mathbb{C}$ are the proability amplitudes associated with each $|v_i\rangle$ when the state $|psi\rangle$ is represented as in Eq. (1.11a). We show some examples of expectation values for the observable Pauli matrices in Fig. 1.3.

An underlying theme of this thesis is to flip the usual logic: instead of using knowledge of the system to derive the expectation value, per Eq. (1.17), we will *estimate* expectation values, either through experiment or simulation, and use them to infer the structure of the observable. This trick enables machine learning routines to reverse engineer the processes Q is subject to, as we will describe in Part II. There is a subtlety to be aware of, however: in later chapters, we will make reference to the expectation value and *likelihood* almost interchangeably – these are distinct concepts that *sometimes* overlap, but not in all cases, as we explain in Chapter 3.

1.3 QUANTUM SIMULATION AND COMPUTATION

Relying on the premise and language of quantum information processing – states, qubits, operators, measurements and expectation values – the growing field of *quantum technology* aims to exploit the non-classical statistics yielded by quantum systems in order to retrieve outcomes beyond the capability of their classical counterparts [**?**]. Applications range from enhanced sensing and metrology [**?**, **?**], to highly-secure communication and cryptography protocols [**?**, **?**, **?**]. The initial motivation for the development of quantum technologies, however, was the observation that simulating nature at a quantum level would require exponential resources and is therefore only feasible given controllable quantum systems, which can accurately emulate the true dynamics [**?**, **?**, **?**, **?**].

The notion of controlling quantum systems to mimic the dynamics of real quantum systems is tantamount to *quantum simulation* [**?**, **?**]. In particular, simulating quantum systems is believed to be of interest for quantum chemistry [**?**, **?**, **?**], for example leading to advances in the simulation of molecular dynamics [**?**, **?**]. More generally, however, this led to research into a wider domain of calculations called *quantum computation* which considers the information processing capability

6 The terms *eigenstate* and *eigenvector* are interchangeable, although it may be helpful to think of eigenstate as the physical manifestation (horizontal photon), and think of eigenvector as the logical manifestions ($|0\rangle$).

of controllable quantum systems beyond merely simulating quantum systems. Then, *universal quantum computers* (or, *quantum Turing machines*), assume access to *logical* qubits and operations (or *gates*) for the implementation of quantum circuits [**?**]. This ignited interest in *quantum algorithms*, which aim to provide some provable advantage [**?**, **?**, **?**, **?**, **?**]. Indeed, it was found that the space of problems addressible by such devices goes beyond the classical counterpart, suggesting there exists a class of quatum algorithms which can offer significant advantage over any feasible algorithm on classical hardware [**?**].

Of course, while the advances in algorithmic quantum computation promise huge impact, they are tempered by contemporary experimental constraints, which must deal with the reality that construction and control of quantum devices is a significant challenge. In constructing QCs and dealing with their output, we must account for physical effects which lead to errors, requiring expensive error mitigation schemes to be reliable [**?**, **?**]. Furthermore, there are a number of criteria a QC must meet before it can be deemed reliable [**?**].

Any two-level quantum system can be used as a qubit; a range of platforms have emerged in attempts to fulfil the potential of quantum computation [**?**], among the most popular[7]:

- Photonic qubits (linear optical QCs) [**?**]
  - existing infrastructure for commercial production of photonics-based technologies suggests the relatively straightforward fabrication of integrated photonic devices at the scale of millions of degrees of freedom [**?**];
  - photons do not decohere so are useful for encoding information [**?**];
  - photons do not interfere [**?**, **?**], so information processing must be mediated by non-trivial measurement schemes [**?**];
  - they are liable to a unique error mechanism – photon loss – necessitating novel quantum error correcting codes [**?**];
  - on-demand single photon generation has not yet been demonstrated, although there is significant progress in the area of photon generation [**?**].
- Superconducting qubits [**?**, **?**]
  - relatively straightforward to control and couple with each other, enabling high-fidelity two-qubit gates, e.g. 99.7% reached in [**?**];
  - difficult to engineer substantial coherence times, although there has been significant recent progress [**?**, **?**], e.g. $T_1 \sim \mathcal{O}(\text{ms})$ in [**?**];
  - require cryogenic temperatures [**?**];
  - arbitrary qubit connectivity at scale is yet to be demonstrated [**?**];
  - methods for the fabrication of medium-to-large scale devices required for fault tolerant quantum computation are not yet known [**?**].
- Ion traps [**?**, **?**]

7 An incomplete list of quantum architectures together with their primary advantages and limitations.

  - high two qubit gate fidelities, e.g. 99.9% in [**?**];
  - very high coherence times, e.g. $\mathcal{O}(10\text{ min})$ in [**?**];
  - straightforward state preparation and readout, e.g. 99.99% readout fidelity in [**?**];
  - long gate-times, e.g. $\mathcal{O}(\mu\text{s})$ in [**?**];
  - uncertain scalability [**?**].

The ever-increasing space of contenders has led to a growing eco-system for quantum software [**?**], promising a wide range of applications in the era of noisy intermediate scale quantum devices [**?**]. Following numerous proposoals [**?**], recent efforts have married state-of-the-art hardware with bespoke algorithms in order to achieve quantum advantage [**?**, **?**]. Evidently there is vast effort in bringing quantum computational resources to reality; in this thesis, however, we are not concerned with the architecture underlying our presumed quantum simulator – we perform simulations only on classical hardware. In principle, however, any quantum simulator – universal or otherwise – capable of implementing the time evolution operator, Eq. (1.10), can be called upon as a co-processor by the algorithms presented.

Our restriction to classical resources leads to a few remarks:

- given access to a fault-tolerant QC/simulator, the algorithms described would enjoy an automatic exponential speedup:
  - the classical bottleneck is the calculation of the time evolution dynamics, Eq. (1.10), according to the matrix exponential, of dimension 2^n, where n is the dimension of the system;
  - it is believed that the same calculation can be performed in polynomial time on a QC [**?**].
- the results achieved in this thesis are limited by the capability of classical computers in simulating quantum systems
  - we study only up to 8-qubit systems, whereas it would be of interest to extend these methods to higher dimensions, which is expected to be feasible when reliable quantum simulators/computers are available.

The remit of this thesis – given these limitations – is therefore to robustly test the presented algorithms, and provide a benchmark achieved through classical facilities, against which the same algorithm can be run in conjunction with quantum hardware.

2

MACHINE LEARNING

Machine learning (ML) is the application of statistics, algorithms and computing power to discover meaning and/or devise actions from data. ML has become an umbrella term, encompassing the family of algorithms which aim to leverage computers to learn without being explicitly programmed, as opposed to the more general artificial intelligence (AI), which seeks to make computers behave intelligently, admitting explicit programs to achieve tasks [**?**]. Its history is therefore imprecise since a number of early, apparently unrelated algorithms were proposed independently, which now constitute ML routines [**?**, **?**]. Nevertheless, the field of ML has been advancing rapidly since the second half of the 20$^{\text{th}}$ century [**?**], especially recently due to the availability of advanced hardware such as graphics processing units (GPUs), facilitating significant progress through an ever-increasing aresnal of powerful open source software [**?**, **?**, **?**].

Throughout this thesis, we endeavour to combine known methods from the ML literature with capabilities of QCs[1]. Typical ML algorithms, which rely on central processing units (CPUs) or GPUs, are deemed *classical* machine learning, in contrast with quantum machine learning (QML), where QCs are central to processing the data. Similarly to the remit of Chapter 1, here we do not provide an exhaustive account of ML algorithms: rather, we describe only the algorithms which are used in later chapters, referring readers to standard texts for a wider discussion [**?**, **?**].

2.1 CLASSICAL MACHINE LEARNING

Of course the first step in any ML application is to consider the types of available data, with respect to the ensemble of known algorithms. Classical ML is usually described in three categories, broadly based on the format of data on which the insight can be built; we will briefly describe each to provide context to discussions throughout this thesis. Later in this thesis we will use the word *model* for descriptions of quantum systems, but here *model* refers to the mapping between inputs and outputs which the ML algorithm devises.

2.1.1 *Supervised machine learning*

Models are trained using *labelled* data, i.e. each training sample has a known label y_i; or, a set of *feature vectors* $\{\vec{x}_i\}$ are associated with the set of corresponding *classes* $\{y_i\}$ [**?**]. The output is a predictive tool which aims to reconstruct the classes of unseen feature vectors: in general, we can view the role of ML in this setting as distilling the function f such that

$$f : \vec{x}_i \longmapsto y_i \quad \forall(\vec{x}_i, y_i). \tag{2.1}$$

1 Or simulated QCs, in this thesis.

There are a number of families of algorithms even within the broad category of supervised ML, we define them as

CLASSIFICATION models aim to produce models which can assign unseen instances to the most appropriate label, from a fixed set of available labels [**?**];

- e.g. labels indicate animals' species, and the feature vector for each sample (data point) encodes the animals' height, weight, number of legs, etc.

REGRESSION models capture the formulaic relationship – which can be either linear or polynamial – between numerical features a the target scalar value, by determining coefficients for each feature. e.g. y is the salary of employees in a company, and the feature vector consists of the individual employees' age, seniority, experience in years, etc.

NEURAL NETWORKS *Universal function approximators*[2]. By invoking a set of linear and non-linear transformations on input data, the *network* is a function of some paramterisation w; neural networks aim to find the optimal network, w', such that Eq. (2.1) is satisfied, $f(w') : \vec{x}_i \longmapsto y_i$.

- Usually used for classification.
- e.g. input *neurons*[3] encode the pixel values of images. The neural network can be used to classify the objects it detects within the image.

SUPPORT VECTOR MACHINE (SVM) Distinguish similar data points by projecitng data into higher dimensional space, and therein finding the hypersurface which separates classes [**?**].

- Usually used for classification tasks.
- For data $\mathcal{D} \in \mathbb{R}^n$, a hypersurface in $\mathbb{R}^{n-1}$, can be drawn arbitrarilily through the space (e.g. a 2D plane in a 3D space).
- Unseen data can then classified by which partition they are reside in when projected into the n-dimensional space.
- The task of the SVMs is to orient the hypersurface in such a way as to separate distinct classes.

Supervised ML algorithms rely on the existence of a body of labelled samples – the dataset $\mathcal{D}$ – upon which the model can be trained. Training is typically performed on a subset of the data, $\mathcal{D}_t$, usually 80% of samples chosen at random. The remaining (20%) of samples, $\mathcal{D}_v$, are retained for the evaluation of the resultant model: $d \in \mathcal{D}_v$ are not trained upon, so do not contribute to

2 Including deep learning networks [**?**].

3 The term *neuron*, also known as *node* or *unit*, derives from the motivation for this class of algorithm: the cells in the brain used for processing information.

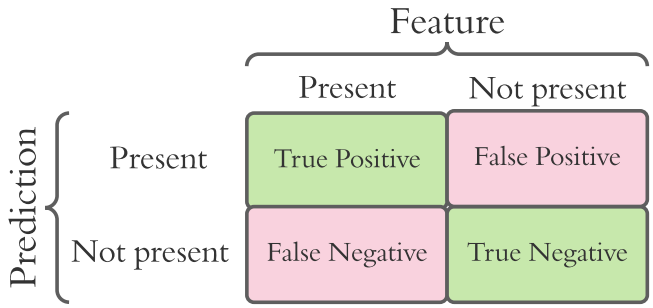

Figure 2.1: Confusion matrix showing the meaning of true positives, true negatives, false positives, false negatives.

the structure of f as returned by the algorithm. The model therefore can not *overfit*, i.e. simply recognise particular samples and label them correctly, without any meaningful inference. The evalutation thus captures how the model can be expected to perform on future, unlabelled data.

2.1.2 *Performance metrics*

An important step is the fair assessment of algorithms, then, which is achieved through a number of *performance metrics*. In each supervised ML, the machine attempts to learn the structure of f that optimises some internal objective function (OF), e.g. minimising the average distance between predicted and target labels for regression, $\sum_{d \in \mathcal{D}_t} y_d - y'_d$. To assess the resultant model, we introduce a number of *performance metrics*, which aim to measure serveral perspectives of the model's efficacy, by considering the model's predictions with respect to $\mathcal{D}_v$.

By definition of the data format, it is relatively straightforward to define metrics for supervised routines: the classes assigned to feature vectors, y'_i, can be quantitatively assessed with respect to their true class, y_i. For example, in *binary classification*, the output of the model is either correct or incorrect, allowing us to meaningfully assess its average performance. Likewise, for numerical targets, the difference $\left|y_i - y'_i\right|$ between the output, y'_i, and the target, y_i for each sample cumulatively indicate the strength of the model.

There are a large number of quantities and performance metrics against which to judge models' outputs. In binary classification, we care about whether the model predicts that a given feature is present, and whether it predicts features incorrectly. For example, the model aims to classify whether or not a dog is present in an image. These type of binary predictions have four outcomes, which can be summarised in a *confusion matrix* (Fig. 2.1), defined as in Table 2.1.

	y has feature	y' has feature
True positives (TP)	✓	✓
False positives (FP)	×	✓
True negatives (TN)	×	×
False negatives (FN)	✓	×

Table 2.1: Classification metrics. We define classification outcomes based on whether the considered feature was present and/or predicted.

We can use the concepts of Table 2.1 to define a series of *rates* which characterise the model's predictions.

ACCURACY The overall rate at which the algorithm predicts the correct result.

$$\frac{TP + TN}{TP + TN + FN + FP} \tag{2.2a}$$

PRECISION Positive predicitve rate. Of those *predicted to have* the feature of interest, what percentage *actually have* the feature.

$$\frac{TP}{TP + FP} \tag{2.2b}$$

SENSITIVITY True positive rate (also known as *recall*). Of those which *actually have* the feature, what percentage are *predicted to have* the feature.

$$\frac{TP}{TP + FN} \tag{2.2c}$$

SPECIFICITY True negative rate. Of those which *do not actually have* the feature of interest, how many are *predicted not to* have the feature.

$$\frac{TN}{TN + FP} \tag{2.2d}$$

Each metric has clear advantages, but consider also their drawbacks:

- Accuracy can be extremely misleading. for example, in a dataset with only 100 instances of the feature of interest, a model predicting 9,900 true negatives and 1,100 false negatives will give 99% accuracy, despite not having found a single positive sample. This is clearly of no use in identifying the minority of cases which are of actual interest.
- Sensitivity can be inflated by over-fitting to positive cases. That is, by predicting the feature as present in all cases, all true instances of the feature will be found, however all false

True positives	False negatives	False positives	Precision	Sensitivity	F_1-score
500	500	1000	33	50	$(\frac{2\times33\times50}{33+50}) = 37$
500	500	500	50	50	$(\frac{2\times50\times50}{50+50}) = 50$
1000	0	1000	50	100	$(\frac{2\times50\times100}{50+100}) = 67$
1000	0	0	100	100	$(\frac{2\times100\times100}{100+100}) = 100$

Table 2.2: F_1-score examples.

instances will be labelled as having the feature, so the model has not helped separate the data. The model willl yield a high rate of true positives (TP) but also a high rate of false positives (FP).

- Precision can be high for extremely selective models, i.e. those which are conservative in predicting the presence of the feature. By predicting relatively few positive instances, it can ensure that a high proportion of its predictions are correct. The absolute number of instances identified, however, is relatively low, as a proportion of the total number in the dataset.
- Specificity, similar to sensitivity, can easily mislead by identifying very few instances as having the target feature. Then, it will correctly predict most non-present instances as false, but will not identify the few instance of interest.

Clearly, the performance metric must be chosen with due consideration for the application; e.g. in testing for a medical condition, rather than incorrectly telling a patient they do not have the condition because the model predicted they were feature-negative, it is preferable to incorrectly identify some patients as feature-positive (since they can be retested). In this case, high accuracy is crucial, at the expense of precision. It is clearly appropriate to blend together the usual metrics, in order to derive performance metrics which balance the priorities of the outcomes. In general – including in this thesis – the most important aspects of a ML are precision and sensitivity: a model which performs well with respect to *both* of these is sensitive to the feature, but precise in its predictions. A quantity which captures both of these is the F_β-score,

$$f_\beta = \left(1+\beta^2\right) \frac{\text{precision} \times \text{sensitivity}}{(\beta^2 \times \text{precision}) + \text{sensitivity}}, \tag{2.3}$$

where $\beta \in \mathbb{R}$ is the relative weight of importance between sensitivity and precision. In particular, considering precision and sensitivity as equally important, i.e. $\beta = 1$, we have the F_1-score,

$$f_1 = \frac{2 \times \text{precision} \times \text{sensitivity}}{\text{precision} + \text{sensitivity}}. \tag{2.4}$$

For examples of how F_1-score balances these considerations, see Table 2.2.

2.1.3 *Unsupervised machine learning*

Contrary to supervised algorithms, unsupervised methods operate on *unlabelled* data, $\mathcal{D}$. This is often summarised as finding structure within unstructured data. Again, we can further compartmentalise methods under this umbrella [**?**]. Although we do not utilise these methods in this thesis, we briefly summarise them here for completeness.

CLUSTERING Finding datapoints which are similar to each other, according to some distance metric.

- e.g. online retailers grouping together customers with similar preferences, in order to tailor advertising campaigns.

DIMENSIONALITY REDUCTION Reducing the feature vector of each sample in a dataset to essential components, which may be amalgamations of original features, while retaining structure within the data.

- this can be used for visualisation to allow for inspection of complex datasets, e.g. plotting users of a social network as nodes on a 2D map, where distinct social groups are kept distant.

ASSOCIATION LEARNING Discover correlations among data.

- For instance, a supermarket may find that purchasers of certain products are likely also to buy others, providing actionable insight e.g. purchases involving bread also include butter in 50% of cases, so positioning these nearby may increase sales by reminding consumers of their compatibility.

SEMI-SUPERVISED LEARNING Combine elements of supervised and unsupervised algorithms, to achieve a task beyond the remit of either alone. This often means classifying data where only occur a small subset of the total dataset is labelled.

- e.g. in facial recognition, a clustering algorithm finds similarities between individual people in photos, and identifies a single person present across a number of photos, and associates those photos together. It combines this with a small set of photos for which people have been tagged, locates the same person and automatically tags them in the wider set of photos.

2.1.4 *Reinforcement learning*

A third category of ML algorithms are reinforcement learning (RL). These are methods where an *agent* interacts with some environment, and refines a *policy* for reacting to different stimuli. As such, the agent can, in principle, deal with a wide array of situations. These methods

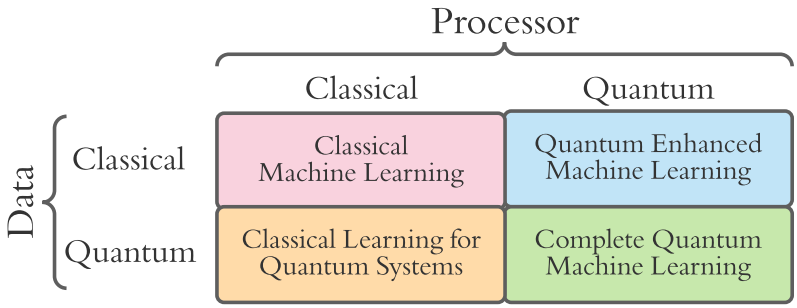

Figure 2.2: Types of quantum machine learning.

underly technologies such as self-driving cars, which inspect their surroundings through *sensors*; compute an *action* according to the policy; implement that action through *actuators*. Following an action, the agent senses whether that action was beneficial or detrimental, and receives a *reward* or *punishment* accordingly. Highly rewarded actions are likely to be repeated in future, allowing the agent to learn what response is appropriate to situational parameters, e.g. a self-driving car braking at a red light is rewarded, while braking at a green light is punished.

The concept of a machine's *agency* is an ongoing discussion in the ML community [**?**, **?**], and is important in this thesis also, when we define our model learning protocol as an agent, since it designs models by interacting with the envinroment of the target quantum systems. We will revisit the concept in Section 4.5.1.

2.2 QUANTUM MACHINE LEARNING

A growing domain is the development of ML algorithms which run on quantum hardware, or exploit data from quantum systems; generally referred to as QML [**?**, **?**]. There are a number of metehodologies which are referred to as QML; for clarity, we define the main branches here, as shown in Fig. 2.2.

CLASSICAL MACHINE LEARNING refers to standard ML as described in Section 2.1, i.e. where the processors are CPUs or GPUs, and the applications are not of specific interest to problems in the quantum domain. Recently, this branch has encompassed quantum *inspired* ML, which still target classical problems, but use subroutines which were orginally found in the context of QML [**?**].

QUANTUM ENHANCED MACHINE LEARNING A quantum co-processor is leveraged on classical data for some provable speedup, i.e. data that could otherwise be processed purely classically, is encoded, loaded onto and processed by quantum hardware. The quantum

counterparts of classical ML algorithms aim to solve the same problems, e.g. as neural networks (NNs) [**?**, **?**] and principle component analysis [**?**].

classical learning for quantum systems Classical processors are employed to extract insight on problems arising from quantum systems, e.g. data is taken from a quantum system and analysed via purely classical methods. For instance, methods which aim to represent quantum states efficiently by leveraging NNs [**?**, **?**].

complete quantum machine learning Data of a quantum nature is processed – at least partially – by quantum processors. The most common technique here is variational quantum eigensolver (VQE), which simulates quanutm systems on QCs, in order to retrieve quantum systems' ground states [**?**]. The algorithm relies on a classical optimisation routine, but was devised explicitly for implementation on quantum hardware.

The algorithms described in Part II and the applications in Parts IV to III can be described as classical learning for quantum systems. This is because the data upon which the applications are built represent quantum systems, but are processed through classical ML algorithms in order to derive insight about those systems. We caveat that it is feasible, and indeed the long term intention of such algorithms, to run in conjunction with a quantum co-processor, which would represent and evolve quantum systems, but all processing presented here are through strictly classical architecture.

2.3 Genetic algorithms

In later chapters we will use a class of optimisation techniques known as *evolutionary algorithms* [**?**, **?**]. In particular, *genetic algorithms (GAs)* are central to our primary applications, specifically in Chapter 8. Here we describe GAs in general terms for reference in later chapters.

GAs work by assuming a given problem can be optimised, if not solved, by a single candidate among a fixed, closed space of candidates, called the population, $\mathcal{P}$. A number of candidates are sampled at random from $\mathcal{P}$ into a single *generation*, and evaluated through some objective function (OF), which assesses the fitness of the candidates at solving the problem of interest. Candidates from the generation are then mixed together to produce the next generation's candidates: this *crossover* process aims to combine only relatively strong candidates, such that the average candidates' fitness improve at each successive generation, mimicing the biological mechanism whereby the genetic makeup of offspring is an even mixture of both parents through the philosophy of *survival of the fittest*. The selection of strong candidates as parents for future generations is therefore imperative; in general parents are chosen according to their fitness as determined by the OF. Buidling on this biological motivation, much of the power of GAs comes from the concept of *mutation*: while offspring retain most of the genetic expressions of their parents, some elements are mutated at random. Mutation is crucial in avoiding local optima of the OF landscape by maintaining diversity in the examined subspace of the population.

GAs are not defined either as supervised or unspervised methods; this designation depends on the OF. If candidates are evaluated with respect to labelled data, we can consider that GA supervised, otherwise unsupervised. Pseudocode for a generic GA is given in Algorithm 1, but we can also informally define the procedure as follows. Given access to the population, $\mathcal{P}$,

1. Sample N_m candidates from the population at random
   (a) call this group of candidates the first generation, μ.
2. Evaluate each candidate $\gamma_j \in \mu$
   (a) each γ_j is assigned a fitness, g_j;
   (b) the fitness is computed through an objective function acting on the candidate, i.e. $g_j = g(\gamma_j)$.
3. Map the fitnesses of each candidate, $\{g_j\}$, to selection probabilities for each candidate, $\{s_j\}$
   (a) e.g. by normalising the fitnesses, or by removing some poorly-performing candidates and then normalising.
4. Generate the next generation of candidates
   (a) Reset $\mu = \{\}$;
   (b) Select pairs of parents, $\{\gamma_{p_1}, \gamma_{p_2}\}$, from μ
      i. Each candidate's probability of being chosen is given by their s_j.
   (c) Cross over $\{\gamma_{p_1}, \gamma_{p_2}\}$ to produce children candidates, $\{\gamma_{c_1}, \gamma_{c_2}\}$
      i. mutate $\gamma_{c_1}, \gamma_{c_2}$ according to some random probabilistic process;
      ii. keep γ_{c_i} only if it is not already in μ, to ensure N_m unique candidates are tested at each generation.
   (d) until $|\mu| = N_m$, iterate to step (b).
5. Until the N_g^{th} generation is reached, iterate to step 2.;
6. The strongest candidate on the final generation is deemed the solution to the posed problem.

Candidates are manifested as *chromosomes*, i.e. strings of fixed length, whose entries, called *genes*, each represent some element of the system. In general, genes can have continuous values, although usually, and for all purposes in this thesis, genes are binary, capturing simply whether or not the gene's corresponding feature is present in the chromosome.

2.3.1 *Example: knapsack problem*

One commonly referenced combinatorial optimisation problem is the *knacksack problem*: given a set of objects, where each object has a defined mass and also a defined value, determine the set of objects to pack in a knapsack which can support a limited weight, such that the value of the packed objects is maximised. Say there are n objects, we can write the vector containing

Algorithm 1: Genetic algorithm

Input: $\mathcal{P}$ // Population of candidate models
Input: $g()$ // objective funtion
Input: map_g_to_s() // function to map fitness to selection probability
Input: select_parents() // function to select parents among generation
Input: crossover() // function to cross over two parents to produce offspring
Input: N_g // number of generations
Input: N_m // number of candidates per generation

Output: γ' // strongest candidate

$\mu \leftarrow \text{sample}\,(\mathcal{P}, N_m)$
for $i \in 1, ..., N_g$ **do**
  for $\gamma_j \in \mu$ **do**
    $g_j \leftarrow g(\gamma_j)$ // assess fitness of candidate
  end
  $\{s_j\} \leftarrow$ map_g_to_s($\{g_j\}$) // map fitnesses to normalised selection probability
  $\mu_c = \arg\max_{s_j}\{\gamma_j\}$ // record champion of this generation

  $\mu \leftarrow \{\}$ // empty set for next generation
  while $|\mu| < N_m$ **do**
    $p_1, p_2 \leftarrow$ select_parents($\{s_j\}$) // choose parents based on candidates' s_j
    $c_1, c_2 \leftarrow$ crossover(p_1, p_2) // generate offspring candidates based on parents
    for $c \in \{c_1, c_2\}$ **do**
      if $c \notin \mu$ **then**
        $\mu \leftarrow \mu \cup \{c\}$ // keep if child is new
      end
    end
  end
end
$\gamma' \leftarrow \arg\max_{s_j}\{\gamma_j \in \mu\}$ // strongest candidate on final generation

return γ'

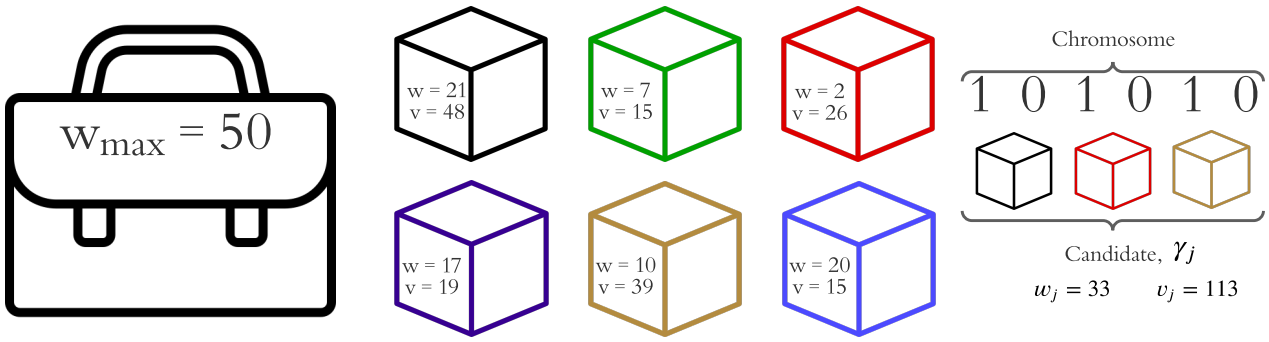

Figure 2.3: Depiction of the knapsack problem. **Left**, A knapsack which can hold any number of objects but is constrained by the total weight it can support, $w_{max} = 50$. **Centre**, A set of objects are available, each with associated weight, w, and value v. The objective is to find the subset of objects which maximise the total value, while not exceeding the capacity of the knapsack. **Right**, An example chromosome, i.e. candidate γ_j, where the bits of the chromosome indicate whether the corresponding object is included, allowing for calculation of the total weight and value of the candidate, w_j, v_j.

the values of those objects as $\vec{v}$, and the vector of their weights as $\vec{w}$. We can then represent configurations of object sets as candidate vectors $\vec{\gamma}_j$, whose genes are binary, and simply indicate whether or not the associated object is included in the set. For example, with $n = 6$,

$$\gamma_j = 100001 \implies \vec{\gamma}_j = (1 \quad 0 \quad 0 \quad 0 \quad 0 \quad 1), \tag{2.5}$$

indicates a set of objects consisting only of those indexed first and last, with none of the intermediate objects included.

The fitness of any candidate is then given by the total value of that configuration of objects, $v_j = \vec{v} \cdot \vec{\gamma}_j$, but candidates are only admitted[4] if the weight of the corresponding set of objects is less than the capacity of the knapsack, i.e. $\vec{w}_j \cdot \vec{\gamma}_j \leq w_{max}$.

For example where each individual object has value < 50 and weight < 25 and $w_{max} = 50$, recalling $\gamma_j = 100001$, say,

$$\vec{v} = (48 \quad 15 \quad 26 \quad 19 \quad 39 \quad 15) \implies v_j = \vec{\gamma}_j \cdot \vec{v} = 48 + 15 = 63; \tag{2.6a}$$

$$\vec{w} = (21 \quad 7 \quad 2 \quad 17 \quad 10 \quad 20) \implies w_j = \vec{\gamma}_j \cdot \vec{w} = 21 + 20 = 41. \tag{2.6b}$$

We can hence assess the fitness of γ_j as 63 and deem it a valid candidate since it does not exceed the weight threshold. We can likewise compute the total weight and value of a series

4 Note there are alternative strategies to dealing with candidates who violate the weight condition, such as to impose a penalty within the OF, but for our purposes let us assume we simply disregard violators.

of randomly generated candidates, and deem them valid or not. Table 2.3 shows a set of 12 randomly generated candidates, of which ten are valid.

Name	Candidate	Value	Weight	Valid
γ_1	110011	117	58	No
γ_2	101010	113	33	Yes
γ_3	011110	99	36	Yes
γ_4	011011	95	39	Yes
γ_5	111000	89	30	Yes
γ_6	010111	88	54	No
γ_7	100010	87	31	Yes
γ_8	110001	78	48	Yes
γ_9	011101	75	46	Yes
γ_{10}	110000	63	28	Yes
γ_{11}	000011	54	30	Yes
γ_{12}	000101	34	37	Yes

Table 2.3: Candidate solutions to the knapsack problem for randomly generated chromosomes.

The strongest (valid) candidates from Table 2.3 are $101010, 011110$. By spawning from these candidates through a one-point crossover at the midpoint[5], we get $\gamma_{c_1} = 101110, \gamma_{c_2} = 011010$, from which we can see $v_{c_1} = 132, w_{c_1} = 50$, i.e. by combining two strong candidates we produce the strongest-yet-seen valid candidate.

By repeating this procedure, it is expected to uncover candidates which optimise v_j while maintining $w_j \leq w_{max}$, or at least to produce near-optimal solutions, using far less time/resources than brute-force evaluation of all candidates, which is usually sufficient. For instance, with $n = 100$ objects to consider, there are $2^{100} \approx 10^{30}$ candidates to consider; the most powerful supercomputers in the world currently claim on the order of Exa-FLOPs, i.e. 10^{18} operations per second, of which say $\mathcal{O}(1000)$ operations are required to test each candidate, meaning 10^{15} candidates can be checked per second in a generous example. This would still require 10^{12} seconds to solve absolutely, so it is reasonable in cases like this to accept *approximately optimal* solutions[6].

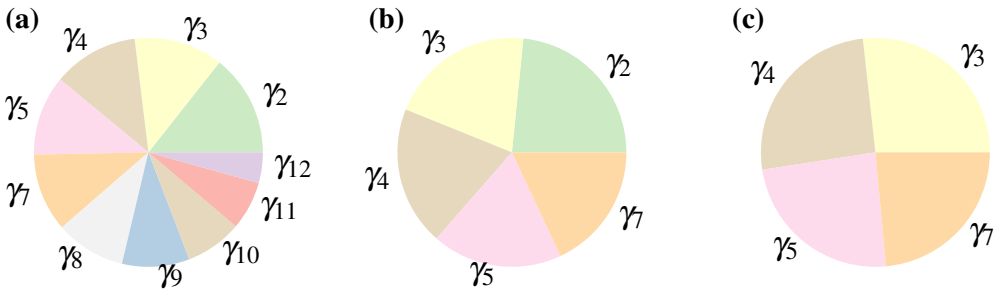

Figure 2.4: Roulette wheels showing selection probability s_i for corresponding candidates γ_i. Colours here only distinguish candidates, they do not encode any information. **b**, The set of potential parents is truncated to include only the strongest five candidates. **a**, All valid candidates are assigned selection probability based on their value in Table 2.3. **c**, After one parent (γ_2) has been chosen, it is removed from the roulette wheel and the remaining candidates' probabilities are renormalised for the selection of the second parent.

2.3.2 *Selection mechanism*

A key subroutine of every GA is the mechanism through which it nominates candidates from generation μ as parents to offsping candidates in $\mu + 1$ [**?**]. All mechanisms have in common that they act on a set of candidates from the previous generation, where each candidate, γ_j, has been evaluated and has fitness value, g_j. Among the viable schemes for selecting individual parents from the set of candidates, μ are

- Rank selection: candidates are selected with probabilty proportional to their ranking relative to the fitness of contemporary candidates in the same generation;
- Tournament selection: a subset of k candidates are chosen at random from μ, of which the candidate with the highest fitness is taken as the parent;
- Stochastic universal sampling: candidates are sampled proportional to their fitness, but the sampling algorithm is biased to ensure high-fitness candidates are chosen at least once within the generation.

We will only detail the mechanism used in later applications within this thesis: fitness proportional selection, known as *roulette selection* [**?**]. This is a straightforward strategy where we directly map candidates' fitness, g_i to a selection probability, s_i, simply by normalising $\{g_i\}$, allowing us to visualise a roulette wheel of uneven wedges, each of which correspond to a candidate. Then we need only conceptually spin the roulette wheel to select the first parent, γ_{p_1}.

5 One-point crossovers are detailed in Section 2.3.3 with this example shown in Fig. 2.5.
6 Simply put: in machine learning, *good enough* is good enough. We will adopt this philosophy for the remainder of this thesis and life.

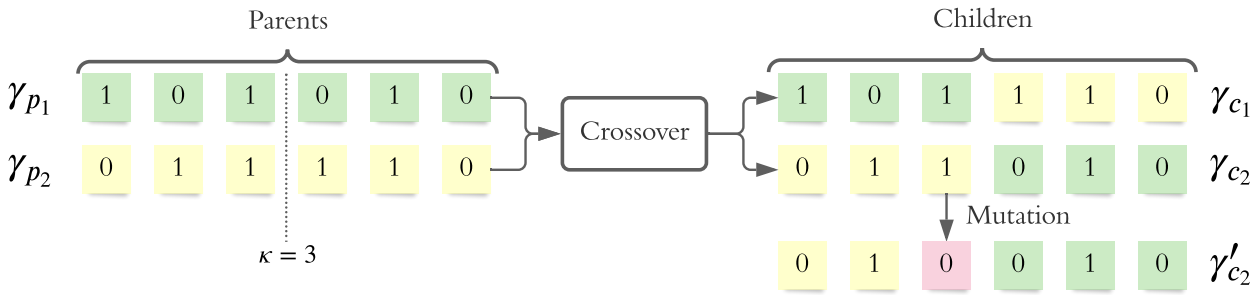

Figure 2.5: Crossover and mutation of chromosomes. Two parents, $\{\gamma_{p_1}, \gamma_{p_2}\}$, are nominated from the process in Fig. 2.4. They are then crossed-over via a one-point crossover with crossing point $\kappa = 3$, resulting in children candidates $\{\gamma_{c_1}, \gamma_{c_2}\}$. One child chromosome is mutated to yield a new candidate, γ'_{c_2}. The candidates added to the next generation are then $\{\gamma_{c_1}, \gamma'_{c_2}\}$.

We then remove γ_{p_1} from the set of potential parents, renormalise the remaining $\{s_i\}$, and spin the wheel again to choose the second parent, γ_{p_2}. The roulette selection is shown in Fig. 2.4.

Practically, we repeat the process outlined until the next generation is filled, usually we have $|\mu| = N_m$, and desire that every generation should contain the same N_m candidates, so we repeat the roulette selection $N_m/2$ times per generation, since every pair of parents yield two offspring. It is important that meaningful differences in fitness are reflected by the selection probability, which is difficult to ensure for large N_m, e.g. with ten models, the strongest candidate is only a marginally more probable parent than the worst – this effect is amplified for larger N_m. We therefore wish to reduce the set of potential parents to ensure high quality offspring: we truncate μ and retain only the highest-fitness $\frac{N_m}{2}$ models as selectable parents.

2.3.3 *Reproduction*

When a pair of parents have been nominated by the selection mechanism above, it remains to use those parents to *reproduce*, i.e. to produce offspring which should inherit and improve upon the properties of their parents. Here we use a *one point crossover*, whereby the two parent chromosomes are mixed together to form two offspring, about a single point, κ: for candidates of n genes, the first κ genes of γ_{p_1} are conjoined with the latter $n - \kappa$ genes of γ_{p_2}. Often κ is restricted to the midpoint of the chromosomes, although in general we need not impose this: we will instead consider $\kappa \in \left(\frac{n}{4}, \frac{3n}{4}\right)$, e.g. with $n = 12$, $\kappa \in (3, 9)$. The one-point crossover is shown for $n = 6$ with $\kappa = 3$ in Fig. 2.5, recalling the chromosome structure from Section 2.3.1.

By allowing κ other than the midpoint, we drastically increase the number of combinations of parents available for reproduction. Finally, then, parent selection is done by constructing a database of pairs of potentital parents with all available crossover points, with selection

probability given by the product of their individual fitnesses. This is conceptually equivalent to selection via roulette wheel as above. Recalling the fitnesses (values) of Table 2.3, we generate the parent selection database:

Parent 1	Parent 2	κ	s_{ij}
γ_2	γ_3	2	$11,187\ (= 113 \times 99)$
γ_2	γ_3	3	$11,187$
γ_2	γ_3	4	$11,187$
γ_2	γ_4	2	$10,735\ (= 113 \times 95)$
γ_2	γ_4	3	$10,735$
γ_2	γ_4	4	$10,735$
		$\vdots$	
γ_5	γ_7	2	$7,743\ (= 89 \times 87)$
γ_5	γ_7	3	$7,743$
γ_5	γ_7	4	$7,743$

Table 2.4: Example of parent selection database. Pairs of parents are selected together, with the (unnormalised) selection probability, s_{ij}, given by the product of the individual candidates' fitnesses. Pairs of parents are repeated in the database for differing κ, and all κ are equally likely.

The GA maintains diversity in the subspace of $\mathcal{P}$ it studies, by *mutating* some of the newly proposed offspring candidates. Again, there are a multitude of approaches for this step [**?**], but for brevity we only describe those used in this thesis. For each proposed child candidate, γ_c, we probabilistically mutate each gene with some mutation rate r_m: if a mutation occurs, the child is replaced by γ_c'. That is, γ_c' is added to the next generation, and γ_c is discarded. r_m is a *hyperparameter* of the GA: the performance of the algorithm can be optimised by finding the best r_m for a given problem.

2.3.4 *Candidate evaluation*

Within every generation of the GA, each candidate must be evaluated, so that the relative strength of candidates can be exploited in constructing candidates for the next generation. In the example of the knapsack problem used above, candidates were evaluated by the value of their contents, but also by whether they would fit in the knapsack. Idenitfiyng the appropriate method by which to evaluate candidates is arguably the most important aspect of designing a GA: while the choice of hyperperameters (N_g, N_m, r_m) dictate the efficacy of the search, the lack of an effective metric by which to distinguish candidates would render the procedure pointless. Considerations are hence usually built into the objective function (OF); GAs implementations later in this thesis therefore demand we design OFs with respect to the individual application.

Part II

ALGORITHMS

3

QUANTUM HAMILTONIAN LEARNING

First suggested in [**?**] and since developed [**?**, **?**] and implemented [**?**, **?**], quantum Hamiltonian learning (QHL) is a machine learning algorithm for the optimisation of a given Hamiltonian parameterisation against a quantum system whose model is known apriori. Given a target quantum system Q known to be described by some Hamiltonian $\hat{H}(\vec{\alpha})$, QHL optimises $\vec{\alpha}$. This is achieved by interrogating Q and comparing its outputs against proposals $\vec{\alpha}_p$. In particular, an experiment is designed, consisting of an input state, $|\psi\rangle$, and an evolution time, t. This experiment is performed on Q, whereupon its measurement yields the datum $d \in \{0, 1\}$, according to the expectation value $\left|\langle\psi| e^{-i\hat{H}_0 t} |\psi\rangle\right|^2$. Then on a trusted (quantum) simulator, proposed parameters $\vec{\alpha}_p$ are encoded to the known Hamiltonian, and the same probe state is evolved for the chosen t and projected on to d, i.e. $\left|\langle d| e^{-i\hat{H}(\vec{\alpha}_p)t} |\psi\rangle\right|^2$ is computed. The task for QHL is then to find $\vec{\alpha}'$ for which this quantity is close to 1 for all values of $(|\psi\rangle, t)$, i.e. the parameters input to the simulation produce dynamics consistenst with those measured from Q.

The procedure is as follows. A *prior* probability distribution $\Pr(\vec{\alpha})$ of dimension $|\vec{\alpha}|$ is initialised to represent the constituent parameters of $\vec{\alpha}$. $\Pr(\vec{\alpha})$ is typically a multivariate normal (Gaussian) distribution; it is therefore necessary to pre-suppose some mean and width for each parameter in $\vec{\alpha}$. This imposes prior knowledge on the algorithm whereby the programmer must decide the range in which parameters are *likely* to fit: although QHL is generally robust and capable of finding parameters outside of this prior, the prior must at least capture the order of magnitude of the target parameters. An example of imposing such domain-specific prior knowledge is, when choosing the prior for a model representing an e^- spin in a nitrogen-vacancy (NV) centre, to select GHz parameters for the electron spin's rotation terms, and MHz terms for the spin's coupling to nuclei, as proposed in literature. It is important to understand, then, that QHL removes the prior knowledge of precisely the parameter representing an interaction in Q, but does rely on a ball-park estimate thereof from which to start.

In short, QHL samples parameter vectors $\vec{\alpha}_p$ from $\Pr(\vec{\alpha})$, simulates experiments by computing the *likelihood* $\left|\langle d| e^{-i\hat{H}(\vec{\alpha}_p)t} |\psi\rangle\right|^2$ for experiments $(|\psi\rangle, t)$ designed by a QHL heuristic subroutine, and iteratively improves the probability distribution of the parameterisation $\Pr(\vec{\alpha})$ through standard *Bayesian inference*. A given set of $(|\psi\rangle, t)$ is called an experiment, since it corresponds to preparing, evolving and measuring Q once[1]. QHL iterates for N_e experiments. The parameter vectors sampled are called *particles*: there are N_p particles used per experiment. Each particle used incurs one further calculation of thelikelihood function – this calculation, on a classical

1 experimentally, this may involve repeating a measurement many times to determine a majority result and to mitigate noise

computer, is exponential in the number of qubits of the model under consideration (because each unitary evolution relies on the exponential of the $2^n \times 2^n$ Hamiltonian matrix of n qubits). Likewise, each additional experiment incurs the cost of calculation of N_p particles, so the total cost of running QHL for a single model is $\propto N_e N_p$. It is therefore preferable to use as few particles and experiments as possible, though it is important to include sufficient resources that the parameter estimates have the opportunity to converge. Access to a fully operational, trusted quantum simulator admits an exponential speedup by simulating the unitary evolution instead of computing the matrix exponential classically.

3.1 BAYES RULE

Bayes' rule is used to update a probability distribution describing hypotheses, Pr(hypothesis), when presented with new information (data). That is, the probabilty that a hypothesis is true is replaced by the initial probability that is was true, Pr(hypothesis), multiplied by the likelihood that the new data would be observed were that hypothesis true, Pr(data|hypothesis), normalsied by the probability of observing that data in the first place, Pr(data). It is stated as

$$\Pr(\text{hypothesis}|\text{data}) = \frac{\Pr(\text{data}|\text{hypothesis}) \times \Pr(\text{hypothesis})}{\Pr(\text{data})}. \tag{3.1}$$

We wish to represent our knowledge of Hamiltonian parameters with a distribution, $\Pr(\vec{\alpha})$: in this case hypotheses $\vec{\alpha}$ attempt to describe data, $\mathcal{D}$, measured from the target quantum system, from a set of experiments $\mathcal{E}$, so we can rewrite Bayes' rule as

$$\Pr(\vec{\alpha}|\mathcal{D};\mathcal{E}) = \frac{\Pr(\mathcal{D}|\vec{\alpha};\mathcal{E})\ \Pr(\vec{\alpha})}{\Pr(\mathcal{D}|\mathcal{E})}. \tag{3.2}$$

We can then discretise Eq. (3.2) to the level of single particles (individual vectors in the parameter space), sampled from $\Pr(\vec{\alpha})$:

$$\Pr(\vec{\alpha}_p|d;e) = \frac{\Pr(d|\ \vec{\alpha}_p;\ e)\ \Pr(\vec{\alpha}_p)}{\Pr(d|e)} \tag{3.3}$$

where

- e are the experimental controls of a single experiment, e.g. evolution time and input probe state;
- d is the datum, i.e. the binary outcome of measuring Q under conditions e;
- $\vec{\alpha}_p$ is the *hypothesis*, i.e. a single parameter vector, called a particle, sampled from $\Pr(\vec{\alpha})$;
- $\Pr(\vec{\alpha}_p|d;e)$ is the *updated* probability of this particle following the experiment e, i.e. accounting for new datum d, the probability that $\vec{\alpha} = \vec{\alpha}_0$;
- $\Pr(d|\vec{\alpha}_p;e)$ is thelikelihood function, i.e how likely it is to have measured the datum d from the system assuming $\vec{\alpha}_p$ are the true parameters and the experiment e was performed;

- $\Pr(\vec{\alpha}_p)$ is the probability that $\vec{\alpha}_p = \vec{\alpha}_0$ according to the prior distribution $\Pr(\vec{\alpha})$, which we can immediately access;
- $\Pr(d|e)$ is a normalisation factor, the chance of observing d from experiment e irrespective of the underlying hypothesis.

In order to compute the updated probability for a given particle, then, all that is required is a value for thelikelihood function. This is equivalent to the expectation value of projecting $|\psi\rangle$ onto d, after evolving $\hat{H}(\vec{\alpha}_p)$ for t, i.e.

$$\Pr(d|\vec{\alpha}; e) = \left| \langle d| \, e^{-i\hat{H}(\vec{\alpha}_p)t} \, |\psi\rangle \right|^2, \tag{3.4}$$

which can be simulated clasically or using a quantum simulator (see Section 3.3). It is necessary first to know the datum d (either 0 or 1) which was projected by Q under real experimental conditions. Therefore we first perform the experiment e on Q (preparing the state $|\psi\rangle$ evolving for t and projecting again onto $\langle\psi|$) to retrieve the datum d. d is then used for the calculation of thelikelihood for each particle sampled from $Pr(\vec{\alpha})$. Each particle's probability can be updated by Eq. (3.3), allowing us to redraw the entire probability distribution – i.e. we compute a *posterior* probability distribution by performing this routine on N_p particles.

3.2 SEQUENTIAL MONTE CARLO

In practice, QHL samples from and updates $\Pr(\vec{\alpha})$ via SMC. SMC samples the N_p particles from $\Pr(\vec{\alpha})$, and assigns each particle a weight, $w_0 = 1/N_p$. Each particle corresponds to a unique position in the parameters' space, i.e. $\vec{\alpha}_p$. Following the calculation of the likelihood, $\Pr(d|\vec{\alpha}_p; e)$, the weight of particle p are updated by Eq. (3.5).

$$w_p^{new} = \frac{\Pr(d|\vec{\alpha}_p; e) \times w_p^{old}}{\sum_p w_p \Pr(\vec{\alpha}_p|d; e)} \tag{3.5}$$

In this way, strong particles (high $\Pr(d|\vec{\alpha}_p; e)$) have their weight increased, while weak particles (low $\Pr(d|\vec{\alpha}_p; e)$) have their weights decreased, and the sum of weights remains normalised. Within a single experiment, the weights of all N_p particles are updated thus: we *simulataneously* update sampled particles' weights as well as $\Pr(\vec{\alpha})$. This iterates for the following experiment, using the *same* particles: we do *not* redraw N_p particles for every experiment. Eventually, the weights of most particles fall below a threshold, r_t, meaning that only that fraction of particles have reasonablelikelihood of being $\vec{\alpha}_0$. At this stage, SMC *resamples*, i.e. selects new particles, according to the updated $\Pr(\vec{\alpha})$, according to the Liu-West resampling algorithm [**?**]. Then, the new particles are in the range of parameters which is known to be more likely, while particles in the region of low-weight are effectively discarded. Usually, we set $r_t = 0.5$, although this hyperparameter can have a large impact on the rate of learning, so can be optimised in particular circumstances, see Fig. 3.2. This procedure is easiest understood through the example presented in Fig. 3.1, where a two-parameter Hamiltonian is learned starting from a uniform distribution.

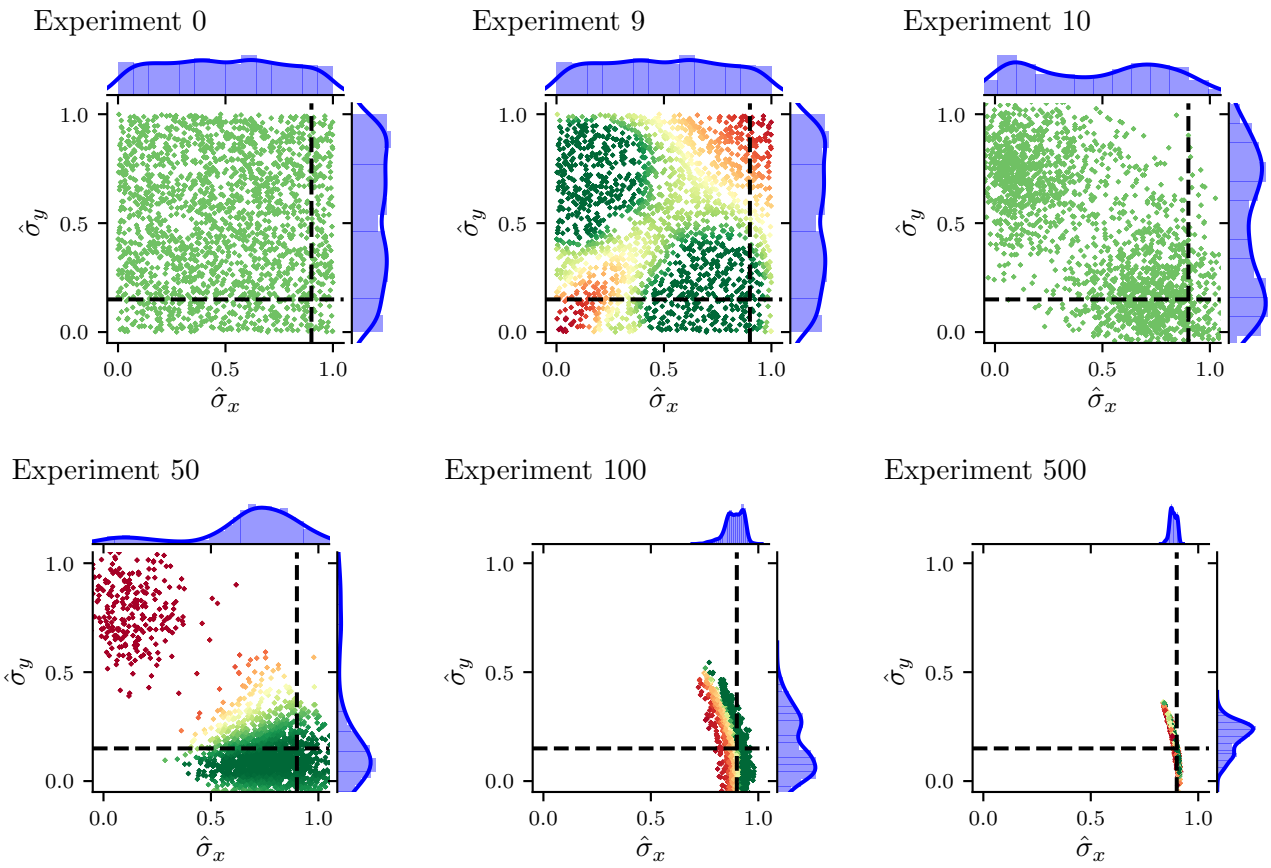

Figure 3.1: Quantum Hamiltonian learning (QHL) via sequential monte carlo (SMC). The studied model has two terms, $\{\hat{\sigma}_x, \hat{\sigma}_y\}$ with true parameters $\alpha_x = 0.9, \alpha_y = 0.15$ (dahsed lines), with $N_e = 500, N_p = 2000$. Crosses represent particles, while the distribution $\Pr(\alpha_p)$ for each parameter can be seen along the top and right-hand-sides of each subplot. Both parameters are assigned a uniform probability distribution $\mathcal{U}(0,1)$, representing our prior knowledge of the system. **(a),** sequential monte carlo (SMC) samples N_p particles from the initial joint probability distribution, with particles uniformly spread across the unit square, each assigned the starting *weight* w_0. At each experiment e, each of these particles'likelihood is computed according to Eq. (3.3) and its weight is updated by Eq. (3.5). **(b),** after 9 experiments, the weights of the sampled particles are sufficintly informative that we know we can discard some particles while most likely retaining the true parameters. **(c),** SMC resamples according the current $\Pr(\vec{\alpha})$, i.e. having accounted for the experiments and likelihoods observed to date, a new batch of N_p particles are drawn, and each reassigned weight w_0, irrespective of their weight prior to resampling. **(d, e),** Afer further experiments and resamplings, SMC narrows $\Pr(\vec{\alpha})$ to a region around the true parameters. **(f),** The final *posterior* distribution consists of two narrow distributions centred on α_x and α_y.

very

3.3 LIKELIHOOD

The fundamental step within QHL is the calculation of likelihood in Eq. (3.3). The core of this learning algorithm is that this likelihood can be retrieved from the Born rule, although in principle *any* validlikelihood function can fulfil this equation, provided the calculation of thelikelihood captures the probabilty that the present hypothesis produced the present datum.

In general, it is not always possible to derive the analytical likelihood, especially in cases where we wish to vary the probe. When Eq. (3.4) can be computed classically, QHL relies on classicallikelihood estimation (CLE), i.e. involving the exponential calculation of Eq. (3.4), whereas quantumlikelihood estimation (QLE) uses the samelikelihood function computed on a quantum simulator; this is the sole application of quantum simulators in this protocol and indeed the remainder of this thesis. Access to such hardware, operating perfectly, would provide exponential speedup in the calculation of this term, rendering both QHL and the wider QMLA formalism scalable, although in this thesis we do not implement QLE so everything can be viewed as CLE. QLE was implemented in [**?**].

We adopt notation used by QInfer, which QMLA for thelikelihood estimation stage [**?**]. The expectation value for a the unitary operator is given by

$$\Pr(0) = |\langle\psi| e^{-i\hat{H}_p t} |\psi\rangle|^2 = l(d=0|\hat{H}_p; e), \tag{3.6}$$

i.e. the input basis is assigned the measurement label $d = 0$, and this quantity is the probability of measuring $d = 0$, i.e. measuring the same state as input. However, we assume a binary outcome model, i.e. that the system is measured either in $|\psi\rangle$ (labelled $d = 0$), or it is not ($d = 1$); thelikelihood for the latter case is

$$\Pr(1) = l(d=1|\hat{H}_p; e) = \sum_{\{|\psi_\perp\rangle\}} |\langle\psi_\perp| e^{-i\hat{H}_p t} |\psi\rangle|^2 = 1 - \Pr(0). \tag{3.7}$$

Usually we will refer to the case where Q is projeced onto the input state $|\psi\rangle$, so the terms *likelihood*, *expectation value* and $\Pr(0)$ are synonymous, unless otherwise stated.

3.3.1 *Interactive Quantumlikelihood Estimation*

An important extension to QLE is interactive quantumlikelihood estimation (IQLE), which follows SMC but uses an alternative likelihood function in order to overcome some of its inherent challenges [**?**]. Two almost identical Hamiltonians will diverge after exponentially small evolution time [**?**]. This is problematic for QHL because it relies on thelikelihood function which is built on the assumption that increasing accuracy of $\hat{H}(\vec{\alpha})$ approximating $\hat{H}_0$ should result in rising likelihood; this result indicates that even extremely accurate approximations become unreliable after very short evolution times. Coupled with the result that small time experiments are uninformative [**?**], this observation demands exponentially many measurements to approximate the exponentially small likelihoods , rendering the approach inefficient.

The Loschmidt echo (LE) is the measure of the revival resulting from an imperfect time-reversal operation implemented after the standard time evolution. The reversal operation corresponds to some Hamiltonian, $\hat{H}_-$, which is seen as an attempt to un-do the evolution according to the original Hamiltonian, $\hat{H}_+$. As such we say that $\hat{H}_-$ is evolved for $-t$, so its unitary is $e^{-i\hat{H}_-(-t)}$ after $\hat{H}_+$ is evolved for t. The LE can be written and characterised as

$$M(t) = \left|\langle\psi|e^{+i\hat{H}_- t}e^{-i\hat{H}_+ t}|\psi\rangle\right|^2 \sim \begin{cases} 1-\mathcal{O}(t^2), & t \leq t_c \\ e^{-\mathcal{O}(t)}, & t_c \leq t \leq t_s \\ 1/\|\hat{H}\|, & t \geq t_s \end{cases} \tag{3.8}$$

where $\hat{H}_-, \hat{H}_+$ are backward and forward time evolutions respsectively, which are assumed almost identical; $\|\hat{H}\|$ is their dimension, and t_c, t_s are bounds on the evolution time marking the transition between the *parabolic decay*, *asymptotic decay* and *saturation* of the echo [**?**]. In effect, the LE gaurantees that if $\hat{H}_- \not\approx \hat{H}_+$, then $M(t) \ll 1$, while $\hat{H}_- \approx \hat{H}_+$ gives $M(t) \approx 1$. This can be exploited for learning: by taking $\hat{H}_+$ as either $\hat{H}_0$ (true) or $\hat{H}(\vec{\alpha})$ (particle or hypothesis), and sampling $\hat{H}_-$ from $\Pr(\vec{\alpha})$, we can adopt Eq. (3.8) as thelikelihood function in Eq. (3.4), in the knowledge that this will disinguish between hypotheses based on their similarity to $\hat{H}_0$.

Importantly, IQLE can only be used where we can *reliably* evolve the system under study. In order that the reverse evolution is relibable, it must be performed on a trusted simulator, restricting IQLE to cases where a coherent quantum channel exists between the target system and a trusted simulator. This automatically excludes any open quantum systems, as well as most realistic experimental setups, although such channels can be achieved [**?**]. The remaining application for IQLE, and correspondingly QHL, is in the characterisation of untrusted quantum simulators, which can realise such coherent channels [**?**].

3.3.2 *Analytical likelihood*

In some cases, analyticallikelihood functions can be derived to describe the dynamics of simple quantum systems [**?**, **?**], for instance encoding the Rabi frequency ω of an oscillating electron spin in an NVC,

$$\hat{H}(\omega) = \frac{\omega}{2}\hat{\sigma}_z. \tag{3.9}$$

Then, bearing in mind that $\hat{\sigma}_z\hat{\sigma}_z = \hat{\mathbb{1}}$, so $\hat{\sigma}_z^{2k} = \hat{\mathbb{1}}$ and $\hat{\sigma}_z^{2k+1} = \hat{\sigma}_z$, using MacLaurin expansion, the unitary evolution of Eq. (3.9) is given by

$$\begin{aligned} U = e^{-i\hat{H}(\omega)t} = e^{-i\frac{\omega t}{2}\hat{\sigma}_z} &= \cos\left(\frac{\omega t\hat{\sigma}_z}{2}\right) - i\sin\left(\frac{\omega t\hat{\sigma}_z}{2}\right) \\ &= \left(\sum_{k=0}^{\infty}\frac{(-1)^k}{(2k)!}\left(\frac{\omega t}{2}\right)^{2k}\hat{\sigma}_z^{2k}\right) - i\left(\sum_{k=0}^{\infty}\frac{(-1)^k}{(2k+1)!}\left(\frac{\omega t}{2}\right)^{2k+1}\hat{\sigma}_z^{2k+1}\right) \\ &= \left(\sum_{k=0}^{\infty}\frac{(-1)^k}{(2k)!}\left(\frac{\omega t}{2}\right)^{2k+1}\right)\hat{\mathbb{1}} - i\left(\sum_{k=0}^{\infty}\frac{(-1)^k}{(2k+1)!}\left(\frac{\omega t}{2}\right)^{2k+1}\right)\hat{\sigma}_z \\ &= \cos\left(\frac{\omega t}{2}\right)\hat{\mathbb{1}} - i\sin\left(\frac{\omega t}{2}\right)\hat{\sigma}_z \end{aligned} \tag{3.10}$$

Then, evolving a probe $|\psi_0\rangle$ and projecting onto a state $|\psi_1\rangle$ gives

$$\langle\psi_1|\, U\, |\psi_0\rangle = \cos\left(\frac{\omega t}{2}\right)\langle\psi_1|\psi_0\rangle - i\sin\left(\frac{\omega t}{2}\right)\langle\psi_1|\hat{\sigma}_z|\psi_0\rangle\,. \tag{3.11}$$

By initialising and projecting into the same state, say $|\psi_0\rangle = |\psi_1\rangle = |+\rangle$, we have

$$\begin{aligned} \hat{\sigma}_z|+\rangle = |-\rangle \implies \langle\psi_1|\hat{\sigma}_z|\psi_0\rangle &= 0 \\ \langle\psi_1|\psi_0\rangle &= 1 \\ \implies \langle\psi_1|U|\psi_0\rangle &= \cos\left(\frac{\omega t}{2}\right), \end{aligned} \tag{3.12}$$

i.e. if the system measures in $|+\rangle$, we set the datum $d = 1$, otherwise $d = 0$. Then, from Born's rule, and in analogy with Eq. (3.4), we can formulate thelikelihood function, where the hypothesis is the single parameter ω, and the sole experimental control is t,

$$\Pr(d = 1|\omega; t) = |\langle\psi_1|U|\psi_0\rangle|^2 = \cos^2\left(\frac{\omega t}{2}\right) \tag{3.13}$$

This analyticallikelihood will underly the simulations used in the following introductions, except where explicitly mentioned.

3.4 TOTAL LOG TOTAL LIKELIHOOD

We have already used the concept of likelihood to update our parameter distribution during SMC; we can consolidate the likelihoods of all particles with respect to a single datum, d, from a single experiment e, in the *total likelihood*,

$$l_e = \sum_{p\in\{p\}} \Pr(d|\vec{\alpha}_p; e) \times w_p^{old}. \tag{3.14}$$

For each experiment, we use totallikelihood as a measure of how well the distribution performed, i.e. we care about how well all particles, $\{p\}$, perform as a collective, representative of how well $\Pr(\vec{\alpha})$ approximates the system, equivalent to the noramlisation factor in Eq. (3.5), [**?**].

l_e are strictly positive, and because the natural logarithm is a monotonically increasing function, we can equivalently work with the log total likelihood (LTL), since $ln(l_a) > ln(l_b) \iff l_a > l_b$. LTL are also beneficial in simplifying calculations, and are less susceptible to system underflow, i.e. very small values of l will exhaust floating point precision, but $ln(l)$ will not.

Note, we know that

$$\begin{aligned} w_p^0 = \frac{1}{N_p} &\implies \sum_p^{N_p} w_p^0 = 1; \\ \Pr(d|\vec{\alpha}_p; e) \leq 1 &\implies \Pr(d|\vec{\alpha}_p; e) \times w_p^{old} \leq w_p^{old} \\ &\implies \sum_{\{p\}} \Pr(d|\vec{\alpha}_p; e) \times w_p^{old} \leq \sum_{\{p\}} w_p^{old} \leq \sum_p^{N_p} w_p^0; \\ &\implies l_e \leq 1. \end{aligned} \tag{3.15}$$

Eq. (3.14) essentially says that a good batch of particles, where on average particles perform well, will mean that most w_i are high, so $l_e \approx 1$. Conversely, a poor batch of particles will have low average w_i, so $l_e \approx 0$.

In order to assess the quality of a *model*, $\hat{H}_i$, we can consider the performance of a set of particles throughout a set of experiments $\mathcal{E}$, through its total log total likelihood (TLTL),

$$\mathcal{L}_i = \sum_{e \in \mathcal{E}} ln(l_e). \tag{3.16}$$

The set of experiments on which $\mathcal{L}_i$ is computed, $\mathcal{E}$, as well as the particles whose sum constitute each l_e can be the same experiments on which $\hat{H}_i$ is trained, $\mathcal{E}_i$, but in general need not be, i.e. $\hat{H}_i$ can be evaluated by considering different experiments than those on which it was trained. For example, $\hat{H}_i$ can be trained with $\mathcal{E}_i$ to optimise $\vec{\alpha}_i'$, and thereafter be evaluated using a different set of experiments $\mathcal{E}_v$, such that $\mathcal{L}_i$ is computed using particles sampled from the distribution after optimising $\vec{\alpha}$, $\Pr(\vec{\alpha}_i')$, and may use a different number of particles than the training phase.

Perfect agreement between the model and the system would result in $l_e = 1 \Rightarrow ln(l_e) = 0$, as opposed to poor agreement $l_e < 1 \Rightarrow ln(l_e) < 0$. Then, in all cases Eq. (3.16) is negative, and across a series of experiments, strong agreement gives low $|\mathcal{L}_i|$, whereas weak agreement gives large $|\mathcal{L}_i|$.

3.5 PARAMETER ESTIMATION

QHL is a parameter estimation algorithm, so here we introduce some methods to evaluate its performance, which we can reference in later sections of this thesis.

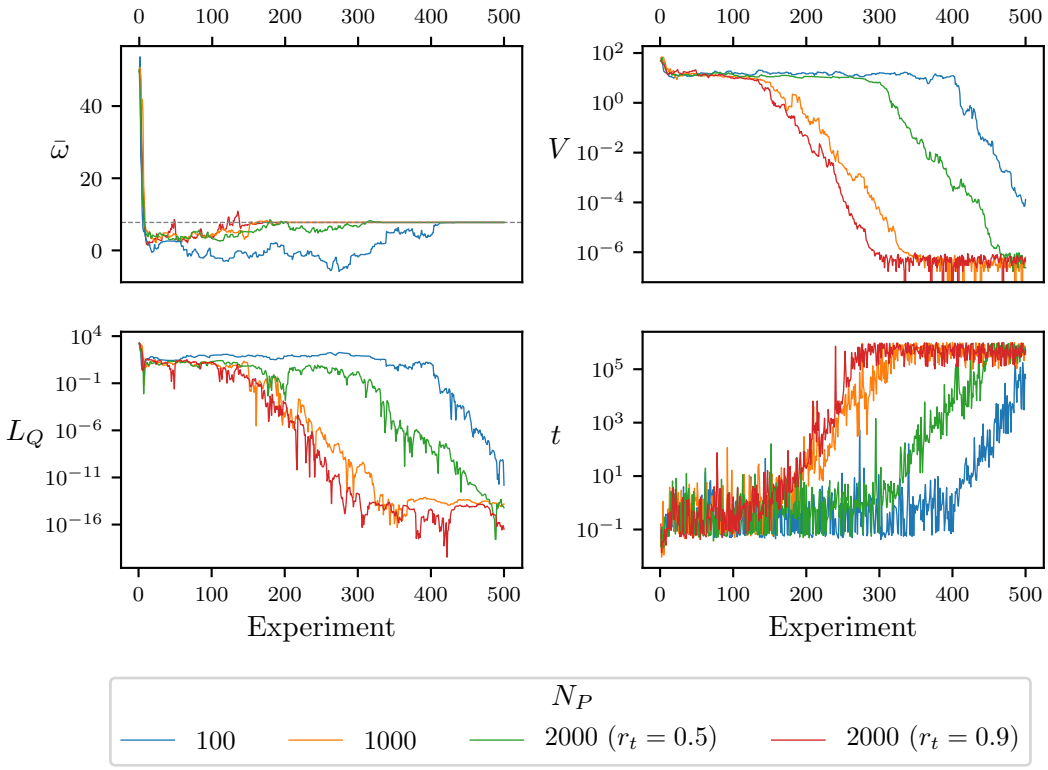

Figure 3.2: Parameter learning for the analyitcallikelihood Eq. (3.13) for varying numbers of particles N_p, for $N_e = 500$. For $N_p = 2000$, we show the resampler threshold set to $r = 0.5$ and $r = 0.9$. (a) the parameter estimate, i.e. $\bar{\omega}$, the mean of the posterior distribution after each experiment, approaching $\omega_0 = 7.75$ (dashed line), where the prior is centred on $\omega = 50 \pm 25$. Decrease in (b) volume, V, (c) quadratic loss, L_Q, and (d) evolution time, t, are shown against experiment number.

The most obvious meausre of the progression of parameter estimation is the error between the true parameterisation, $\vec{\alpha}_0$, and the approximation $\vec{\alpha}_p = \text{mean}\left(\Pr(\vec{\alpha})\right)$, which can be captured by a large family of loss functions. Here we use the quadratic loss (QL), which captures this error through the sum of the square difference between each parameter's true and estimated values symetrically, i.e. error above the true parameter is as impactful as error below. We can record the QL at each experiment of our training regime and hence track its performance.

Definition 3.5.1 (Quadratic Loss)**.** For a true parameterisation $\vec{\alpha}_0$, and a hypothesis $\vec{\alpha}$, the quadratic loss is given by

$$L_Q = \|\vec{\alpha}_0 - \vec{\alpha}\|^2 . \tag{3.17}$$

3.5.1 *Volume*

We also care about the range of parameters supported by $\Pr(\vec{\alpha})$ at each experiment: the volume of the particle distribution can be seen as a proxy for our certainty that the approximation mean $(\Pr(\vec{\alpha}))$ is accurate. For example, for a single parameter ω, our best knowledge of the parameter is mean $(\Pr(\omega))$, and our belief in that approximation is the standard deviation of $\Pr(\omega)$; we can think of volume as an n-dimensional generalisation of this intuition [**?**, **?**].

In general, a confidence region, defined by its confidence level κ, is drawn by grouping particles of high particle density (HPD), $\mathcal{P}$, such that $\sum_{p \in \mathcal{P}} w_p \geq \kappa$. We use the concept of minimum volume enclosing ellipsoid (MVEE) to capture the confidence region [**?**], calculated as in [**?**], which are characterised by their covariance matrix, Σ, which allows us to calculate the volume,

do we posteri credibl

$$V(\Sigma) = \frac{\pi^{|\vec{\alpha}|/2}}{\Gamma(1 + \frac{|\vec{\alpha}|}{2})} \det\left(\Sigma^{-\frac{1}{2}}\right), \tag{3.18}$$

where Γ is the Gamma function, and $|\vec{\alpha}|$ is the cardinality of the parameterisation. This quantity allows us to meaningfully compare distributions of different dimension, but we must be cautious of drawing strong comparisons between models based on their volume alone, for instance because they may have started from vastly different prior distributions.

Within SMC, we assume the credible region is simply the posterior distribution, such that we can take $\Sigma = \mathrm{cov}(\Pr(\vec{\alpha}))$ after each experiment, and hence track the uncertainty in our parameters across the training experiments [**?**]. We use volume as a measure of the learning procedure's progress: slowly decreasing or static volume indicates poor learning, possibly highlighting poor experiment design, while fast or exponentially decreasing volume indicates that the parameters are being learned well. When the volume has converged, the learning has saturated and there is little benefit to running further experiments.

3.6 EXPERIMENT DESIGN HEURISTIC

A key consideration in QHL is the choice of experimental controls implemented in attempt to learn from the system. The experimental controls required are dictated by the choice of likelihood function used within SMC, though typically there are two primary controls we will focus on: the evolution time, t, and the probe state evolved, $|\psi\rangle$. The design of experiments is handled by an experiment design heuristic (EDH), whose structure can be altered to suit the user's needs. Usually, the EDH attempts to exploit the information available, adaptively accounting for some aspects of the inference process performed already, although there may be justification for enforcing a non-adaptive schedule, for instance to force QHL to train on a full set of experimental data rather than a restricted set which adaptive methods would advise. We can categorise each EDH as either *online* of *offline*, depending on whether it accounts for the current state of the inference procedure, i.e. the posterior. The EDH is modular and can be

replaced by any method that returns a valid set of experimental controls, so we can consider numerous approaches, for instance those described in [**?**, **?**].

3.6.1 *Particle Guess Heuristic*

The default EDH is the particle guess heuristic (PGH) [**?**], an online method which attempts to design the optimal evolution time based on the posterior. Note PGH does not specify the probe, so is coupled with a probe selection routine to comprise a complete EDH.

The principle of PGH is that the uncertainty of the posterior limits how well the Hamiltonian is currently approximated, and therefore limits the evolution time for which the posterior can be expected to reasonably mimic $\hat{H}_0$. For example, consider Eq. (3.9) with a single parameter with $\omega_0 = 10$, and current mean $(\Pr(\omega)) = 9, \text{std}\,(\Pr(\omega)) = 2$, we can expect that the approximation $\omega' = \text{mean}\,(\Pr(\omega))$ is valid up to $t_{max} = 1/\text{std}(\Pr(\omega))$. It is sensible, then, to use $t \sim t_{max}$ for two reasons: (i) smaller times are already well explained by the posterior, so offer little opportunity to learn; (ii) t_{max} is at or near the threshold the posterior can comfortably explain, so it will expose the relative difference inlikelihood between the posterior's particles, providing a strong capacity to learn. Informally, as the uncertainty in the posterior shrinks, PGH selects larger times to ensure the training is based on informative eperiments simulataneously with increasing certainty about the paraemters. In the one-dimensional case, this logic can be used to find an optimal time heuristic, where experiment k is assigned $t_k = 1.26/\text{std}(\Pr(\omega))$ [**?**].

Rather than directly using the inverse of the standard deviation of $\Pr(\vec{\alpha})$, which relies on the expensive calculation of the covarinace matrix, PGH uses a proxy whereby two particles are sampled from $\Pr(\vec{\alpha})$. The experimental evolution time for experiment k is then given by

$$t_k = \frac{1}{\|\vec{\alpha}_i - \vec{\alpha}_j\|}, \tag{3.19}$$

where $\vec{\alpha}_i, \vec{\alpha}_j$ are distinct particles sampled from $\mathcal{P}$ where $\mathcal{P}$ is the set of particles under consideration by SMC after experiment $k-1$, which had been recently sampled from $\Pr(\vec{\alpha})$.

3.6.2 *Alternative experiment design heuristics*

The EDH can be used to suit the requirements of the target system; we test four such examples against a series of models. Here the EDH must only design the evolution time for the experiment, with probe design discussed in the next section. The heuristics tested are:

- Random$(0, t_{max})$: Randomly chosen time up to some arbitrary maximum, we set $t_{max} = 1000$. This approach is clearly subobtimal, since it does not account whatsoever for the knowledge of the training so far, and demands the user choose a suitable t_{max}, which is not gauranteed to be meaningful.

- t list: forcing the training to consider a set of times decided in advance. For instance, when only a small set of experimental measurements are available, it is sensible to train on all of them, perhaps repeatedly. We test uniformly spaced times between 0 and t_{max}, and train on the list twice. Again this EDH fails to account for the performance of the trainer so far, so may use times either far above or below the ability of the parameterisation.
- $(9/8)^k$: An early attempt to match the expected exponential decrease in volume from the training, was to set $t = (9/8)^k$ [**?**]. Note we increment k after 10 experiments in the training regime, rather than after each experiment, which would result in extremely high times which flood memory.
- PGH: as in Section 3.6.1.

We show how the choie of EDH within this set can influence the training procedure, by testing models of various complexity amd dimension. In particular, we first test a simple 1-qubit model, Eq. (3.20a); followed by more complicated 1-qubit model, Eq. (3.20b); as well as randomly generated 5-qubit Ising, Eq. (3.20c), and 4-qubit Heisenberg models, Eq. (3.20d). Each $\hat{H}_i$ have randomly chosen parameters implicitly assigned to each term.

$$\hat{H}_1 = \hat{\sigma}_1^z \tag{3.20a}$$

$$\hat{H}_2 = \hat{\sigma}_1^x + \hat{\sigma}_1^y + \hat{\sigma}_1^z \tag{3.20b}$$

$$\hat{H}_3 = \hat{\sigma}_1^z\hat{\sigma}_3^z + \hat{\sigma}_1^z\hat{\sigma}_4^z + \hat{\sigma}_1^z\hat{\sigma}_5^z + \hat{\sigma}_2^z\hat{\sigma}_4^z + \hat{\sigma}_2^z\hat{\sigma}_5^z + \hat{\sigma}_3^z + \hat{\sigma}_4^z + \hat{\sigma}_3^z + \hat{\sigma}_5^z \tag{3.20c}$$

$$\hat{H}_4 = \hat{\sigma}_1^z\hat{\sigma}_2^z + \hat{\sigma}_1^z\hat{\sigma}_3^z + \hat{\sigma}_2^x\hat{\sigma}_3^x + \hat{\sigma}_2^z\hat{\sigma}_3^z + \hat{\sigma}_2^x\hat{\sigma}_4^x + \hat{\sigma}_3^z\hat{\sigma}_4^z \tag{3.20d}$$

We show the performance of each of the listed EDHs in Fig. 3.3. We will have cause to use alternative EDHs in paricular circumstances, but we adopt PGH as the default EDH throughout this thesis, unless otherwise stated.

3.7 PROBE SELECTION

A final consideration for experiments within QHL is the choice of input probe state, $|\psi\rangle$, which is evolved in the course of finding thelikelihood used during the Bayesian update. We can consider the choice of probe as an output of the EDH, although previous work has usually not considered optimising the probe, instead usually setting $|\psi\rangle = |+\rangle^{\otimes n}$ for n qubits [**?**, **?**]. In principle it is possible for the EDH to design a new probe at each experiment, although a more straightforward approach is to compose a set of probes offline, $\Psi = \{|\psi\rangle\}$, of size $N_\psi = |\Psi|$. Then, a probe is chosen at each experiment from Ψ, allowing for the same $|\psi\rangle$ to be used for the multiple experiments within the training, e.g. by iterating over Ψ. Ψ can be generated with

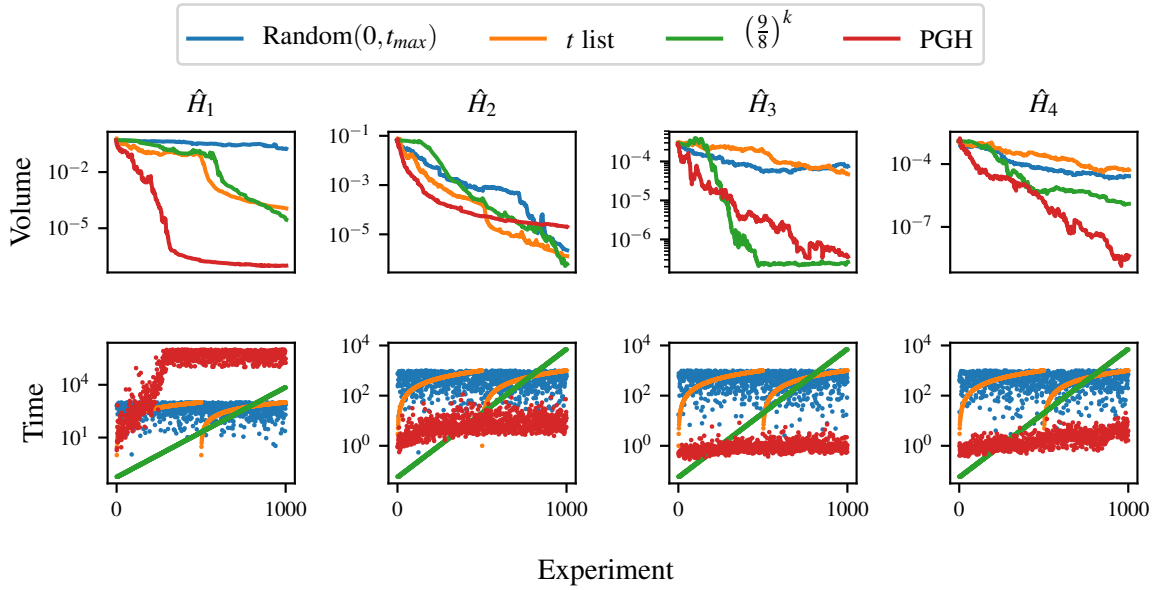

Figure 3.3: The volume of various models when trained through QHL using different EDHs. We show models of various complexity and dimension, each trained using four heuristics, outlined in the main text. Implementation details are listed in Table A.1

respect to the individual learning problem as we will examine later, but it is usually sufficient to use generic strategies which should work for all models; some straightforward examples are

i. $|0\rangle$: $\Psi = \{|0\rangle^{\otimes n}\}$, $N_\psi = 1$;

ii. $|+\rangle$: $\Psi = \{|+\rangle^{\otimes n}\}$, $N_\psi = 1$;

iii. $|t\rangle$: Ψ is the tomographic basis set, $N_\psi = 40$;

iv. $|r\rangle$: $|\psi\rangle$ are random, separable probes, $N_\psi = 40$.

We show the 1-qubit probes within Ψ under each of these strategies on the Bloch sphere in Fig. 3.4.

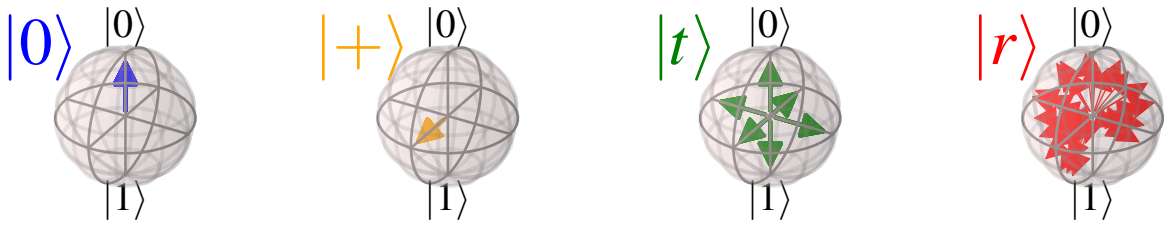

Figure 3.4: 1-qubit probes used for tests in Fig. 3.5.

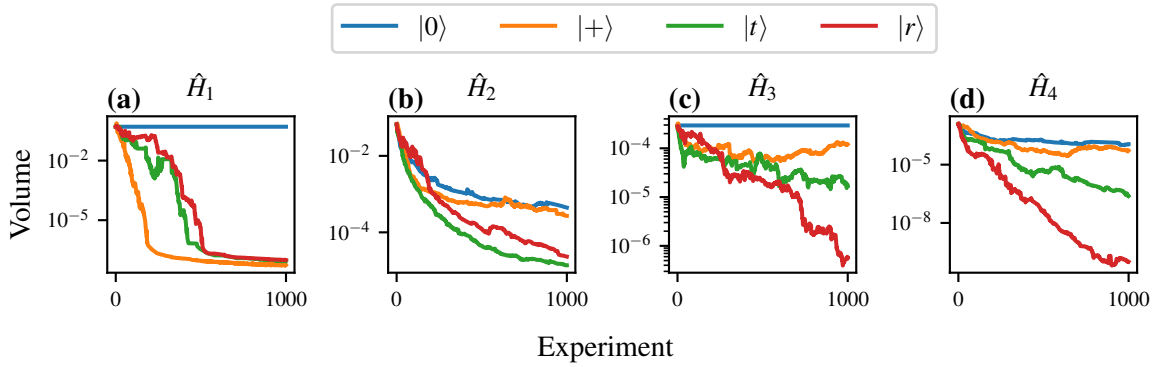

Figure 3.5: The volume of various models when trained through QHL using different initial probe sets. We show models of various complexity and dimension, each trained using random probes, $|r\rangle$, tomographic basis set probes, $|t\rangle$, as well as $|0\rangle$ and $|+\rangle$ probes. In each case the probes are generated for arbitrary numbers of qubits; for $|0\rangle, |1\rangle$, the number of probes generated is $N_\psi = 1$, and for $|t\rangle, |r\rangle$, $N_\psi = 40$. Implementation details are listed in Table A.1

We test the same set of models as Eq. (3.20) and test each of these probe construction strategies in Fig. 3.5. We can draw a number of useful observations from these simple tests:

- Training on an eigenstate, $|0\rangle$, of the model yields no information gain. This is because all particles give likelihoods $l = 1$, so no weight update can occur, meaning the parameter distribution does not change when presented new evidence.
- Training on an even superposition of the model's eigenstates, $|+\rangle$, is maximally informative: any deviations from the true parameterisation are registered most dramatically in this basis, providing the optimal training probe for this case.
- These observations are reinforced by Fig. 3.5**c**, where a 5-qubit Ising model also fails to learn from one of its eigenstates, $|0\rangle^{\otimes 5}$. Of note, however, is that $|+\rangle^{\otimes 5}$ is not the strongest probe here: the much larger Hilbert space here can not be scanned sufficiently using a single probe; using a larger number of probes is more effective, even if those are randomly chosen.
- In general the tomographic and random probe sets perform reliably.

It is an open challenge to identify the optimal probe for training any given model, and the choice of such informative probes could be built into the EDH in general, for example by computing the eigenstates of the candidate, and generating a probe set from superposition between those eigenstates. However, a further consideration is that, for model comparison purposes, it is helpful to have a universal set of probes, upon which all models are learned. This would minimise bias towards particlar models, which might arise from probes which are favourable bases for a subset of models, for example $|+\rangle$ in Fig. 3.5**a**. Careful consideration should be given to N_ψ in the choice of the probe generator, since it is important to ensure probes

test the parameterisation across the Hilbert space robustly, However this must be balanced by ensuring SMC has sufficient opportunity to learn within a subspace before moving to the next; we can mitigate this concern by instructing the EDH to repeatedly select a probe from Ψ for a batch of experiments, say five, before moving to the next available probe.

As standard for the remainder of this thesis, unless otherwise stated, we adopt the random probe generator as the defualt mechanism for selecting probes, only iterating between probes after batches of 5 experiments.

4

QUANTUM MODEL LEARNING AGENT

Quantum Model Learning Agent (QMLA) is an algorithm that extends the concept of applying machine learning to the characterisation of Hamiltonians we've seen so far. The extension, and central question of QMLA is: if we do not even have the structure of the model which describes a target quantum system, can we still learn about the physics of the system? That is, we remove the assumption about the form of the Hamiltonian model, and attempt to uncover which *terms* constitute the Hamiltonian, and in so doing, learn what interactions the system is subject to. Throughout this thesis, we are concerned solely with Hamiltonian models. although, in general, the description of a quantum system of interest need not be Hamiltonian, e.g. it could be Lindbladian for open quantum systems, so we generalise the effort to the search for the most suitable *model*.

For the remainder of this thesis, our objective is to learn the model underlying some target system Q. We will first introduce some concepts which will prove useful when discussing QMLA, before describing the protocol in detail in Section 4.3.

4.1 MODELS

Models are simply the mathematical objects which can be used to predict the behaviour of a system. In this thesis, models are synonymous with Hamiltonians, composed of a set of *terms*, $\mathcal{T} = \{\hat{t}\}$, where each $\hat{t}$ is a matrix. Each term is assosiated with a multipicative scalar, which may be referred to as that term's *parameter*: we impose order on the terms and parameters such that we can succinctly summarise any model as

$$\hat{H} = \begin{pmatrix} \alpha_0 & \dots & \alpha_n \end{pmatrix} \begin{pmatrix} \hat{t}_1 \\ \vdots \\ \hat{t}_n \end{pmatrix} = \vec{\alpha} \cdot \vec{T} \tag{4.1}$$

where $\vec{\alpha}, \vec{T}$ are the model's parameters and terms, respectively.

For example, a model which is the sum of the (non-identity) Pauli operators is given by

$$\begin{aligned} \hat{H} &= \begin{pmatrix} \alpha_x & \alpha_y & \alpha_z \end{pmatrix} \cdot \begin{pmatrix} \hat{\sigma}_x \\ \hat{\sigma}_y \\ \hat{\sigma}_z \end{pmatrix} \\ &= \alpha_x \hat{\sigma}_x + \alpha_y \hat{\sigma}_y + \alpha_z \hat{\sigma}_z \\ &= \begin{pmatrix} \alpha_z & \alpha_x - i\alpha_y \\ \alpha_x + i\alpha_y & \alpha_z \end{pmatrix}. \end{aligned} \tag{4.2}$$

Through this formalism, we can say that the sole task of QHL was to optimise $\vec{\alpha}$, given $\vec{T}$. The principle task of QMLA is to identify $\vec{T}$ with the most statistical evidence for describing the target system Q. In short, QMLA proposes candidate models $\hat{H}_i$ as hypoteses to explain Q; we *train* each model independently through a parameter learning routine, and finally nominate the model with the best performance after training. In particular, QMLA uses QHL as the parameter learning subroutine, but in principle this step can be performed by any algorithm which learns $\vec{\alpha}$ for given $\vec{T}$, [**?**, **?**, **?**, **?**, **?**, **?**, **?**, **?**]. While discussing a model $\hat{H}_i$, their *training* then simply means the implementation of QHL, where $\hat{H}_i$ is assumed to represent Q, such that $\vec{\alpha}_i$ is optimised as well as it can be, even if $\hat{H}_i$ is entirely inaccurate.

4.2 BAYES FACTORS

We can use the tools introduced in Section 3.4 to *compare* models. Of course it is first necessary to ensure that each model has been adequately trained: while inaccurate models are unlikely to strongly capture the system dynamics, they should first train on the system to determine their best attempt at doing so, i.e. they should undergo the process in Chapter 3. It is statistically meaningful to compare models via their TLTL, $\mathcal{L}_i$, if and only if they have considered the same data, i.e. if models have each attempted to account for the same set of experiments, $\mathcal{E}$ [**?**].

We can then exploit direct pairwise comparisons between models, by imposing that both models' TLTL are computed based on *any* shared set of experiments $\mathcal{E}$, with corresponding measurements $\mathcal{D} = \{d_e\}_{e\in\mathcal{E}}$. Pairwise comparisons can then be quantified by the Bayes factor (BF),

$$B_{ij} = \frac{\Pr(\mathcal{D}|\hat{H}_i;\mathcal{E})}{\Pr(\mathcal{D}|\hat{H}_j;\mathcal{E})}. \tag{4.3}$$

Intuitively, we see that the BF is the ratio of the likelihood, i.e. the performance, of model $\hat{H}_i$'s attempt to account for the data set $\mathcal{D}$ observed following the experiment set $\mathcal{E}$, against the samelikelihood for model $\hat{H}_j$. BFs are known to be statistically signicative of the stronger model from a pair, at explaining observed data, while favouring models of low cardinality, thereby supressing overfitting models.

We have that, for independent experiments, and recalling Eq. (3.14),

$$\begin{aligned}\Pr(\mathcal{D}|\hat{H}_i;\mathcal{E}) &= \Pr(d_n|\hat{H}_i;e_n)\times\Pr(d_{n-1}|\hat{H}_i;e_{n-1})\times\cdots\times\Pr(d_0|\hat{H}_i;e_0)\\ &= \prod_{e\in\mathcal{E}}\Pr(d_e|\hat{H}_i;e)\\ &= \prod_{e\in\mathcal{E}}(l_e)_i.\end{aligned} \tag{4.4}$$

We also have, from Eq. (3.16)

$$\begin{aligned} \mathcal{L}_i &= \sum_{e\in\mathcal{E}} ln\left((l_e)_i\right) \\ \implies e^{\mathcal{L}_i} &= \exp\left(\sum_{e\in\mathcal{E}} ln\left[(l_e)_i\right]\right) = \prod_{e\in\mathcal{E}} \exp\left(ln\left[(l_e)_i\right]\right) = \prod_{e\in\mathcal{E}} (l_e)_i. \end{aligned} \tag{4.5}$$

So we can write

$$B_{ij} = \frac{\Pr(\mathcal{D}|\hat{H}_i;\mathcal{E})}{\Pr(\mathcal{D}|\hat{H}_j;\mathcal{E})} = \frac{\prod_{e\in\mathcal{E}}(l_e)_i}{\prod_{e\in\mathcal{E}}(l_e)_j} = \frac{e^{\mathcal{L}_i}}{e^{\mathcal{L}_j}} \tag{4.6}$$

$$\implies B_{ij} = e^{\mathcal{L}_i - \mathcal{L}_j} \tag{4.7}$$

This is simply the exponential of the difference between two models' total log-likelihoods when presented the same set of experiments. Intuitively, if $\hat{H}_i$ performs well, and therefore has a high TLTL, $\mathcal{L}_i = -10$, and $\hat{H}_j$ performs worse with $\mathcal{L}_j = -100$, then $B_{ij} = e^{-10-(-100)} = e^{90} \gg 1$. Conversely for $\mathcal{L}_i = -100, \mathcal{L}_j = -10$, then $B_{ij} = e^{-90} \ll 1$. Therfore $\left|B_{ij}\right|$ is the strength of the statistical evidence in favour of the interpretation

$$\begin{cases} B_{ij} > 1 & \Rightarrow \hat{H}_i \text{ stronger than } \hat{H}_j \\ B_{ij} < 1 & \Rightarrow \hat{H}_j \text{ stronger than } \hat{H}_i \\ B_{ij} = 1 & \Rightarrow \hat{H}_i \text{ as strong as } \hat{H}_j \end{cases} \tag{4.8}$$

4.2.1 *Experiment sets*

As mentioned it is necessary for the TLTL of both models in a BF calculation to refer to the same set of experiments, $\mathcal{E}$. There are a number of ways to achieve this, which we briefly summarise here for reference later.

During training (the QHL subroutine), candidate model $\hat{H}_i$ is trained against $\mathcal{E}_i$, designed by an EDH to optimise parameter learning specifically for $\hat{H}_i$; likewise $\hat{H}_j$ is trained on $\mathcal{E}_j$. The simplest method to compute the BF is to enforce $\mathcal{E} = \mathcal{E}_i \cup \mathcal{E}_j$ in Eq. (4.3), i.e. to cross-train $\hat{H}_i$ using the data designed specifically for training $\hat{H}_j$, and vice versa. This is a valid approach because it challenges each model to attempt to explain experiments designed explicitly for its competitor, at which only truly accurate models are likely to succeed.

A second approach builds on the first, but incorporates *burn–in* time in the training regime: this is a standard technique in the evaluation of ML models whereby its earliest iterations are discounted for evaluation so as not to skew its metrics, ensuring the evaluation reflects the strength of the model. In BF, we achieve this by basing the TLTL only on a subset of the training experiments. For example, the latter half of experiments designed during the training of $\hat{H}_i$, $\mathcal{E}_i'$.

This does not result in less predictive BF, since we are merely removing the noisy segments of the training for each model, e.g. the first half of experiments in Fig. 3.2. Moreover it provides a benefit in reducing the computation requirements: updating each model to ensure the TLTL is based on $\mathcal{E}' = \mathcal{E}'_i \cup \mathcal{E}'_j$ requires only half the computation time, which can be further reduced by lowering the number of particles used during the update, N'_p, which will give a similar result as using N_p, assuming the posterior has converged. We will verify this claim later, after we have introduced some relevant concepts, in Section 8.1.2.1.

figures points.

A final option is to design a set of *evaluation* experiments, $\mathcal{E}_v$, that are valid for a broad variety of models, and so will not favour any particular model. Again, this is a common technique in ML: to use one set of data for training models, and a second, unseen dataset for evaluation. This is clearly a favourable approach: provided for each model we compute Eq. (3.16) using $\mathcal{E}_v$, we can automatically select the strongest model based solely on their TLTLs, meaning we do not have to perform further computationally-expensive updates, as required to cross-train on opponents' experiments during BF calculation. However, it does impose on the user to design a *fair* $\mathcal{E}_v$, requiring unbiased probe states $\{|\psi\rangle\}$ and times $\{t\}$ on a timescale which is meaningful to the system under consideration. For example, experiments with $t > T_2$, the decoherence time of the system, would result in measurements which offer little information, and hence it would be difficult to extract evidence in favour of any model from experiments in this domain. It is difficult to know, or even estimate, such meaningful time scales a priori, so it is difficult for a user to design $\mathcal{E}_v$. Additionally, the training regime each model undergoes during QHL is designed to provide adaptive experiments that take into account the specific model entertained, to choose an optimal set of evolution times, so it is likely that the set of times in $\mathcal{E}_i$ is *reasonable* by default. This approach would be favoured in principle, in the case where such constraints can be accounted for, e.g. an experiment repeated in a laboratory where the available probe states are limited and the timescale achievable is understood.

4.3 QUANTUM MODEL LEARNING AGENT PROTOCOL

Given a target quantum system, Q, described by some *true* model $\hat{H}_0$, QMLA distills a model $\hat{H}' \approx \hat{H}_0$. We can think of QMLA as a forest search algorithm[1]: consisting of a number of trees, each of which can have an arbitrary number of branches, where each leaf on each branch is an individual model, QMLA is the search for the leaf in the forest with the strongest statistical evidence of representing Q. Each tree in the QMLA forest corresponds to an independent *model search* , structured according to a bespoke exploration strategy (ES), which we detail in Section 4.4. In short, the model search proceeds by grouping models in *layers*, training each model on each layer independently, layers are then *consolidated* to rank their performance, and new models are then *spawned*.

1 Note QMLA is not a random forest, where decision trees are added at random, because in QMLA trees are highly structured and included manually.

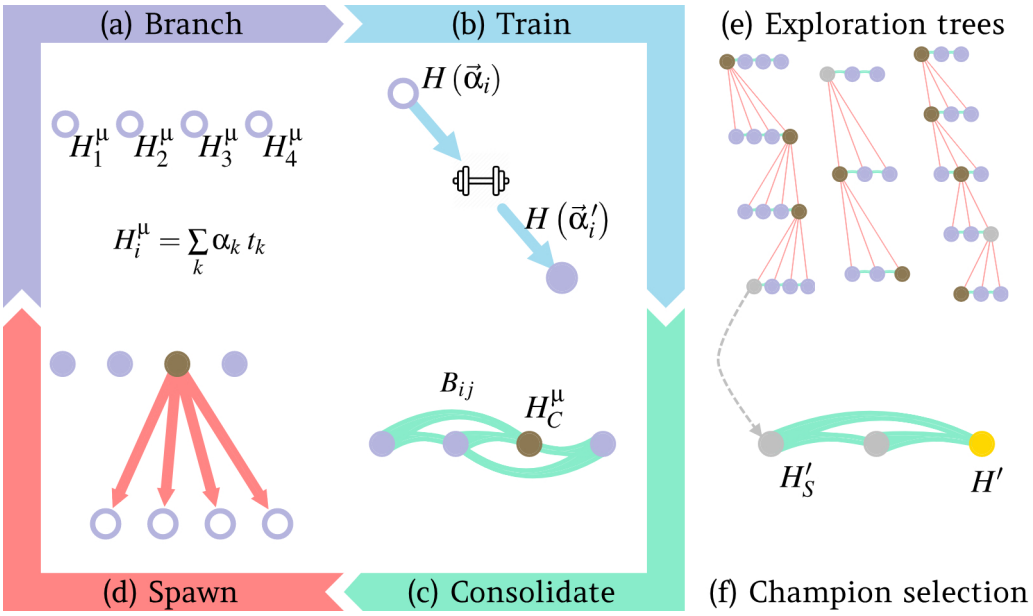

Figure 4.1: Schematic of Quantum Model Learning Agent (QMLA). **(a-d)** () phase within an Exploration strategy (ES). **(a)** Models are placed as (empty, purple) nodes on the *active branch* μ, where each model is a sum of terms $\hat{t}_k$ multiplied by a scalar parameter α_k. **(b)** Each active model is trained according to a subroutine such as quantum Hamiltonian learning to optimise $\vec{\alpha}_i$, resulting in the trained $\hat{H}(\vec{\alpha}_i')$ (filled purple node). **(c)** μ is consolidated, i.e. models are evaluated relative to other models on μ, according to the consolidation mechanism specificed by the ES. In this example, pairwise Bayes factors B_{ij} between $\hat{H}_i, \hat{H}_j$ are computed, resulting in the election of a single branch champion $\hat{H}_C^\mu$ (bronze). **(d)** A new set of models are *spawned* according to the chosen ES's model genertion strategy. In this example, models are spawned from a single parent. The newly spawned models are placed on the next layer $\mu + 1$, iterating back to **(a)**. **(e-f)** Higher level of entire QMLA procedure. **(e)** The model search phase for a unique ES is presented on an *exploration tree*. Multiple ES can operate in parallel, e.g. assuming different underlying physics, so the overall QMLA procedure involves a *forest search* across multiple exploration trees. Each ES nominates a champion, $\hat{H}_S'$ (silver), after consolidating its branch champions (bronze). **(f)** $\hat{H}_S'$ from each of the above exploration trees are gathered on a single layer, which is consolidated to give the final champion model, $\hat{H}'$ (gold).

4.4 EXPLORATION STRATEGIES

QMLA is implemented by running N_t exploration trees (ETs) concurrently, where each ET corresponds to a unique model search and ultimately nominates a single model as its favoured approximation of $\hat{H}_0$. An ES is the set of rules which guide a single ET throughout its model search . We elucidate the responsibilities of ESs in the remainder of this section, but in short they can be summarised as:

i. model generation: combining the knowledge progressively acquired on the ET to construct new candidate models;

ii. decision criteria for the model search phase: instructions for how QMLA should respond at predefined junctions, e.g. whether to cease the model search after a branch has completed;

iii. true model specification: detailing the terms and parameters which constitute $\hat{H}_0$ (in the case where Q is simulated);

iv. modular functionality: subroutines called throughout QMLA are interchangeable such that each ES specifies the set of functions to achieve its goals.

QMLA acts in tandem with one or more ESs, through the process depicted in Fig. 4.2. In summary: QMLA sends a request to the ES for a set of models; ES designs models and places them as leaves on one of its branches, and returns the set $\mathbb{H}$; QMLA places $\mathbb{H}$ on a unique layer; QMLA trains the models in $\mathbb{H}$; QMLA consolidates $\mathbb{H}$; QMLA informs the ES of the results of training/consolidation of $\mathbb{H}$; ES decides whether to continue the search, and informs QMLA.

4.4.1 *Model generation*

The main role of any ES is to design candidate models to test against $\hat{H}_0$. This can be done through any means deemed appropriate, although in general it is sensible to exploit the information gleaned so far in the ET, such as the performance of previous candidates and their comparisons, so that successfel models are seen to *spawn* new models, e.g. by combining previously successful models, or by building upon them. Conversely, model generation can be completely determined in advance or entirely random. This alludes to the central design choice in composing an ES: how broad and deep should the searchable *model space* be, considering that adequately training each model is expensive, and that model comparisons are similarly expensive. The model search occurs within some *model space*, the size of which can usually be easily found by assuming that terms are binary – either the interaction they represent is present or not. If all possible terms are accounted for, and the total set of terms is $\mathcal{T}$, then there are $2^{|\mathcal{T}|}$ available candidates in the model space. The model space encompasses the closed[2]set of models construable by the set of terms considered by an ES. Because training models is slow in general, a central aim of QMLA is to search this space efficiently, i.e. to minimise the number of models considered, while retaining high quality models and providing a reasonable prospect of uncovering the true model , or a strong approximation thereof.

2 It is feasible to define an ES which uses an open model space, that is, there is no pre-defined $\mathcal{T}$, but rather the ES determines models through some other heuristic mechanism. In this thesis, we do not propose any such ES, but note that the QMLA framework facilitates the concept, see Chapter 5.

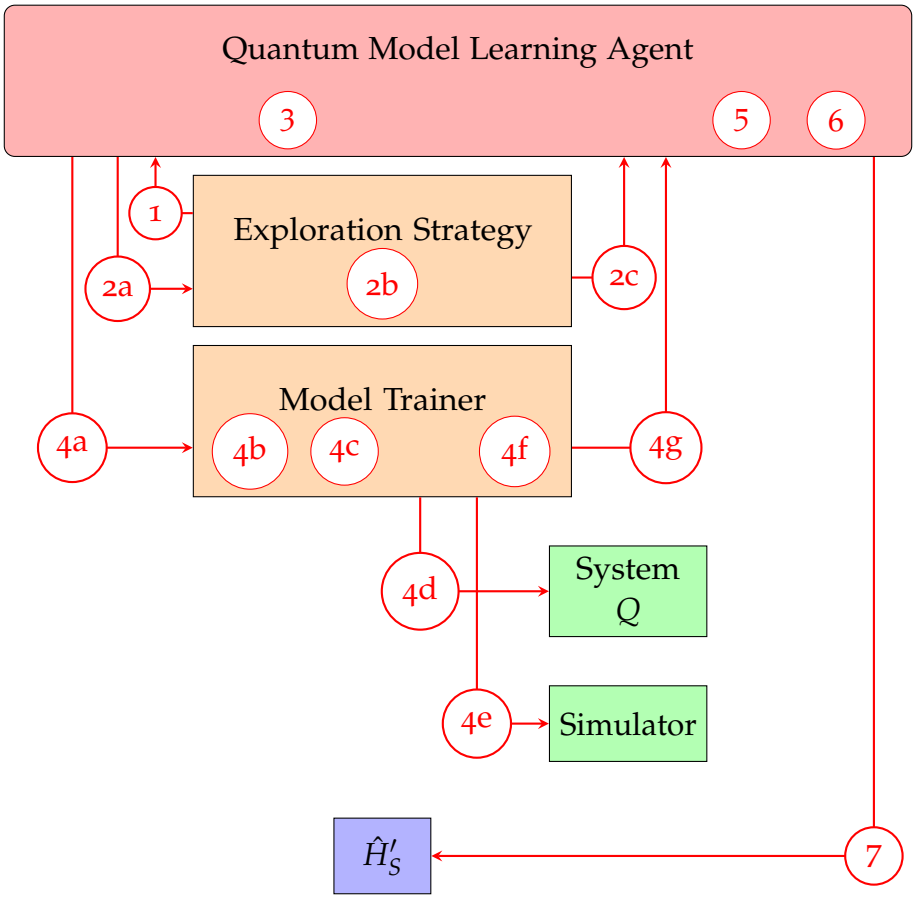

Figure 4.2: Interface between Quantum Model Learning Agent (QMLA) and a single exploration strategy (ES) The main components are the ES, model training subroutine, target quantum system (i.e. black box, Q), and (quantum) simulator. The main steps of the algorithm, shown in red with arrows denoting data transferred during that step, are as follows. **1**, QMLA retrieves decision infrastructure from ES, such as the consolidation mechanism and termination criteria. **2**, models are designed/spawned; **2a**, QMLA signals to ES requesting a set of models, passing the results of the previous layers' models if appropriate. **2b**, ES spawns new models, $\mathbb{H}$; **2c**, ES passes $\mathbb{H}$ to QMLA. **3**, QMLA assigns a new layer $(\mu \leftarrow \mu + 1)$ and places the newly proposed models upon it. **4**, Model training subroutine (here quantum Hamiltonian learning), performed independently for each model $\hat{H}_i \in \mu$; **4a**, QMLA passes $\hat{H}_i$ to the model trainer; **4b**, construct a prior distribution P_i describing the model's parameterisation $\vec{\alpha}_i$; **4c**, design experiment e to perform on Q to optimise $\vec{\alpha}_i$; **4d**, perform e on Q to retrieve a datum d; **4e**, simulate e for particles $\{\vec{\alpha}_1, \ldots, \vec{\alpha}_N\}$ sampled from P_i to retrieve a *likelihood* l_e; **4e**, update the prior P_i based on (d, l_e). **5**, Evaluate and rank $\hat{H}_i \in \mu$ according to the ES's consolidation mechanism. **6**, Check ES's termination criteria; if reached, proceed to **(7)**, otherwise return to **(2)**. **7**, Nominate champion model, $\hat{H}'_S$.

4.4.2 *Decision criteria for the model search phase*

Further control parameters, which direct the growth of the ET, are set within the ES. At several junctions within Algs. Algorithm 2, Algorithm 3, QMLA queries the ES in order to decide what happens next. Here we list the important cases of this behaviour.

i. Parameter-learning settings
   (i) such as the prior distribution to assign each parameter during QHL, and the parameters needed to run SMC.
   (ii) the time scale on which to examine Q.
   (iii) the input probes to train upon.

ii. Branch comparison strategy
   (i) How to compare models within a branch (or QMLA layer). Some examples used in this work are (a) a points-ranking where each points are assigned according to Eqn. Eq. (4.8) (b) ranking reflecting each model's log-likelihood after training. All methods in §**??** can be thought of as branch comparison strategies.

iii. model search termination criteria
   (i) e.g. instruction to stop after a fixed number of iterations, or when a certain fitness has been reached.

iv. Champion nomination
   (i) when a single tree is explored, identify a single champion from the branch champions
   (ii) if multiple trees are explored, how to compare champions across trees.

4.4.3 *True model specification*

It is necessary also to specify details about the true model $\hat{H}_0$, at least in the case where QMLA acts on simulated data. Within the ES, we can set $\vec{T}_0$ as well as $\vec{\alpha}_0$. For example where the target system is an untrusted quantum simulator to be characterised, S_u, by interfacing with a trusted (quantum) simulator S_t, we decide some $\hat{H}_0$ in advance: the model training subroutine calls for likelihoods, those corresponding to $\hat{H}_0$ are computed S_u, while particles' likelihood are computed on S_t.

4.4.4 *Modular functionality*

Finally, there are a number of fundamenetal subroutines which are called upon throughout the QMLA algorithm. These are written independently such that each subroutine has a number of available implementations. These can be chosen to match the requirements of the user, and are set via the ES.

i. Model training procedure
   (a) i.e. whether to use QHL or quantum process tomography, etc.
   (b) In this work we always used QHL. likelihood function: the method used to estimate thelikelihood for use during QLE within QHL, which ultimately depends on the measurement scheme.
      i. By default, here we use projective measurement back onto the input probe state, $\left|\langle\psi| e^{-i\hat{H}t} |\psi\rangle\right|^2$.
   (c) The role of these functions is to compute $\Pr(0)$ to be used by QInfer, which is not always the same as computing the likelihood, although these are equiavelent when we measure $d = 0$, see .
      i. Generically, without referring to the likelihood, these functions are to compute the expectation value of the unitary operator corresponding to the model of the system.
   (d) It is possible to change this to implement any measurement procedure, for example an experimental procedure where the environment is traced out.

ii. Probes: defining the input probes to be used during training.
   (a) In general it is preferable to use numerous probes in order to avoid biasing particular terms.
   (b) In some cases we are restricted to a small number available input probes, e.g. to match experimental constraints.

iii. Experiment design heuristic: bespoke experiments to maximise the information on which models are individually trained.
   (a) In particular, in this work the experimental controls consist solely of $\{|\psi\rangle, t\}$.
   (b) Currently, probes are generated once according to Section 4.4.4, but in principle it is feasible to choose optimal probes based on available or hypothetical information. For example, probes can be chosen as a normalised sum of the candidate model's eigenvectors.
   (c) Choice of t has a large effect on how well the model can train. By default times are chosen proportional to the inverse of the current uncertainty in $\vec{\alpha}$ to maximise Fischer information, through the multi-particle guess heuristic [**?**]. Alternatively, times may be chosen from a fixed set to force QHL to reproduce the dynamics within those times' scale. For instance, if a small amount of experimental data is available offline, it is sensible to train all candidate models against the entire dataset.

iv. Model training prior: change the prior distribution, e.g. Fig. Fig. 3.1(a)

4.4.5 *Exploration strategy examples*

To solidifiy the concept of ESs, and how they affect the overall, reach and runtime of a given ET, consider the following examples, where each strategy specifies how models are generated, as well as how trained models are compared within a branch. Recall that all of these strategies rely on QHL as the model training strategy, so that the run time for training, is $t_{\text{QHL}\sim N_e N_p t_U}$, where $t_U(n)$ is the time to compute the unitary evolution via the matrix exponential for an n-qubit model All models are trained using the default likelihood in Eq. (3.4). Assume the conditions

- all models considered are represented by 4-qubit models;
  - $t_{U(4)} \sim 10^{-3}$sec.
- each model undergoes a reasonable training regime;
  - $N_e = 1000, N_p = 3000$;
  - $\implies t_{\text{QHL}} = N_e \times N_p \times t_{U(4)} = 3000s \sim 1\text{h}$;
- Bayes factor calculations use
  - $N_e = 500, N_p = 3000$
  - $\implies t_{\text{BF}} \sim 2 \times 500 \times 3000 \times 10^{-3} \sim 1\text{h}$;
- there are 12 available terms
  - allowing any combination of terms, this admits a model space of size $2^{12} = 4096$
- access to 16 computer cores to parallelise calculations over
  - i.e. we can train 16 models or perform 16 BF comparisons in $1h$.

Then, consider the following model generation/comparison strategies.

a. Predefined set of 16 models, comparing every pair of models
   (i) Training takes $1h$, and $\binom{16}{2} = 120$ comparisons need $8h$
   (ii) total time is $9h$.

b. Generative procedure for model design, comparing every pair of models, running for 12 branches
   (i) One branch takes $9h \implies$ total time is $12 \times 9 = 108h$;
   (ii) total number of models considered is $16 \times 12 = 192$.

c. Generative procedure for model design, where less model comparisons are needed (say one third of all model pairs are compared), running for 12 branches
   (i) Training time is still $1h$
   (ii) One third of comparisons, i.e. 40 BF to compute, requires $3h$
   (iii) One branch takes $4h \implies$ total time is $36h$
   (iv) total number of models considered is also 192.

These examples illustrate some of the design decisions involved in ESs, namely whether timing considerations are more important than thoroughly exploring the model space. They also show considerable time–savings in cases where it is acceptable to forego all model comparisons. The approch in Section 4.4.5 is clearly limited in its applicability, mainly in that there is a heavy requirement for prior knowledge, and it is only useful in cases where we either know $\hat{H}_0 \in \mathbb{H}$, or would be satisfied with approximating $\hat{H}_0$ as the closest available $\hat{H}_j \in \mathbb{H}$. On the opposite end of this spectrum, Section 4.4.5 is an excellent approach with respect to minimising prior knowledge required by the algorithm, although at the significant expense of testing a much larger number of candidate models. There is no optimal strategy for all use–cases: specific quantum systems of study demand particular considerations, and the amount of prior information available informs how wide the model search should reach.

In this work we have used two straightforward model generation routines. Firstly, during the study of various physical classes (Ising, Heisenberg, Fermi-Hubbard), a list of lattice configurations were chosen in advance, which were then mapped to Hamiltonian models. This ES is non-adaptive and indeed the model search consists merely of a single branch with no subsequent calls to the model generation routine, as in Section 4.4.5. In the latter section instead we use a GA: this is clearly a far more general strategy, at a significant computational cost, but is suitable for systems where we have less knowledge in advance. In this case, new models are designed based heavily on results from earlier branches of the ET. The genetic algorithm model generation subroutine is listed in Algorithm 4, and can broadly be summed up thus: the best models in a generation μ produce offspring which constitute models on the next generation. These types of evolutionary algorithms ensure that newly proposed candidates inherit some of the structure which rendered previous candidates (relatively) successful, in the expectation that this will yield ever-stronger candidates.

4.5 GENERALITY

Several aspects of QMLA are deliberately vague in order to facilitate generality.

MODEL can mean any description of a quantum system which captures the interactions it is subject to.

- Here we exclusively consider Hamiltonian models, but Lindbladian models can also be considered as generators of quantum dynamics.

MODEL TRAINING is any subroutine which can train a given model, i.e. optimise a given parameterisation under the assumption that represents the target system.

- Currently only QHL has been used, but tomography is valid in principle, albeit slower.
- QHL relies on the calculation of a characteristic likelihood function; this too is not restricted to the generic form of Eq. (3.4) and can be replaced by any form which represents

thelikelihood that experimental conditions e result in measurement datum d. We will see examples of this in Chapter 9 where we trace out part of the system in order to represent open systems.

MODEL SELECTION or *consolidation* can be as rigourous as desired by the user.

- Consolidation occurs at the branch level of each ET, but also in finding the tree champion, and ultimately the global champion.
- In practice, we use either BF or a related concept such as TLTL which are statistically signicative. However, in **??** we will consider a number of alternative schemes for discerning the strongest models.

4.5.1 *Agency*

While the concept of *agency* is contentious [**?**], we can view our overall protocol as a multi-agent system [**?**], or even an agent based evolutionary algorithm [**?**], because any given ES satisfies the definition, *the population of individuals can be considered as a population of agents*, where we mean the population of models present on a given ET. More precisely, we can view individual models as *learning agents* according to the criteria of [**?**], i.e. that a learning agent has

- a *problem generator*: designs actions in an attempt to learn about the system – this is precisely the role of the EDH;
- a *performance element*: implements the the designed actions and measures the outcome – the measurement of a datum following the experiment chosen by the EDH;
- a *critic*: the likleihood function informs whether the designed action (experiment) was successful;
- a *learning element*: the updates to the weights and overall parameter distribution improve the model's performance over time.

We depict this analogy in Fig. 4.3. Finally, the model design strategy encoded in the ES *can* allow agency, by permitting the spawn rules autonomy, so we label the entire procedure as the quantum model learning agent.

4.6 ALGORITHMS

We conclude this chapter by listing the algorithms used most frequently, in order to clarify each of their roles, and how they interact. Algorithm 2 shows the overall QMLA algorithm, which is simplified greatly to a loop over the model search of each ES. The model search iteself is listed in Algorithm 3, which contains calls to subroutines for model learning (QHL, Algorithm 5), branch evaluation (which can be based upon BF, Algorithm 6) and centers on the generation of new models, an example of which – based on a genetic algorithm – is given in Algorithm 4.

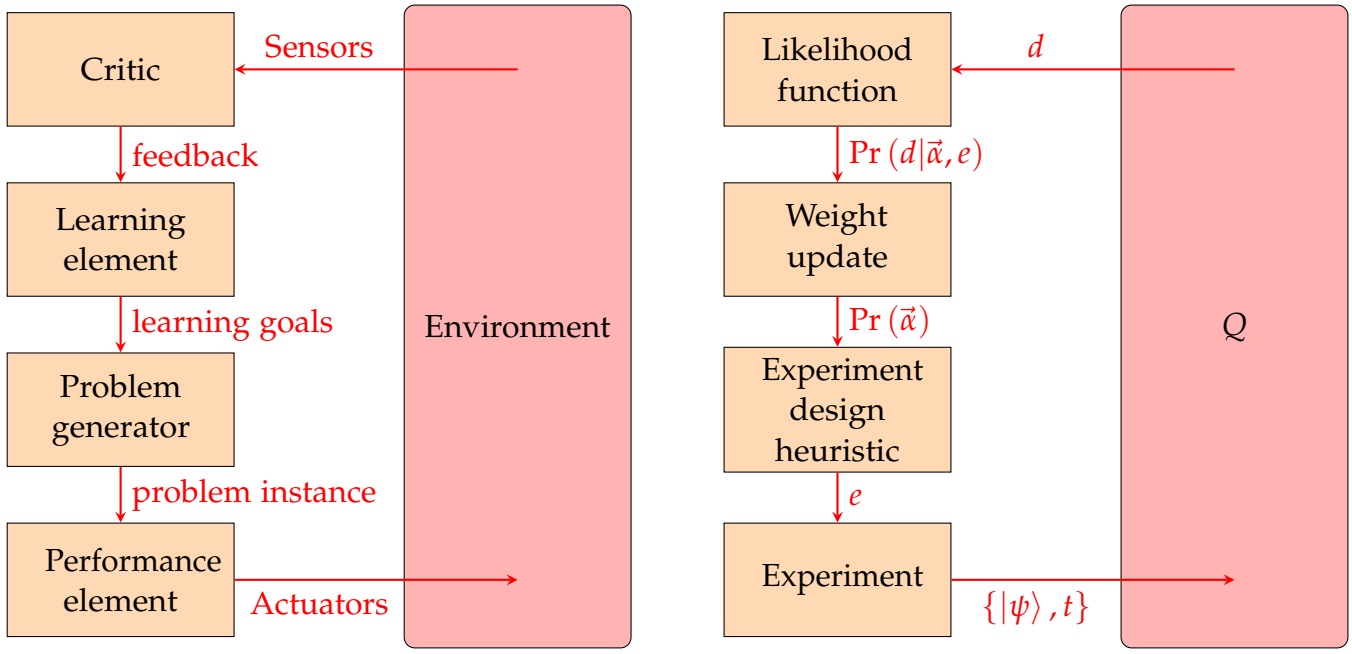

Figure 4.3: Learning agents. **Left**: definition of a learning agent, where an *environment* is affected by *actuators* which realise a *problem instance*, designed by a *problem generator*, through some *performance element*. The result of the agent's action is detected by *sensors*, which the *critic* interprets with respect to the agent's *learning goals*, by providing *feedback* to the *learning element*. *Right*: mapping of the concept of a learning agent on to an individual model. A target quantum system, Q, is queried by performing some experiment e, designed by an experiment design heuristic, and implemented by evolving a probe state $|\psi\rangle$ for time t. The systems is measured, and the datum d is sent to the likelihood function, which sends thelikelihood $\Pr(d|\vec{\alpha}, t)$ to the weight update (and the parameter distribution update), before designing another experiment.

Algorithm 2: Quantum Model Learning Agent

Input: Q // some physically measurable or simulateable quantum system
Input: $\mathbb{S}$ // set of exploration strategies

Output: $\hat{H}'$ // champion model

$\mathbb{H}_c \leftarrow \{\}$
for $S \in \mathbb{S}$ **do**
  $\hat{H}'_S \leftarrow$ model_search(Q, S)
  $\mathbb{H}_c \leftarrow \mathbb{H}_c \cup \{\hat{H}'_S\}$ // add ES champion to collection
end
$\hat{H}' \leftarrow$ final_champion($\mathbb{H}_c$)
return $\hat{H}'$

Algorithm 3: ES subroutine: model_search

Input: Q // some physically measurable or simulateable quantum system
Input: S // Exploration strategy: collection of rules/subroutines

Output: $\hat{H}'_S$ // Exploration strategy's nominated champion model

$\nu \leftarrow \{\}$
$\mathbb{H}_c \leftarrow \{\}$
while !S.terminate() **do**
  $\mu \leftarrow$ S.generate_models(ν) // e.g. Algorithm 4
  for $\hat{H}_i \in \mu$ **do**
    $\hat{H}'_i \leftarrow$ S.train($\hat{H}_i$) // e.g. Algorithm 5
  end
  $\nu \leftarrow$ S.evaluate(μ) // e.g. pairwise via Algorithm 6
  $\hat{H}^{\mu}_c \leftarrow$ S.branch_champion(ν) // use ν to select a branch champion
  $\mathbb{H}_c \leftarrow \mathbb{H}_c \cup \{\hat{H}^{\mu}_c\}$ // add branch champion to collection
end
$\hat{H}'_S \leftarrow$ S.nominate_champion($\mathbb{H}_c$)
return $\hat{H}'_S$

Algorithm 4: ES subroutine: generate_models (example: greedy spawn)

Input: ν // information about models considered to date

return $\mathbb{H}$

Algorithm 5: Quantum Hamiltonian Learning

Input: Q // some physically measurable or simulatable quantum system, described by $\hat{H}_0$
Input: $\hat{H}_i$ // Hamiltonian model attempting to reproduce data from $\hat{H}_0$
Input: $\Pr(\vec{\alpha})$ // probability distribution for $\vec{\alpha} = \vec{\alpha}_0$
Input: N_e // number of epochs to iterate learning procedure for
Input: N_p // number of particles to draw from $\Pr(\vec{\alpha})$
Input: $\Lambda(\Pr(\vec{\alpha}))$ // Heuristic algorithm which designs experiments
Input: $\mathrm{RS}(\Pr(\vec{\alpha}))$ // Resampling algorithm for redrawing particles
Output: $\vec{\alpha}'$ // estimate of Hamiltonian parameters

Sample N_p times from $\Pr(\vec{\alpha}) \leftarrow \mathcal{P}$ // particles

for $e \in \{1 \rightarrow N_e\}$ **do**
  $t, |\psi\rangle \leftarrow \Lambda(\Pr(\vec{\alpha}))$ // design an experiment
  for $p \in \mathcal{P}$ **do**
    Retrieve particle $p \leftarrow \vec{\alpha}_p$
    Prepare Q in $|\psi\rangle$, evolve and measure after $t \leftarrow d$ // datum
    $|\langle d| e^{-iH(\vec{\alpha}_p)t} |\psi\rangle|^2 \leftarrow Pr(d|\vec{\alpha}_p; t)$ // likelihood
    $w_p \leftarrow w_p \times Pr(d|\vec{\alpha}_p; t)$ // weight update
  end
  if $1/\sum_p w_p^2 < N_p/2$ // check whether to resample (are weights too small?)
  then
    $\mathrm{RS}(\Pr(\vec{\alpha})) \leftarrow \mathcal{P}$ // Redraw particles via resampling algorithm
  end
end
$\mathrm{mean}(\Pr(\vec{\alpha})) \leftarrow \vec{\alpha}'$
return $\vec{\alpha}'$

Algorithm 6: Bayes Factor calculation

Input: Q // some physically measurable or simulateable quantum system.
Input: $\hat{H}'_j, \hat{H}'_k$ // Hamiltonian models after QHL (i.e. $\vec{\alpha}_j, \vec{\alpha}_k$ already optimised), on which to compare performance.
Input: $\mathcal{E}_j, \mathcal{E}_k$ // experiments on which $\hat{H}'_j$ and $\hat{H}'_k$ were trained during QHL.
Output: B_{jk} // Bayes factor between two candidate Hamiltonians

$\mathcal{E} = \{\mathcal{E}_j \cup \mathcal{E}_k\}$
for $\hat{H}'_i \in \{\hat{H}'_j, \hat{H}'_k\}$ **do**
  $\mathcal{L}_i = 0$ // total log-likelihood of $\hat{H}_i$
  for $e \in \mathcal{E}$ **do**
    $e \leftarrow t, |\psi\rangle$ // assign time and probe from experiment control set
    Prepare Q in $|\psi\rangle$, evolve and measure after $t \leftarrow d$ // datum
    $\left|\langle d| e^{-i\hat{H}'_i t} |\psi\rangle\right|^2 \leftarrow Pr(d|\hat{H}_i, t)$ // totallikelihood for $\hat{H}'_i$ on e
    $log\left(Pr(d|\hat{H}_i, t)\right) \leftarrow l_e$ // log totallikelihood for $\hat{H}'_i$ on e
    $\mathcal{L}_i + l_e \leftarrow \mathcal{L}_i$ // add l_e to total log totallikelihood
  end
end
$\exp\left(\mathcal{L}_j - L_k\right) \leftarrow B_{jk}$ // Bayes factor between models

return B_{jk}

5

SOFTWARE

All of the details in Chapter 3 and Chapter 4 are implemented in the QMLA software framework, a (mostly) Python codebase which underlies all of the arguments, results and figures in this thesis. The codebase is designed to simplify the process of running QMLA or QHL on novel systems. In particular, the core QMLA algorithm can support a wide range of ESs, allowing for the design of bespoke ESs to account for the specific requirements of any given system. In this chapter we give an overview of the QMLA software, implementation and instructions for its use.

5.1 IMPLEMENTATION

In this section we describe the technical details of the implementation of the algorithm described in Chapter 4, as well as a number of relevant subroutines. We do not introduce new mathematical, physical or algorithmic concepts, so readers interested in applications of the techniques may prefer to skip to Part III.

5.1.1 *Object oriented programming*

We first introduce the concepts of object-oriented programming, and in particular *inheritance* between objects, since this will feature in later discussion about the implementation of QMLA and ESs. Python is a robust object-oriented language [**?**], meaning that we can frame concepts as objects which permit actions to be performed by/to them. In particular, objects in Python are formulated as *classes*, which can have associated *attributes* and *methods*. For example, we can encode the concept of a footballer as an object, such that the player object has attributes, e.g. number of games played and goals scored in a season, as well as methods for specific calculations, e.g. to summarise their record. We can then utilise the footballer class to store information about an *individual* player, by making an instance of the class.

A fundamental concept in object-oriented programming is *inheritance* between objects, such that a *child* objects inherit properties of its *parent*. In general, a parent object can be thought of as an abstract concept, which provides basic functionality and reasonable default properties, while a child object can specify further details. For example, an Athlete class can act as a parent to the footballer class, where the Athlete class holds core information such as date of birth. This allows for the Athlete class to be recycled as the *base* class for other child classes which have the same underlying requirements, e.g RubgyPlayer. We list this example in Listings C.6 to 5.2.

```
class Athlete():
```

```
    def __init__(
        self,
        name,
        birth_day,
        birth_month,
        birth_year,
    ):
        # Use information given
        self.name = name
        self.date_of_birth = datetime.date(
            birth_year, birth_month, birth_day
        )

    def age(self, round_down=True):
        days_since_birth = datetime.date.today() - self.
           date_of_birth
        age = days_since_birth.days / 365

        if round_down:
            age = int(age)

        return age

    def summary(self):
        summary = "{name} is a {age}-year old athlete.".format(
            name = self.name,
            age = self.age()
        )
        print(summary)


bob = Athlete(
    name='Bob',
    birth_day = 11,
    birth_month = 11,
    birth_year = 1993,
)
bob.summary()
```

Listing 5.1: Parent class, encoding the concept of an athlete.

```
class Footballer(Athlete):
    def __init__(
        self,
        footed,
        team,
        size = 'medium',
        **kwargs
    ):
        # Pass arguments to the parent class
        super().__init__(**kwargs)

        # Use information given
        self.team = team
        self.footed = footed
        self.size = size

        # Default attributes
        self.goals_scored = 0

    def summarise(self):
        summary = "{size} {player} plays for {team} and has
           scored {num_goals} goals.".format(
            size = self.size,
            player = self.name,
            team = self.team,
            num_goals = self.goals_scored
        )
        print(summary)

    def record_goals(self, num_new_goals):
        self.goals_scored += num_new_goals


mickey = Footballer(
    name = 'Mickey',
    footed = 'left',
    team = 'QECDT-FC',
    birth_day = 1,
    birth_month = 1,
```

```
    birth_year = 1990,
    size = 'Big'
)
mickey.record_goals(num_new_goals = 10)
mickey.summarise()
```

Listing 5.2: Child class, encoding the concept of a footballer, which adopts the abstrat representation of an athlete.

5.2 PYTHON FRAMEWORK

A driving motivation for the development of QMLA is generality: we endevaour to make QMLA applicable to any target quantum system. We provide a framework, where users can tailor the inputs and methodology to their needs: we depict the main components of the framework in Fig. 5.1, broadly grouping concepts as part of its *infrastructure*, *algorithm* or *application*. In short, users need only specify the elements of the framework in the *application* segment, without concern for the underlying mechanics of QMLA; in particular, users interface with the framework through the design of a bespoke ES, described next.

5.2.1 *Application*

The application of QMLA refers to the choice of target system, Q, and how QMLA searches the model search in attempt to discover its model. As outlined in Section 4.4, ESs play the role of defining QMLA's objectives, guiding the steps it takes, and designing the models to be tested. We facilitate the study of any system by providing a robust $\mathrm{ExplorationStrategy}$ base class, with all of the functionality expected of a generic ES, allowing users to inherit and build upon it. In particular, ESs allow users to specify the implementation of aspects listed in Section 4.4, as well as further details.

5.2.1.1 *Modular functionality*

The most crucial methods[1] of the ES class are modular, described in Section 5.2.1.1, meaning that they can be directly replaced, provided the alternative method fulfils the same role. Our base ES class uses sensbile defaults for this modular functionality, but this flexible mechanism allows for adapting QMLA by choosing an approach for each of the following subroutines.

likelihood function. By default, QHL calls a subroutine to compute Eq. (3.4). This can be replaced by any function which, given a Hamiltonian, evolution time and probe state,

1 The words *method* and *function* are mostly interchangeable, although methods are specifically associated with a class, while functions are stand-alone.

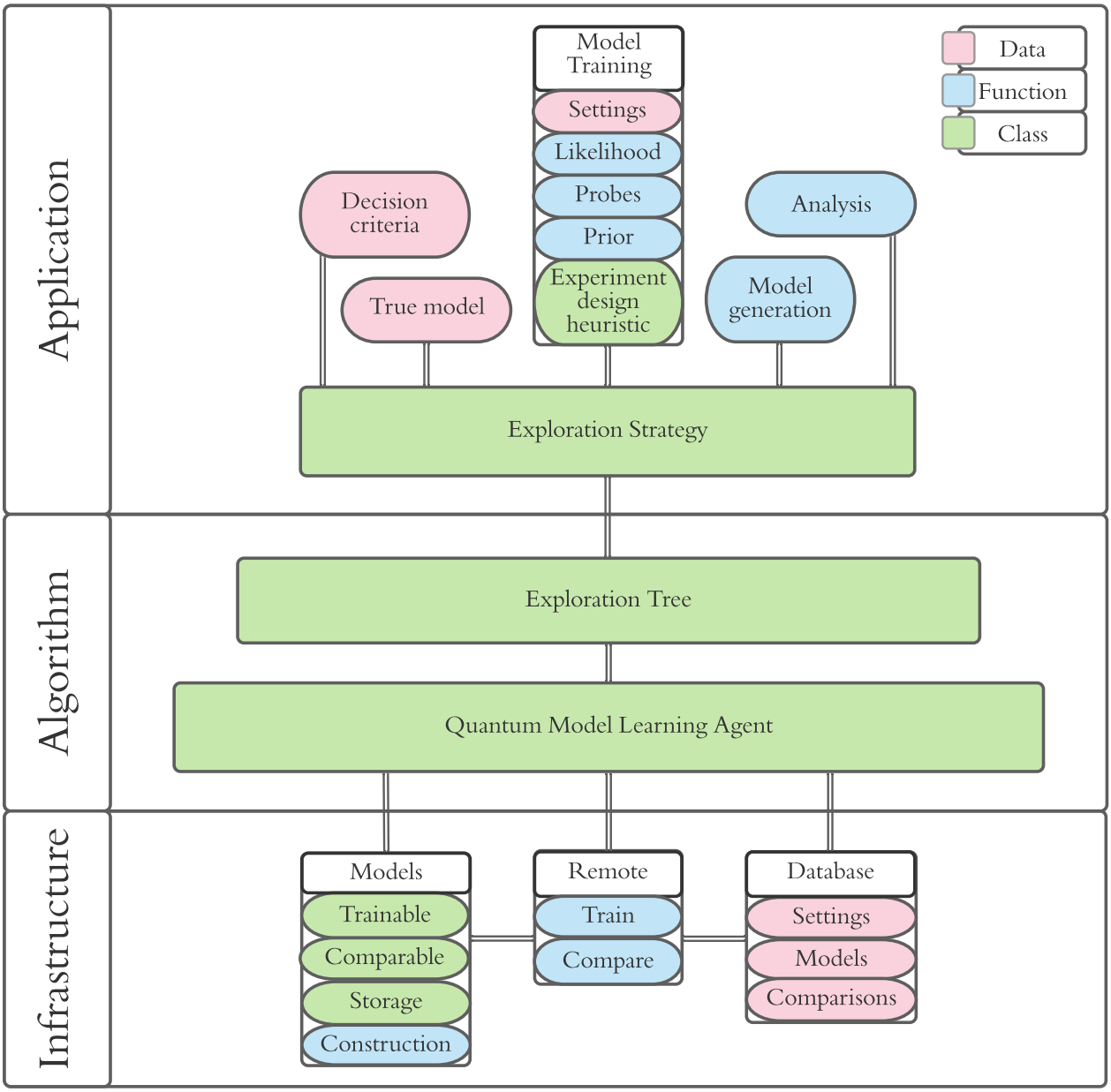

Figure 5.1: Overview of important *objects* in the QMLA framework. Colours encdoe the type of object: red objects are *data*, blue are *functions/methods* and green are *classes*. Objects are grouped broady, with double lines showing communication channels between (groups of) objects. *Infrastructure*: functions for the implementation of model training/comparisons on a remote server. *Algorithm*: implementation of the iterative procedures and decision-making laid out in Chapter 4. *Application*: inter-changeable data/functionality for the unique requirements of a given target system. Users wishing to customise QMLA must choose a valid object for each of those in *applications*, and need not alter any of the underlying framework.

returns the likelihood, according to the experiment you wish to simulate. For example, in Chapter 9, the data on which models are trained comes from experimental measurements, so we replace thelikelihood function with a calculation corresponding to the experimental procedure. Importantly, QInfer requires the quantity $\Pr(0)$, see Eq. (3.6), so that is the output of these functions.

  - Probe generation. The training phase requires a set of probes against which to optimise individual models. Users may wish to specify the design of such probes, for example to match experimental constraints which restrict the realisible probes in the performance of the experiment. Alternatively, it may be feasible to design probes which increase the information gained per experiment, enabling faster learning.

- Experiment design heuristic (EDH). The choice of EDH greatly influences how the training will perform. We provide a base class implementing PGH, as well as child classes for each of the EDHs listed in Section 3.6.2.
- Prior. The method of drawing the prior distribution can be replaced, for example, with a method for constructing a uniform distribution on each parameter. A key input to the procedure is the initial knowledge the user has about the system, which is encoded in the prior, for instance varying orders of magnitude of the viable terms.

Additionally, applications require a series of settings for the model training phase, such as the hyperparameters required by the resampling algorithm, [**?**], as well as detailing the true (target) model, $\hat{H}_0$, in the case where Q is a simulated quantum system. We can also specify some ES-specific analyses to examine its internal performance, although this is generally required during development/testing, and less useful thereafter.

5.2.2 *Algorithm*

The algorithm layer of Fig. 5.1 implements the core steps of QMLA, as shown in Fig. 4.1, by running a set of exploration trees (ETs), each of which communicate with a unique ES. The core QMLA class manages the database of models and their comparisons, and decides how to react at certain stages, by consulting the decision criteria set by the ES.

5.2.2.1 *Parallel implementiation*

The implementation of QMLA seeks to separate the organisation of the model search from the cumbersome calculations which enable the search. We can offload those calculations to a compute cluster (server) to run *in parallel*, allowing for significant speedup of the entire QMLA procedure, limited by Amdahl's law. QMLA distributes jobs to *worker* processes in a server, i.e. we assume that QMLA is run on a machine with N_c available parallel *processes*[2]. Then, the expensive calculations, namely training and comparing models, are not performed directly within the QMLA class, but instead are farmed out across the server. The role of QMLA then is to collate the outcome of those calculations in conjunction with the set of ETs, until each ET

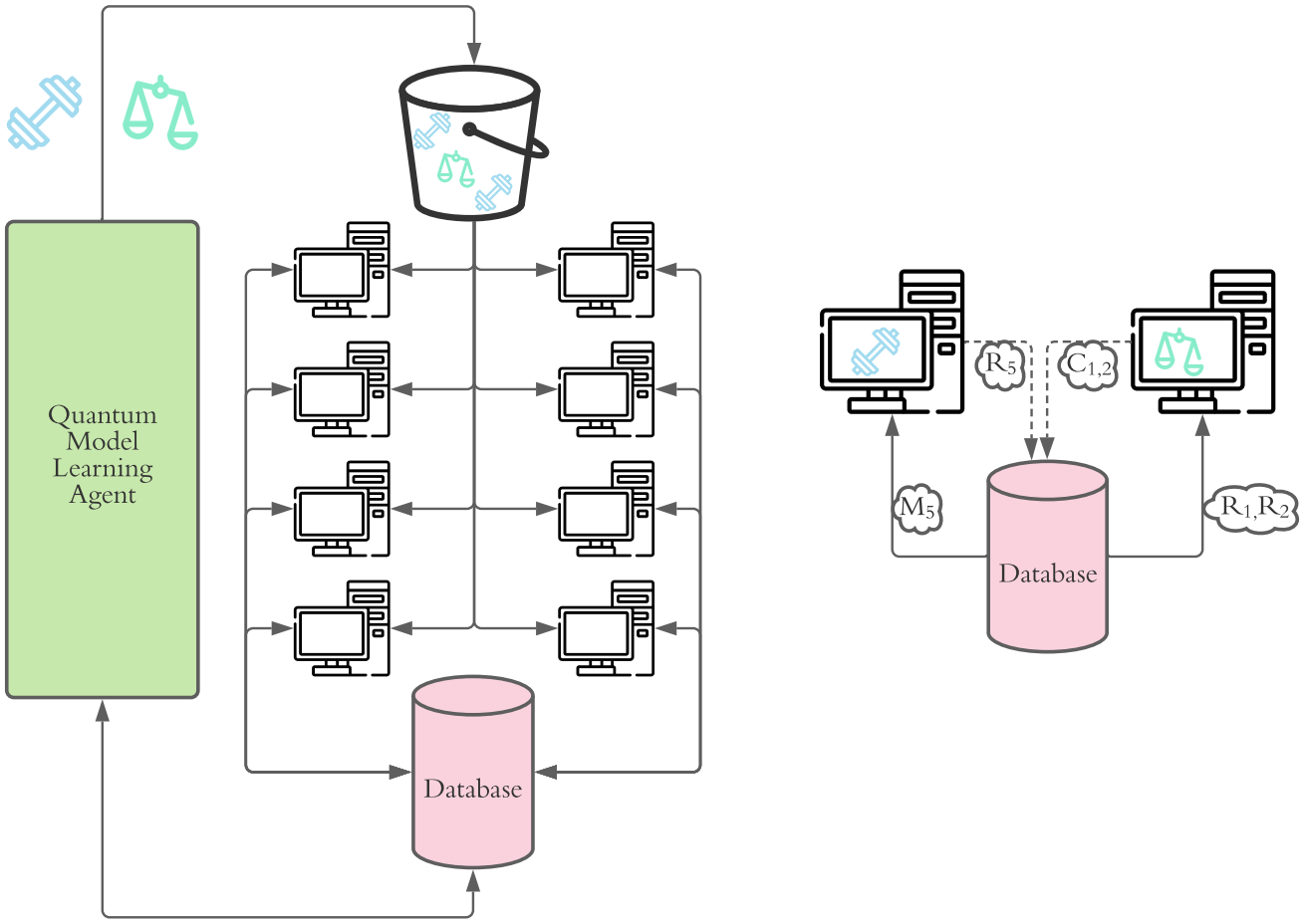

Figure 5.2: Parallel architecture for QMLA. **Left**, QMLA generates tasks – either to train (blue dumbbells) or compare (oragne scales) models – and places them in a task queue. Worker processes (depicted as computers) retrieve those tasks and compute them in parallel, and interact with a database. **Right**, Distributed tasks occuring in parallel. The left-hand process assumes the task of training the model with ID 5: it first queries the database for a packet of core information, M_5, which informs the model training procedure, for example the terms and parameters of model 5. After training, it sends a packet, R_5, summarising the result of model 5's training. The right-hand process compares two models with IDs 1 and 2, by first retrieivng the results packets R_1, R_2, then storing the comparison $C_{1,2}$ on the database.

is deemed complete, and then to consolidate the set of ET champions, ultimately setting the global champion, $\hat{H}'$. Thereafter it can perform some analysis, e.g. to generate a series of plots which demonstrate how the model search progressed, as well as the evidence in favour of $\hat{H}'$, including for example the reproduction of Q's dynamics by $\hat{H}'$. See **??** for further details.

While there are a number of strategies for parallelising code over a cluster, we use the *master-worker* strategy, where one process acts as the *master*, determining which calculations are required at any given moment, then brokering self-contained tasks to *workers*, which blindly solve a small problem, without knowledge of the wider context or algorithm [**?**]. The mapping here is trivial: the master of our algorithm is QMLA, while workers can be used for the tasks of training and comparing models. The QMLA class is hence assigned a single process solely for its considerations, e.g. for the ranking of models and determination of the next models to tests, while the remaining $N_c - 1$ processes lay dormant until QMLA requests that they perform a job.

We use a simple *task queue* for the distribution of jobs: QMLA adds tasks to the queue and any available worker can take the next job and compute it. There are two types of task for workers:

- to train a candidate model $\hat{H}_i$: the worker first requests some essenital information about the model from the databse, e.g. the name, terms and prior associated with the model, packaged in M_i; following completion, the worker compresses the result, R_i, and sends it to the database for storage.
- to compare two models, $\hat{H}_i, \hat{H}_j$: the worker retrieves R_i, R_j from the database, performs the calculation, and returns the compressed outcome of the comparison, C_{ij}, to the database.

The master QMLA class can also access said database, and copies the compressed results packets R_i and C_{ij}, in order to account for the results in its decision-making. It is worth noting that tasks are completely independent, so some worker processes may compute comparisons while others train models simultaneously, although obviously the comparison can not begin until both R_i, R_j are available. This is dealt with easily by using a *blocking* protocol, where new batches of jobs are not released until the master receives all the results of jobs on which the new tasks depend. QMLA simply waits until all models on a given layer have been trained before queueing comparisons on that layer, to ensure a comparison can not start without the data needed to compute that comparison.

Models are assigned a unique ID upon creation; models are uniquely described by their name, represented as a string in the QMLA class, such that newly proposed models can be checked against the set of previously considered models before being added to the database. QMLA can hence check whether a proposed model has already been trained, in which case it does not resubmit the model, but instead relies on the previous result. Likewise QMLA can check for the presence of any comparison result C_{ij} before setting it as a new task, ensuring we do not duplicate expensive calculation.

We use a redis database and task queue [**?**, **?**]. We depict the structure of this parallel architecture, and the master-worker strategy, in Fig. 5.2.

2 Note when running in *serial* (e.g. running locally on a personal machine), it is valid to simply set $N_c = 1$.

5.2.3 *Infrastructure*

The infrastructure enabling the distribution of QMLA's tasks across a set of worker processes can be summarised as

- a set of classes representing the objects on which we must perform expensive calculations;
- functions to launch those calculations independently of any other calculation;
- a database which can be accessed by all workers as well as QMLA.

We need a series of distinct classes to represent models, for use in each stage of QMLA: a *trainable* class is used for the parameter optimisation, while *comparable* classes are used for computing BFs, Crucially, this separation allows us to perform data-heavy calculations independently, e.g. on a remote process within a compute cluster, and discard the class instance used for the calculation and the large amount of data it generates, while only the relatively small *storage* classs is retained by QMLA for later use.

The tasks which actually implement the calculations (Section 5.2.2.1) are captured by standalone *remote* functions. These functions receive instructions such as $\mathrm{train\ model\ 10}$; they then contact the database for the set of shared settings, such as N_e, N_p and the set of probes, before performing the task, and then sending the compressed result to the database for storage.

To achieve this separation between calculation and analysis, we use a redis database [**?**], which holds the core implementation settings, e.g. N_e, N_p and the set of probes to train upon, as well as the compressed summaries of the outcomes of tasks

5.3 USAGE

Several aspects of QMLA are *probabilistic*. Firstly, the Bayesian updates within model training of QHL relies on likelihoods which implicitly depend on the measurement datum of a quantum system; in the case where the the measurement collapses Q into the less-likely basis, the likelihoods will reflect that accurate hypotheses were poor, resulting in misguided posterior distributions. It is thus *possible* that the parameter learning will converge on incorrect values. Moreover, the model design subroutine is not gauranteed to exploit the aspects of favoured models which are actually informative, e.g. given a favoured model with four correct terms and two incorrect terms, the model generator may opt to build on the incorrect terms, in the common situation where it does not know which constituent terms are helpful and which aren't.

Overall, then, it is pertinent to run QMLA many times and gather statistics about its performance, rather than making overly-strong claims about Q based on a single *instance* of the algorithm. We say that a QMLA *run* consists of N_r independent *instances*, which can be run in parallel, such that we are primarily concerned with the performance of the run instead of any individual instance. For example, with $N_r = 100$, we can interpret the *win rate* of every model in the model space as evidence for that model being $\hat{H}_0$. For the sake of evaluating QMLA itself, as in Part III, we can use the win rate of $\hat{H}_0$ as indication of the *success rate*, i.e. the fraction of

instances within a run where QMLA identifies precisely $\hat{H}' = \hat{H}_0$. Note, however, that neither the win rate nor success rate are singularly informative of QMLA's performance: in some cases, we can deem QMLA successful even if it does not identify $\hat{H}_0$ exactly, e.g. if it finds the majority of terms present in $\mathcal{T}_0$ from a large space, i.e. a high F_1-score, see Section 8.1.2.

5.3.1 *Outputs and analysis*

When a run is launched, QMLA generates a *results directory* unique to that run, identified by the time and date of its launch, in which all the pertinent information for that run, including raw data and figures, are stored. It includes an analyse.sh script to generate analysis after all instances have completed[3]. QMLA provides a large amount of anaytics to assess the performance of the protocol. These range from *big picture* perspectives such as the win rate across the entire run, to zooming in on the internal metrics for training individual models. Some of these analyses are generated by default, while others are optional depending on the level of detail the user requires. A number of sub-directories are produced in the results directory, each containing data/figures from a different view of the run; these are listed in Appendix A.

The user has control on which plots are generated, in order that the appropriate level of degree is presented, without producing an excessive number of images which can slow the protocol down. Results are categorised across the levels of the framework, for example:

- Run: results across a number of instances.
  - the number of instance wins for champion models.
  - average dynamics reproduced by champion models.
- Instance: performance of a single insance.
  - models generated and the branches on which they reside
- Model: Individual model performance within an instance.
  - parameter estimation through QHL.
- Comparisons Pairwise comparison of models' performance.
  - dynamics of both candidates (with respect to a single basis).
- Exploration strategy: figures specific to the ES
  - model generation metrics

Most plots used in this thesis are generated directly by the QMLA framework[4]; the ES class and implementation parameters of each figure is listed in Table A.1.

3 Note this script is not run automatically since, on remote servers, instances finish independently without any central process noticing. Therefore this script must be run by the user when the run is complete.

4 Or are minor modifications of auto-generated plots.

Part III

THEORETICAL STUDY

6

PRESCRIBED MODEL SETS

A sensible first case study for the QMLA framework is to prescribe a set of models, where we know that the true model is among them, or at least that we would be satisfied with approximating $\hat{H}_0$ as the best model in the set. This application can be useful, for example, for expedited device calibration; suppose we wish to characterise a new, *untrustued* quantum simulator/device, S_u, and we have access to a *trusted*[1] simulator, S_t. In order to perform this calibration, we treat S_u as the system, Q, i.e. we call upon it to retrieve the datum d in Eq. (3.4), where the calculation of the likelihoods for each particle are computed through S_t. If S_u is reliable, the data from its calculations will be consistent with some $\hat{H}_0$ of our choosing, while miscalibrations will mainfest as imperfectly implemented gates/steps in the calculation of the system's likelihood, and so would result in data inconsistent with $\hat{H}_0$. Therefore, if we can prescribe the most likely miscalibrations, it may be feasible to compose a set of models, $\mathbb{H}$, which represent those cases, and search for $\hat{H}'$ only within $\mathbb{H}$, to find identify the miscalibrations. For example, by encoding connections between every pair of device qubits in $\hat{H}_0$, we can compose models with restricted connectivity, for instance where some pairs of qubits are disconnected, and hence discover whether the device allows arbitrary two-qubit gates, and which pairs are disallowed.

6.1 LATTICES

We first consider Q as some lattice, where QMLA attempts to identify the structure of the lattice. The set of viable models then comprises alternative lattices. Due to simluation constraints, because we train models through exact unitary evolution, we are restricted to $\sim$ 8-qubit Hamiltonians, so we only consider lattices which can be simulated in this limit. The ES in this chapter is then simply to propose a set of models with no further model generation, with comparisons between all pairs of models through BFs.

Connectivity between lattice sites is achieved within the specific Hamiltonian formalisms introduced in the following sections, although in general we write $\mathcal{C} = \{\langle k, l\rangle\}$ as the set of connected pairs $\langle k, l\rangle$, such that the Hamiltonian for a given lattice can be thought of as some function of its configuration, $\hat{H}(\vec{\alpha}, \mathcal{C})$. Then, we can specify candidate models only by their $\mathcal{C}$, e.g. a 3-site chain can be summarised by $\mathcal{C} = \{\langle 1,2\rangle, \langle 2,3\rangle\}$, whereas a fully connected 3-site lattice (i.e. a triangle) is given by $\mathcal{C} = \{\langle 1,2\rangle, \langle 1,3\rangle, \langle 2,3\rangle\}$. We can then summarise the set of candidate models through the descriptions of lattice configurations, corresponding to those depicted in Fig. 6.1:

1 Note: here a classical computer can fulfil the role of the trusted simulator.

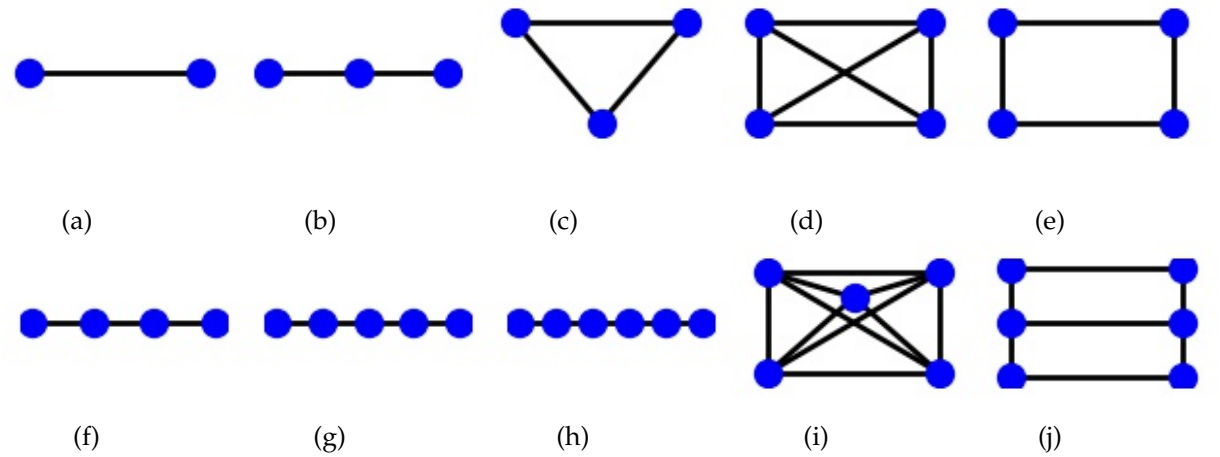

Figure 6.1: Lattices used for prescribed models test for QMLA. Lattices are characterised by the connectivity of their sites; dotted lines show connection between pairs of sites.

- 2-site chain
- 3-site chain
- 3-site fully connected (triangle)
- 4-site fully conneted (square)
- 4-site linearly connected (loop)
- 4-site chain
- 5-site chain
- 6-site chain
- 5-site fully connected (pentagon)
- 6-site partially connected (grid)

We will use this set of lattice configurations throughout the remainder of this chapter.

6.2 ISING MODEL

The Ising model is one of the most studied concepts in all of physics, representing electrons on a lattice of N sites, where each electron can have *spin* up or down [**?**, **?**, **?**]. Interactions between spins $\langle k, l \rangle$ have strength J_{kl}, and the transverse magnetic field acts on spin k with strength h_k. It is usually stated as

$$\hat{H}_I(\mathcal{C}) = \sum_{\langle k,l \rangle \in \mathcal{C}} J_{kl} \, \hat{\sigma}_k^z \, \hat{\sigma}_l^z + \sum_{k=1}^{N} h_k \hat{\sigma}_k^x. \tag{6.1}$$

The interaction term indicates the class of magnetism of the pair's interaction, i.e.

$$\begin{cases} J_{kl} < 0, & \text{ferromagnetic;} \\ J_{kl} > 0, & \text{antiferromagnetic;} \\ J_{kl} = 0, & \text{noninteracting.} \end{cases} \tag{6.2}$$

If all interaction pairs are described by the same case in Eq. (6.2), the entire system can be said belong to that class of magnetism.

6.2.1 *Note on optimising the Ising model*

Many treatments of the Ising model seek to find the ground state of the system by optimising the configuration of spins in the system. This involves neglecting the transverse magnetic field, and treating Ising model classically, such that the ground state is found by minimising the energy function

$$E_I = \langle \psi | H_I | \psi \rangle = \sum_{\langle k,l \rangle \in \mathcal{C}} J_{kl} \ \langle \psi | \hat{\sigma}_k^z \ \hat{\sigma}_l^z | \psi \rangle \,, \tag{6.3}$$

where $|\psi\rangle = |\psi_1\rangle \otimes |\psi_2\rangle \cdots \otimes |\psi_N\rangle$.

This optimisation relies on the relationship between the Ising model with its eigenvalues and eigenstates: Eq. (6.3) consists only of $\hat{\sigma}_z$ terms, and we have that

$$\hat{\sigma}_z \, |+\rangle = +1 \, |+\rangle \quad ; \quad \hat{\sigma}_z \, |-\rangle = -1 \, |-\rangle \,. \tag{6.4}$$

Then, for a single pair of spins $\langle k, l \rangle$, we have

$$\begin{aligned} \langle +_k \, +_l | \, \hat{\sigma}_k^z \ \hat{\sigma}_l^z \, | +_k \, +_l \rangle &= \langle +_k \, +_l | \, (+1)(+1) \, | +_k \, +_l \rangle = +1, \\ \langle +_k \, -_l | \, \hat{\sigma}_k^z \ \hat{\sigma}_l^z \, | +_k \, -_l \rangle &= \langle +_k \, -_l | \, (+1)(-1) \, | +_k \, -_l \rangle = -1, \\ \langle -_k \, +_l | \, \hat{\sigma}_k^z \ \hat{\sigma}_l^z \, | -_k \, +_l \rangle &= \langle -_k \, +_l | \, (-1)(+1) \, | -_k \, +_l \rangle = -1, \\ \langle -_k \, -_l | \, \hat{\sigma}_k^z \ \hat{\sigma}_l^z \, | -_k \, -_l \rangle &= \langle -_k \, +_l | \, (-1)(1) \, | -_k \, -_l \rangle = +1. \end{aligned} \tag{6.5}$$

So, by restricting the individual spins to $|\psi_k\rangle \in \{|+\rangle \,, |-\rangle\}$, we can equivalently consider every spin s_k in the system as a binary variable $s_k \in \{\pm 1\}$, i.e. $s_k s_l = \pm 1$ in Eq. (6.5), such that the energy function

$$E_I(\mathcal{S}) = \langle \psi | \hat{H}_I | \psi \rangle = \sum_{\langle k,l \rangle \in \mathcal{C}} J_{kl} \ \ s_k s_l \tag{6.6}$$

can be minimised by optimising the configuration $\mathcal{S}$, when the interaction terms $\{J_{\langle k,l \rangle}\}$ are known. The optimal configuration $\mathcal{S}_0$ can then be mapped to a state vector $|\psi_0\rangle$, i.e. the ground state of the system.

While this task can be greatly simplified by the reduction in Eq. (6.5), meaning we do not have to compute any unitary evolution to evaluate Eq. (6.6), it is still an expensive optimisation,

because effectively it is a search over $\{|\psi\rangle\}$, so the search space has 2^N candidates [**?**, **?**]. This allows for a straightforward mapping between ground state search and solving combinatorial optimsiation algorithms, namely MAX-CUT, known to be NP-complete [**?**], allowing for proposed advantage in mapping computationally challenging problems to quantum hardware [**?**]. This mapping underlies ongoing research into quantum annealing as a computational platform capable of providing advantage for a specific family of problems [**?**, **?**, **?**].

Crucially, our goal is *not* to find the ground state of Q, but instead to find the generator of its dynamics. Therefore, we treat the Ising *quantum mechanically*: instead of treating Eq. (6.1) as the underlying mechanism for a cost function to be optimised, i.e. Eq. (6.6), we use quantum operators and do not necessarily restrict the probe state $|\psi\rangle$, allowing us to use Eq. (6.1) within thelikelihood function Eq. (3.4).

6.2.2 *Ising model cases*

We consider two cases: firstly, where it is assumed that the strength of interactions $J_{k,l}$ are uniform (given by J); and secondly, where each interaction is assigned a unique parameter (J_{kl}). In the first case, we can represent the Ising model for a given lattice configuration $\mathcal{C}$ as

$$\hat{H}(\mathcal{C}) = J \sum_{\langle k,l\rangle \in \mathcal{C}} \hat{\sigma}_k^z \hat{\sigma}_l^z + h \sum_{k=1}^{N} \hat{\sigma}_k^x, \tag{6.7}$$

allowing for the compact representation, following Section 4.1,

$$\vec{\alpha}_I = \begin{pmatrix} J & h \end{pmatrix} \tag{6.8a}$$

$$\vec{T}_I = \begin{pmatrix} \sum\limits_{\langle k,l\rangle \in \mathcal{C}} \hat{\sigma}_k^z \hat{\sigma}_l^z \\ \sum\limits_{k=1}^{N} \hat{\sigma}_k^x \end{pmatrix}. \tag{6.8b}$$

In the more general second case, termed the *fully parameterised* Ising model, we instead have the term set

$$\mathcal{T}_I = \left\{ \hat{\sigma}_k^z \hat{\sigma}_l^z, \ \sum_{k=1}^{N} \hat{\sigma}_k^x \right\}_{\langle k,l\rangle \in \mathcal{C}}. \tag{6.9}$$

with unique parameters J_{kl} associated with each interaction term $\hat{\sigma}_k^z \hat{\sigma}_l^z$. We summarise these cases in Table 6.1.

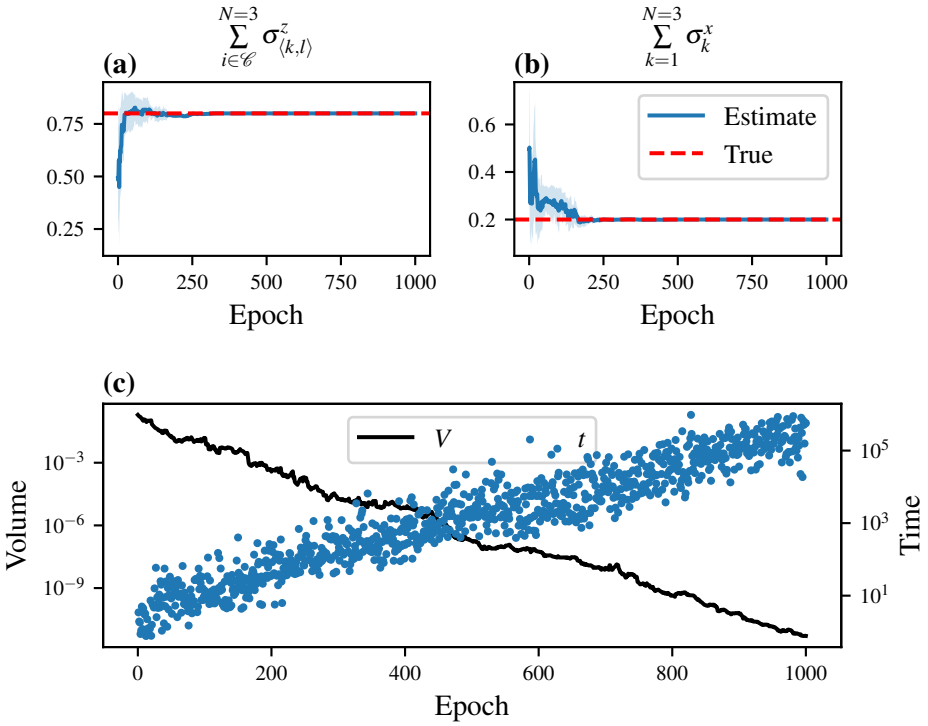

Figure 6.2: Quantum Hamiltonian learning for standard Ising model, where terms are grouped by their functionality, as in Eq. (6.1). (a,b) show the parameter estimates progression against epochs (experiments), with the corresponding term written on top of the plot; (c) shows the volume of the parameter distribution at each epoch, as well as the evolution time chosen by the EDH. Implementation details are listed in Table A.1

	$J_{\langle k,l\rangle}$	h_k
Standard	J	h
Fully parameterised	$J_{\langle k,l\rangle}$	h_k

Table 6.1: Types of Ising model. Varying whether parameters $J^z_{\langle k,l\rangle}, h_k$ are shared across sites gives distinct models.

We first construct models under each of these forms to verify QHL is capable of learning in this regime. The former case is the standard form of the Ising model; its training is shown in Fig. 6.2, while the fully paramterised model is shown in Fig. 6.3. Ultimately, these two cases give the same Hamiltonian when $J_{\langle k,l\rangle} = J;\ h_k = h\ \forall k,l$. So, the fully parameterised model will learn the same parameters as the standard Ising model, and we can take the BF between them to determine which parameterisation is favourable. Encouragingly, both models learaned the parameters to high precision, and neither model converged; the volume continues to reduce

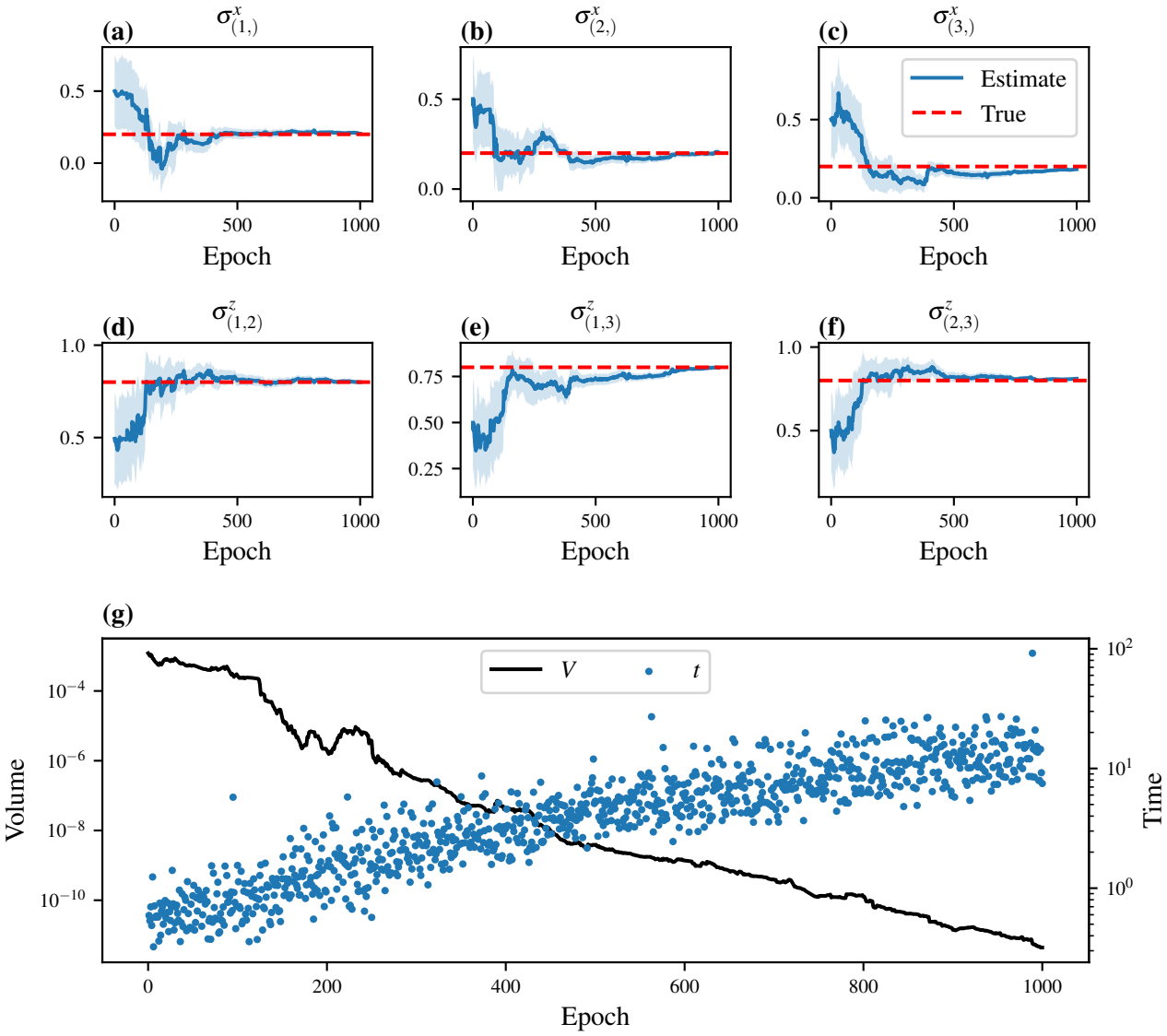

Figure 6.3: QHL for fully parameterised Ising model, where every interaction between pairs of sites are assigned unique parameters, here neglecting the transverse field, as in Eq. (6.9). (a)-(f) show the parameter estimates progression against epochs (experiments), with the corresponding term written on top of the plot; (g) shows the volume of the parameter distribution at each epoch, as well as the evolution time chosen by the EDH. Implementation details are listed in Table A.1

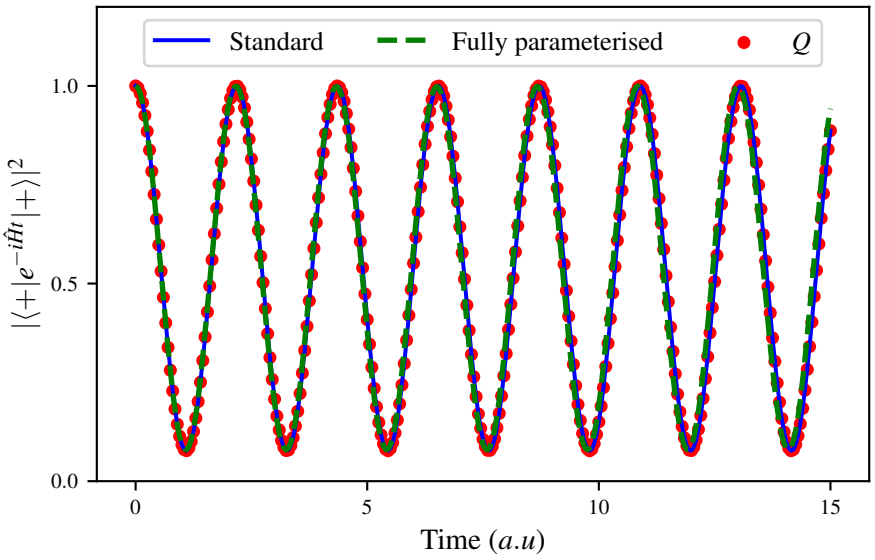

Figure 6.4: Dynamics reproduced by Ising models under standard and fully parameterised formalisms, compared with dynamics for the true system. Implementation details are listed in Table A.1

exponentially in both cases, suggesting it may be impractical to seek saturation in the model training phase for every model, since this may require a very large number of experiments and particles.

The dynamics produced by both models are shown in Fig. 6.4: the dynamics are almost indistinguishable by eye, but the standard Ising model, which in this case is $\hat{H}_0$, outperforms the fully parameterised model, by a BF of 10^{19}. This serves as a good *sanity check*, confirming our expectation that the BF will favour the simpler model (i.e. fewer parameters) even when both models are trained to a high precision to very similar parmaeters, and are difficult to distinguish through human intuition.

6.3 HEISENBERG MODEL

Generalising the Ising model, the Heisenberg Hamiltonian is another model for magnetic systems consisting of a set of spins on a lattice [**?**]. It builds on the Ising model by additionally considering the spins' rotations about the $x-$ and $y-$ axes, generally stated as

$$\hat{H}_H(\mathcal{C}) = \sum_{\langle k,l\rangle\in\mathcal{C}} J^x_{kl}\,\hat{\sigma}^x_k\hat{\sigma}^x_l + \sum_{\langle k,l\rangle\in\mathcal{C}} J^y_{kl}\,\hat{\sigma}^y_k\hat{\sigma}^y_l + \sum_{\langle k,l\rangle\in\mathcal{C}} J^z_{kl}\,\hat{\sigma}^z_k\hat{\sigma}^z_l + \sum_{k=1}^{N} h_k\hat{\sigma}^z_k. \tag{6.10}$$

We can consider a number of formulations of the Heisenberg model, by considering whether the interaction parameters are completely unique for each pair of spins in each axis, or are shared by pairs of spins; we list the instances within the family of Heisenberg models in Table 6.2.

	J^x_{kl}	J^y_{kl}	J^z_{kl}	h_k
XXX	J^x	J^x	J^x	h
XXZ	J^x	J^x	J^z	h
XYZ (standard)	J^x	J^y	J^z	h
Fully parameterised	J^x_{kl}	J^y_{kl}	J^z_{kl}	h_k

Table 6.2: Heisenberg model types: varying whether the interaction parameters J^w_{kl} are shared among pairs of spins give distinct descriptions which are all in the family of Heisenberg models.

Again, there are a number of possibile models to test, although we can reasonably expect these to follow the same arguments as for the Ising model cases: increasing generality at the expense of larger parameter dimension requires more resources to learn to a reasonable level. In this chapter we will refer to the Heisenberg-XYZ model, and will consider the fully parameterised Heisenberg model in Chapter 8; the parameters and terms of interest are then captured by Eq. (6.11).

$$\vec{\alpha}_H = \begin{pmatrix} J^x & J^y & J^z & h \end{pmatrix} \tag{6.11a}$$

$$\vec{T}_H = \begin{pmatrix} \sum\limits_{\langle k,l\rangle \in \mathcal{C}} \hat{\sigma}^x_k \hat{\sigma}^x_l \\ \sum\limits_{\langle k,l\rangle \in \mathcal{C}} \hat{\sigma}^y_k \hat{\sigma}^y_l \\ \sum\limits_{\langle k,l\rangle \in \mathcal{C}} \hat{\sigma}^z_k \hat{\sigma}^z_l \\ \sum\limits_{k=1}^{N} \hat{\sigma}^z_k \end{pmatrix} \tag{6.11b}$$

6.4 HUBBARD MODEL

Another representation of solid state matter systems is given by the Hubbard model [**?**, **?**, **?**]. The Hubbard model deals with systems of correlated fermions, allowing spins to *hop* between sites. Note the Hubbard model is synonymous with the Fermi-Hubbard (FH) model, which can be used to distinguish this model of fermions from a similar model of bosons, named the Bose-Hubbard model, which is not studied in this thesis. We use the subscript FH to distinguish

the (Fermi-)Hubbard model from the Heisenberg model $\hat{H}_H$, Eq. (6.10). The Hubbard model is generally stated in second quantisation as

$$\hat{H}_{FH}(\mathcal{C}) = \sum_{s\in\{\uparrow,\downarrow\}} \sum_{\langle k,l\rangle\in\mathcal{C}} t^s_{\langle k,l\rangle} \left(\hat{c}^\dagger_{ks} c_{ls} + \hat{c}^\dagger_{ls} c_{ks}\right) + \sum_k^N U_k \hat{n}k\uparrow \hat{n}_{k\downarrow} + \sum_k^N \mu_k \left(\hat{n}_{k\uparrow} + \hat{n}_{k\downarrow}\right) \tag{6.12}$$

where

- $\hat{c}_{ks}$ and $\hat{c}^\dagger_{ks}$ are respecitvely the fermionic annihilation and creation operators for spin $s \in \{\uparrow,\downarrow\}$ on site k;
- $\hat{n}_{ks} = \hat{c}^\dagger_{ks}\hat{c}_{ks}$ is a counting operator to count the number of spins s on site k;
- $t^s_{\langle k,l\rangle}$ is the kinetic (hopping) term for spin s between sites k and l;
- U_k is the onsite (repulsion) energy for site k;
- μ_k is the chemical energy for k;
- N is the number of sites in the system.

Again, we can achieve differing physics by controlling whether the parameters are shared, with similar consequences to the Ising and Heisenberg models, where additional parameterisation comes at the expense of slower/worse performance in training. We list a subset of possible configurations in Table 6.3; we will use the standard form in this chapter, i.e.

$$\vec{\alpha}_{FH} = (t^\uparrow \quad t^\downarrow \quad U \quad \mu) \tag{6.13a}$$

$$\vec{T}_{FH} = \begin{pmatrix} \sum_{\langle k,l\rangle\in\mathcal{C}} (\hat{c}^\dagger_{k,\uparrow}\hat{c}_{l,\uparrow} + \hat{c}^\dagger_{l,\uparrow}\hat{c}_{k,\uparrow}) \\ \sum_{\langle k,l\rangle\in\mathcal{C}} (\hat{c}^\dagger_{k,\downarrow}\hat{c}_{l,\downarrow} + \hat{c}^\dagger_{l,\downarrow}\hat{c}_{k,\downarrow}) \\ \sum_{k=1}^N \hat{n}_{k\uparrow}\hat{n}_{k\downarrow} \\ \sum_{k=1}^N \left(\hat{n}_{k\uparrow} + \hat{n}_{k\downarrow}\right) \end{pmatrix} \tag{6.13b}$$

	$t^\uparrow_{\langle k,l\rangle}$	$t^\uparrow_{\langle k,l\rangle}$	U_k	μ_k
Standard	$t^\uparrow$	$t^\downarrow$	U	μ
Fully parameterised	$t^\uparrow_{\langle k,l\rangle}$	$t^\downarrow_{\langle k,l\rangle}$	U_k	μ_k

Table 6.3: Types of Hubbard model. Varying whether parameters $t^s_{\langle k,l\rangle}, U_k, \mu_k$ are shared across sites gives distinct models.

6.4.1 *Jordan Wigner transformation*

In order that the Hubbard model is simulateable with qubits[2], it must first undergo a mapping from the fermionic representation to a spin system representation; such a mapping is given by the Jordan Wigner transformation (JWT) [**?**, **?**]. We implement the JWT within QMLA through OpenFermion's fermilib package [**?**].

In second quantisation, the fermions on the lattice can occupy one (or a superposition of) *modes*, for example, spin $\uparrow$ on the site indexed 3 is a mode. The system can then be given by a state in the *number basis*,

$$|\psi_f\rangle = |n_{m_1}, n_{m_2}, \dots, n_{m_n}\rangle\,, \tag{6.14}$$

where n_{m_i} is the number of fermions on mode m_i and there are n modes in total.

$\hat{c}^\dagger_{m_i}$ ($\hat{c}_{m_i}$) is the creation (annihilation) operator on the mode m_i: it acts on the system by adding (removing) a fermion from (to) m_i:

$$\hat{c}^\dagger_{m_i}|\psi_f\rangle = |n_{m_1}, \dots, n_{m_i}+1, \dots, n_{m_n}\rangle\,, \tag{6.15a}$$

$$\hat{c}_{m_i}|\psi_f\rangle = |n_{m_1}, \dots, n_{m_i}-1, \dots, n_{m_n}\rangle\,. \tag{6.15b}$$

In the Hubbard model, we assign a mode for each combination of spin $s \in \{\uparrow, \downarrow\}$ with each site k, i.e. the system is in the state

$$|\psi_{FH}\rangle = |n_{1\uparrow}, n_{1\downarrow}, \dots, n_{N\uparrow}, n_{N\downarrow}\rangle\,. \tag{6.16}$$

In particular, since fermions obey the Pauli exclusion principle, i.e. every spin/site can be occupied by at most one electron, and we can view them as two-level systems, so we have $n_{sk} \in \{0, 1\} \forall s, k$, We therefore use a similar system to the number basis: a qubit registered as $|0\rangle$ corresponds to an empty mode, while $|1\rangle$ holds a fermion. Empty lattices are thus given by $|0\rangle^{\otimes 2N}$. Then, in analogue with the annihilation and creation operators, we introduce oeprators $\hat{\sigma}^+, \hat{\sigma}^-$ such that

$$\hat{\sigma}^+ = \begin{pmatrix} 0 & 0 \\ 1 & 0 \end{pmatrix} \implies \hat{\sigma}^+|0\rangle = |1\rangle \tag{6.17a}$$

$$\hat{\sigma}^- = \begin{pmatrix} 0 & 1 \\ 0 & 0 \end{pmatrix} \implies \hat{\sigma}^-|1\rangle = |0\rangle \tag{6.17b}$$

Then, to map the number basis of Eq. (6.16) to a state which can be prepared on qubits, the JWT assigns a single qubit to each mode, where qubits are ordered simply by the site index and spin type, as shown in Table 6.4. The JWT can be summarised by mapping – for the mode m – the

2 Or simulations of qubits, as in this thesis.

Mode	Site	Spin	Qubit
1	1	↑	1
2	1	↓	2
3	2	↑	3
4	2	↓	4
	⋮		
$2N-1$	N	↓	$2N-1$
$2N$	N	↑	$2N$

Table 6.4: Jordan Wigner mode/qubit indices.

creation (annihilation) operator $\hat{c}_m^\dagger$ ($\hat{c}_m$), to an operator which adds a spin to the corresponding state through the operator $\hat{\sigma}_m^+$ ($\hat{\sigma}_m^-$).

$$\hat{c}_m \to (\hat{\sigma}^z)^{\otimes k-1} \otimes \hat{\sigma}^- \otimes (\hat{\sigma}^z)^{\otimes 2N-1} \tag{6.18a}$$

$$\hat{c}_m^\dagger \to (\hat{\sigma}^z)^{\otimes k-1} \otimes \hat{\sigma}^+ \otimes (\hat{\sigma}^z)^{\otimes 2N-1} \tag{6.18b}$$

Note the JWT acts on all modes/qubits other than the target with $\hat{\sigma}^z$, since

For example, an empty 2-site lattice $|\psi_0\rangle$ is acted on by a creation operator on mode 3, corresponding to spin ↑ on site 2:

$$\hat{c}_{2\uparrow}^\dagger |0000\rangle = \hat{c}_3^\dagger |0000\rangle = \hat{\sigma}_1^z \hat{\sigma}_2^z \hat{\sigma}_3^+ \hat{\sigma}_4^z |0000\rangle = |0010\rangle \tag{6.19}$$

6.4.2 *Half filled basis*

In principle there can be $2N$ spins on a lattice of N sites, although in general we will restrict to the case where there are N spins in the lattice, known as *half-filling*, such that Eq. (6.16) is effectively projected into the subspace spanned by half-filled basis states. For example, with $N = 2$

$$\{|1100\rangle, |1010\rangle, |1001\rangle, |0101\rangle, |0110\rangle, |0011\rangle\} \tag{6.20}$$

Therefore, in the design of probes for training Hubbard models, we can generate probes in the subspace spanned by half-filled states.

6.5 MODEL LEARNING FOR LATTICES

Finally, then, we can use the lattice systems introduced in Sections 6.1 to 6.4 as first case studies for QMLA. Each $\mathcal{C} \in \mathbb{C}$ can specify a unique model under the standard model formalism for

each of Ising (Eq. (6.8)), Heisenberg (Eq. (6.11)) and Hubbard (Eq. (6.13)) models. We can then devise a simple ES which only tests the models corresponding to $\mathbb{C}$, with no further model generation, i.e. Algorithm 7, and compares every pair of models through BF, deeming the champion as that which wins the largest number of comparisons, as in Algorithm 8.

Algorithm 7: Lattice exploration strategy: model generation

Input: $\mathbb{C}$ // Set of lattice configurations
Output: $\{\hat{H}_i\}$ // Set of models to tests

$\mathbb{H} = \{\ \}$
for $\mathcal{C} \in \mathbb{C}$ **do**
  $\hat{H}_i \leftarrow$ map_lattice_to_model($\mathcal{C}$)
  $\mathbb{H} \leftarrow \mathbb{H} \cup \{\hat{H}_i\}$
end
return $\mathbb{H}$

Algorithm 8: Lattice exploration strategy: consolidation

Input: $\mathbb{H}$ // Set of trained models
Output: $\hat{H}'$ // Favoured model

for $\hat{H}_i \in \mathbb{H}$ **do**
  $s_i \leftarrow 0$ // Score for every model
end
for $\hat{H}_i \in \mathbb{H}$ **do**
  for $\hat{H}_j \in \mathbb{H} \setminus \{\hat{H}_i\}$ **do**
    $B_{ij} \leftarrow BF(\hat{H}_i, \hat{H}_j)$ // Compute Bayes factor via Algorithm 6
    if $B_{ij} > 1$ **then**
      $s_i \leftarrow s_i + 1$ // $\hat{H}_i$'s score increases if it is the stronger model
    end
  end
end
$\hat{H}' \leftarrow \arg\max_{s_i} (\hat{H}_i)$
return $\hat{H}'$

For example, we adopt the fully connected four site lattice (d in Fig. 6.1) as the true lattice specifying $\hat{H}_0$, under the Ising formalism (Eq. (6.7)). We run QMLA by training the ten models corresponding to the ten lattices, Fig. 6.5**a-b**; comparing the models predictive power, Fig. 6.5**c-d**,

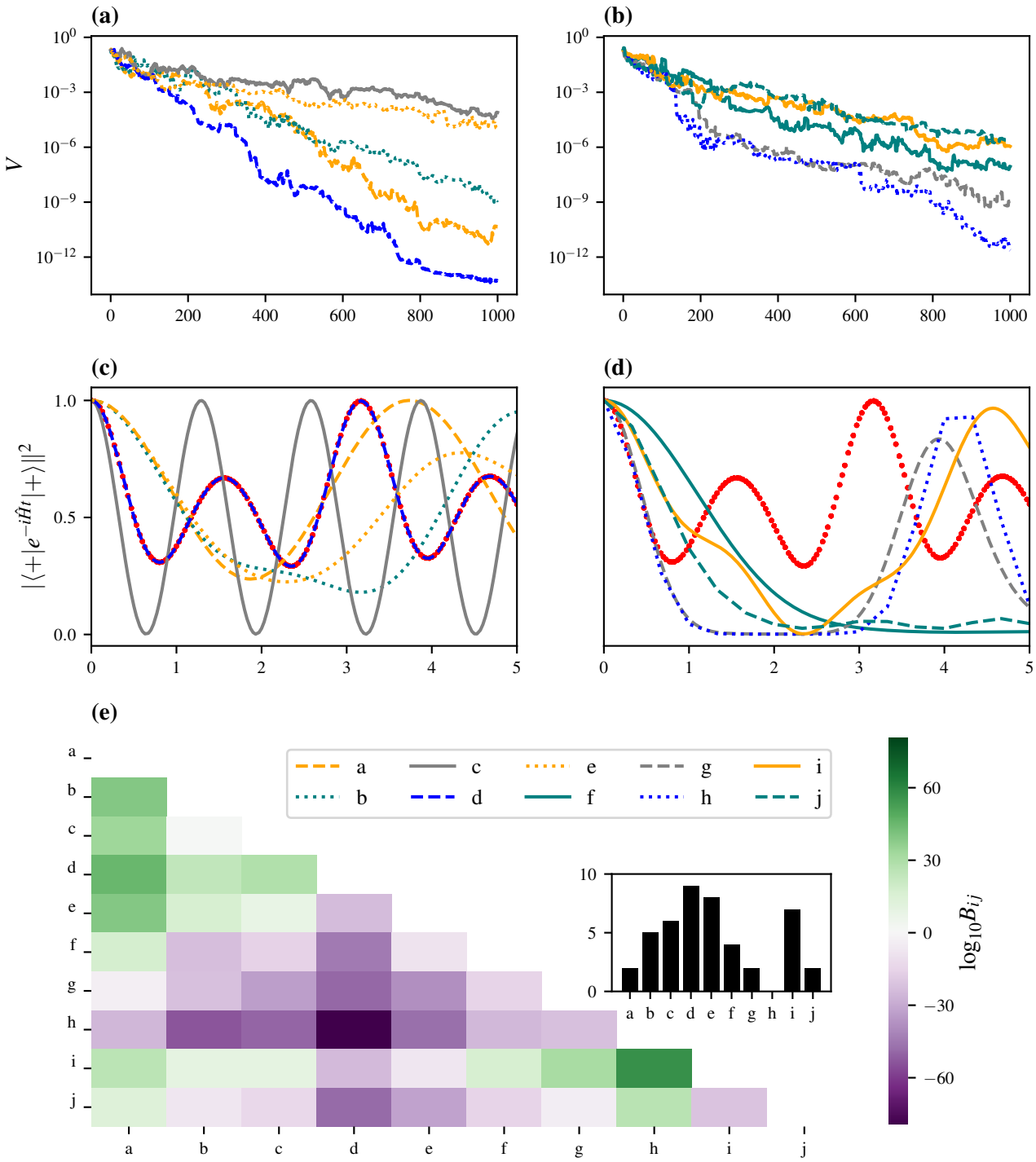

Figure 6.5: QMLA for prescribed set of lattices under Ising formalism. The lattice indices correspond to those in Fig. 6.1, and the true system is given by lattice d. (a,b) show the decrease in volume for each model's training phase. (spread over two plots for readibility) (c,d), trained models are used to reproduce dynamics, compared with the dynamics of the true system. (e) Heatmap of $\log_{10} B_{ij}$ between every pair of models. The BF is read as i versus j, where i is the model on the y-axis and j is the model on the x-axis. $\log_{10} B_{ij} > 0$ (green) favours the model listed on the y-axis; $\log_{10} B_{ij} < 0$ (purple) favours the model listed on the x-axis. The inset shows the number of BF comparisons won by each model, i.e. the models' scores. Implementation details are listed in Table A.1

through BF (Fig. 6.5**e**), and choosing the model which wins the largest number of BF contests. In this example, $\hat{H}_0$ is stronger than every alternative model according to the BFs, and is hence determined as $\hat{H}'$.

6.6 COMPLETE QUANTUM MODEL LEARNING AGENT RUNS FOR LATTICE SETS

In order to test QMLA robustly, we can use each of the lattices shown in Fig. 6.1 to specify $\hat{H}_0$, to ensure the algorithm is capable of finding the underlying model of arbitrary complexity, within the constraints of a prescribed model set[3]. Moreover, we can extend this test to the Heisenberg and Hubbard formalisms; note that due to the overhead given by the JWT (Section 6.4.1), i.e. the requirement of two qubits per site, we restrict study of the Hubbard model to lattices $a - e$ for practicality. By running 10 independent QMLA instances for each lattice under each formalism, we can gauge the success rate of the algorithm for distinguishing basic lattices from each other. We present the result of these tests in Fig. 6.6, finding in all cases that QMLA identifies $\hat{H}_0$ with success rates at least 70%.

We take this test case as evidence that the BF is a fair mechanism by which to distinguish between models. In general it will not be possible to prescribe the set of models to test, although this might serve as a straightforward mechanism for the calibration of quantum devices: suspected miscalibrations can be used in the design of such a set of models, along with a target $\hat{H}_0$ which the device should be able to implement. Then, by testing such a prescribed set and determining $\hat{H}'$, we can map the miscalibration between the intended and actual operations. In the ideal case, where it is mostly believed the device works, this application of QMLA may allow for fast, automated *verification* of the device: if QMLA finds $\hat{H}' = \hat{H}_0$ with high success given reasonable opportunity to miscompute, it may be sufficient verification that the device behaves as desired, or at least part thereof.

3 The remainder of this thesis is dedicated to cases where we do not prescribe the model set, but instead generate models dynamically.

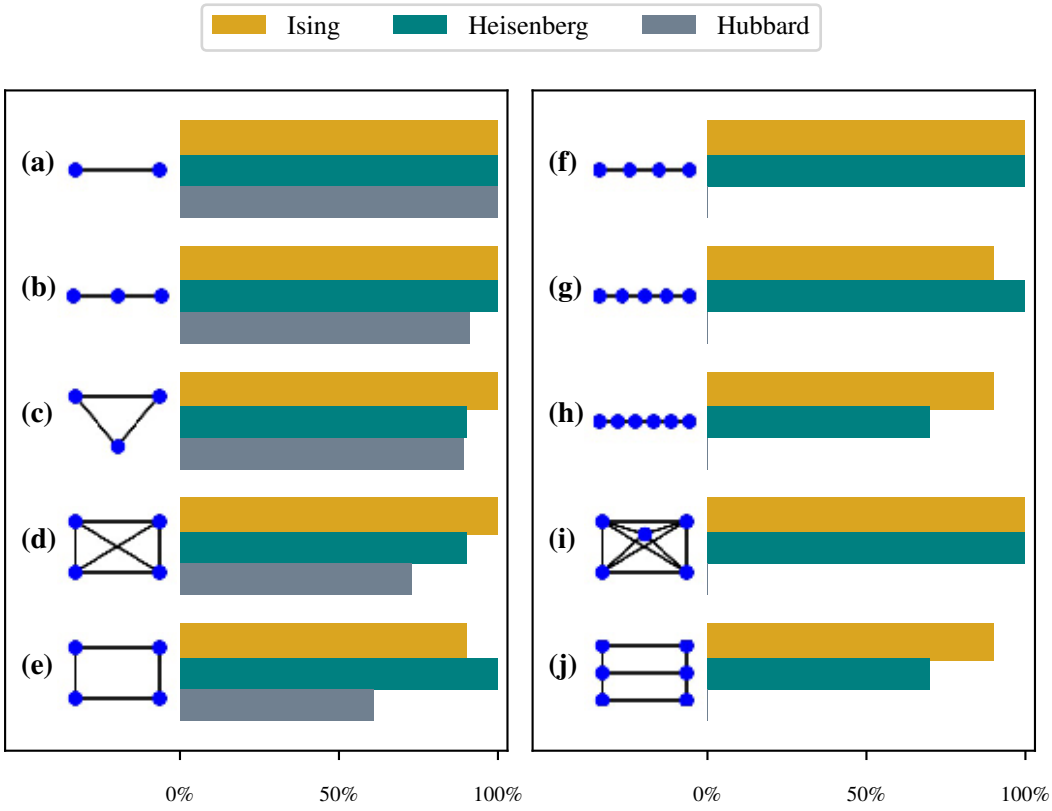

Figure 6.6: Rates of success for QMLA under various conditions. Each lattice is set as the true model $\hat{H}_0$ for ten independent instances. In each instance, the ES considers the available lattices (**a-j** for Ising and Heisenberg cases and **a-e** for the Hubbard case), and selects a champion model $\hat{H}'$ as that most consistent with data generated by $\hat{H}_0$. The figure displays the rate at which each lattice is correctly identified as $\hat{H}_0$ under standard Ising, Heisenberg and Hubbard formalisms. Implementation details are listed in Table A.1

7

BLACK BOX QUANTUM SYSTEMS

8

GENETIC ALGORITHMS

The QMLA framework lends itself easily to the family of optimsation techniques called *evolutionary algorithms*, where individuals, sampled from a population of candidates, are considered, in generations, as solutions to the given problem, and iterative generations aim to efficiently search the available population, by mimicing biological evolutionary mechanisms [**?**]. In particular, we develop a ES which incorporates an GA in the generation of models; GAs are a subset of evolutionary algorithms where candidate solutions are expressed as strings of numbers representing some configuration of the system of interest [**?**]. We describe the concepts of GAs in Section 2.3, so we begin by before describing the adaptations which allow us to build a genetic exploration strategy (GES).

8.1 ADAPTATION TO QMLA FRAMEWORK

Unlike the generic aspects of GAs described in Section 2.3, in the context of QMLA, here we must deviate from default mechanisms. Recalling the overarching goal of QMLA, to characterise some black box quantum system, Q, we do not have access to a natural OF. We wish to optimise the modelling of $\hat{H}'$, but assume we do not know the target $\hat{H}_0$, so we can not simply invoke some loss function, for example. Instead, we must devise schemes which exploit the knowledge we *do* have about each candidate $\hat{H}_j$, which is the primary challenge in building an ES based on a GA. We propose and discuss a number of options in Section 8.2.

Common to all proposed OFs, however, is that candidates should first be trained before evaluation, so that their assessment is based on their actual power in explaining the target system, rather than some initial paramterisation which may not capture their potential. This is a tenet of QMLA: for each candidate $\hat{H}_j(\vec{\alpha}_j)$, we use a subroutine to optimise $\vec{\alpha}_j$, again for this study we rely on QHL.

Ultimately, the conceived role of a GA within QMLA is to generate the sets of models to place on successive branches of the ETs in Fig. 4.1. The apparatus for this is to implement an exploration strategy (ES) whose model generation subroutine calls an external GA. Recall from Section 4.4.1, that we capture the space of available terms as $\mathcal{T}$, i.e. we list – in advance – the feasible terms which may be included in models[1], with $N_t = |\mathcal{T}|$ the number of terms considered. QMLA is then an optimisation algorithm, attempting to find the set $\mathcal{T}'$ which *best* represents the true terms $\mathcal{T}_0$. Note, this does not require idenitifcation of the precise true model to be successful, as insight can be gained from approximate models which capture the physics of the target system. We introduce metrics for success in Section 8.1.2. We recognise the limitations this structure imposes: we can only identify terms which were conceived in advance; this may

restrict QMLA's applicability to entirely unknown systems, where such a primitive set can not even be compiled.

The structure of the overall QMLA algorithm, recall Fig. 4.1, is unchanged. In a genetic exploration strategy (GES):

- models are still grouped in branches, here called generations;
- models are still trained, again through QHL;
- branches are evaluated according the the OF to be described in Section 8.2;
- new models are spawned through the genetic algorithm by selecting pairs of parents for crossover, with the resultant offspring models probabilistically mutated.

We detail the corresponding generate_models subroutine in Algorithm 9. We can restate the informal description of GAs, now in the context of QMLA, as

1. Sample N_m models from $\mathcal{P}$ at random
   (a) this is the first generation, μ.
2. Evaluate each model $\hat{H}_j \in \mu$.
   (a) train $\hat{H}_j$ through QHL
   (b) apply the objective function to assign the model's fitness g_j
3. Map the fitnesses of each model, $\{g_j\}$, to selection probabilities for each model, $\{s_j\}$
   (a) e.g. by normalising the fitnesses, or by removing some poorly-performing models and then normalising.
4. Generate the next generation of models
   (a) Reset $\mu = \{\}$
   (b) Select pairs of parents, $\hat{H}_{p_1}, \hat{H}_{p_2}$, from μ
      i. Each model's probability of being chosen is given by their s_j
   (c) Cross over $\hat{H}_{p_1}, \hat{H}_{p_2}$ to produce children models, $\hat{H}_{c_1}, \hat{H}_{c_2}$.
      i. mutate $\hat{H}_{c_1}, \hat{H}_{c_2}$ according to some random probabilistic process
      ii. keep $\hat{H}_{c_i}$ only if it is not already in μ, to ensure N_m unique models are tested at each generation.
   (d) until $|\mu| = N_m$, iterate to step (b).
5. Until the N_g^{th} generation is reached, iterate to step 2..
6. The strongest model on the final generation is deemed the approximation to the system, $\hat{H}'$.

1 Recall that models impose structure on sets of terms: $\hat{H}_j = \vec{\alpha}_j \cdot \vec{T}_j = \sum_{k \in \mathcal{T}_j} \alpha_k \hat{t}_k$.

Model		Chromosome					
	$\vec{T}$	$\hat{\sigma}^x_{(1,2)}$	$\hat{\sigma}^z_{(1,2)}$	$\hat{\sigma}^y_{(2,3)}$	$\hat{\sigma}^x_{(2,3)}$	$\hat{\sigma}^y_{(2,3)}$	$\hat{\sigma}^x_{(2,3)}$
γ_{p_1}	$(\hat{\sigma}^x_{(1,2)}\ \hat{\sigma}^z_{(1,2)}\ \hat{\sigma}^y_{(2,3)})$	1	0	1	0	1	0
γ_{p_2}	$(\hat{\sigma}^z_{(1,2)}\ \hat{\sigma}^y_{(2,3)}\ \hat{\sigma}^z_{(2,3)})$	0	0	1	0	1	1
γ_{c_1}	$(\hat{\sigma}^x_{(1,2)}\ \hat{\sigma}^z_{(1,2)}\ \hat{\sigma}^y_{(2,3)}\ \hat{\sigma}^z_{(2,3)})$	1	0	1	0	1	1
γ_{c_2}	$(\hat{\sigma}^z_{(1,2)}\ \hat{\sigma}^y_{(2,3)})$	0	0	1	0	1	0
γ'_{c_2}	$(\hat{\sigma}^z_{(1,2)}\ \hat{\sigma}^x_{(2,3)}\ \hat{\sigma}^y_{(2,3)})$	0	0	1	1	1	0

Table 8.1: Mapping between QMLA's models and chromosomes used by a genetic algorithm. Example shown for a three-qubit system with six possible terms, $\hat{\sigma}^w_{i,j} = \hat{\sigma}^w_i \hat{\sigma}^w_j$. Model terms are mapped to binary genes: if the gene registers 0 then the corresponding term is not present in the model, and if it registers 1 the term is included. The top two chromosomes are *parents*, $\gamma_{p_1} = 101010$ (blue) and $\gamma_{p_2} = 001011$ (green): they are mixed to spawn new models. We use a one–point cross over about the midpoint: the first half of γ_{p_1} is mixed with the second half of γ_{p_2} to produce two new children chromosomes, $\gamma_{c_1}, \gamma_{c_2}$. Mutation occurs probabilistically: each gene has a 25% chance of being mutated, e.g. a single gene (red) flipping from $0 \to 1$ to mutate γ_{c_2} to γ'_{c_2}. The next generation of the genetic algorithm will then include $\gamma_{c_1}, \gamma'_{c_2}$ (assuming γ_{c_1} does not mutate). To generate N_m models for each generation, $N_m/2$ parent couples are sampled from the previous generation and crossed over.

8.1.1 *Models as chromosomes*

We first need a mapping from models to chromosomes; this is straightforward given the description of chromosomes as binary strings, exemplified in Section 2.3.1. We assign a gene to every term in $\mathcal{T}$, so that candidate models are succinctly represented by bit strings of length N_t. We give an example of the mapping between models and chromosomes in Table 8.1.

8.1.2 *F_1-score*

We need a metric against which to evaluate models, and indeed the entire QMLA procedure. We can gauge the performance of QMLA's model search by the quality of candidate models produced at each generation, so we introduce a mertic to act as proxy for model quality: the

F_1-score. In short, $f \in (0,1)$ indicates the degree to which $\hat{H}_i$ captures the physics of the target system: $f = 0$ indicates that $\hat{H}_i$ shares no terms with $\hat{H}_0$, while $f = 1$ is found uniquely for $\hat{H}_i = \hat{H}_0$. We will define the concept formally next. Note that here we are able to compute f for candidate models because the target $\hat{H}_0$ is simulated, i.e. we know the true terms $\mathcal{T}_0$; this would not be available for a real system with unknown $\hat{H}_0$, but is useful for the analysis of the algorithm itself.

We emphasise that the goal of this work is to identify the *model* which best describes quantum systems, and not to improve on parameter-learning when given access to particular models, since those already exist to a high standard [**?**, **?**]. Therefore we can consider QMLA as a classification algorithm, with the goal of classifying whether individual terms $\hat{t}$ from a set of available terms $\mathcal{T} = \{\hat{t}\}$ are helpful in describing data which is generated by $\hat{H}_0$, which has $\mathcal{T}_0$. Candidate models $\hat{H}_i$ then have $\mathcal{T}_i$. We can assess $\hat{H}_i$ using standard metrics used regularly in the ML literature, which simply count the number of terms identified correctly and incorrectly,

- TP: number of terms in $\mathcal{T}_0$ which are in $\mathcal{T}_i$;
- true negatives (TN): number of terms not in $\mathcal{T}_0$ which are also not in $\mathcal{T}_i$;
- FP: number of terms in $\mathcal{T}_i$ which are not in $\mathcal{T}_0$;
- false negatives (FN): number of terms in $\mathcal{T}_0$ which are not in $\mathcal{T}_i$.

These concepts allow us to define

- *precision*: how precisely does $\hat{H}_i$ capture $\hat{H}_0$, i.e. if a term is included in $\mathcal{T}_i$ how likely it is to actually be in $\mathcal{T}_0$, Eqn 8.1a;
- *sensitivity*: how sensitive is $\hat{H}_i$ to $\hat{H}_0$, i.e. if a term is in $\mathcal{T}_0$, how likely $\mathcal{T}_i$ is to include it, Eqn. 8.1b.

$$\text{precision} = \frac{TP}{TP + FP} \tag{8.1a}$$

$$\text{sensitivity} = \frac{TP}{TP + FN} \tag{8.1b}$$

Informally, precision prioritises that predicted terms are correct, while sensitivity prioritises that true terms are identified. In practice, it is important to balance these considerations. F_β-score is a measure which balances these, with F_1-score in particular giving them equal importance.

$$F_1 = \frac{2 \times (precision) \times (sensitivity)}{(precision + sensitivity)} = \frac{TP}{TP + \frac{1}{2}(FP + FN)}. \tag{8.2}$$

We give an example of these quantities in Fig. 8.1, where $TP = 3, TN = 4, FP = 1, FN = 2$, giving precision $= 3/4$ and sensitivity $= 3/5$, with a final $f = 0.67$, i.e. the average of the indicators of model quality which we care about.

We adopt F_1-score as an indication of model quality because we are concerned both with precision and sensitivity of output models. We can use F_1-score to measure the success of the

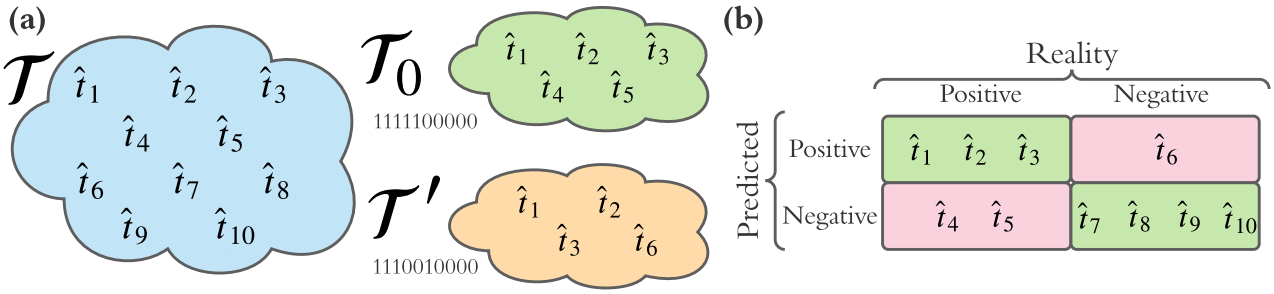

Figure 8.1: Concepts used for classification. **a**, the set of available terms $\mathcal{T}$ containing individual terms $\hat{t}_1$ to $\hat{t}_{10}$. The true model $\hat{H}_0$ is constructed from the set $\mathcal{T}_0$. Suppose a candidate $\hat{H}'$ has the set $\mathcal{T}'$. **b**, the confusion matrix for $\hat{H}'$. Correctly classified terms are true positives and true negatives (green), and incorrectly classified terms are false positives and true negatives (red).

algorithm, by recording f for all models in all generations, allowing us to see whether or not the approximation of the system is improving on average.

Of course in realistic cases we can not assume knoweldge of $\mathcal{T}_o$ and therefore cannot compute F_1-score, but it is a useful tool in the development of the GES itself, or in cases where $\hat{H}_0$ is known, such as when the target system is simualated, e.g. in the case of device calibration. Our search for an effective OF can then be guided by seeking the method which correlates most strongly with F_1-score in test-cases.

8.1.2.1 *Distinguishing F_1-score through Bayes factors*

We have so far relied on BF as the means by which to distinguish models' ability to explain data from the target system. We conjecture that models of higher F_1-score are usually stronger at this task than those of lower F_1-score, which will allow us to incorporate these statistical tools into the design of OFs. We can test this simply by training models of equally spaced F_1-score, and computing BF between all pairs.

In Fig. 8.2, we show the relationships between F_1-score and BF for various conditions: Firstly, under a standard training regime with full BF comparisons between all pairs, we see that in most cases, the model with higher F_1-score is favoured by BF. In Fig. 8.2b, we run a complete model training subroutine, but compute the BF based on fewer experiments and particles (retaining a fraction 0.2). This verifies an earlier claim from Section 4.2.1: although the strength of evidence is weaker given reduced BF resources, the direction of the evidence is usually the same, i.e. the insight is indicative of the true physics, so we can save considerable compute time by trusting these restricted BFs calculations. On the other extreme, we see in Fig. 8.2**c**, where models are trained with, and BFs based upon, even greater resources, we see a similar effect: adding resources strengthens the evidence, but does not fundamentally change the outlook.

Algorithm 9: ES subroutine: generate_models via genetic algorithm

Input: ν // information about models considered to date

Input: $g(\hat{H}_i)$ // objective function

Output: $\mathbb{H}$ // set of models

$N_m = |\nu|$ // number of models
for $\hat{H}_i \in \nu$ **do**
  $g_i \leftarrow g(\hat{H}_i)$ // model fitness via objective function
end
$r \leftarrow \text{rank}(\{g_i\})$ // rank models by their fitness
$\mathbb{H}_t \leftarrow \text{truncate}(r, \frac{N_m}{2})$ // truncate models by rank: only keep $\frac{N_m}{2}$
$s \leftarrow \text{normalise}(\{g_i\})\ \forall \hat{H}_i \in \mathbb{H}_t$ // normalise remaining models' fitness
$\mathbb{H} = \{\}$ // new batch of chromosomes/models
while $|\mathbb{H}| < N_m$ **do**
  $p_1, p_2 = \text{roulette}(s)$ // use s to select two parents via roulette selection
  $c_1, c_2 = \text{crossover}(p_1, p_2)$ // produce offspring models
  $c_1, c_2 = \text{mutate}(c_1, c_2)$ // probabilistically mutate
  $\mathbb{H} \leftarrow \mathbb{H} \cup \{c_1, c_2\}$ // add new models to batch
end
return $\mathbb{H}$

Finally, in addition to reducing the resources used per BF calculation, we reduce the number of comparisons computed, as would be required for rating models according to Bayes factor enhanced Elo ratings (BFEER), in Fig. 8.2**d**. In essence, we can see that the insight is largely the same from the most and least expensive training/comparison strategies, and by exploiting the available evidence through Elo ratings, rather than brute-force computing as much evidence as possible, we can achieve similar results. Note that the time saving reported between full and partial connectivity between models scales with N_m: here, with $N_m = 10$, the former computes 45 BFs, while the latter computes 17; for $N_m = 60$, as used in full instances/runs, these rise to 600 and 1770 respectively, so the benefit of the Elo scheme is amplified. This saving depends on the user's choice of graph connectivity, see **??**, though is typically a factor between 2-3; in general, though, assuming we can reduce the resources used within the BF, this phase is considerably less cumbersome than the model training itself, so it is feasible to compute all available BFs to inform the BFEER.

8.1.3 *Hyperparameter search*

Firstly we will validate our reasoning that F_1-score is a sensible figure of merit, by directly invoking it as the objective function. That is, we first implement a GA, using the mapping between models and chromosomes outlined above, where we fix the numbers of sites $d = 4$, and assume full connectivity between the sites, with $x-$, $y-$ and $z-$ couplings available, such that there are $N_t = 3 \times \binom{4}{2} = 18$ terms in $\mathcal{T}$, so that the total population is of size 2^{18} chromosomes. We can then sweep over the GA hyperparameters to find a suitable configuration: in Fig. 8.3 we show how the choice of parameters affect the success rate of preciesly identifying the target chromosome, which is chosen at random for each instance, and we run 20 instances of each configuration. The studied hyperparameters[2] are

i. number of generations;
ii. number of models per generation;
iii. mutation rate, r_m;
iv. number of generation a candidate must reign as the strongest observed, before the search terminates, the *cutoff*.

Naturally, we expect that running for more generations with more models per generation will result in a more effective search in the model space, having examined $N_g N_m$ models. We must also consider, however, that – in realistic cases of QMLA – the total computation time scales badly with these, since training and comparing models are such expensive subroutines. Our goal is therefore to identify the set of hyperparameters which best searches the model space with minmial N_g, N_m. We see that, unsurprisingly, the GA performs poorly when run with few resources, but broadly the performances are similiar provided it is run with sufficient resources.

2 These and further hyperparameters can be swept using code given in the QMLA codebase, in the directory scripts/genetic_alg_param_sweep.

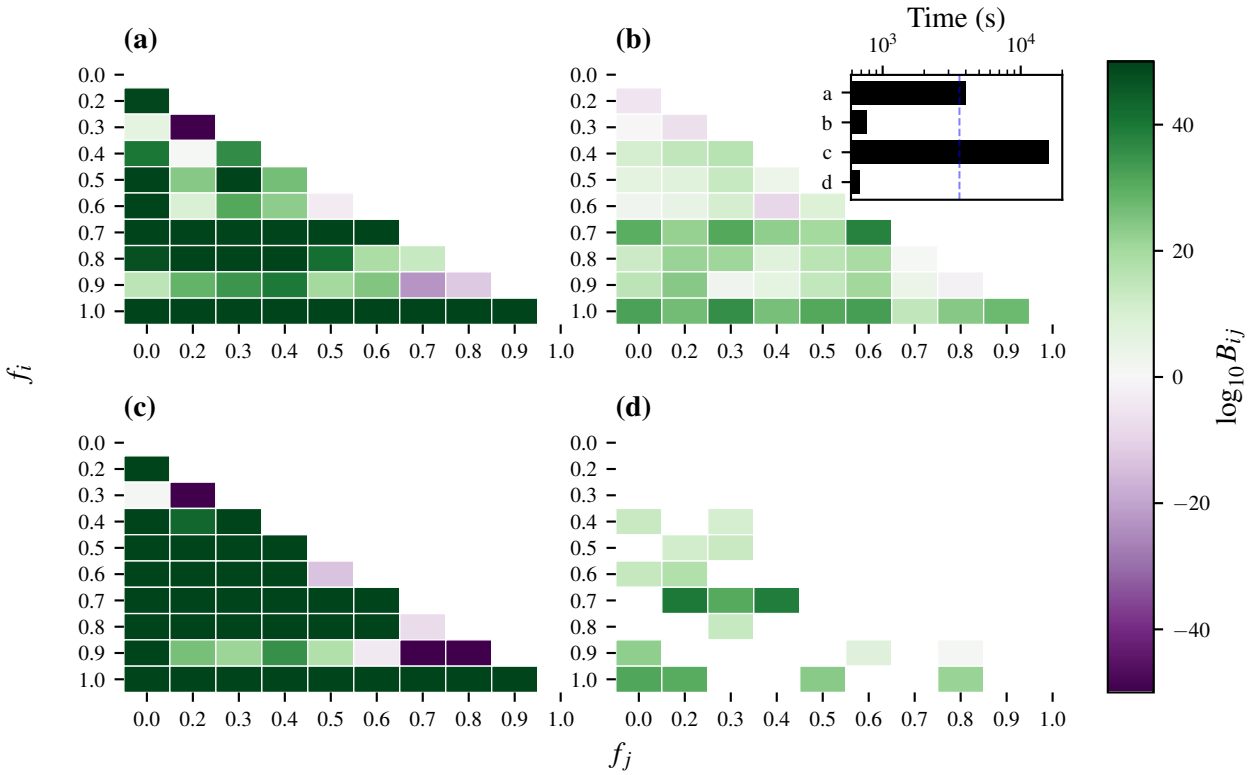

Figure 8.2: Pairwise Bayes factor, B_{ij} by F_1-score of candidates $\hat{H}_i$ (f_i on the y-axis) and $\hat{H}_j$ (f_j on the x-axis). $\log_{10} B_{ij} > 0$ (< 0), green (purple), indicates statistical evidence that $\hat{H}_i$ ($\hat{H}_j$) is the better model with respect to the observed data. Visualisation is curtailed to $\log_{10} B_{ij} = \pm 50$. **a**, Models are trained with $N_e = 500, N_p = 2500$, and all available data uis used in the calculation of BFs. **b**, $N_e = 500, N_p = 2500$ using only a fraction (0.2) of experiments/particles for BF calculation. **c**, $N_e = 1000, N_p = 5000$, using all available data in the calculation of BF. **d**, $N_e = 500, N_p = 2500$, comparing only a subset of pairs of models through BF, and using only a fraction (0.2) of experiments/particles for those calculations. This pairwise comparison strategy is used for the BFEER OF. **Inset**, timings for each approach in seconds, with $t = 1$hr marked vertically in blue.

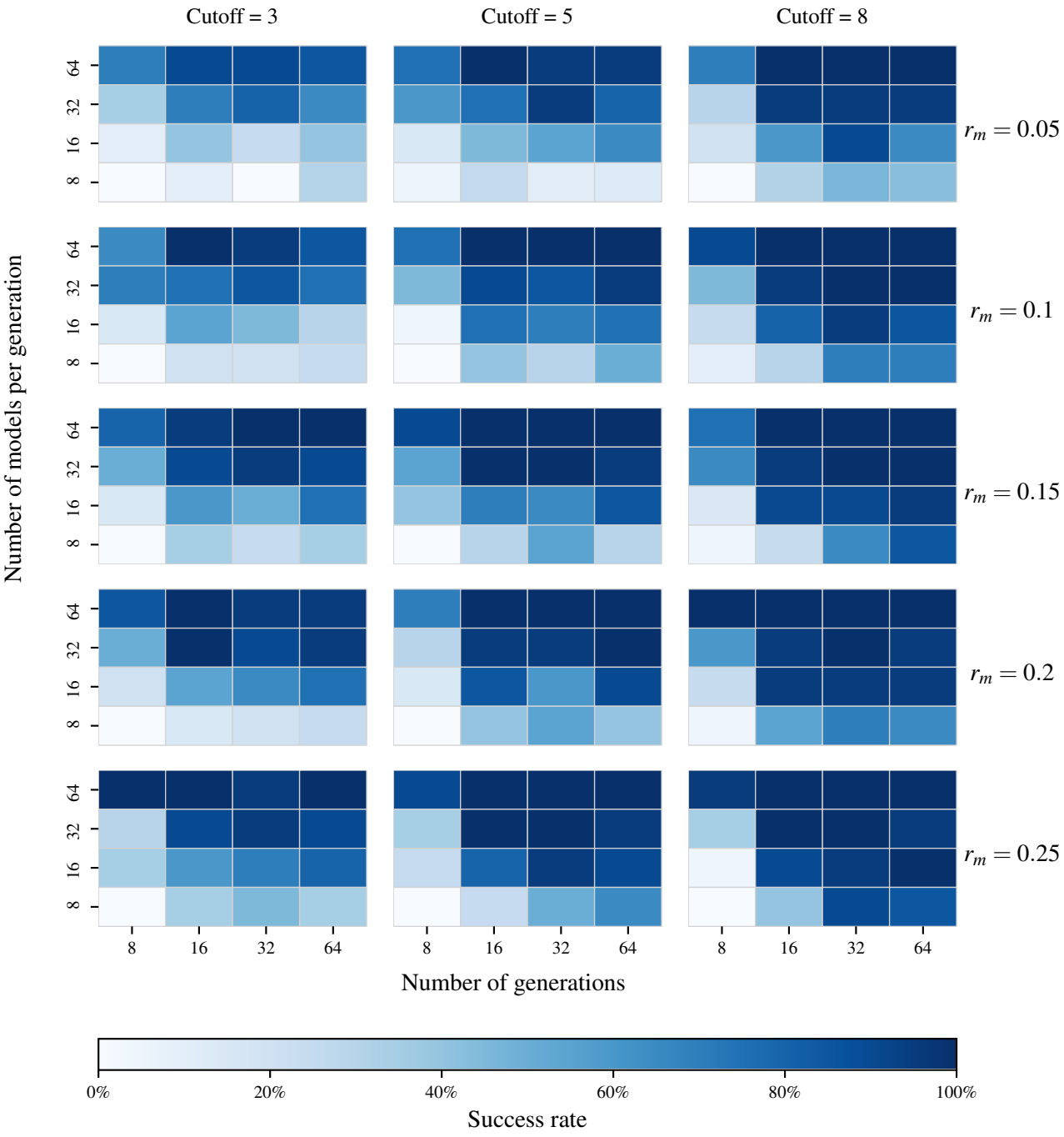

Figure 8.3: Genetic algorithm parameter sweep. Each subplot shows the success rates for varying numbers of generations, $N_G \in \{8, 16, 32, 64\}$, and numbers of models per generation, $N_m \in \{8, 16, 32, 64\}$. A subplot is generated for ranges of the mutation rate, r_m and the number of generations for which the elite model is unchanged after which the GA is cut off.

Table 8.2: Examples of how each objective function, g as described in Section 8.2.1 to Section 8.2.7, assign selection probability (denoted %) to the same set of candidate models, $\{\hat{H}_i\}$, when attempting to learn data from $\hat{H}_0$, listed in Eq. (8.3). For each model we first summarise its averagelikelihood l_e (Eqn. 4.5), total log-likelihood $\mathcal{L}_i$ (Eqn. 3.16), as well as F_1-score and number of terms k. We use $n = 250$ samples, i.e. $\mathcal{L}_i$ is a sum of n likelihoods . The set of models is truncated so that only the strongest four are assigned selection probability.

We can bound the parameters $r_m \geq 0.1, cutoff \geq 5, N_m \geq 16, N_g \geq 16$ to ensure a reasonable search through the model space, without having to consider a prohibitive number of models. We must bear in mind, however, that this parameter sweep refers only to the trivial case where the F_1-score is used as the OF, so we do not expect such high success rates in realistic cases.

8.2 OBJECTIVE FUNCTIONS

We have alluded to the central probelm in building a GA into QMLA: how to evaluate trained candidate models in the absence of a natural OF. Here we will propose and analyse a number of potential OFs, some of which will underlie later studies in this thesis. Readers may prefer to skip to Section 8.2.8, where we conclude this study by choosing a single OF for consideration in this chapter.

We will show how each OF computes g_i for candidate models $\hat{H}_i$, and summarise the outcomes in Table 8.2. For each $\hat{H}_i$, we may refer to

- $\mathcal{L}_i$, total log total likelihood (TLTL), introduced in Section 3.4
- k_i: the model's cardinality, i.e. number of terms in its parameterisation;
- $\mathcal{E}_i$: the bespoke set of experiments composed by the EDH solely for trainng $\hat{H}_i$;
- $n = |\mathcal{E}_i|$: the number of samples used in trainng $\hat{H}_i$.

In Table 8.2, we consider six models as examples of the outcome using each OF; the models, randomly generated of varying quality with respect to the target $\hat{H}_0$, are

$$\begin{aligned}
\hat{H}_0 &= \sigma^z_{(1,2)}\sigma^z_{(1,3)}\sigma^z_{(2,3)}\sigma^z_{(2,5)}\sigma^z_{(3,5)};\\
\hat{H}_a &= \sigma^z_{(1,5)}\sigma^z_{(3,4)}\sigma^z_{(4,5)};\\
\hat{H}_b &= \sigma^z_{(1,4)}\sigma^z_{(1,5)}\sigma^z_{(2,5)}\sigma^z_{(3,4)};\\
\hat{H}_c &= \sigma^z_{(1,2)}\sigma^z_{(1,5)}\sigma^z_{(2,4)}\sigma^z_{(2,5)}\sigma^z_{(4,5)};\\
\hat{H}_d &= \sigma^z_{(1,3)}\sigma^z_{(1,4)}\sigma^z_{(1,5)}\sigma^z_{(2,4)}\sigma^z_{(2,5)}\sigma^z_{(3,4)}\sigma^z_{(3,5)};\\
\hat{H}_e &= \sigma^z_{(1,2)}\sigma^z_{(1,3)}\sigma^z_{(1,5)}\sigma^z_{(2,3)}\sigma^z_{(2,5)}\sigma^z_{(4,5)};\\
\hat{H}_f &= \sigma^z_{(1,2)}\sigma^z_{(1,3)}\sigma^z_{(2,3)}\sigma^z_{(2,4)}\sigma^z_{(2,5)}\sigma^z_{(3,4)}\sigma^z_{(3,5)}.
\end{aligned} \tag{8.3}$$

8.2.1 *Inverse Log-likelihood*

$\mathcal{L}_i$ can be thought of as a measure of the success of a given model at explaining data from any set of experiments, $\mathcal{E}$. This can be immediately interpreted as an OF, provided each candidate model computes a meaningful TLTL, requiring that they are all based on the same set of experiments, $\mathcal{E}_v$, which are designed explicitly for the purpose of model evaluation.

TLTL are negative and the strongest model has lowest $|\mathcal{L}_i|$ (or highest $\mathcal{L}_i$ overall), so the corresponding OF for candidate $\hat{H}_i$ is

$$g_i^L = \frac{-1}{\mathcal{L}_i}. \tag{8.4}$$

In our tests, Eqn. 8.4 is found to be too generous to poor models, assigning them non-negligible probability. Its primary flaw, however, is its reliance on $\mathcal{E}_v$: in order that the TLTL is significant, it must be based on meaningful experiments, the design of which can not be gauranteed in advance, or at least risks introducing strong bias.

8.2.2 *Akaike Information Criterion*

A common metric in model selection is Akaike information criterion (AIC) [**?**]. Incorporating TLTL, AIC objectively quantifies how well a given model accounts for data from the target system, and punishes models which use extraneous parameters, by incurring a penalty on k_i. AIC is given by

$$AIC_i = 2k_i - 2\mathcal{L}_i. \tag{8.5}$$

In practice we use a slightly modified form of Eqn. 8.5 which corrects for the number of samples $n = |\mathcal{E}_i|$, called the Akaike information criterion corrected (AICC),

$$AICC_i = AIC_i + 2k_i \frac{k_i + 1}{n - k_i - 1}. \tag{8.6}$$

Model selection from a set of candidates occurs simply by selecting the model with $AICC_{\min}$. A suggestion to retrieve selection probability, by using Eqn. 8.6 as a measure of *relative likelihood*, is to compute *Akaike weights* (as defined in in Chapter 2 of [**?**]),

$$w_i^A = exp\left(\frac{AICC_{\min} - AICC_i}{2}\right), \tag{8.7}$$

where $AICC_{\min}$ is the lowest $AICC$ observed among the models under consideration e.g. all models in a given generation.

Clearly, Akaike weights impose quite strong penalties on models which do not explain the data well, but also punish models with extra parameters, i.e. overfitting models, effectively searching for the strongest and simplest model simultaneously. The level of punishment for poorly performing models is likely too drastic: very few models will be in a range sufficiently

close to $AICC_{\min}$ to receive a meaningful Akaike weight, suppressing diversity in the model population. Indeed, we can see from Table 8.2 that this results in most models being assigned negligible weight, which is not useful for parent selection. Instead we compute a straightforward quantity as the AIC–inspired fitness, Eqn. 8.8,

$$g_i^A = \left(\frac{1}{AICc_i}\right)^2, \tag{8.8}$$

where we square the inverse AIC to amplify the difference in quality between models, such that stronger models are generously rewarded.

8.2.3 *Bayesian Information Criterion*

Related to the idea of AIC, Eqn. 8.5, is that of Bayesian information criterion (BIC),

$$BIC_i = k_i\, ln(n_i) - 2\mathcal{L}_i, \tag{8.9}$$

where k_i, n_i and $\mathcal{L}_i$ are as defined on Page 96. Analagously to Akaike weights, *Bayes weights* as proposed in §7.7 of [**?**], are given by

$$w_i^B = exp\left(-\frac{BIC_i}{2}\right). \tag{8.10}$$

BIC is harsher than AIC in its punishment of the number of parameters in each model, therefore requiring strong statistical justification for the addition of any parameters. Again, this may be overly cumbersome for our use case: with such a relatively small number of parameters, the punishment is disproportionate; moreover since we are trying to uncover physical interactions, we do not necessarily want to suppress models merely for their cardinality, since this might result in favouring simple models which do not capture the physics. As with Akaike weights, then, we opt instead for a simpler objective function,

$$g_i^B = \left(\frac{1}{BIC_i}\right)^2. \tag{8.11}$$

8.2.4 *Bayes factor points*

A cornerstone of model selection within QMLA is the calculation of Bayes factor (BF) (see Section 4.2). We can compute the pairwise BF between two candidate models, B_{ij}, according to Eqn. 4.7. B_{ij} can be based on some evaluation dataset, $\mathcal{E}_v$, but can also be calculated from $\mathcal{E}_i \cup \mathcal{E}_j$: this is a strong advantage since the resulting insight (Eqn. 4.8) is based on experiments which were bespoke to both $\hat{H}_i, \hat{H}_j$. As such we can be confident that this insight accurately points us to the stronger of two candidate models.

We can utilise this facility by simply computing the BF between all pairs of models in a set of N_m candidates $\{\hat{H}_i\}$, i.e. compute $\binom{N_m}{2}$ BFs. Note that this is computationally expensive: in order to train $\hat{H}_i$ on $\mathcal{E}_j$ requires a further $\left|\mathcal{E}_j\right|$ experiments, each requiring N_P particles[3], where each particle corresponds to a unitary evolution and therefore the caluclation of a matrix exponential. The combinatorial scaling of the model space is then quite a heavy disadvantage. However, in the case where all pairwise BF are performed, we can assign a point to $\hat{H}_i$ for every comparison which favours it.

$$g_i^p = \sum_{j \in \mu} b_{ij}, \quad b_{ij} = \begin{cases} 1, & B_{ij} > 1 \\ 0, & \text{otherwise} \end{cases} \tag{8.12}$$

This is a straightforward mechanism, but is overly blunt because it does not account for the strength of the evidence in favour of each model. For example, a dominant model will receive only a slightly higher selection probability than the second strongest, even if the difference between them was $B_{ij} = 10^{100}$. Further, the unfavourable scaling make this an expensive method.

8.2.5 *Ranking*

Related to Section 8.2.4, we can rank models in a generation based on their number of BF points. BF points are assigned as in Eqn. 8.12, but instead of corresponding directly to fitness, we assign models a rank R, i.e. the model with highest g_i^p gets $R = 1$, and the model with n^{th} highest g_i^p gets $R = n$. Note here we truncate μ, meaning we remove the worse-performing models and retain only N'_m models, before calculating R. This is because computing R using all N_m models results in less distinct selection probabilities.

$$g_i^R = \frac{N'_m - R_i + 1}{\sum_{n=1}^{N'_m} n}, \tag{8.13}$$

where R_i is the rank of $\hat{H}_i$ and N'_m is the number of models retained after truncation.

8.2.6 *Residuals*

Recall at each experiment, N_P particles are compared against a single experimental datum, d. For consistency with QInfer [**?**] – on which QMLA's code base extends – we call the expectation value for the system $\Pr_Q(0)$, and that of each particle $\Pr_p(0)$, recall Section 3.3. Typically, $\Pr_Q(0) = \left|\langle\psi| e^{-i\hat{H}_0 t} |\psi\rangle\right|^2$, but this can be changed to match given experimental schemes, e.g. the Hahn-echo sequence applied in [**?**]. By definition, the datum d is the binary outcome of the measurement on the system under experimental conditions e. That is, d encodes the answer to the question: after time t under Hamiltonian evolution, did Q project onto the basis we

3 Caveat the reduction in overhead outlined in Section 4.2.1.

have labelled 0 (usually the same as the input probe state $|\psi\rangle$)? However, in practice we often have access also to the likelihood , i.e. rather than a binary value, a number representing the probability that Q will project on to 0 for a given experiment e, $\Pr_Q(0|e)$. Likewise, we can simulate this quantity for each particle, $\Pr_p(0|e)$. This allows us to calculate the *residual* between the system and individual particles' likelihoods , r_p^e, as well as the mean residual across all particles in a single experiment r^e:

$$\begin{aligned} r_p^e &= \left| Pr_Q(0|e) - Pr_p(0|e) \right| \\ r^e &= \underset{p}{\text{mean}}\{r_p^e\} \end{aligned} \tag{8.14}$$

Residuals capture how closely the particle distribution reproduced the dynamics from Q: $r_p^e = 0$ indicates perfect prediction, while $r_p^e = 1$ is completely incorrect. We can therefore maximise the quantity $1 - r$ to find the best model, using the OF

$$g_i^r = \left| 1 - \underset{e \in \mathcal{E}}{\text{mean}}\{r^e\} \right|^2. \tag{8.15}$$

This OF can be thought of in frequentist terms as similar to the residual sum of squares, although instead of summing the residual squares, we average to ensure $0 \leq r \leq 1$. g_i^r encapsulates how well a candidate model can reproduce dynamics from the target system, as a proxy for whether that candidate describes the system. This is not always a safe figure of merit: in most cases, we do not expect parameter learning to perfectly optimise $\vec{\alpha}_i$. Reproduced dynamics alone can not capture thelikelihood that $\hat{H}_i = \hat{H}_0$. However, this OF provides a useful test for QMLA's GA: by simulating the case where parameters *are* learned perfectly, such that we know that g_i^r truly represents the ability of $\hat{H}_i$ to simulate $\hat{H}_0$, then this OF gaurantees to promote the strongest models, especially given that $\hat{H}_i = \hat{H}_0 \implies r_p^e = 0 \; \forall \; \{e, p\}$. In realistic cases, however, the non-zero residuals – even for strong $\hat{H}_i$ – may arise from imperfectly learned parameters, rendering the usefulness of this OF uncertain. Finally, it does not account for the cardinality, k_i, of the candidate models, which could result in favouring severely overfitting models in order to gain marginal improvement in residuals, which all machine learning protocols aim to avoid in general.

8.2.7 *Bayes factor enhanced Elo-ratings*

A popular tool for rating individual competitors in sports and games is the *Elo rating* scheme, e.g. used to rate chess players and soccer teams [**?**, **?**], also finding application in the study of animal hierarchies [**?**]. Elo ratings allow for evaluating relative quality of individuals based on incomplete pairwise competitions, e.g. despite two football teams having never played against each other before, it is possible to quantify the difference in quality between those teams, and therefore to predict a result in advance [**?**]. We recognise a parallel with these types of

competitions by noting that in our case, we similarly have a pool of individuals (models), which we can place in direct competition, and quantify the comparitive outcome through BF.

Elo ratings are transitive: given some interconnectivity in a generation, we need not compare *every* pair of models in order to make meaningful claims about which are strongest; it is sufficient to perform a subset of comparisons, ensuring each individual is tested robustly. We can take advantage of this transitivity to reduce the combinatorial overhead usually associated with computing bespoke BF between all models (i.e. using their own training data $\mathcal{E}_i$ instead of a generic $\mathcal{E}_v$). In practice, we map models within a generation to nodes on a graph, which is then sparsely connected. In composing the list of edges for this graph, we primarily prioritise each node having a similar number of edges, and secondarily the distance between any two nodes. For example, with 14 nodes we overlay edges such that each node is connected with 5,6 or 7 other nodes, and all nodes at least share a competitor in common.

The Elo rating scheme is as follows: upon creation, $\hat{H}_i$ is assigned a rating R_i; every comparison with a competitor $\hat{H}_j$ results in B_{ij}; R_i is updated according to the known strength of its competitor, R_j, as well as the result B_{ij}. The Elo update ensures that winning models are rewarded for defeating another model, but that the extent of that reward reflects the quality of its opponent. As such, this is a fairer mechanism than BF points, which award a point for every victory irrespective of the opposition: if $\hat{H}_j$ is already known to be a strong or poor model, then ΔR_i proportionally changes the credence we assign to $\hat{H}_i$. It achieves this by first computing the *expected* result of a given comparison with respect to each model, based on the current ratings,

$$E_i = \frac{1}{1 + 10^{\frac{R_j - R_i}{400}}}; \tag{8.16a}$$

$$E_i + E_j = 1, \tag{8.16b}$$

Then, we find the binary *score* from the perspective of each model:

$$\begin{cases} B_{ij} > 1 & \Rightarrow \; S_i = 1; \; S_j = 0 \\ B_{ij} < 1 & \Rightarrow \; S_i = 0; \; S_j = 1 \end{cases} \tag{8.17}$$

which is used to determine the change to each model's rating:

$$\Delta R_i = \eta \times (S_i - E_i)\,. \tag{8.18}$$

An important detail is the choice of η, i.e. the *weight* of the change to the models' ratings. In standard Elo schemes this is a fixed constant, but here – taking inspiration from football ratings where η is the number of goals by which one team won – we weight the change by the strength of our belief in the outcome: $\eta \propto \left|B_{ij}\right|$. That is, similarly to the interpretation of Eqn. 4.8, we use the evidence in favour of the winning model to transfer points from the loser to the winner, albeit we temper this by instead using $\eta = log_{10}(B_{ij})$, since BF can give very large numbers. In

	Model	R_i	E_i	S_i	B_{ij}	$\log_{10}(B_{ij})$	ΔR_i	R'_i
$\hat{H}_a > \hat{H}_b$	$\hat{H}_a$	1000	0.76	1	1e+100	100	0.24	1024.0
	$\hat{H}_b$	800	0.24	0	1e-100	100	-0.24	776.0
$\hat{H}_b > \hat{H}_a$	$\hat{H}_a$	1000	0.76	0	1e-100	100	-0.76	924.0
	$\hat{H}_b$	800	0.24	1	1e+100	100	0.76	876.0

Table 8.3: Example of Elo rating updates. We have two models, where $\hat{H}_a$ is initially believed to be a stronger candidate than $\hat{H}_b$, i.e. has a higher starting Elo rating. We show the effect of strong evidence[4] in favour of each model following BF comparison, $B_{ij} \sim 10^{100}$. In the case where $\hat{H}_a$ defeats $\hat{H}_b$, because this was so strongly expected given their initial ratings, the reward for $\hat{H}_a$ (and cost to $\hat{H}_b$) is relatively small, compared with the case where – contrary to prediction – $\hat{H}_b$ defeats $\hat{H}_a$.

total, then, following the comparison between models $\hat{H}_i, \hat{H}_j$, we can perform the Elo rating update

$$R'_i = R_i + \log_{10}(B_{ij}) \left(S_i - \frac{1}{1 + 10^{\frac{R_j - R_i}{400}}} \right). \tag{8.19}$$

This procedure is easiest to understand by following the example in Table 8.3.

Finally, it remains to select the starting rating R_i^0 to assign models upon creation. Although this choice is arbitrary, it can have a strong effect on the progression of the algorithm. Here we impose details specific to the QMLA GA: at each generation we admit the top two models automatically for consideration in the next generation, such that strongest models can stay alive in the population and ultimately win. These are called *elite* models, $\hat{H}_e^1, \hat{H}_e^2$. This poses the strong possibility for a form of generational wealth: if elite models have already existed for several generations, their Elo ratings will be higher than all alternatives by defintion. Therefore by maintaining a constant R_i^0, i.e. a model born at generation 12 gets the same R_i^0 as $\hat{H}_e^1$ – which was born several generations prior and has been winning BF comparisons ever since – we bias the GA to continue to favour the elite models. Instead, we would prefer that newly born models can overtake the Elo rating of elite models. We achieve this through an imprecise mechanism: newly born models are given the Elo rating of the second-most-elite model, $\hat{H}_e^2$. This performs three key functions:

i. new models are immediately *within range* of the elite models; if they perform well enough, they have a realistic and fair chance of overtaking them;

4 Note to achieve $B_{ij} = 10^{100} = e^{\mathcal{L}_i - \mathcal{L}_j} \implies \mathcal{L}_i - \mathcal{L}_j = ln(10^{100}) \approx 7$.

ii. the strongest model retains some of its advantage gained over previous generations – in order that the ratings are meaningful, there must be some advantage accrued over series of victories;

iii. $\hat{H}_e^2$ is allowed continue to compete, but has no advantage: in order to retain its status as elite, it must perform well *again* in this generation, so it can not simply rely on results from previous generations – against inferior opposition – to remain active in the gene pool.

Given the arbitrary scaling of the Elo rating scheme, and in order to derive a meaningful selection probability, we ought to ground the raw Elo rating somehow at each generation μ. We do this by subtracting the lowest rating among the entertained models, R^{μ}_{min}. This serves to ensure the range of remaining R_i is defined only by the difference between models as assessed within μ: a very strong model might have much higher R_i than its contemporaries, but that difference was earned exclusively by comparison within μ, so it deserves higher fitness. We perform this step before truncation, so that the reamining models post-truncation all have non-zero fitness. Finally, then, we name this OF the *Bayes-factor enhanced Elo rating*, whereby the fitness of each model is attained directly from its rating after undergoing Elo updates in the current generation minus the minimum rating of any model in the same generation μ,

$$g_i^E = R_i^{\mu} - R^{\mu}_{\text{min}}. \tag{8.20}$$

The advantage of this OF is that it gives a meaningful value on the absolute quality of every model, allowing us to determine the strongest, and importantly to find the relative strength between models. Further, it exploits bespoke BFs, i.e. based on the considered models' individually designed $\mathcal{E}_i$, removing the impetus to design $\mathcal{E}_v$ which can evaluate models definitively. One disadvantage is that it does not explicitly punish models based on their cardinality, however this feature is partially embedded by adopting BF for the comparisons, which are known to protect against overfitting.

8.2.8 *Choice of objective function*

Having proposed a series of possible objective functions, we are now in a position to analyse which of those are most appropriate for QMLA. Recall from Section 8.1.2 the figure of merit we use for models, F_1-score, which we will use to distinguish between the outputs of each OF.

First we can remark on the examples listed in Table 8.2. The OFs which rely on the TLTL, i.e. g^L, g^A, g^B, g^r, are effectively tricked by the log likelihood, which appears reasonably convincing for poor models, e.g. $\hat{H}_a, \hat{H}_c$. This underlines the risk in buidling $\mathcal{E}_v$, which can be biased towards weak models, for example resulting in high selection probability for $\hat{H}_a$ which has $f = 0$, while $\hat{H}_d$, with $f = 0.4$ is discarded. On the other hand, OFs grounded by the BF (g^p, g^R, g^E) invariably promote models of higher F_1-score, justifying the role of statistical evidence used for those calculations. Overall, however, the insights from this complete example are insufficient to

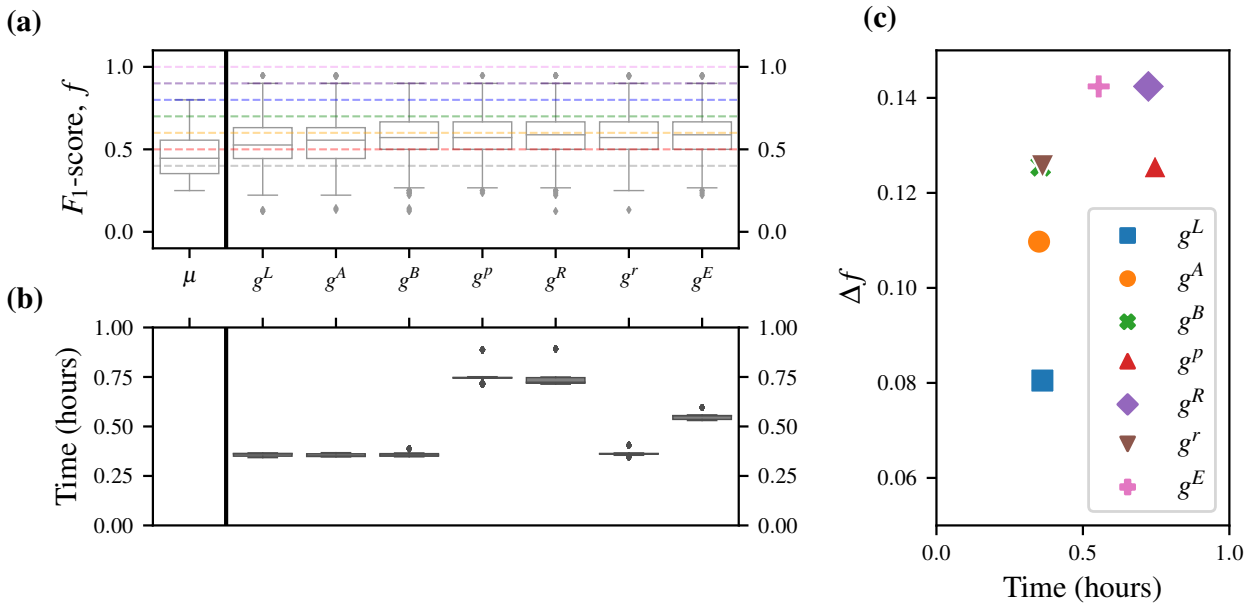

Figure 8.4: Comparison between proposed objective functions (OFs). Each OF trains the same initial generation of $N_m = 28$ models with resources $N_E = 500, N_P = 2000$, and then design a new set of N_m models through the same roulette strategy, such that the only difference between OF's output is how they assign selection probability. We run each OF 25 times for the same target system, a 4–qubit Heisenberg–XYZ model. **(a)** shows the box–plot of new models' F_1-score, f, where the median and inter–quartile ranges are indicated by the boxes, as well as those of the initial generation μ centered on $f_\mu = 0.45$. We mark $f = \{0.4, 0.5, ..., 1.0\}$ for ease of interpretation. **(b)** shows box–plots of the time taken to compute the single generation in each case. In **(c)** we report the difference between the median f among the newly proposed models from f_μ, Δf, plotted against the time to achieve the result.

make general claims about the performance of each OF, so here we examine their outputs systematically.

Returning to the task of determining our favoured OF, we choose some random target $\hat{H}_0$, and run a single generation using each OF, judging them by the quality of models they produce. We train the same batch of $N_m = 28$ random models in each case, and allow each OF to compute the selection probabilities for those models, and therefore direct the design of the hypothetical next generation of models. We plot the distribution of F_1-score that each OF produces in Fig. 8.4, also accounting for the time taken in each case, i.e. we report the time to train and evaluate the single generation on a 16–core node.

Overall, then, we can see that a strong balance of outcome with resource considerations are achieved by the Bayes factor enhanced Elo rating strategy, Section 8.2.7 so we use that for the case study presented in this chapter. We strongly emphasise, however, that the performance of each objective function can vary under alternative conditions, and therefore similar analysis may be warranted for future applications. For instance, if t_{max} is known to be small, in smaller model spaces, using g^r results in higher success rates. We retain BFEER, however, for generality and novelty, but it is important to recognise that the results listed do not reflect an upper limit of QMLA's performance, but rather reflect the constraints of the system under study; each Q will bring its own unique considerations which can result in significantly stronger or weaker performance. In particular, we will later use the OF based on residuals, Section 8.2.6, to study a much larger model space under assumptions of perfect parameter learning, Chapter 10.

8.3 APPLICATION

Having introduced all the necessary concepts of GAs, mapped them to the QMLA framework and chosen a suitable OF, we can finally use the GES for model search. In summary of this chapter so far, we use the following settings.

- Models are mapped to a bit string (chromosome), where each bit represents whether a given model term (gene) is present; chromosomes are of length N_t genes.
- A maximum of N_g generations are run, each with N_m unique models.
- Candidate models are trained using QHL, specifically by using IQLE[5]for parameter estimation.
- Models' fitness are determined by their BFEER, after having been trained by QHL and compared against some set of competing candidate models.
- For generating models on $\mu + 1$, the models on μ are first truncated (the worst-performing $N_m/2$ are discarded), and then assigned selection probability based on their fitness.
- Models are selected to become parents sequentially using roulette selection. Highly favoured models can parent many children models.

- Selected parent models are crossed over via a one point cross-over, at crossover location $\kappa \in \left(\frac{N_t}{4}, \frac{3N_t}{4}\right)$, and probabilistically mutated with rate $r_m = 0.25$.
- The top two elite models from μ are included on the $\mu + 1$.
- If, after 5 generations, the highest-fitness (elite) model is unchanged, we terminate the search and declare that model as the champion, $\hat{H}'$.
- Otherwise, after N_g generations, the highest-fitness model on the final generation is declared $\hat{H}'$.

We will use a four-qubit model space under the Heisenberg formalism, Eq. (6.10), such that any pair of sites $\langle k, l\rangle$ can be coupled by any of $\hat{\sigma}^x_{\langle k,l\rangle}, \hat{\sigma}^y_{\langle k,l\rangle} m \hat{\sigma}^z_{\langle k,l\rangle}$, so in total there are $N_t = |\mathcal{T}| = 3 \times \binom{4}{2} = 18$ terms, giving a model space of $2^{18} \approx 250,000$ viable models/chromosomes. For practical reasons[6], we set $N_m = 60$ and $N_g = 16$, although in most cases the elitism clause is triggered so the search terminates long before N_g is reached. The true parameters $\vec{\alpha}_0$ are assigned randomly in the range $(0.25, 0.75)$; within QHL the prior is set as a multivariate normal distribution 0.5 ± 0.125. We choose $\hat{H}_0$ at random to contain half the available terms[7],

$$\hat{H}_0 = \sigma^{yz}_{(1,2)} \sigma^{z}_{(1,3)} \sigma^{y}_{(1,4)} \sigma^{xy}_{(2,3)} \sigma^{x}_{(2,4)} \sigma^{xz}_{(3,4)}. \tag{8.21}$$

8.3.1 *Analysis*

We will analyse the GES from four perspectives: a single model, a single generation, a single QMLA instance, and the overall performance across many instances, i.e. a run.

Recall that BFEER are mediated through random graphs: given N_m models on μ, a given model $\hat{H}_i$ undergoes some $N^i_{BF} < N_m$ BF comparisons. In Fig. 8.5 we show the BF results and effects on the rating of a random model, $\hat{H}_i$, where $N_m = 60$ and $N^i_{BF} = 12$, i.e. $\hat{H}_i$ is directly compared against $\sim 20\%$ of contemporary models on μ. We see that $\hat{H}_i$'s rating is effected by whether it wins a given comparison, but also by the strength of evidence provided by the comparison (the BF), and the quality of its opposition (its rating).

We extend the single model analysis of Fig. 8.5 to all N_m models in the first generation in Fig. 8.6. The general trend is that models of higher F_1-score have their ratings increased, at the expense of models of lower F_1-score. After assessing models thus, the set of models is truncated to retain only the strongest candidates, which are assigned probability of being chosen to become a parent during roulette selection, as in Section 2.3.3. The very strongest two models are granted a position in the subsequent generation: these are the *elite* models.

5 IQLE assumes complete access to the target system see Section 3.3.1. This restricts the present analysis to simulateable, rather than physical, use cases, e.g. device calibration.

6 This is to ensure, with 15 available worker nodes, and accounting for some slowly-learning models, that all N_m models in a generation are trained within $2t_{qhl}$, where t_{qhl} is the time to train a single model.

7 Note we use a compact model representation, e.g. $\hat{H}_i = \sigma^{yz}_{(1,2)} \sigma^{z}_{(1,3)} = \sigma^{y}_{(1,2)} + \sigma^{z}_{(1,2)} + \sigma^{z}_{(1,3)}$.

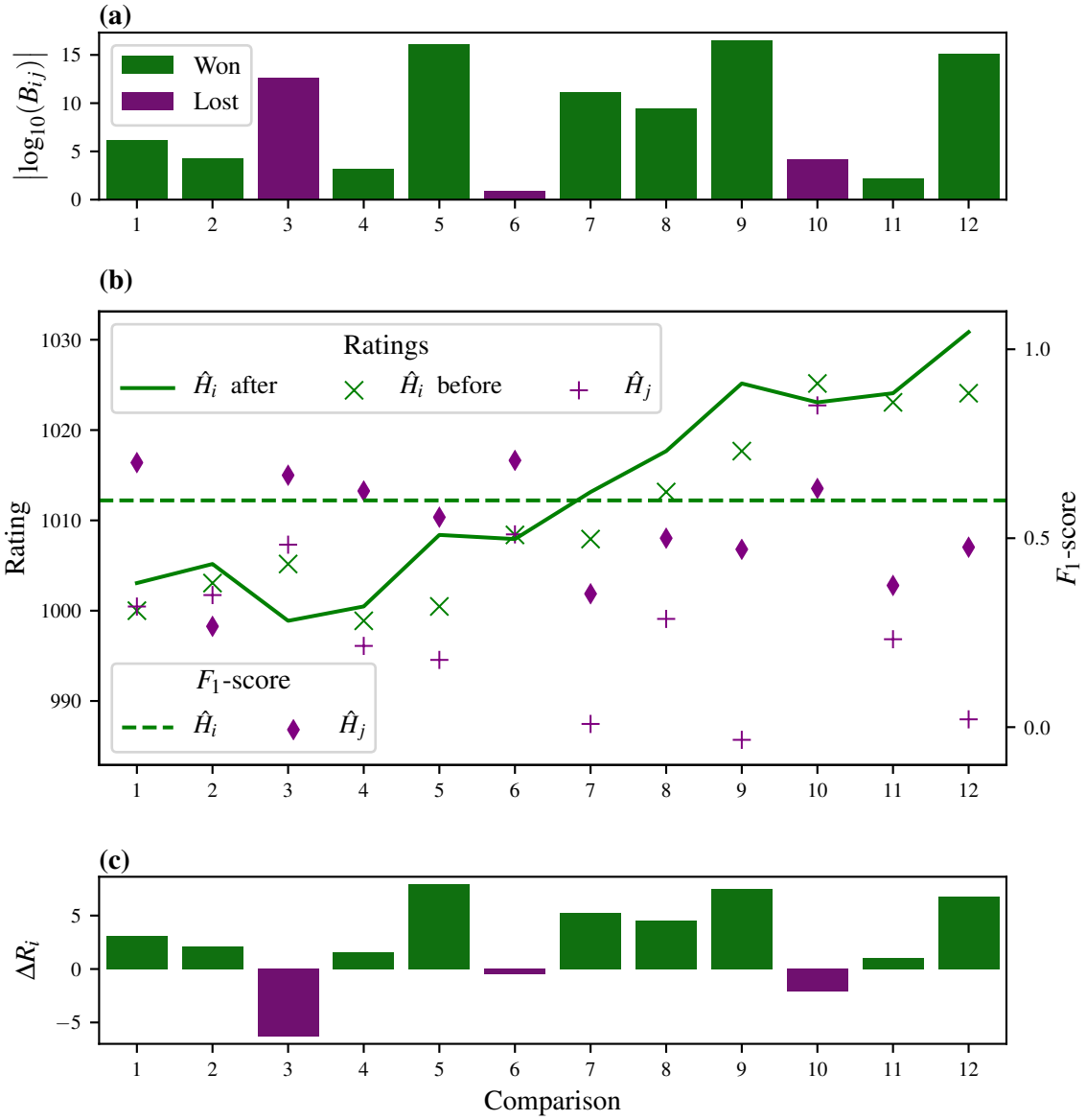

Figure 8.5: Bayes factor enhanced Elo ratings progression for a single candidate, $\hat{H}_i$, within a single generation. **a**, The BFs between $\hat{H}_i$ and some opponents, $\{\hat{H}_j\}$, from the perspective where $\hat{H}_i$ *wins* given $B_{ij} > 1 \Rightarrow \log_{10} B_{ij} > 0$, and loses otherwise. **b**, $\hat{H}_i$'s rating is shown (solid green line) changing according to the BFs comparisons with 12 other models from the same generation. Before each comparison, $\hat{H}_i$'s rating is shown (green cross) as well as the rating of its opponent, $\hat{H}_j$ (purple plus). The F_1-scores are also shown for $\hat{H}_i$ (dashed green line) and $\hat{H}_j$ (purple diamond). **c**, The corresponding change in $\hat{H}_i$'s rating, ΔR_i.

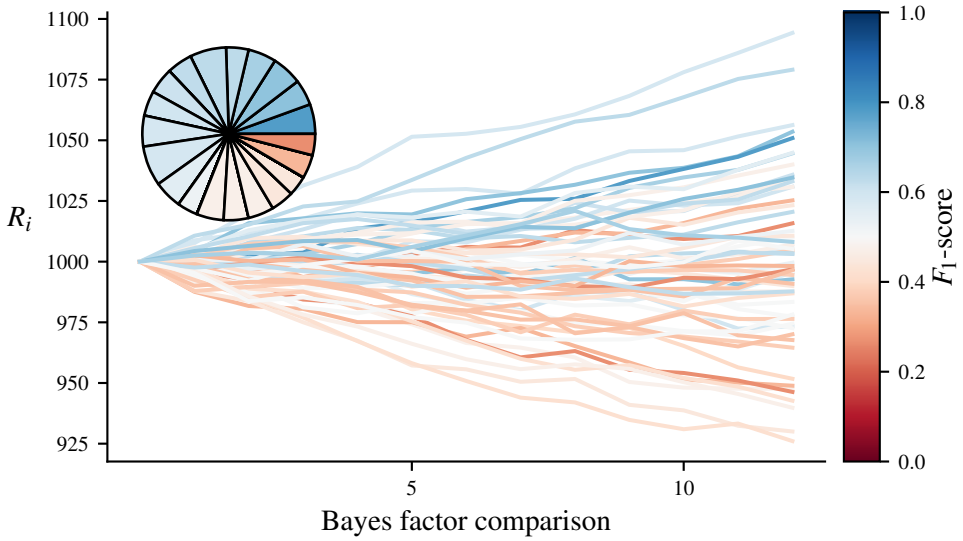

Figure 8.6: Ratings of all models in a single genetic algorithm generation. Each line represents a unique model and is coloured by the F_1-score of that model. **Inset**, the selection probabilities resulting from the final ratings of this generation. Only a fraction of models are assigned selection probability, while the remaining poorer-performing models are truncated.

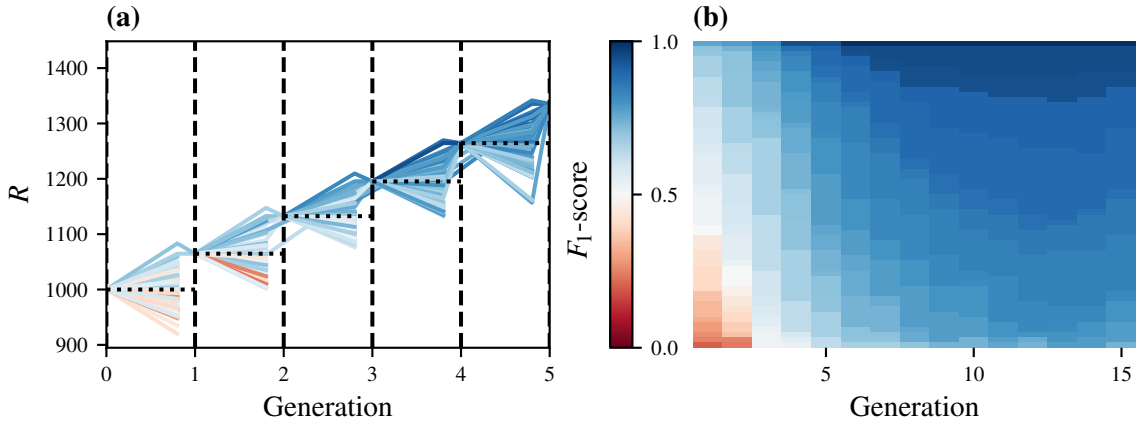

Figure 8.7: A single instance of the QMLA ga. **a**, Ratings of all models for the first five generations. Each line in each generation represents a model by its F_1-score. Horizontal dotted lines show the starting rating at that generation. **b**, Gene pool progression for $N_m = 60, N_g = 15$. Each time at each generation represents a model by its F_1-score.

Similarly we can consider the quality of models across at each generation, and their ratings. In Fig. 8.7 we see the trend suggested by Fig. 8.6 continue, i.e. that models of higher quality overall tend to achieve higher BFEER. The gene pool as a whole tends towards a homogeneous set of models, all with $f \geq 0.85$. Consequently, even in cases where the precise model, $\hat{H}_0$, is not identified, the champion model is highly informative, in that it captures many of the same interactions, therefore most-likely providing meaningul insight on the system's physics.

Finally, to understand the performance of the QMLA algorithm overall, we run 100 independent instances in a run, Fig. 8.8. We see that, while the overall model space can be characterised by the distribution of models' F_1-score, where we sample where $\bar{f} = 0.5 \pm 0.14$, that QMLA quickly moves to the subspace of high-quality models, i.e. the models explored have median $f = 0.76 \pm 0.15$. This exploration is based on 430 ± 45 chromosomes per instance, i.e. QMLA trains only 0.16% of the 2^{18} potential models. Ultimately QMLA nominates champion models, $\{\hat{H}'\}$ with $f \geq 0.88$ in all instances, and precisely identifies $\hat{H}' = \hat{H}_0$ in 72% of instances. Considering the big picture, where the remit of QMLA is to identify the interactions the target system is subject to, we show how often each term/gene is included in $\hat{H}'$ in Fig. 8.8**d**. Crucially, we see that terms which really are within the true Hamiltonian, $\hat{t} \in \mathcal{T}_0$, are found significantly more frequently than those without, $\hat{t} \notin \mathcal{T}_0$. This level of analysis can be used to post-validate the outcome of QMLA, i.e. rather than relying on $\hat{H}'$ from a single instance, trusting the terms' individual frequencies as evidence that they are of importance when describing the system of interest.

8.3.2 *Device characterisation*

This adaptive GES may prove a useful application of QMLA in the domain of device calibration, in particular to characterise some untrusted quantum simulator. That is, by using the simulator to implement some target $\hat{H}_0$, QMLA can identify which operator is *actually* implemented. For instance, implementation of a four–qubit model relies on high-fidelity two-qubit gates between arbitrary qubit pairs, and QMLA can effectively reconstruct which operations were and were not faithfully computed.

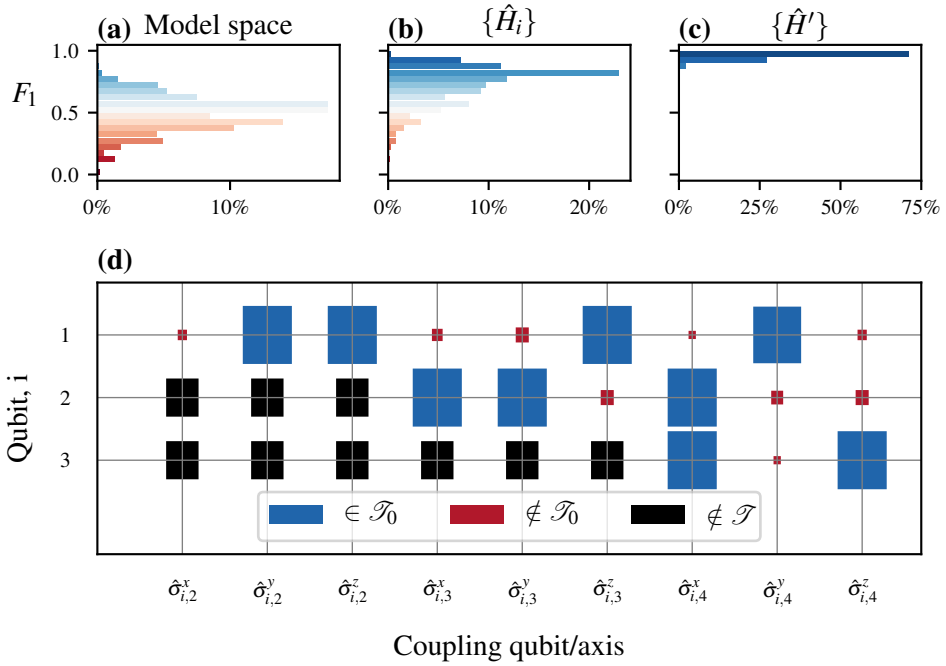

Figure 8.8: A run of the QMLA genetic algorithm (GA), consisting of 100 independent instances. **(a)**, The model space contains $2^{18} \approx 250,000$ candidate models; normally distributed around $f = 0.5 \pm 0.14$. **(b)**, The models explored during the model search of all instances combined, $\{\hat{H}_i\}$, show that QMLA tends towards stronger models overall, with $f = 0.76 \pm 0.15$ from $\sim$ 43,000 chromosomes across the instances, i.e. each instance trains $\sim$ 430 distinct models. **(c)**, Champion models from each instance, showing QMLA finds strong models in general, and in particular finds the true model $\hat{H}_0$ (with $f = 1$) in 72% of cases, and $f \geq 0.88$ in all instances. **(d)**, Hinton diagram showing the rate at which each term is found in the winning model. The size of the blocks show the frequency with which they are found, while the colour indicates whether that term was in the true model (blue) or not (red). Terms are couplings between two qubits, e.g $\hat{\sigma}^x_{(1,3)}$ couples the first and third qubits along the x-axis. We test four qubits with full connectivity, resulting in 18 unique terms (terms with black rectangles are not considered by the GA).

Part IV

EXPERIMENTAL STUDIES

9 NITROGEN VACANCY CENTRE

It is of primary interest to apply the QMLA algorithm to real-life, experimental systems. In this chapter we devise an ES to operate in conjunction with experimental data in order to characterise an electron spin in an NV centre in diamond. In particular, we model, through Hamiltonian terms, interactions between the spin and the spin bath in which it resides, so that QMLA is finding an effective model for the open system dynamics.

Here we will first introduce a basic picture of NVCs, using basic but nonstandard nomenclature for simplicity; for thorough descriptions of the underlying physics, readers are referred to [**?**]. We next discuss the target system with respect to its modelling, determining the suitable terms which *might* represent the NVC's interactions, to inform the starting point for the QMLA. Finally we describe the implementation of an ES for the examination of the NVC, and the results of the QMLA procedure.

9.1 NITROGEN-VACANCY CENTRE

NV centers are point defects in diamond, occuring naturally [**?**] or synthetically [**?**, **?**]. A substitutional nitrogen-14 (^{14}N) isotope is embedded in a lattice of carbon atoms in diamond, adjacent to a lattice vacancy, such that it is surrounded by three carbon-13s (^{13}Cs) [**?**]. Of the ^{14}N atom's five valence electrons, three bond with nearby ^{13}Cs; the remaining two unbonded electrons for a lone pair and can be thought of as a single spin-$\frac{1}{2}$ particle. The adjacent lattice vacancy has three unbonded electrons, two of which bond together leaving a single unpaired electron. The single electron in the lattice vacancy, together with the effective lone pair of the ^{14}N, form a a system of two spin-$\frac{1}{2}$ particles. Such systems have been thoroughly studied; of particular interest are the resultant *triplet* states, i.e. the allowed permutations of the two particles with total quantum spin $S = 1$, with magnetic spin multiplicity allowing $m_s = -1, 0, 1$, giving rise to three distinct energy levels for the system.

A *manifold* is a set of states differing only slightly, for example states near the absolute ground state manifold might differ only in magnetic spin quantum number, and can be characterised as the ground state manifold. We consider two principle manifolds of the system: the ground state and excited manifolds, each consisting of three states, corresponding to the allowed values for magnetic spin m_s, see Fig. 9.1a. For brevity, we denote states with reference to their magnetic spin and manifold, e.g. the state in the ground state manifold with $m_s = 0$ is denoted $|m_s = 0\rangle_g$. In the absence of a magnetic field, the states corresponding to $|m_s = \pm 1\rangle$ are degenerate, but in the presence of a magnetic field, B, they have distinct energy levels, referred to as the Zeeman effect, Fig. 9.1b.

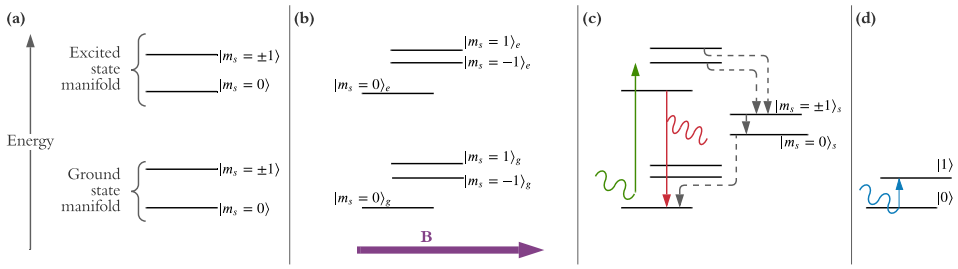

Figure 9.1: Simplified depiction of energy levels of the nitrogen-vacancy centre, corresponding to its triplet state. **a**, With no external field, the system simply has excited and ground-state manifolds, each of which consist of two energy levels depending on the magnetic spin, m_s. **b**, In the presence of a magnetic field (purple, B), the magnetic spins have distinct energy levels, i.e. Zeeman splitting. States are denoted by their magnetic spin and subscripted by their manifold. **c**, Application of a green ($532nm$) laser excites the NVC from any of the states in the ground state manifold to the excited manifold. The dominant decay mechanism for the excited states are shown: (i) $|m_s = 0\rangle_e \to |m_s = 0\rangle_g$ (red line) through the emission of a red ($637nm$) photon; (ii) $|m_s = \pm 1\rangle_e \to |m_s = 0\rangle_g$ (dotted grey lines) via the shelving manifold which allows for non-spin-preserving transition, and does not emit a photon. **d**, Computational basis states $|0\rangle$ and $|1\rangle$ are assigned to the two lowest energy states. The difference in energy between these states is such that a microwave (MW, blue) photon can trigger transition from $|0\rangle$ to $|1\rangle$, as well as states in between such as $|+\rangle$, allowing for the implementation of quantum logic gates.

We designate the state $|m_s = 0\rangle_g$ as the basis state $|0\rangle = \begin{pmatrix} 1 \\ 0 \end{pmatrix}$, and $|m_s = -1\rangle_g$ as $|1\rangle = \begin{pmatrix} 0 \\ 1 \end{pmatrix}$, such that we have defined a qubit and computational basis, Fig. 9.1d. By shining a laser of 532nm (green) on the NVC, it is excited to the excited manifold, from which it decays back to the ground state manifold. Importantly, the process of this decay can be exploited for the preparation of the NVC in the computational basis state $|0\rangle$. That is, the dominant decay process from $|m_s = 0\rangle_e$ is spin-preserving, so it ends in $|m_s = 0\rangle_g$. On the other hand, had the NVC been in the $|m_s = \pm 1\rangle_e$, the dominant decay process is through a shelving (singlet) state, and does not preserve spin, such that it also decays to the $|m_s = 0\rangle_g$. Therefore, irrespective of the initial state, by shining the green laser on the NVC, it is most likely that it has been prepared in $|m_s = 0\rangle_g = |0\rangle$, providing us a starting point from which to perform computation.

The difference in energy between $|0\rangle$ and $|1\rangle$ is addressible optically: by shining a microwave (MW) pulse at the NVC, we can oscillate the qubit between the two levels. Likewise, having initialised the state to $|0\rangle$, we can perform a $\pi/2$ rotation about the logical z-axis, by running the MW laser for half the time, resulting in the state $|+\rangle$. We can similarly devise MW radiation to achieve quantum gates and operations on our NVC qubit. We depict these cycles in Fig. 9.1c.

We can further exploit the decay mechanism to compose a readout procedure, to infer the population of $\{|0\rangle, |1\rangle\}$ at a given instant, for example following the application of gates to the system. We know that the excitation due to the green laser is spin-preserving, i.e. when the NVC has been excited to $|m_s = 0\rangle_e$, it had originated in $|m_s = 0\rangle_g$. We also know that the decay $|m_s = 0\rangle_e \to |m_s = 0\rangle_g$ is spin preserving, with the emission of a red photon: by simply counting the number of photons emitted, we quantify the population of $|0\rangle$ at the time of query. On the contrary, when the $|m_s = -1\rangle_g$ is excited, spin is also preserved, so it goes to $|m_s = -1\rangle_e$; but $|m_s = -1\rangle_e$ decays through the shelving state as outlined earlier, *without* the emission of a photon. We can hence infer the population of $|m_s = -1\rangle_g$ at the time of query by the fraction of incidents which don't emit a photon. That is, say we first calibrate the system by retaining the green laser for some time: after a few μs, a steady state is achieved where the majority of the time, the triplet is in the state $|0\rangle = |m_s = 0\rangle_g$. Then, excitation from the same laser results in the excitation to $|m_s = 0\rangle_e$, which decays back to $|m_s = 0\rangle_g$ and emits a photon in the process; by counting the red photons emitted in a certain time window – equivalently, measuring the photoluminescence (PL) signal – we benchmark the population of $|0\rangle$ when nothing else has happened as p_0. Now, when we apply gates (i.e. MW pulses) to the NVC, we can similarly read out the population of $|0\rangle$ as p_0', and infer that thelikelihood that the NVC is found in the initial state $|0\rangle$ is p_o'/p_0. We can use this quantity as the likelihood within QLE, allowing us to learn from the NVC, as we will discuss in the next sections.

In summary then, by assigning basis states $|0\rangle, |1\rangle$ to energy levels of the ground state manifold, we are able to ensure the preparation of the NVC in $|0\rangle$ by first shining a green laser on the NVC. We can then apply MW radiation to achieve quantum logical gates on the system, and read out the final state of the system, again by shining a green laser and observing the emitted photons (PL) and inferring the population level of each basis state. We represent these concepts in a simplified format in Fig. 9.1.

9.2 TARGET SYSTEM

We take the axis of the NVC, i.e. the axis connecting the ^{14}N with the lattice vacancy, as the z-axis. There are clearly a huge number of interactions to which the NVC is subject: we choose to focus on its interactions with the environment, i.e. with nuceli in the same diamond, which dictate its decoherence. These interactions are characterised by hyperfine terms [**?**]. The overall Hamiltonian for such systems, where the set of nuclear sites is $\{\chi\}$, is given by

$$\hat{H}_{\text{full}} = \Delta_{\text{gs}}\hat{S}_z^2 + \mu_B g\mathbf{B}\cdot\mathbf{S} + \mathbf{S}\cdot\sum_\chi\left(\mathbf{A}_\chi\cdot\hat{I}_\chi\right) + P\hat{I}_z^2 + \mu_n g\mathbf{B}\cdot\sum_\chi\hat{I}_\chi. \tag{9.1}$$

We will describe each term, as well as approximations which enable us to simplify the space considerably.

- Isolated-spin terms, i.e. describing the spin independent of the environmental nuclei

  - $\Delta_{gs}\hat{S}_z^2$: the *zero-field* splitting, i.e. without any external (magnetic) field, the spin oscillates rapidly, with $\Delta_{gs} \sim$ GHz.
  - $\mu_B g \mathbf{B} \cdot \mathbf{S}$: the spin's precession about the magnetic field, $\mathbf{B} = \begin{pmatrix} B_x & B_y & B_z \end{pmatrix}$, via the total spin operator[1] $\mathbf{S} = \begin{pmatrix} \hat{S}_x & \hat{S}_y & \hat{S}_z \end{pmatrix}$, where μ_B is the Bohr magneton and g is the g-factor (≈ 2, simplified from the g-factor tensor).
- Hyperfine terms
  - $\hat{S} \cdot \sum_\chi \left(\mathbf{A}_\chi \cdot \hat{I}_\chi \right)$: The NVC total spin operator $\mathbb{S}$ couples with each site, χ. At each site there is a nucleus which has total spin operator $\mathbf{I}_\chi = \begin{pmatrix} \hat{I}_x & \hat{I}_y & \hat{I}_z \end{pmatrix}_\chi$. $\mathbf{A}$ is the hyperfine tensor, containing the hyperfine parameters of interest.
- Bath-only terms, i.e. describing the other nuceli independent of the spin
  - $P\hat{I}_z^2$: the quadrupole splitting, i.e. this term gives the splitting of the ^{14}N's hyperfine splitting, which does not meaningfully contribute to the short-decay processes in the experiments described in the next section.
  - $\mu_n g \mathbf{B} \cdot \sum_\chi \hat{I}_\chi$: μ_n is the nuclear magneton and g is again the g-factor.

Given that we are interested in the spin and its interactions with the environment only, we can immediately drop the bath-only terms, by assuming the bath is static apart from its interactions with the NVC. This is a usual assumption in the treatment of open system dynamics, to allow for focus on the dominant interactions for the system of interest [**?**]. Additionally, since the zero field splitting contributes a constant shift in energy, we can safely omit it by moving to the rotating frame. We are then left only with the second and third terms of Eq. (9.1).

9.2.1 *Mapping to model terms*

Next we will focus on mapping the remaining terms to operators to compose the set of terms $\mathcal{T}$ to use in our ES. In our modelling, the NVC spin is represented by the first logical qubit, with a further $|\{\chi\}|$ qubits, each representing a unique nuclear site, as discussed later in this section. As standard, we take the axis[2]of the NVC as parallel to the qubit's z-axis.

The first terms included come from the spin's precession about the magnetic field. It is usually assumed that the external, applied magnetic field is well-aligned with the spin qubit's z-axis; here we will treat this determination as the role of QMLA, i.e. we will endeavour to establish whether the x-, y-axis components of the magnetic field are important for describing the spin's dynamics. Then, we have

$$\mu_B g \mathbf{B} \cdot \mathbf{S} = \mu_B g \begin{pmatrix} B_x & B_y & B_z \end{pmatrix} \cdot \begin{pmatrix} \hat{S}_x & \hat{S}_y & \hat{S}_z \end{pmatrix} \rightarrow \alpha_x \hat{S}_x + \alpha_y \hat{S}_y + \alpha_z \hat{S}_z, \tag{9.2}$$

1 We invoke an inexact representation of high dimensional tensors here for ease of interpretation. For instance, the total nuclear spin operator exists in arbitrary dimension (depending on the number of sites modelled), but we present it simply as $\mathbf{I} = \begin{pmatrix} \hat{I}_x & \hat{I}_y & \hat{I}_z \end{pmatrix}$ at each site to convey that we can separate the terms in the construction of models.

2 The axis connecting the ^{14}N with the lattice vacancy.

with $\alpha_i = \mu_B g B_i$. The spin's rotation terms to be included in QMLA's deliberations are therefore

$$\mathcal{T}_s = \{\hat{S}_x, \hat{S}_y, \hat{S}_z\} \tag{9.3}$$

Next, let's focus on the hyperfine coupling term. In general we sum over the nuclear sites $\{\hat{H}_i\}$, since the spin will interact with every nucleus to some extent; We show in **[?]** that a realistic system requires modelling a finite-size bath of $|\{\chi\}| \sim 15$ nuclei to capture the dynamics of interest, which is infeasible for complete characterisation via classical simulation, where we are limited to ~ 11 qubit calculations[3]. Instead, by focusing only on the *short-time* dynamics of the NVC, we can isolate the effects of dominant interactions, most notably with a single nearby ^{13}C. Indeed, by assigning a first qubit as representing the NVC spin, we can map the entire environment onto a generic second *environmental qubit*, representing the amalgamation of said interactions, though we can think of the two-qubit system as the NVC coupled with a single ^{13}C **[?]**.

$$\mathbf{S} \cdot \sum_{\chi} (\mathbf{A}_\chi \cdot \mathbf{I}_\chi) \rightarrow \mathbf{S} \cdot \mathbf{A} \cdot \mathbf{I} \tag{9.4}$$

This clearly reduces the dimension of our approximation, the number of qubits, n_q from $n_q = 1 + |\{\chi\}|$ to $n_q = 2$, since now we only retain qubits for the NVC and the ^{14}N (which also represents the entire bath). The hyperfine tensor $\mathbf{A}$ consists of the hyperfine parameters, i.e. the strength of correspdoning interactions.

$$\mathbf{A} = \begin{pmatrix} A_\perp & 0 & 0 \\ 0 & A_\perp & 0 \\ 0 & 0 & A_\parallel \end{pmatrix}, \tag{9.5}$$

where $A_\perp$ is the non-axial hyperfine coupling term and $A_\parallel$ is the axial coupling term, since the axis of the NVC is used to define the z-axis for our qubits.

The total spin operators – of the NVC operating on the first logical qubit and the environmental qubit on the second – can be thought of as

$$\begin{aligned} \mathbf{S} &= (\hat{S}_x^{(1)} \quad \hat{S}_y^{(1)} \quad \hat{S}_z^{(1)}) \\ \mathbf{I} &= (\hat{I}_x^{(2)} \quad \hat{I}_y^{(2)} \quad \hat{I}_z^{(2)}) \end{aligned} \tag{9.6}$$

So we can write,

$$\begin{aligned} \mathbf{S} \cdot \mathbf{A} \cdot \mathbf{I} =& A_\perp \hat{S}_x \hat{I}_x + A_\perp \hat{S}_y \hat{I}_y + A_\parallel \hat{S}_y \hat{I}_y \\ &+ A_{xy} \left(\hat{S}_x \hat{I}_y + \hat{S}_y \hat{I}_x \right) \\ &+ A_{xz} \left(\hat{S}_x \hat{I}_z + \hat{S}_z \hat{I}_x \right) \\ &+ A_{yz} \left(\hat{S}_y \hat{I}_z + \hat{S}_z \hat{I}_y \right) \end{aligned} \tag{9.7}$$

Off-diagonal terms, referred to hereafter as *transverse* terms ($\hat{S}_i\hat{I}_j$ where $i \neq j$), are usually neglected [**?**]; here we will emply QMLA to determine whether their contributions are worthy of inclusion, although we consider only $\{\hat{S}_x\hat{I}_y, \hat{S}_x\hat{I}_z, \hat{S}_y\hat{I}_z\}$ for brevity. In total then, the hyperfine terms to be entertained by QMLA are

$$\mathcal{T}_{HF} = \begin{Bmatrix} \hat{S}_x\hat{I}_x, & \hat{S}_y\hat{I}_y, \hat{S}_z\hat{I}_z, \\ \hat{S}_x\hat{I}_y, & \hat{S}_x\hat{I}_z, \hat{S}_y\hat{I}_z \end{Bmatrix}. \tag{9.8}$$

Finally, combining Eq. (9.3) and Eq. (9.8), we have the full set of terms to incorporate into QMLA ES:

$$\mathcal{T}_{NV} = \begin{Bmatrix} \hat{S}_x, & \hat{S}_y, \hat{S}_z, \\ \hat{S}_x\hat{I}_x, & \hat{S}_y\hat{I}_y, \hat{S}_z\hat{I}_z, \\ \hat{S}_x\hat{I}_y, & \hat{S}_x\hat{I}_z, \hat{S}_y\hat{I}_z \end{Bmatrix}. \tag{9.9}$$

We introduce a shorthand notation to ease model representation for the remainder of this chapter. Recall that we have defined a two-qubit Hilbert space for model construction. Terms which affect only the spin act only on the first qubit, $\hat{S}_i = \hat{\sigma}_i \otimes \hat{\mathbb{1}}$, where $\hat{\sigma}_i$ is the Pauli operator giving rotation about the i-axis, and $\hat{\mathbb{1}}$ is the one-qubit identity matrix. Retaining the hyperfine notation, for the expectedly-dominant diagonal terms, we denote $\hat{A}_i = \hat{S}_i\hat{I}_i = \hat{\sigma}_i \otimes \hat{\sigma}_i$. We refer to the less-dominant off-diagonal terms as *transverse* terms, $\hat{T}_{kl} = \hat{S}_k\hat{I}_l = \hat{\sigma}_k \otimes \hat{\sigma}_l$. We can hence rewrite Eq. (9.9) as

$$\mathcal{T}_{NV} = \begin{Bmatrix} \hat{S}_x, & \hat{S}_y, \hat{S}_z, \\ \hat{A}_x, & \hat{A}_y, \hat{A}_z, \\ \hat{T}_{xy}, & \hat{T}_{xz}, \hat{T}_{yz} \end{Bmatrix}. \tag{9.10}$$

We also use a succinct representation for brevity, e.g. $\hat{S}_{xy}\hat{A}_z = \hat{S}_x + \hat{S}_y + \hat{A}_z$, where parameters $\alpha_x, \alpha_y, \alpha_z$ are implicitly assumed.

9.2.2 *Prior knowledge*

The spin-only terms, $\hat{S}_i$, are consequences of the magnetic field, which is usually assumed as aligned with z-axis, such the x-, y-axis compoenents are negligible; $\hat{S}_z$ is expected in the range $\sim 2 - 3$MHz. Likewise, the hyperfine terms, $\hat{A}_i$ are expected in the range of $\sim$ MHz [**?**], while in the *secular approximation* only the z-component is expected to contribute substantially [**?**]. The non axial hyperfine terms, i.e. the transverse terms $\hat{T}_{kl}$ are not usually included in effective models, but can be found of order $\sim \mathcal{O}(10\text{kHz})$ [**?**]. We utilise this prior understanding of the system to inform the parameter range used for training candidate models: for each of the terms

3 This limitation arises from the requirement to compute the total evolution of the global state, involving calculation of $e^{-i\hat{H}t}$, i.e. the characterisation of an n_q-qubit model depends on classical exponentiation of the $2n_q \times 2n_q$ Hamiltonian for each particle and experiment in CLE, which is a prohibitive expense.

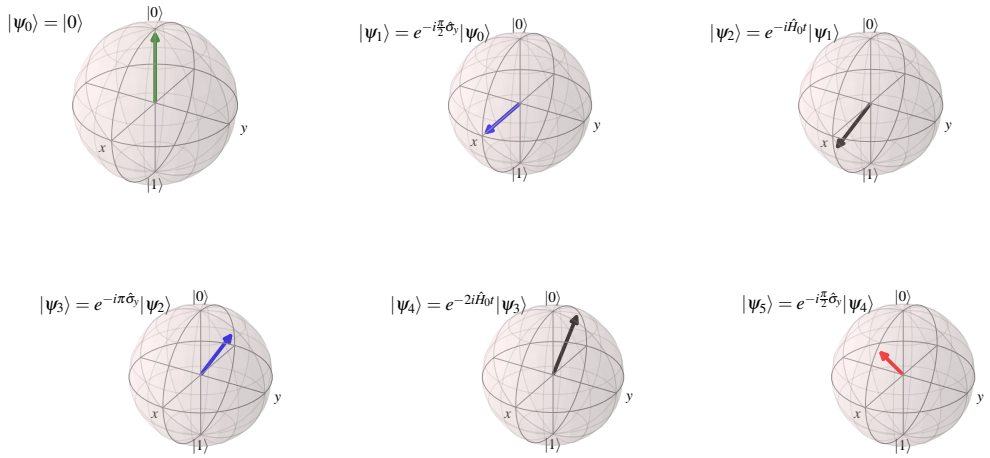

Figure 9.2: States of spin qubit at each stage of Hahn echo sequence.
The state of the NVC spin is initialised by a green laser into state $|\psi_0\rangle = |0\rangle$. We then apply a rotation about the y-axis (i.e. a MW pulse), yielding the state $|\psi_1\rangle = |+\rangle$. The system is then allowed to evolve according to its own $\hat{H}_0$ for t, $|\psi_2\rangle = e^{-i\hat{H}_0 t}|+\rangle$. We apply a second MW pulse, this time for a π-rotation about the y-axis, $|\psi_3\rangle = e^{-i\pi\hat{\sigma}_y}e^{-i\hat{H}_0 t}|+\rangle$. Again the system evolves according to interactions with the environment, this time for $t' = 2t$. We apply a final MW pulse to rotate about the y-axis again, effectively either returning the spin to near the $|0\rangle$ axis, or near the $|1\rangle$ axis. Here $|\psi_5\rangle$ is roughly half way between $|0\rangle$ and $|+\rangle$, i.e. along the z-axis. The spin is read out from $|\psi_5\rangle$ via the NVC's photoluminescence. Here $\hat{H}_0 = 0.25\,\hat{\sigma}_y$ was evolved for $t = 0.5$ (arbitrary units), and the final state overlap with the initial state, i.e. thelikelihood of measuring the spin in $|0\rangle$ is $\Pr(0|\hat{H}_0, t) = 0.865$.

in Eq. (9.10), we will adopt a normal prior distribution of 4 ± 1.5MHz. This is sufficiently specific to ensure the training subroutine operates in a physically meaningful – and likely appropriate – space, whlie also broad enough to allow for significant differences between expectation and reality, as well as supporting hypotheses where each parameter is zero, such that such negligible contributions can be identified.

9.2.3 *Experimental procedure*

We have decided to characterise the hyperfine interactions of the NVC; these are evident most strongly at very short timescales [**?**]. To isolate the effects of the hyperfine interactions, we run Hahn echo experiments, which are known to emphasise weak interactions. Hahn echo sequences attempt to decouple the spin's dynamics from the nuclear bath [**?**, **?**, **?**, **?**, **?**] providing a helpful platform for studying residual contributions of terms in Eq. (9.10). The NVC qubit undergoes

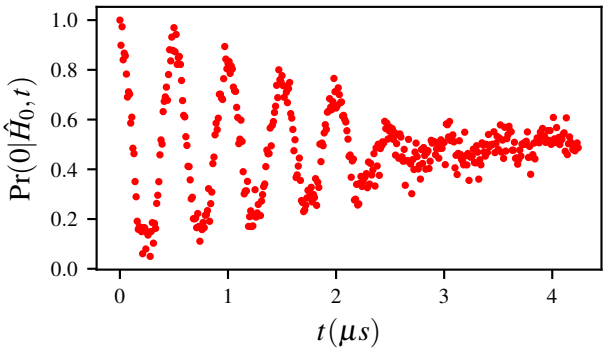

Figure 9.3: Raw data for the nitrogen-vacancy centre's dynamics. The y-axis shows the photoluminescence of the NVC, equivalently thelikelihood $\Pr(0|\hat{H}_0, t)$.

a series of evolutions – either according to application of quantum logic gates or the natural evolution of the system interacting with its environmen We depict the stages of the experiment in Fig. 9.2, starting from the initialised $|0\rangle$ through to its final state which is read out through PL, both of which as described in Section 9.1.

In particular, the final state, $|\psi\rangle_5$, is read out, effectively by projection onto $|0\rangle$; we can interpret the PL after evolution time t as the likelihood that the NVC is found in $|0\rangle$ after evolution of its *true* Hamiltonian, $\hat{H}_0$. That is, we assign this projection as the quantity $\Pr(0|\hat{H}_0, t)$ (the likelihood), and it can be used withinlikelihood estimation in order to refine a candidate model $\hat{H}_j$, effectively[4] by changing the structure of $\hat{H}_j$ until $\Pr(0|\hat{H}_0, t) \approx \Pr(0|\hat{H}_j, t)\ \forall t$.

By varying the evolution time of the Hahn-echo sequence, we can map thelikelihood against time, which we can view as capturing the dynamics of the NVC spin **??**. We vary time up to $t \sim 4\mu s$ in the short-time range in intervals of $\Delta t = 50ns$, so we have 425 data points. Importantly, the data for the studied NVC is taken once and analysed offline, i.e. QMLA does not have complete authority to design experiments to run on the NVC, although it can aim to choose the most informative t available in the predefined set; we will discuss the consequences of this restriction later in this chapter.

9.3 Exploration strategy

Finally, then, we are in a position to describe the specific implementation details which allow QMLA to study this NVC system. Recalling the terminology of QMLA from Chapter 4, we design an exploration strategy (ES) specifically for the system under study. The ES will account for the details listed in this chapter so far, in summary:

- we attempt to assign a model, $\hat{H}'$, to the NVC;

4 Of course this is a gross simplification of QHL which is described fully in **??**

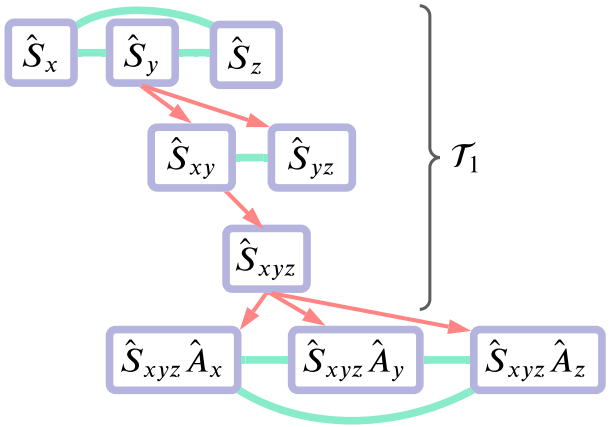

Figure 9.4: Greedy model search. Models (purple) are placed on branches, trained and consolidated (green) as in Fig. 4.1, with the branch champion spawning (red) candidates to place on the subsequent branch. Branches are grouped in tiers, correspdoning to levels of approximation: the first tier of the model generation strategy is shown, where $\mathcal{T}_1 = \{\hat{S}_x, \hat{S}_y, \hat{S}_z\}$ is explored. The final champion from the first tier seeds the second tier.

  - we especially focus on its hyperfine interactions;
- in particular, we use a 2-qubit approximation;
  - the first qubit represent the spin itself;
  - the second qubit represents the environment in which the NVC resides;
- we query the NVC by performing Hahn echo experiments (Fig. 9.2);
- the outcome of those experiments are thought of as the system's likelihoods (Fig. 9.3);
- likelihoods are used for the training of individual candidate models;
- candidate models are composed of the terms defined in Eq. (9.10).

As outlined in Section 4.4, the central role of any ES is to specify the model generation procedure, which QMLA relies upon for deciding the next set of candidate models to test. In this case, we exploit some intuition and prior knowledge of how such systems work, to design a bespoke model generation subroutine: we can think of this as a midway point between the completely specified ESs used for identifying the underlying lattices from a prescribed set in Chapter 6, and the entirely general genetic algorithm which does not restrict model generation, of Chapter 8. We use the standart structure of ETs introduced in Section 4.4, where models are placed on consecutive branches, μ, with branches consolidated by complete pairwise comparisons, mediated through BFs, resulting in the selection of a single branch champion, $\hat{H}_{C(\mu)}$.

We use a *greedy search rule*: terms are added one-by-one to gradually increase the complexity of candidate models until terms are exhausted [**?**]. We break the ET into three distinct tiers, each corresponding to an intuitive degree of complexity: the first tier involves the spin-only terms, $\mathcal{T}_1 = \{\hat{S}_i\}$; the second considers the hyperfine terms, $\mathcal{T}_2 = \{\hat{A}_i\}$; the final tier the transverse terms, $\mathcal{T}_3 = \{\hat{T}_i\}$. Within each tier, terms are added greedily to the previous branch's champion, $\hat{H}_{C(\mu)}$. So, the first branch is given by $\mu = \{\hat{S}_x, \hat{S}_y, \hat{S}_z\}$; say $\hat{H}_{C(\mu)} = \hat{S}_y$, then $\mu + 1$ determines that $\hat{S}_x, \hat{S}_z$ are not yet considerd, so it constructs the models $\hat{S}_{x,y}, \hat{S}_{y,z}$, e.g. Fig. 9.4. After exhausting all tiers, we consolidate the set of branch champions, $\mathbb{H}_C = \{\hat{H}_{C(\mu)}\}$, to determine the best model considered globally, $\hat{H}'$.

Clearly, this growth rule is partially deterministic, insofar as some models are gauranteed to be considered, while others are not reachable; indeed, the space of available models are heavily constrained, in particular models in later tiers will always involve all of the tier 1 models, e.g. $\hat{S}_x\hat{A}_y$ does not occur naturally. We account for this shortcoming with a final redcibility test, triggered if any of the parameters of $\hat{H}'$ are potentially negligible, i.e. are within one standard deviation of 0. This test simply removes such low-parmeter terms from $\hat{H}'$, giving a reduced global champion, $\hat{H}'_r$, and computes the BF between $\hat{H}', \hat{H}'_r$: if the BF indicates strong evidence in favour of the reduced version, we replace the champion model, $\hat{H}' \leftarrow \hat{H}'_r$. In effect, we thus verify the statistical significance of each term included in $\hat{H}'$.

The total model in Eq. (9.1) supports $N_t = 1 + 3 + 6|\chi| + 3 + 3|\chi| = 7 + 9|\chi|$ terms, which we reduced to a space of $N_t = 3 + 6|\chi| = 9$ through several approximations[5]; even so, the remainng 2^9 permitted models were reduced further by building the logic of this ES from our intuition aroud existing knowledge of typical NVC systems, such the ES will only ever consider < 20 models per instance. The described ES seems overly perscriptive, but should be viewed as a first attempt at a generalisable approach: essentially we can view the tiers of the greedy search as characterising the system at various approximations, e.g. the first tier examines one-qubit terms, while subsequent tiers inspect 2-qubit terms. We can envision future work where the greedy search is gradually extended to less rigid approximations, enabling study of more complex quantum systems. This leads to some important remarks:

1. Realistic, near-term applications of QMLA can not be thought of as a solution to black-box characterisation problems: it must be used in conjunction with domain expertise for the system under study.
2. While this test-case yields promising results, the outcome of QMLA here may not be especially insightful, since the available model terms were so deliberately constrained – we demonstrate a use-case in Chapter 10 where a broader scope is enabled in simulation.

A common charge against QMLA supposes to first write down the most complex model, train it fully, and then infer which terms are negligible, in a similar process to the champion reduction test outlined here. While this may be feasible in the case described here, with $N_t = 9$ and a closed term set, this would scale poorly: adding just a second nuclear site increases the model search to a space of $N_t = 15$. Models of higher cardinality ($|\vec{\alpha}|$) demand higher N_e, N_p to train well, so immediately trainng the most involved model would require infeasible resources[6], and

risks significantly overfitting the data. It seems more appropriate to work "from the ground up", testing terms and keeping them only when justified, instead of training all terms and attempting to decouple their effects post-hoc.

9.3.1 *Test in simulation*

Before considering the real experimental data (Fig. 9.3), we first test the ES in simulation under ideal conditions. That is, we assume the ability to prepare arbitrary probe states, and use a random probe set (see **??**), and use the full expectation value as the likelihood, $|\langle\psi|e^{-i\hat{H}_j t}|\psi\rangle|^2$. Of course, this is infeasible since we presume access to the full state at the time of measurement, but this can be seen as a best-case scenario for this application, because the realistic case loses information by tracing out the environmental qubit at measurement. We vary the target $\hat{H}_0$, among a series of ten models, which are all valid models achievable by the ES.

Varying $\hat{H}_0$, allowing arbitrary probe preparation and PGH EDH, i.e. case (i) from [**?**].

9.4 EXPERIMENT DESIGN CONSTRAINTS

Moving to analyse the experimental setup, there are a number of constraints which we must account for in training models. Firstly, the $\pi/2$-pulse applied to the prepared qubit ($|\psi_0\rangle \rightarrow |\psi_1\rangle$ in Fig. 9.2) means that the state before evolution is always $|+\rangle$ in the computational basis; this is a severe limitation on model training, as we saw in **??**. Moreover, this puts a bias on the interactions QMLA is likely to identify: we show in Fig. 9.2 how QHL performs in training the same model using (i) the probe set available experimentally; (ii) a more general (random) probe set. This has a noteworthy impact on the outcome of this study, since this suppression of terms means we are more likely to find some interactions than others, so we must add this caveat to the champion model.

The experiment was run until the NVC was deemed to have decohered, so Fig. 9.3 ceases at $t_{\text{max}} \sim 4\mu s$. As discussed in **??**, usually it is helpful to allow a experiment design heuristic (EDH) to choose the experimental controls, including the evoltuion time, t, against which the model is trained at each experiment; the default particle guess heuristic (PGH) attempts to select t at the upper boundary of times where the model is expected to be predictive, such as to maximise the information gained by the experiment (see Section 3.6.1). Here, however, we can not allow the EDH to select arbitrary t, since we do not have data beyond t_{max}.

Clearly, we require a custom EDH to account for the constraints outlined, with the following considerations:

1. We may only assume access to the probe $|+\rangle$ on the spin qubit

6 Note: in the case studies presented in this thesis, it was found that the same resources were sufficient for the simplest and most complex models, due to the relatively small number of terms therein. We expect for larger models, e.g. $|\vec{\alpha}| > 10$, that the resources allocated ought to be proportional to the cardinality, which is an in-built option in the QMLA software.

   (a) we further assume the environmental spin is polarised by the same microwave pulse, such that the global probe available is $|\psi\rangle = |+\rangle\,|+'\rangle$, with $|+'\rangle = \frac{|0\rangle + e^{i\phi}|1\rangle}{\sqrt{2}}$ and ϕ is random [**?**].

2. We can not allow the choice of any t
   (a) Any $t > t_{\text{max}}$, arising from a thin parameter distribution, must be mapped to some $0 < t \leq t_{\text{max}}$.
   (b) All nominated t must be mapped to the nearest available t in the dataset so that the likelihoods are as close as possible to simulating the true system.
3. Much of the physics of interest occurs at relatively high times, i.e. because the rotation (MHz) terms dominate, the decay of the peaks can be seen as evidence of the bath, notably through hyperfine terms in the model.
   (a) We therefore wish to enforce that all models are trained on those data ($t \geq 2\mu s$), even if their parameter distribution is insufficiently narrow to yield those times naturally.

Accounting for these, we construct an EDH which mixes the robust, adaptive nature of PGH, useful for refining an initially broad $\Pr(\vec{\alpha})$, with a primitive, linear time-selection, useful to ensure the trained parameters at least attempt to account for the physics we are actually interested in. That is, with each model trained for N_e experiments, we train according to the standard PGH for the first $N_e/2$, but force the training to mediate over the available data for the latter $N_e/2$.

9.5 RESULTS

We apply the ES described in Section 9.3 to the raw data of Fig. 9.3; the results are summarised in Fig. 9.5.

We first focus on the overall outcomes: the most blunt figure of merit of interest is simply whether QMLA overfits or underits the true parameterisation. In preliminary analysis we run 500 instances with varying $\hat{H}_0$, and where the cardinality of $\hat{H}_0$ ranges, so we can broadly gauge the tendency towards over- and under-fitting: we see that in $\sim$ 50% of instances the correct cardinality is found, rising to $\sim$ 86% by allowing one fewer (additional) terms, Fig. 9.5**(b)**. Moreover, the champion models' are highly predictive: the median coefficient of determination between the systems' and corresponding champion models' data is $R^2 = 0.84$.

Then, considering the performance of the algorithm on whole, we perform runs of 100 instances on the exerpimental data as well as simulated data, where the simulation assumes[7] $\hat{H}_0 = \hat{S}_{xyz}\hat{A}_z$, The set of models selected most frequently are shown in Fig. 9.5**(c)**, and each model is trained with $N_e = 1000, N_p = 3000$, with the volumes of those models (in

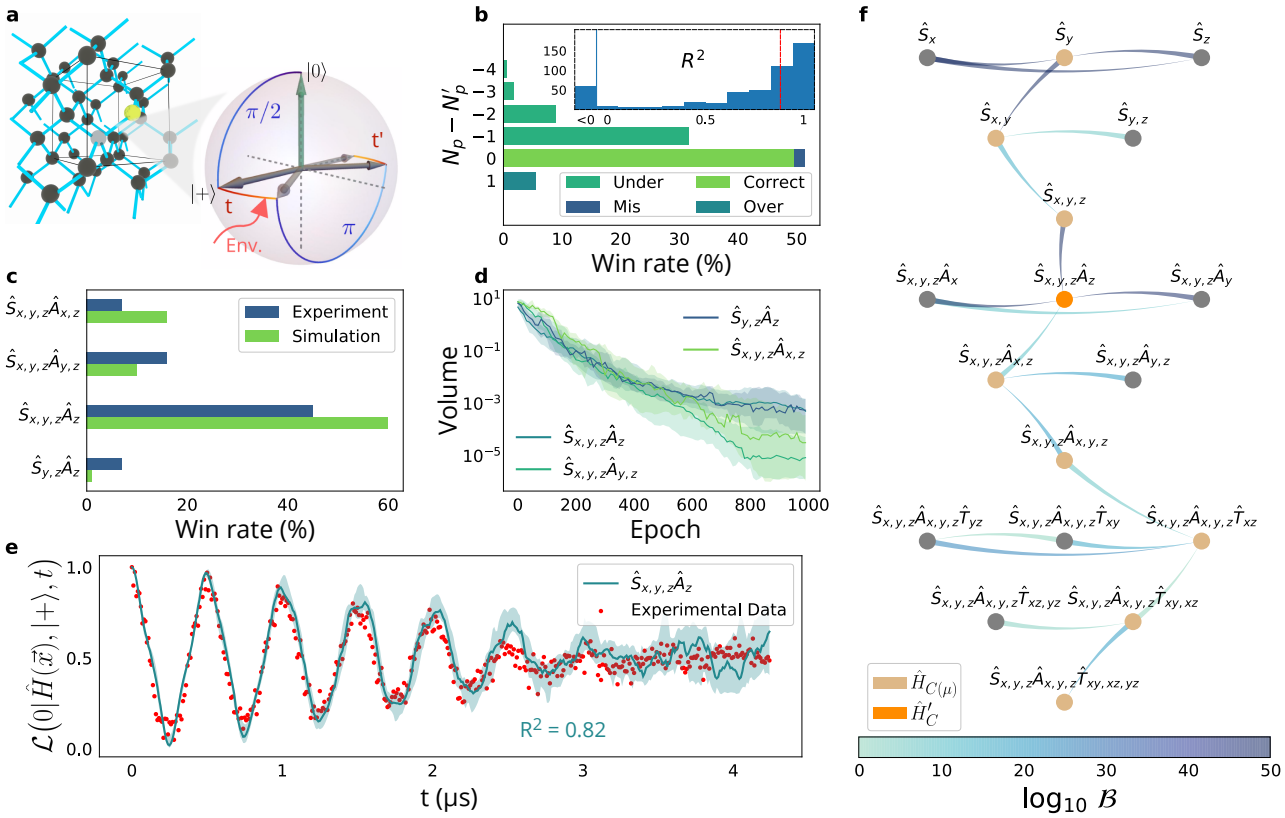

Figure 9.5: **a**, The carbon lattice providing the outer environment for the NV centre, along with the time evolution of the electron spin state (represented on a Bloch sphere) during the pulses for the Hahn-echo sequences. The final $\pi/2$ pulse is omitted. **b**, Simulation of 500 independent QMLA instances, where $\hat{H}_0$ is chosen randomly. The win rate is reported against the difference $(N_p - N'_p)$ between the number of parameters in $\hat{H}'$ and $\hat{H}_0$, respectively. The *under-parameterised (over-parameterised)* class refers to models with less (more) parameters than $\hat{H}_0$. *Correct* indicates that exactly $\hat{H}_0$ was found. The *mis-parameterised* class groups models with the same parametrisation cardinality as $\hat{H}_0$, but different Hamiltonian terms. **Inset**, Histogram of occurrences of R^2 values for each retrieved $\hat{H}'$ against a sampling of datapoints from $\hat{H}_0$, with median $R^2 = 0.84$ (red dotted line). **c**, Win rates of top four models for 100 QMLA instances, against both simulated and experimental data. Simulations use $\hat{H}_0 = \hat{S}_{x,y,z}\hat{A}_z$. **d**, Total volume spanned by the parameters' prior across epochs, for the models in **c**. Shaded areas indicate 66% credible regions. **e**, Simulated likelihoods reproduced by the model with the highest win rate ($\hat{S}_{x,y,z}\hat{A}_z$, turquoise), compared with corresponding NV-centre system experimental data (red-dots, extracted from the observed PL of the first Hahn-echo decay). Error bars smaller than the dots (see Methods). **f**, A single QMLA instance against experimental data in **e**, depicted as a directed acyclic graph (DAG). The thin end of each edge points to the favoured model; the colour of the edges maps $\log_{10} \mathcal{B}$ as in the bar legend at the bottom. Layer champions $\hat{H}_{C(\mu)}$are in light brown, whereas the global champion $\hat{H}'$ is in orange.

Model	Experiment		Simulation	
	Wins	R^2	Wins	R^2
$\hat{S}_{y,z}\hat{A}_z$	9	0.8	1	0.26
$\hat{S}_y\hat{A}_{x,z}$	2	0.63		
$\hat{S}_{x,y,z}\hat{A}_z$	45	0.86	61	0.97
$\hat{S}_{x,y,z}\hat{A}_y$			1	-0.54
$\hat{S}_{x,y,z}\hat{A}_{x,y}$	3	0.81		
$\hat{S}_{x,y,z}\hat{A}_{y,z}$	14	0.83	10	0.96
$\hat{S}_{x,y,z}\hat{A}_{x,z}$	6	0.64	15	0.99
$\hat{S}_{x,y,z}\hat{A}_{x,y,z}$	2	0.72	5	0.97
$\hat{S}_{x,y,z}\hat{A}_{x,z}\hat{T}_{xz}$			1	0.68
$\hat{S}_{x,y,z}\hat{A}_{x,y,z}\hat{T}_{xz}$			5	0.77
$\hat{S}_y\hat{A}_{x,y,z}\hat{T}_{xy,xz,yz}$	2	0.31		
$\hat{S}_{x,y,z}\hat{A}_{x,y,z}\hat{T}_{xy,xz}$	4	0.67	1	0.32

Table 9.1: QMLA win rate s and R^2 for models based on experimental data and simulations. We state the number of QMLA instances won by each model and the average R^2 for those instances as an indication of the predictive power of winning models.

the experimental case) shown in Fig. 9.5**(d)**. In particular, the most prominent models, $\{\hat{S}_{x,y,z}\hat{A}_z, \hat{S}_{x,y,z}\hat{A}_{y,z}, \hat{S}_{x,y,z}\hat{A}_{x,z}, \hat{S}_{y,z}\hat{A}_z\}$ are found collectively in 74% (87%) of instances on the experimental (simulated) data; the win rate and R^2 of all models (which won at least one instance) are reported in Table 9.1. It is noteworthy that even in the simulated case, the same models mislead QMLA: this suggests that the resultant physics from these models is substantially similar to that of the true model [8]. These models are defensible with respect to the descriptions of Section 9.2, since in each case they detect the interaction between the spin qubit and the environmental qubit, i.e. the hyperfine terms $\hat{A}_i$, especially $\hat{A}_z$ which occurs in 97% (99%) of champions. We discuss some physical insights from these results in Section 9.5.1.

The most frequently found model, $\hat{H}' = \hat{S}_{x,y,z}\hat{A}_z$, is found in 45% (61%) of instances: we show its attempt to reproduce the dynamics of Fig. 9.3 in Fig. 9.5**(e)**, showing excellent agreement with the raw data, with $R^2 = 0.82$. This serves as an essential sanity check: we can intuitively see that QMLA has distilled a model which captures at least *some* of the most important physical

7 Here we work backwards by setting the target model as that which QMLA deemed most appropriate for the available data. We posit that this choice is arbitrary and doesn't fundamentally change the discussion of this chapter, merely aiding in analysing the performance of the algorithm with respect to a concrete example.

8 Alternatively, that the same systematic error misdirects the search in both cases.

interactions the target NVC system is subject to; otherwise we would not see such clear overlap between the prediced and true dynamics.

Finally we display the model search as a DAG in Fig. 9.5**(f)**, where models are represented on nodes on the graphs layers (equivalent to ET branches), and their parents are resident on the branch immediately above their own. Comparisons between models, $\hat{H}_i, \hat{H}_j$, are shown as edges between nodes on the graph, coloured by the strength of evidence of the outcome, the BF, B_{ij}. Each layer, μ, nominates their branch champion, $\hat{H}_{C(\mu)}$; the set of branch champions are consolidated to determine the global champion, $\hat{H}'_C$.

9.5.1 *Analysis*

Considering the runs summarised in Fig. 9.5, here we will present some furhter perspecitives. Fig. 9.6 first details all models considered in the 200 instances comprising the experimental and simulated QMLA runs, as well as the win rate of each model. This ES is designed to study a small subspace of the overall available space: only 40 unique models are constructed. We highlight a number of *credible* models which we deem especially valid approximations of the target system, i.e. which contain the most viable approximations.

Fig. 9.7 shows the reproduction of dynamics of the top four models from both simulated and experimental runs. We see that each model faithfully captures the essential dynamics arising from the respective target systems; this alone is insufficient to conclude that the true model has been identified, but serves as a valuable *sanity-check*, convincing us that the output of QMLA is at least a sensible approximation of $\hat{H}_0$, if not the absolutely true model .

The key insight promised by QMLA is to identfiy the interactions present in the studied system. In Fig. 9.8 we show the number of times each of the terms permitted (Eq. (9.10)) is included in the champion model; we also show the distribution of parameter estimates for those terms. From the simulated case, we see that those terms which are in $\hat{H}_0$, i.e. $\mathcal{T}_0$, are found in almost all instances; furthermore, while some terms are erroneoulsy found in $> 40\%$ of instances, they are found with less than a quarter of the frequency of the true terms, so these may be reasonably ruled out in post-processing the QMLA results. The inaccurate terms found most often are seen to have (almost) negligible parameters: in conjunction with domain expertise, users can determine whether the inclusion of these terms are meaningful or simply artefacts of slight overfitting. In the experimental run, on the other hand, we see a similar gulf in frequency between some terms. Namely, $\{\hat{S}_x, \hat{S}_y, \hat{S}_z, \hat{A}_z\}$ are found in 50+ more instances than all others: we therefore conclude that those terms contribute most strongly to the NVC. The parameters found for these terms are of the same order of magnitude as we would have predicted originally, but disagreee in the precise value. For example, the rotation about the y-axis, $\hat{S}_y$, has frequency 5.7MHz, roughly twice the predicted value of 2.7MHz.

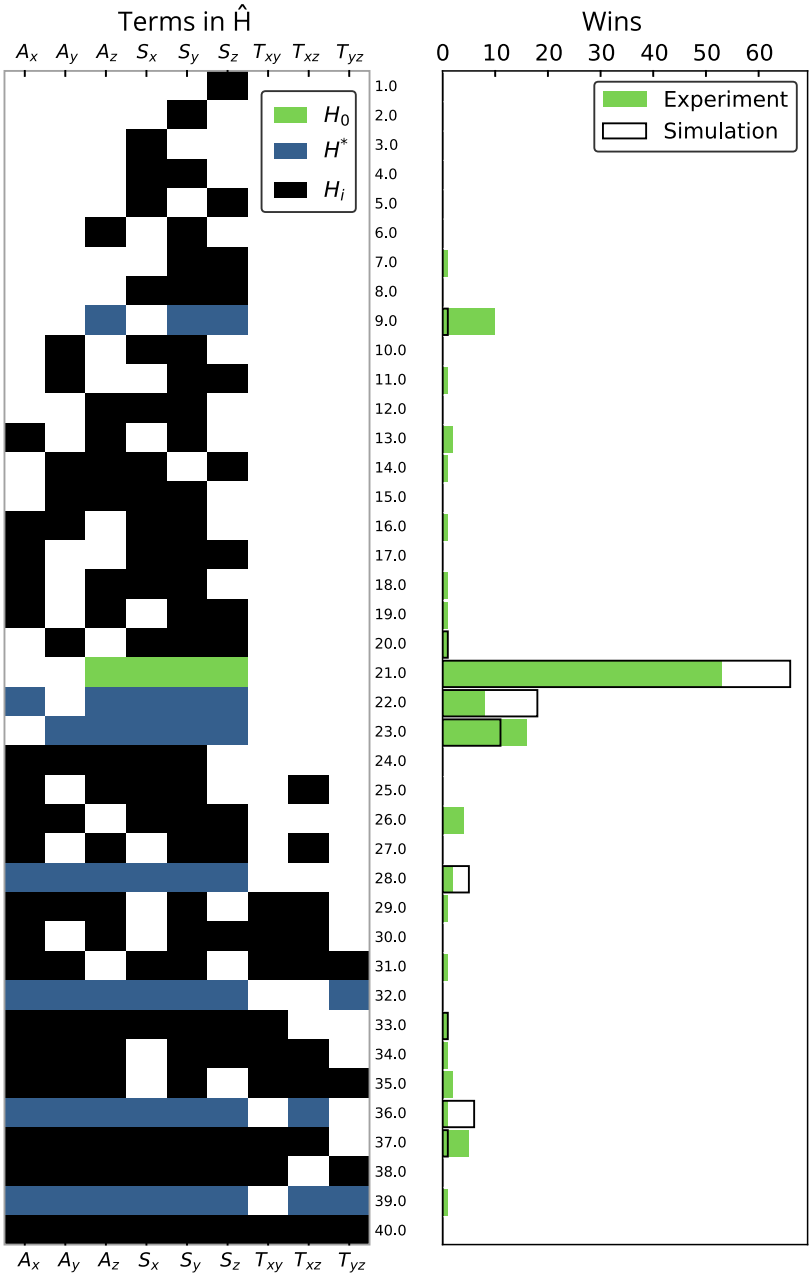

Figure 9.6: **Left**: map of the various Hamiltonian terms included in each of the possible 40 candidate models explored by QMLA during any of the 100 instances on either simulated or experimental data. The explicit form of each operator can be inferred from **??**. IDs of candidate models are on the vertical axis, and labels for the terms on the horizontal axis. The true model $\hat{H}_0$ for the simulated case is highlighted in green and a subset of credible models in blue, i.e. models which may reasonbaly be expected to describe the NVC from theoretical arguments. **Right**: wins for each of the candidate models as above out of 100 independent QMLA runs, reported as a histogram for cases adopting simulated data (empty bars) or the experimental dataset.

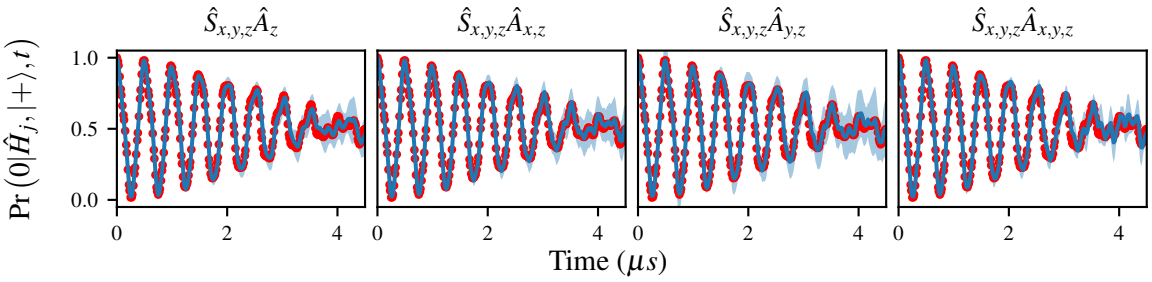

a, Simulated data

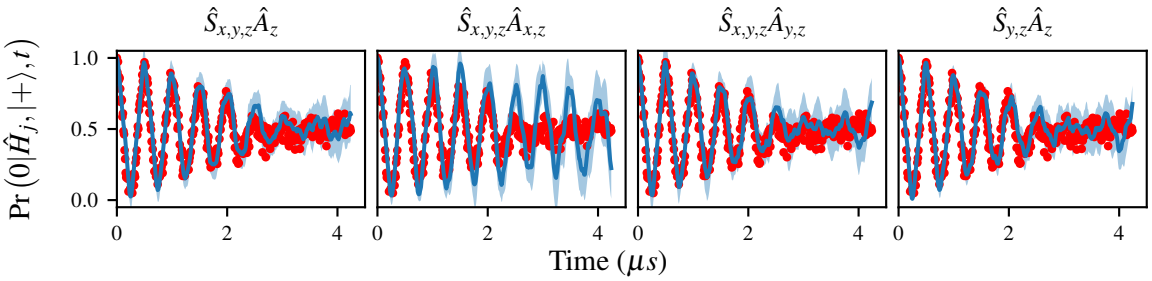

b, Experimental data

Figure 9.7: Dynamics reproduced by various QMLA champion models for simulated/experimental data. Expectation values are shown on y–axis with time on x–axis. Red dots give the true dynamics of $\hat{H}_0$, while the blue lines show the median reconstruction by $\hat{H}'$ from all the instances where that model was deemed $\hat{H}'$, with light blue showing the standard deviation of those likelihoods . $\hat{H}'$ is listed on top of each plot; the number of instances won by each model can be read from Table 9.1.

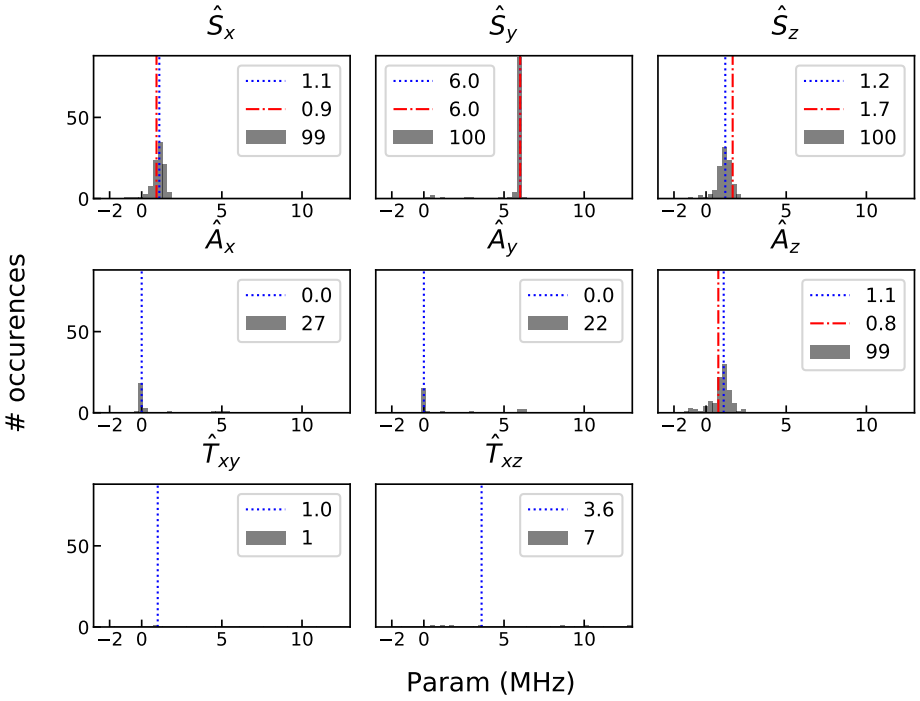

a, Simluated QMLA instances. Red dotted lines show the true parameters.

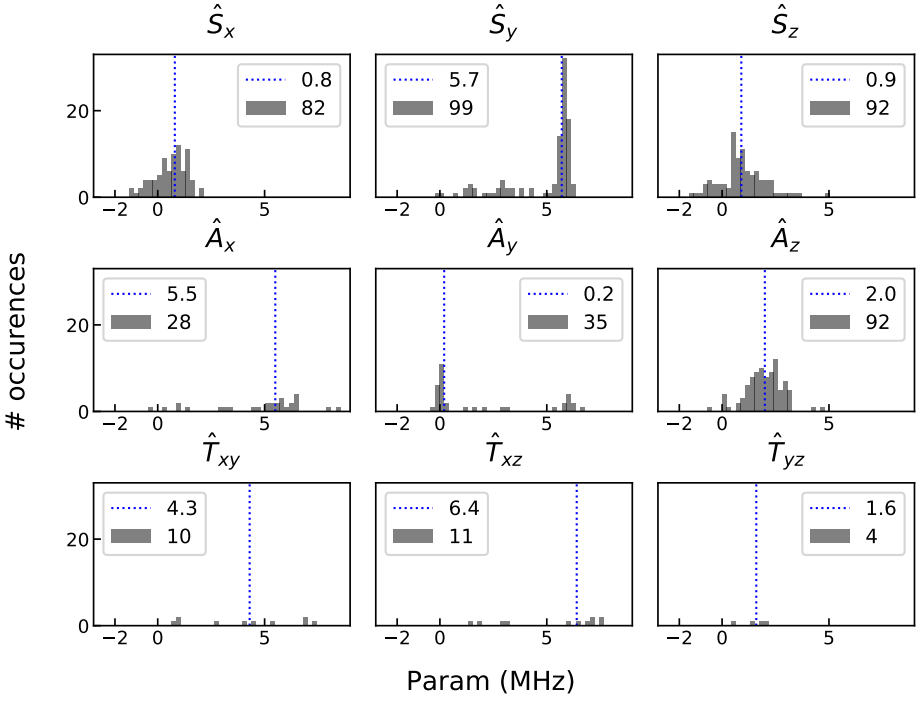

b, Experimental QMLA instances.

Figure 9.8: Histograms for parameters learned by QMLA champion models on (**a**) simulated and (**b**) experimental data. Blue dotted lines indicate the median for that parameter; grey blocks show the number of models which found the parameter to have that value and the number listed in the legend reports how many champion models contained that term.

10 LARGER SYSTEMS

Chapter 9 concerned a two-qubit approximation of the short-time dynamics of an NVC. It is valid criticism of this analysis that the model space searched was reduced substantially from prior knowledge, and it therefore remains to test QMLA in a large model space, on physically meaningful data. In this chapter, we extend QMLA, to consider appoximations of NVC sytems using more qubits, representing several nuclear sites, which aim to capture the interactions between the target NVC and the environment. We will simulate the target system here, allowing us to make definite statements on the performance of QMLA, unlike the experimental data where we can not be sure of the dynamics' genreator.

10.1 TARGET SYSTEM

A more realistic model may be expected from consdiering the environment as a finite-size bath, consisting of n_s nuclear spins in addition to the NVC spin, i.e. the total number of qubits of such a model is $n_q = 1 + n_s$. Such effects can be highlighted by Hahn echo measurements, as in Fig. 9.2, except reversing the evoluting by $t' = t$ instead of $t' = 2t$ [**?**, **?**], so our simulations will use this measurement scheme.

Since we are simulating the target system, we may choose the approximation we wish to invoke. We use the secular approximation, i.e. we assume the magnetic field is perfectly aligned along the z-axis [**?**]: recalling Eq. (9.1), the NVC spin qubit rotates only about the z-axis, and coupling between the electron and nuclear qubits are only via $\hat{S}_z \cdot \hat{A}_z^{\chi}$. We include the effect of the nuclear spins' rotations, which are much weaker. In total then, the set of nuclear spins, $\{\chi\}$, are mapped to n_s qubits:

$$\hat{H}_0 = \hat{S}_z + \sum_{j=2}^{n_q} \hat{S}_z \cdot \hat{A}_z^j + \sum_{w \in \{x,y,z\}} \sum_{j=2}^{n_q} \hat{I}_w^j. \tag{10.1}$$

For simplicity, we restate this in terms only of the Pauli matrices, where the first qubit refers to the NVC and the remaining qubits give the interactions and nuclear terms.

$$\hat{H}_0 = \hat{\sigma}_z^1 + \sum_{j=2}^{n_q} \hat{\sigma}_z^1 \hat{\sigma}_z^j + \sum_{w \in \{x,y,z\}} \sum_{j=2}^{n_q} \hat{\sigma}_w^j, \tag{10.2}$$

so in total, $\mathcal{T}_0$ has 1 term for the NVC qubit, n_s terms for hyperfine couplings and $3n_s$ terms for the nuclei: $|\mathcal{T}_0| = 1 + 4n_s$.

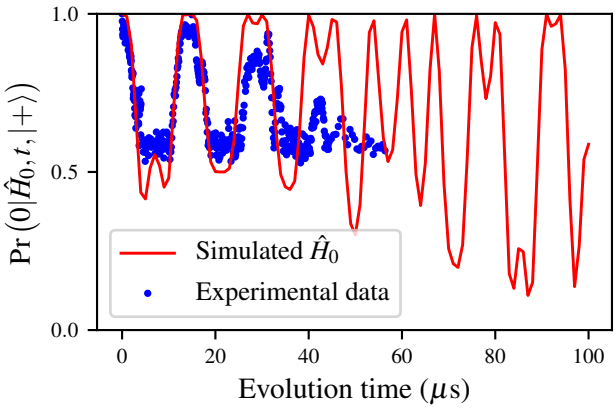

Figure 10.1: Long-time dynamics for nitrogen-vacancy centre, red, showing revivals, generated by $\hat{H}_0$ from Eq. (10.2), via Hahn echo measurement with $t' = t$. For comparison, experimentally generated dynamics are shown in blue.

We set the goal of QMLA as finding the approximation of Eq. (10.2), by allowing it to consider a wider set of terms. The permissible terms are then all spin rotation terms, as well as all nuclei rotation terms, and the coupling terms:

$$\mathcal{T} = \left\{ \begin{array}{c} \hat{S}_w = \hat{\sigma}^1_w, \\ \hat{I}^j_w = \hat{\sigma}^j_w, \\ \hat{S}_w \cdot \hat{A}_w = \hat{\sigma}^1_w \hat{\sigma}^j_w \end{array} \right\} \tag{10.3}$$

for $w = \{x, y, z\}$ and $j \in \{2, ..., n'_q\}$. Importantly, in general $n'_s + 1 = n'_q \neq n_q$, i.e. QMLA can search a space of models with more or less spins, n'_s, than are truly in $\hat{H}_0$. In total then, $|\mathcal{T}| = 3 + 3n'_s + 3n'_s = 3 + 6n'_s$.

We set the system parameters based on theoretical predictions, listed in Table 10.1.

Here our aim is to test QMLA, so the choice of n_s and n'_s are arbitrary; for the target system we use $n_s = 4$ proximal spins, so that, from Eq. (10.2), $|\mathcal{T}_0| = 13$, and we allow candidates to consider $n'_s = 5$, so $|\mathcal{T}| = 33$.

In summary, irrespective of the underlying physics we are simulating, here QMLA is aiming to identify the 13 terms truly present in Q, while searching the space of 33 permissible terms. Without imposing any restrictions on which combinations of terms are allowed, each term is simply either in $\hat{H}'$ or not, so can be thought of as binary variables: the total model space is therefore of size $2^{33} \approx 10^{10}$.

Term	$\hat{t}$	Meaning	Parameter (Hz) $\in \hat{H}_0$	
$\hat{S}_x$	$\hat{\sigma}_x^1$	NVC rotation about x-axis	2×10^9	No
$\hat{S}_y$	$\hat{\sigma}_y^1$	NVC rotation about y-axis	2×10^9	No
$\hat{S}_z$	$\hat{\sigma}_z^1$	NVC rotation about z-axis	2×10^9	Yes
$\hat{S}_x \cdot \hat{A}_x^j$	$\hat{\sigma}_x^1\hat{\sigma}_x^j$	Coupling b/w spin and j^{th} nuclear qubit about x-axis	0.2×10^6	No
$\hat{S}_y \cdot \hat{A}_y^j$	$\hat{\sigma}_y^1\hat{\sigma}_y^j$	Coupling b/w spin and j^{th} nuclear qubit about y-axis	0.2×10^6	No
$\hat{S}_z \cdot \hat{A}_z^j$	$\hat{\sigma}_z^1\hat{\sigma}_z^j$	Coupling b/w spin and j^{th} nuclear qubit about z-axis	0.2×10^6	Yes
$\hat{I}_x^j$	$\hat{\sigma}_x^j$	j^{th} nuclear spin rotation about x-axis	66×10^3	Yes
$\hat{I}_y^j$	$\hat{\sigma}_y^j$	j^{th} nuclear spin rotation about y-axis	66×10^3	Yes
$\hat{I}_z^j$	$\hat{\sigma}_z^j$	j^{th} nuclear spin rotation about z-axis	15×10^3	Yes

Table 10.1: Extended model NVC terms

10.2 GENETIC ALGORITHM

GAs provide a robust and thoroughly tested paradigm for searching large candidate spaces; this is a natural framework through which we can explore such an unresetricted model space. We have already extensively discussed the formalism of GAs in Chapter 8, and specifically in the context of QMLA in Section 8.1. Here we will use the same ES as described in Chapter 8, i.e. where model generation is driven by a GA, and models are cast to chromosomes. In particular, candidate model's fitness will be computed from the residuals between their and the sytem's dynamics, described fully in Section 8.2.6. This objective function (OF) relies on the definition of a validation dataset, $\mathcal{E}_v$, which we compose of tomographic probes and times generated uniformly up to $t_{max} = 100\mu s$, Fig. 10.2.

10.2.1 *Parameter learning*

Here, our primary goal is to validate QMLA's performance in a very large model space, with over 10^{10} valid candidates. Our focus on model generation, then, we do *not* train models individually: instead we assume access to a *perfect* parameter learning subroutine. That is, for each candidate considered, we simply assume knowledge of its parameters, $\vec{\alpha}$. This is a major caveat to the results of this chapter: no such perfect training scheme is known, so it remains to examine the detrimental effects of imprecisely finding $\vec{\alpha}' \approx \vec{\alpha}$. Moreover, while it is possible to extract information on the nuclear qubits from measuring only the NVC qubit, as in the Hahn

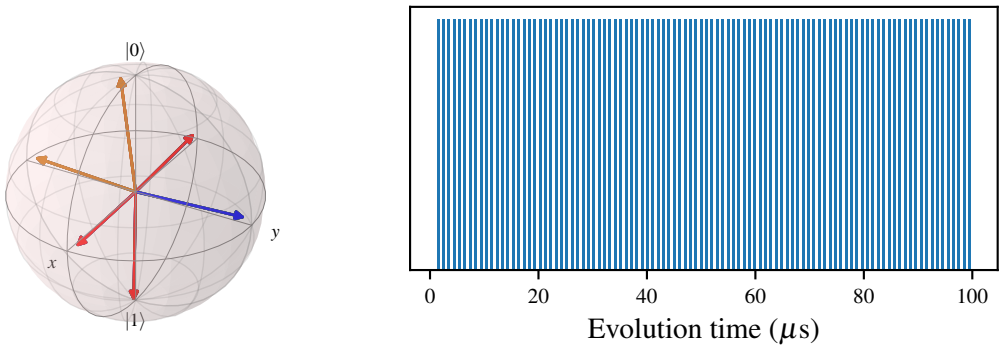

Figure 10.2: Evaluation dataset, $\mathcal{E}_v$, for nitrogen-vacancy centre genetic algorithm. **Left**, Probe state the NVC qubit is prepared in, on the Bloch sphere, i.e. Ψ_v is close to the tomographic basis. **Right**, Time comb evaluated against, i.e. uniformly distributed times up to $t_{max} = 100\mu$s are used for experiments in $\mathcal{E}_v$.

echo measurements, it is uncertain whether any technique can simultaneously detect parameters of significantly varying orders of magnitude; For instance, some terms in Table 10.1 are $\mathcal{O}(\text{GHz})$, while others are $\mathcal{O}(\text{kHz})$; it is likely to prove difficult to discern the kHz parameters well, given that their contribution is equivalent to errors of order $\mathcal{O}(10^{-6})$ in the dominant GHz terms. Therefore we must caution that the results presented here, while demonstrating that QMLA *can* operate in large model spaces, are not immediately applicable to experimental systems, since there are outstanding challenges in the assessment of individual candidates, which must be overcome before the technique outlined can realisitcally succeed.

10.2.2 *Results*

At the instance level, we can see that the gene pool tends towards models of higher quality, captured by their F_1-score, Fig. 10.3**a**. The improvement in modelling is reflected in the branch champions' predictive power at reproducing data generated by the system, Fig. 10.3**b**.

Considering the overall run, we see that QMLA is searching in a vast model space where randomly sampled models have poor F_1-score on average, Fig. 10.4**a**. QMLA efficiently explores the space by quickly moving into a subspace of high F_1-score, nominating $\hat{H}' = \hat{H}_0$ precisely in 85% of instances, Fig. 10.4**b,c**. The number of times each of the terms considered, Eq. (10.3), are present in $\hat{H}_0$ offers the most important insight from QMLA, namely the evidence in favour of each term's presence, which can be used to infer the most likely underlying physics. Here, $\hat{t} \in \mathcal{T}_0$ are found in $\geq 94\%$ of instances, while $\hat{t} \notin \mathcal{T}_0$ are found in $\leq 11\%$, shown in Fig. 10.5 and listed in Table 10.2. Such a discrepency, as well as the win rates for the models, allows for the clear declaration of the model $\hat{H}_0$ as the favoured representation for the quantum system.

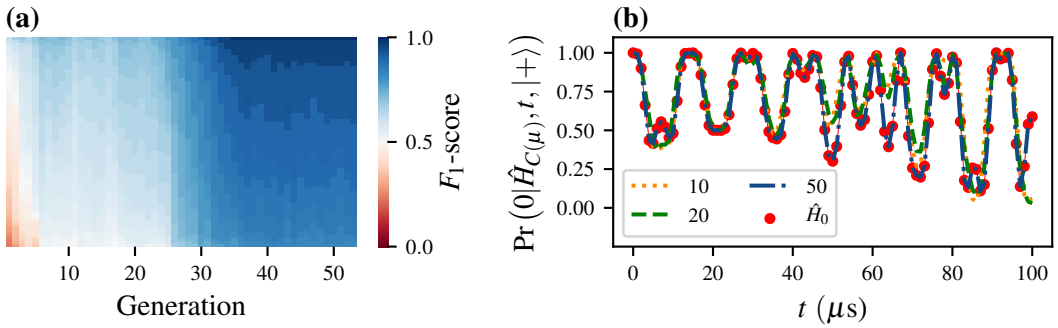

Figure 10.3: Instance of the genetic algorithm for simulated nitrogen-vacancy centre system with four qubits. **a**, Branch champions' dynamics. Each generation, μ, nominates a branch champion, $\hat{H}_{C(\mu)}$. Here, progressive generations' champions dynamics are shown against those of the target system, $\hat{H}_0$ (red). **b**, Gene pool progression for the GA. Each tile represents a candidate model by its F_1-score. Each generation considers $N_m = 72$ models; the GA runs for $N_g = 53$ generations.

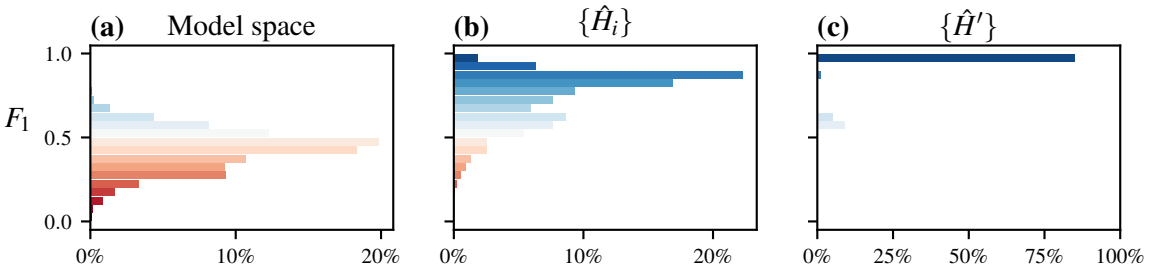

Figure 10.4: Nitrogen-vacancy centre genetic algorithm run. **(a)**, F_1-score of 10^6 samples from the model space of $2^{33} \approx 10^{10}$ candidate models, normally distributed around $f = 0.44 \pm 0.12$. **(b)**, The models explored during the model search of all instances combined, $\{\hat{H}_i\}$, show that QMLA tends towards stronger models overall, with $f = 0.79 \pm 0.16$ from $\sim 140,000$ chromosomes across the 100 instances, i.e. each instance tests $\sim$ 1400 distinct models. **(c)**, Champion models from each instance, showing QMLA finds strong models in general, and in particular finds the true model ($\hat{H}_0$, with $f = 1$) in 85% of cases.

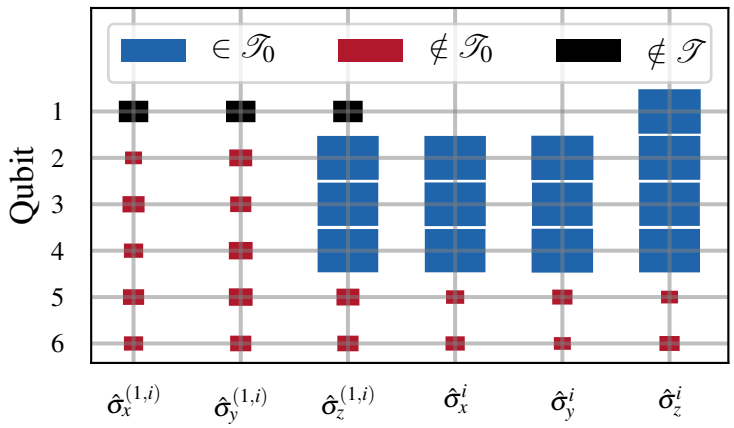

Figure 10.5: Hinton diagram of terms found for 4-qubit nitrogen-vacancy centre model. Terms are either in the target model ($\in \mathcal{T}_0$, blue) or not ($\notin \mathcal{T}_0$, red), or else not considered ($\notin \mathcal{T}$, black). Terms acting solely on the first qubit are the NVC spin's rotation terms, $\hat{\sigma}_w^1$, while each nuclear site also has rotation terms $\hat{\sigma}_w^j$. Hyperfine terms, $\hat{\sigma}_w^{(1,j)}$, couple the NVC qubit with the j^{th} nuclear spin. The precise rate at which each term is detected can be read from Table 10.2.

Qubit	$\hat{\sigma}_x^{(1,i)}$	$\hat{\sigma}_y^{(1,i)}$	$\hat{\sigma}_z^{(1,i)}$	$\hat{\sigma}_x^i$	$\hat{\sigma}_y^i$	$\hat{\sigma}_z^i$
1	-	-	-	0	0	100
2	5	11	97	97	99	97
3	10	9	94	96	94	94
4	7	12	94	94	97	95
5	9	12	11	6	8	5
6	7	9	9	7	5	8

Table 10.2: Percentage of instances for which each term is found by QMLA GA studying NVC system.

APPENDIX

A

FIGURE REPRODUCTION

Most of the figures presented in the main text are generated directly by the QMLA framework. Here we list the implementation details of each figure so they may be reproduced by ensuring the configuration in Table A.1 are set in the launch script. The default behaviour of QMLA is to generate a results folder uniquely identified by the date and time the run was launched, e.g. results can be found at the *results directory* qmla/Launch/Jan_01/12_34. Given the large number of plots available, ranging from high-level run perspective down to the training of individual models, we introduce a plot_level $\in \{1, ..., 6\}$ for each run of QMLA: higher plot_level informs QMLA to generate more plots.

Within the results directory, the outcome of the run's instances are stored, with analysis plots broadly grouped as

4. evaluation: plots of probes and times used as the evaluation dataset.
5. single_instance_plots: outcomes of an individual QMLA instance, grouped by the instance ID. Includes results of training of individual models (in model_training), as well as sub-directories for anlaysis at the branch level (in branches) and comparisons.
6. combined_datasets: pandas dataframes containing most of the data used during analysis of the run. Note that data on the individual model/instance level may be discarded so some minor analyses can not be performed offline.
7. exploration_strategy_plots plots specifically required by the ES at the run level.
8. champion_models: analysis of the models deemed champions by at least one instance in the run, e.g. average parameter estimation for a model which wins multiple instances.
9. performance: evaluation of the QMLA run, e.g. the win rate of each model and the number of times each term is found in champion models.
10. meta analysis of the algorithm' implementation, e.g. timing of jobs on each process in a cluster; generally users need not be concerned with these.

In order to produce the results presented in this thesis, the configurations listed in Table A.1 were input to the launch script. The launch scripts in the QMLA codebase consist of many configuration settings for running QMLA; only the lines in snippet in Listing A.1 need to be set according to altered to retrieve the corresponding figures. Note that the runtime of QMLA grows quite quickly with N_e, N_p (except for the AnalyticalLikelihood ES), especially for the entire QMLA algorithm; running QHL is feasible on a personal computer in < 30 minutes for $N_e = 1000; N_p = 3000$.

```
#!/bin/bash
```

```
###############
# QMLA run configuration
###############
num_instances=1
run_qhl=1 # perform QHL on known (true) model
run_qhl_mulit_model=0 # perform QHL for defined list of models.
exp=200 # number of experiments
prt=1000 # number of particles

###############
# QMLA settings
###############
plot_level=6
debug_mode=0

###############
# Choose an exploration strategy
###############

exploration_strategy='AnalyticalLikelihood'
```

Listing A.1: QMLA Launch scipt

Figure	Exploration Strategy	N_E	N_P	Data
Fig. 3.3	DemoHeuristicPGH	1000	3000	Nov_27/19_39
	DemoHeuristicNineEighths	1000	3000	Nov_27/19_40
	DemoHeuristicTimeList	1000	3000	Nov_27/19_42
	DemoHeuristicRandom	1000	3000	Nov_27/19_47
Fig. 3.4	DemoProbesPlus	1000	3000	Nov_27/14_43
	DemoProbesZero	1000	3000	Nov_27/14_45
	DemoProbesTomographic	1000	3000	Nov_27/14_46
	DemoProbes	1000	3000	Nov_27/14_47
Fig. 3.5	DemoProbesPlus	1000	3000	Nov_27/14_43
	DemoProbesZero	1000	3000	Nov_27/14_45
	DemoProbesTomographic	1000	3000	Nov_27/14_46
	DemoProbes	1000	3000	Nov_27/14_47
Fig. 3.2	AnalyticalLikelihood	500	2000	Nov_16/14_28
Fig. 6.2	DemoIsing	500	5000	Nov_18/13_56
Fig. 6.3	DemoIsing	1000	5000	Nov_18/13_56
Fig. 6.4	DemoIsing	1000	5000	Nov_18/13_56
Fig. 6.5	IsingLatticeSet	1000	4000	Nov_19/12_04
	IsingLatticeSet	1000	4000	Nov_19/12_04
	IsingLatticeSet	1000	4000	Nov_19/12_04
Fig. 6.6	IsingLatticeSet	1000	4000	Sep_30/22_40
	HeisenbergLatticeSet	1000	4000	Oct_22/20_45
	FermiHubbardLatticeSet	1000	4000	Oct_02/00_09

Table A.1: Implementation details for figures used in the main text.

Figure	Exploration Strategy	N_E	N_P	Data
Fig. 8.2	DemoBayesFactorsByFscore	500	2500	Dec_09/12_29
	DemoFractionalResourcesBayesFactorsByFscore	500	2500	Dec_09/12_31
	DemoBayesFactorsByFscore	1000	5000	Dec_09/12_33
	DemoBayesFactorsByFscoreEloGraphs	500	2500	Dec_09/12_32
Fig. 8.5	HeisenbergGeneticXYZ	500	2500	Dec_10/14_40
Fig. 8.6	HeisenbergGeneticXYZ	500	2500	Dec_10/14_40
	HeisenbergGeneticXYZ	500	2500	Dec_10/14_40
Fig. 8.7	HeisenbergGeneticXYZ	500	2500	Dec_10/16_12
	HeisenbergGeneticXYZ	500	2500	Dec_10/16_12
Fig. 9.6	NVCentreExperimentalData	1000	3000	2019/Oct_02/18_01
	SimulatedExperimentNVCentre	1000	3000	2019/Oct_02/18_16
Fig. 9.7	NVCentreExperimentalData	1000	3000	2019/Oct_02/18_01
Fig. 9.6	SimulatedExperimentNVCentre	1000	3000	2019/Oct_02/18_16
Fig. 9.8	SimulatedExperimentNVCentre	1000	3000	2019/Oct_02/18_16
	NVCentreExperimentalData	1000	3000	2019/Oct_02/18_01
Fig. 10.2	NVCentreGenticAlgorithmPrelearnedParameters	2	5	Sep_09/12_00
	NVCentreGenticAlgorithmPrelearnedParameters	2	5	Sep_09/12_00
Fig. 10.3	NVCentreGenticAlgorithmPrelearnedParameters	2	5	Sep_09/12_00
	NVCentreGenticAlgorithmPrelearnedParameters	2	5	Sep_09/12_00

Table A.2: [Continued from Table A.1] Implementation details for figures used in the main text.

B

FUNDAMENTALS

There are a number of concepts which are fundamental to any discussion of QM, but are likely to be known to most readers, and are therefore cumbersome to include in the main body of the thesis. We include them here for completeness[1].

B.1 LINEAR ALGEBRA

Here we review the language of linear algebra and summarise the basic mathematical techniques used throughout this thesis. We will briefly recall some definitions for reference.

- Notation

Definition of	Representation
Vector (or *ket*)	$\|\psi\rangle$
Dual Vector (or *bra*)	$\langle\psi\|$
Tensor Product	$\|\psi\rangle \otimes \|\phi\rangle$
Complex conjugate	$\|\psi^*\rangle$
Transpose	$\|\psi\rangle^T$
Adjoint	$\|\psi\rangle^\dagger = (\|\psi\rangle^*)^T$

Table B.1: Linear algebra definitions.

The dual vector of a vector (ket) $|\psi\rangle$ is given by $\langle\psi| = |\psi\rangle^\dagger$.

The *adjoint* of a matrix replaces each matrix element with its own complex conjugate, and then switches its columns with rows.

$$M^\dagger = \begin{pmatrix} M_{0,0} & M_{0,1} \\ M_{1,0} & M_{1,1} \end{pmatrix}^\dagger = \begin{pmatrix} M^*_{0,0} & M^*_{0,1} \\ M^*_{1,0} & M^*_{1,1} \end{pmatrix}^T = \begin{pmatrix} M^*_{0,0} & M^*_{1,0} \\ M^*_{0,1} & M^*_{1,1} \end{pmatrix} \tag{B.1}$$

1 Much of this description is reproduced from my undergraduate thesis [?].

The *inner product* of two vectors, $|\psi\rangle = \begin{pmatrix} \psi_1 \\ \psi_2 \\ \vdots \\ \psi_n \end{pmatrix}$ and $|\phi\rangle = \begin{pmatrix} \phi_1 \\ \phi_2 \\ \vdots \\ \phi_n \end{pmatrix}$ is given by

$$\langle\phi|\psi\rangle = (|\phi\rangle^\dagger)\,|\psi\rangle = (\phi_1^* \ \phi_2^* \ \dots \ \phi_n^*) \begin{pmatrix} \psi_1 \\ \psi_2 \\ \vdots \\ \psi_n \end{pmatrix} = \phi_1^*\psi_1 + \phi_2^*\psi_2 + \cdots + \phi_n^*\psi_n \tag{B.2}$$

$|\psi\rangle_i, |\phi\rangle_i$ are complex numbers, and therefore the above is simply a sum of products of complex numbers. The inner product is often called the *scalar product*, which is in general complex.

B.2 POSTULATES OF QUANTUM MECHANICS

There are numerous statements of the postulates of quantum mechanics. Each version of the statements aims to achieve the same foundation, so we endeavour to explain them in the simplest terms.

1 Every moving particle in a conservative force field has an associated wave-function, $|\psi\rangle$. From this wave-function, it is possible to determine all physical information about the system.

2 All particles have physical properties called observables (denoted Q). In order to determine a value, Q, for a particular observable, there is an associated *operator* $\hat{Q}$, which, when acting on the particles wavefunction, yields the value times the wavefunction. The observable Q is then the eigenvalue of the operator $\hat{Q}$.

$$\hat{Q}\,|\psi\rangle = q|\psi\rangle \tag{B.3}$$

3 Any such operator $\hat{Q}$ is Hermitian

$$\hat{Q}^\dagger = \hat{Q} \tag{B.4}$$

4 The set of eigenfunctions for any operator $\hat{Q}$ forms a complete set of linearly independent functions.

5 For a system with wavefunction $|\psi\rangle$, the expectation value of an observable Q with respect to an operator $\hat{Q}$ is denoted by $\langle q\rangle$ and is given by

$$\langle q\rangle = \langle\psi|\hat{Q}|\psi\rangle \tag{B.5}$$

6 The time evolution of $|\psi\rangle$ is given by the time dependent *Schrodinger Equation*

$$i\hbar\frac{\partial\psi}{\partial t} = \hat{H}\psi, \tag{B.6}$$

where $\hat{H}$ is the system's Hamiltonian.

Using these building blocks, we can begin to construct a language to describe quantum systems.

B.3 STATES

An orhthonormal basis consists of vectors of unit length which do not overlap, e.g. $|x_1\rangle = \begin{pmatrix}1\\0\end{pmatrix}, |x_2\rangle = \begin{pmatrix}0\\1\end{pmatrix} \Rightarrow \langle x_1|x_2\rangle = 0$. In general, if $\{|x\rangle\}$ are the eigenstates of a system, then the system can be written as some state vector, $|\psi\rangle$, in general a superposition over the basis-vectors:

$$|\psi\rangle = \sum_x a_x|x\rangle \tag{B.7a}$$

$$\text{subject to} \quad \sum_x |a_x|^2 = 1, \quad a_x \in \mathbb{C} \tag{B.7b}$$

The *state space* of a physical system (classical or quantum) is then the set of all possible states the system can exist in, i.e the set of all possible values for $|\psi\rangle$ such that Eq. (B.7b) are satisfied.

For example, photons can be polarised horizontally ($\leftrightarrow$) or vertically ($\updownarrow$); take those two conditions as observable states to define the eigenstates of a two-level system, so we can designate the photon as a qubit. Then we can map the two states to a 2-dimensional, x-y plane: a general vector on such a plane can be represented by a vector with coordinates $\begin{pmatrix}x\\y\end{pmatrix}$. These polarisations can then be thought of as standard basis vectors in linear algebra. Denote $\leftrightarrow$ as the eigenstate $|0\rangle$ and $\updownarrow$ as $|1\rangle$

$$|\leftrightarrow\rangle = |0\rangle = \begin{pmatrix}1\\0\end{pmatrix} \qquad \text{A unit vector along x-axis} \tag{B.8a}$$

$$|\updownarrow\rangle = |1\rangle = \begin{pmatrix}0\\1\end{pmatrix} \qquad \text{A unit vector along y-axis} \tag{B.8b}$$

Now, in relation to the concept of superposition, we can consider, for example, a photon in an even superposition of the vertical and horizontal polarisations, evenly splitting the two basis vectors. As such, we would require that, upon measurement, it is equally likely that the

photon will *collapse* into the polarised state along x as it is to collapse along y. That is, we want $\Pr(\updownarrow) = \Pr(\leftrightarrow)$ so assign equal modulus amplitudes to the two possibilities:

$$|\psi\rangle = a\,|\leftrightarrow\rangle + b\,|\updownarrow\rangle\,, \quad \text{with} \quad \Pr(\updownarrow) = \Pr(\leftrightarrow) \Rightarrow |a|^2 = |b|^2 \tag{B.9}$$

We consider here a particular case, due to the significance of the resultant basis, where $\leftrightarrow$-polarisation and $\updownarrow$-polarisation have real amplitudes $a, b \in \mathbb{R}$.

$$\begin{aligned} &\Rightarrow a = \pm b \quad \text{but also} \quad |a|^2 + |b|^2 = 1 \\ \Rightarrow \quad &a = \frac{1}{\sqrt{2}} \quad ; \quad b = \pm\frac{1}{\sqrt{2}} \\ &\Rightarrow |\psi\rangle = \frac{1}{\sqrt{2}}\,|\leftrightarrow\rangle \pm \frac{1}{\sqrt{2}}\,|\updownarrow\rangle \\ &\Rightarrow |\psi\rangle = \frac{1}{\sqrt{2}}\,|0\rangle \pm \frac{1}{\sqrt{2}}\,|1\rangle \end{aligned} \tag{B.10}$$

These particular superpositions are of significance:

$$|+\rangle = \frac{1}{\sqrt{2}}\,(|0\rangle + |1\rangle) \tag{B.11a}$$

$$|-\rangle = \frac{1}{\sqrt{2}}\,(|0\rangle - |1\rangle) \tag{B.11b}$$

This is called the Hadamard basis: it is an equally valid vector space as the standard basis which is spanned by $\begin{pmatrix}1\\0\end{pmatrix}, \begin{pmatrix}0\\1\end{pmatrix}$, as it is simply a rotation of the standard basis.

B.3.1 *Mulitpartite systems*

In reality, we often deal with systems of multiple particles, represented by multiple qubits. Mathematically, we consider the state vector of a system containing n qubits as being the tensor product of the n qubits' individual state vectors[2]. For instance, suppose a 2-qubit system, $|\psi\rangle$ consisting of two independent qubits $|\psi_A\rangle$ and $|\psi_B\rangle$:

$$|\psi\rangle = |\psi_A\rangle\,|\psi_B\rangle = |\psi_A\psi_B\rangle = |\psi_A\rangle \otimes |\psi_B\rangle \tag{B.12}$$

Consider first a simple system of 2 qubits. Measuring in the standard basis, these qubits will have to collapse in to one of the basis states $|0,0\rangle, |0,1\rangle, |1,0\rangle, |1,1\rangle$. Thus, for such a 2-qubit system, we have the general superposition

$$|\psi\rangle = \alpha_{0,0}|0,0\rangle + \alpha_{0,1}|0,1\rangle + \alpha_{1,0}|1,0\rangle + \alpha_{1,1}|1,1\rangle$$

2 We will later discuss entangled states, which can not be described thus.

where $\alpha_{i,j}$ is the amplitude for measuring the system as the state $|i,j\rangle$. This is perfectly analogous to a classical 2-bit system necessarily occupying one of the four possibilities $\{(0,0),(0,1),(1,0),(1,1)\}$.

Hence, for example, if we wanted to concoct a two-qubit system composed of one qubit in the state $|+\rangle$ and one in $|-\rangle$

$$\begin{aligned}
|\psi\rangle &= |+\rangle \otimes |-\rangle \\
|\psi\rangle &= \frac{1}{\sqrt{2}}\left(|0\rangle + |1\rangle\right) \otimes \frac{1}{\sqrt{2}}\left(|0\rangle - |1\rangle\right) \\
&= \frac{1}{2}\left[|00\rangle - |01\rangle + |10\rangle - |11\rangle\right] \\
&= \frac{1}{2}\left[\begin{pmatrix}1\\0\end{pmatrix} \otimes \begin{pmatrix}1\\0\end{pmatrix} - \begin{pmatrix}1\\0\end{pmatrix} \otimes \begin{pmatrix}0\\1\end{pmatrix} + \begin{pmatrix}0\\1\end{pmatrix} \otimes \begin{pmatrix}1\\0\end{pmatrix} - \begin{pmatrix}0\\1\end{pmatrix} \otimes \begin{pmatrix}0\\1\end{pmatrix}\right] \\
&= \frac{1}{2}\left[\begin{pmatrix}1\\0\\0\\0\end{pmatrix} - \begin{pmatrix}0\\1\\0\\0\end{pmatrix} + \begin{pmatrix}0\\0\\1\\0\end{pmatrix} - \begin{pmatrix}0\\0\\0\\1\end{pmatrix}\right]. \\
\Rightarrow |\psi\rangle &= \frac{1}{2}\begin{pmatrix}1\\-1\\-1\\1\end{pmatrix}
\end{aligned} \tag{B.13}$$

That is, the two qubit system – and indeed any two qubit system – is given by a linear combination of the four basis vectors

$$\{|00\rangle, |0,1\rangle, |10\rangle, |11\rangle\} = \left\{\begin{pmatrix}1\\0\\0\\0\end{pmatrix}, \begin{pmatrix}0\\1\\0\\0\end{pmatrix}, \begin{pmatrix}0\\0\\1\\0\end{pmatrix}, \begin{pmatrix}0\\0\\0\\1\end{pmatrix}\right\}. \tag{B.14}$$

We can notice that a single qubit system can be described by a linear combination of two basis vectors, and that a two qubit system requires four basis vectors to describe it. In general we can say that an n-qubit system is represented by a linear combination of 2^n basis vectors.

B.3.2 *Registers*

A *register* is generally the name given to an array of controllable quantum systems; here we invoke it to mean a system of multiple qubits, specifically a subset of the total number of

available qubits. For example, a register of ten qubits can be denoted $|x[10]\rangle$, and we can think of the system as a register of six qubits together with a register of three and another register of one qubit.

$$|x[10]\rangle = |x_1[6]\rangle \otimes |x_2[3]\rangle \otimes |x_3[1]\rangle$$

B.4 ENTANGLEMENT

Another unique property of quantum systems is that of *entanglement*: when two or more particles interact in such a way that their individual quantum states can not be described independent of the other particles. A quantum state then exists for the system as a whole instead. Mathematically, we consider such entangled states as those whose state can not be expressed as a tensor product of the states of the individual qubits it's composed of: they are dependent upon the other.

To understand what we mean by this dependence, consider a counter-example. Consider the Bell state,

$$|\Phi^+\rangle = \frac{1}{\sqrt{2}}\left(|00\rangle + |11\rangle\right), \tag{B.15}$$

if we measure this state, we expect that it will be observed in either eigenstate $|00\rangle$ or $|11\rangle$, with equal probability due to their amplitudes' equal magnitudes. The bases for this state are simply the standard bases, $|0\rangle$ and $|1\rangle$. Thus, according to our previous definition of systems of multiple qubits, we would say this state can be given as a combination of two states, like Eq. (B.12),

$$\begin{aligned} |\Phi^+\rangle &= |\psi_1\rangle \otimes |\psi_2\rangle \\ &= (a_1|0\rangle + b_1|1\rangle) \otimes (a_2|0\rangle + b_2|1\rangle) \\ &= a_1a_2|00\rangle + a_1b_2|01\rangle + b_1a_2|10\rangle + b_1b_2|11\rangle \end{aligned} \tag{B.16}$$

However we require $|\Phi^+\rangle = \frac{1}{\sqrt{2}}(|00\rangle + |11\rangle)$, which would imply $a_1b_2 = 0$ and $b_1a_2 = 0$. These imply that either $a_1 = 0$ or $b_2 = 0$, and also that $b_1 = 0$ or a_2=0, which are obviously invalid since we require that $a_1a_2 = b_1b_2 = \frac{1}{\sqrt{2}}$. Thus, we cannot express $|\Phi^+\rangle = |\psi_1\rangle \otimes |\psi_2\rangle$; this inability to separate the first and second qubits is what we term *entanglement*.

B.5 UNITARY TRANSFORMATIONS

A fundamental concept in quantum mechanics is that of performing transformations on states. *Quantum transformations*, or *quantum operators*, map a quantum state into a new state within the same Hilbert space. There are certain restrictions on a physically possible quantum transformation: in order that U is a valid transformation acting on some superposition $|\psi\rangle = a_1|\psi_1\rangle + a_2|\psi_2\rangle + \ldots a_k|\psi_k\rangle$, U must be linear

$$U(a_1|\psi_1\rangle + a_2|\psi_2\rangle + \ldots a_k|\psi_k\rangle) = a_1(U|\psi_1\rangle) + a_2(U|\psi_2\rangle) + \cdots + a_k(U|\psi_k\rangle). \tag{B.17}$$

To fulfil these properties, we require that U *preserve the inner product*:

$$\langle \psi_0 | U^\dagger U | \psi \rangle = \langle \psi_0 | \psi \rangle$$

That is, we require that any such transformation be *unitary*:

$$UU^\dagger = I \Rightarrow U^\dagger = U^{-1} \tag{B.18}$$

Unitarity is a sufficient condition to describe any valid quantum operation: any quantum transformation can be described by a unitary transformation, and any unitary transformation corresponds to a physically implementable quantum transformation.

Then, if U_1 is a unitary transformation that acts on the space $\mathcal{H}_1$ and U_2 acts on $\mathcal{H}_2$, the product of the two unitary transformations is also unitary. The tensor product $U_1 \otimes U_2$ acts on the space $\mathcal{H}_1 \otimes \mathcal{H}_2$. So, then, supposing a system of two separable qubits, $|\psi_1\rangle$ and $|\psi_2\rangle$ where we wish to act on $|\psi_1\rangle$ with operator U_1 and on $|\psi_2\rangle$ with U_2, we perform it as

$$(U_1 \otimes U_2)(|\psi_1\rangle \otimes |\psi_2\rangle) = (U_1 |\psi_1\rangle) \otimes (U_2 |\psi_2\rangle) \tag{B.19}$$

B.6 DIRAC NOTATION

In keeping with standard practice, we employ *Dirac notation* throughout this thesis. Vectors are denoted by *kets* of the form $|a\rangle$. For example, the standard basis is represented by,

$$\begin{aligned} |x\rangle = |0\rangle &= \begin{pmatrix} 1 \\ 0 \end{pmatrix} \\ |y\rangle = |1\rangle &= \begin{pmatrix} 0 \\ 1 \end{pmatrix} \end{aligned} \tag{B.20}$$

We saw in Table B.1 that for every such ket, $|\psi\rangle$, there exists a *dual vector*: its complex conjugate transpose, called the *bra* of such a vector, denoted $\langle \psi |$. That is,

$$\begin{aligned} \langle \psi |^\dagger &= |\psi\rangle \\ |\psi\rangle^\dagger &= \langle \psi | \end{aligned} \tag{B.21}$$

$$|\psi\rangle = \begin{pmatrix} \psi_1 \\ \psi_2 \\ \vdots \\ \psi_n \end{pmatrix} \Rightarrow \langle \psi | = \begin{pmatrix} \psi_1^* & \psi_2^* & \dots & \psi_n^* \end{pmatrix} \tag{B.22}$$

Then if we have two vectors $|\psi\rangle$ and $|\phi\rangle$, their *inner product* is given as $\langle\psi|\phi\rangle = \langle\phi|\psi\rangle$.

$$\begin{aligned} |\psi\rangle = \begin{pmatrix} \psi_1 \\ \psi_2 \\ \psi_3 \\ \vdots \\ \psi_n \end{pmatrix} \quad ; \quad |\phi\rangle = \begin{pmatrix} \phi_1 \\ \phi_2 \\ \phi_3 \\ \vdots \\ \phi_n \end{pmatrix} \\ \Rightarrow \langle\phi| = \begin{pmatrix} \phi_1^* & \phi_2^* & \phi_3^* & \dots & \phi_n^* \end{pmatrix} \\ \Rightarrow \langle\phi|\,|\psi\rangle = \begin{pmatrix} \phi_1^* & \phi_2^* & \phi_3^* & \dots & \phi_n^* \end{pmatrix} \begin{pmatrix} \psi_1 \\ \psi_2 \\ \psi_3 \\ \vdots \\ \psi_n \end{pmatrix} \\ \Rightarrow \langle\phi|\,|\psi\rangle = \phi_1^*\psi_1 + \phi_2^*\psi_2 + \phi_3^*\psi_3 + \cdots + \phi_n^*\psi_n \end{aligned} \tag{B.23}$$

Example B.6.1.

$$\begin{aligned} |\psi\rangle = \begin{pmatrix} 1 \\ 2 \\ 3 \end{pmatrix} \quad ; \quad |\phi\rangle = \begin{pmatrix} 4 \\ 5 \\ 6 \end{pmatrix} \\ \Rightarrow \langle\phi|\,|\psi\rangle = \begin{pmatrix} 4 & 5 & 6 \end{pmatrix} \begin{pmatrix} 1 \\ 2 \\ 3 \end{pmatrix} \\ = (4)(1) + (5)(2) + (6)(3) = 32 \end{aligned} \tag{B.24}$$

Similarly, their *outer product* is given as $|\phi\rangle\langle\psi|$. Multiplying a column vector by a row vector thus gives a matrix. Matrices generated by a outer products then define operators:

Example B.6.2.

$$\begin{pmatrix} 1 \\ 2 \end{pmatrix} \begin{pmatrix} 3 & 4 \end{pmatrix} = \begin{pmatrix} 3 & 4 \\ 6 & 8 \end{pmatrix} \tag{B.25}$$

Then we can say, for $|0\rangle = \begin{pmatrix} 1 \\ 0 \end{pmatrix}$ and $|1\rangle = \begin{pmatrix} 0 \\ 1 \end{pmatrix}$

$$|0\rangle\langle 0| = \begin{pmatrix} 1 & 0 \\ 0 & 0 \end{pmatrix} \tag{B.26a}$$

$$|0\rangle\langle 1| = \begin{pmatrix} 0 & 1 \\ 0 & 0 \end{pmatrix} \tag{B.26b}$$

$$|1\rangle\langle 0| = \begin{pmatrix} 0 & 0 \\ 1 & 0 \end{pmatrix} \tag{B.26c}$$

$$|1\rangle\langle 1| = \begin{pmatrix} 0 & 0 \\ 0 & 1 \end{pmatrix} \tag{B.26d}$$

And so any 2-dimensional linear transformation in the standard basis $|0\rangle, |1\rangle$ can be given as a sum

$$\begin{pmatrix} a & b \\ c & d \end{pmatrix} = a|0\rangle\langle 0| + b|0\rangle\langle 1| + c|1\rangle\langle 0| + d|1\rangle\langle 1| \tag{B.27}$$

This is a common method of representing operators as outer products of vectors. A transformation that *exchanges* a particle between two states, say $|0\rangle \leftrightarrow |1\rangle$ is given by the operation

$$\hat{Q} : \begin{cases} |0\rangle \to |1\rangle \\ |1\rangle \to |0\rangle \end{cases}$$

Which is equivalent to the outer product representation

$$\hat{Q} = |0\rangle\langle 1| + |1\rangle\langle 0|$$

For clarity, here we will prove this operation

Example B.6.3.

$$\begin{aligned} \hat{Q} &= |0\rangle\langle 1| + |1\rangle\langle 0| \\ &= \begin{pmatrix} 1 \\ 0 \end{pmatrix}\begin{pmatrix} 0 \\ 1 \end{pmatrix} + \begin{pmatrix} 0 \\ 1 \end{pmatrix}\begin{pmatrix} 1 \\ 0 \end{pmatrix} \\ &= \begin{pmatrix} 0 & 1 \\ 0 & 0 \end{pmatrix} + \begin{pmatrix} 0 & 0 \\ 1 & 0 \end{pmatrix} \\ &= \begin{pmatrix} 0 & 1 \\ 1 & 0 \end{pmatrix} \end{aligned}$$

So then, acting on $|0\rangle$ *and* $|1\rangle$ *gives*

$$\hat{Q}|0\rangle = \begin{pmatrix} 0 & 1 \\ 1 & 0 \end{pmatrix}\begin{pmatrix} 1 \\ 0 \end{pmatrix} = \begin{pmatrix} 0 \\ 1 \end{pmatrix} = |1\rangle$$

$$\hat{Q}\left|1\right\rangle = \begin{pmatrix} 0 & 1 \\ 1 & 0 \end{pmatrix} \begin{pmatrix} 0 \\ 1 \end{pmatrix} = \begin{pmatrix} 1 \\ 0 \end{pmatrix} = \left|0\right\rangle$$

To demonstrate how Dirac notation simplifies this:

$$\begin{aligned} \hat{Q}\left|0\right\rangle &= \left(\left|0\right\rangle\left\langle 1\right| + \left|1\right\rangle\left\langle 0\right|\right)\left|0\right\rangle \\ &= \left|0\right\rangle\left\langle 1\right|\left|0\right\rangle + \left|1\right\rangle\left\langle 0|0\right\rangle \\ &= \left|0\right\rangle\left\langle 1|0\right\rangle + \left|1\right\rangle\left\langle 0|0\right\rangle \end{aligned}$$

Then, since $\left|0\right\rangle$ and $\left|1\right\rangle$ are orthogonal basis, their inner product is 0 and the inner product of a vector with itself is 1, ($\left\langle 1|1\right\rangle = \left\langle 0|0\right\rangle = 1, \left\langle 0|1\right\rangle = \left\langle 1|0\right\rangle = 0$). So,

$$\begin{aligned} \hat{Q}\left|0\right\rangle &= \left|0\right\rangle(0) + \left|1\right\rangle(1) \\ \Rightarrow \hat{Q}\left|0\right\rangle &= \left|1\right\rangle \end{aligned} \tag{B.28}$$

And similarly for $\hat{Q}\left|1\right\rangle$. This simple example then shows why Dirac notation can significantly simplify calculations across quantum mechanics, compared to standard matrix and vector notation. To see this more clearly, we will examine a simple 2-qubit state under such operations. The method generalises to operating on two or more qubits generically: we can define any operator which acts on two qubits as a sum of outer products of the basis vectors $\left|00\right\rangle, \left|01\right\rangle, \left|10\right\rangle$ and $\left|11\right\rangle$. We can similarly define any operator which acts on an n qubit state as a linear combination of the 2^n basis states generated by the n qubits.

Example B.6.4. *To define a transformation that will exchange basis vectors $\left|00\right\rangle$ and $\left|11\right\rangle$, while leaving $\left|01\right\rangle$ and $\left|10\right\rangle$ unchanged (ie exchanging $\left|01\right\rangle \leftrightarrow \left|01\right\rangle, \left|10\right\rangle \leftrightarrow \left|10\right\rangle$) we define an operator*

$$\hat{Q} = \left|00\right\rangle\left\langle 11\right| + \left|11\right\rangle\left\langle 00\right| + \left|10\right\rangle\left\langle 10\right| + \left|01\right\rangle\left\langle 01\right| \tag{B.29}$$

Then, using matrix calculations this would require separately calculating the four outer products in the above sum and adding them to find a 4×4 matrix to represent $\hat{Q}$, which then acts on a state $\left|\psi\right\rangle$. Instead, consider first that $\left|\psi\right\rangle = \left|00\right\rangle$, ie one of the basis vectors our transformation is to change:

$$\hat{Q}\left|00\right\rangle = \left(\left|00\right\rangle\left\langle 11\right| + \left|11\right\rangle\left\langle 00\right| + \left|10\right\rangle\left\langle 10\right| + \left|01\right\rangle\left\langle 01\right|\right)\ \left|00\right\rangle \tag{B.30}$$

And as before, only the inner products of a vector with itself remains:

$$\begin{aligned} &= \left|00\right\rangle\left\langle 11\left|00\right.\right\rangle + \left|11\right\rangle\left\langle 00\left|00\right.\right\rangle + \left|10\right\rangle\left\langle 10\left|00\right.\right\rangle + \left|01\right\rangle\left\langle 01\left|00\right.\right\rangle \\ &= \left|00\right\rangle(0) + \left|11\right\rangle(1) + \left|10\right\rangle(0) + \left|01\right\rangle(0) \\ \Rightarrow &\hat{Q}\left|00\right\rangle = \left|11\right\rangle \end{aligned} \tag{B.31}$$

i.e the transformation has performed $\hat{Q} : |00\rangle \rightarrow |11\rangle$ *as expected. Then, if we apply the same transformation to a state which does not depend on one of the target states, eg,*

$$\begin{aligned} |\psi\rangle =& a\,|10\rangle + b\,|01\rangle \\ \hat{Q}\,|\psi\rangle =& \Big(|00\rangle\langle 11| + |11\rangle\langle 00| + |10\rangle\langle 10| + |01\rangle\langle 01| \Big)\Big(a\,|10\rangle + b\,|01\rangle \Big) \\ =& a\Big(|00\rangle\langle 11|10\rangle + |11\rangle\langle 00|10\rangle + |10\rangle\langle 10|10\rangle + |01\rangle\langle 01|10\rangle \Big) \\ &+ b\Big(|00\rangle\langle 11|01\rangle + |11\rangle\langle 00|01\rangle + |10\rangle\langle 10|01\rangle + |01\rangle\langle 01|01\rangle \Big) \end{aligned} \tag{B.32}$$

And since the inner product is a scalar, we can factor terms such as $\langle 11|10\rangle$ *to the beginning of expressions, eg* $|00\rangle\langle 11|\,|10\rangle = \langle 11\,|10\rangle\,|00\rangle$*, and we also know*

$$\begin{aligned} \langle 11|10\rangle = \langle 00|10\rangle = \langle 01|10\rangle = \langle 11|01\rangle = \langle 00|01\rangle = \langle 10|01\rangle = 0 \\ \langle 10|10\rangle = \langle 01|01\rangle = 1 \end{aligned} \tag{B.33}$$

We can express the above as

$$\begin{aligned} \hat{Q}\,|\psi\rangle =& a\Big((0)\,|00\rangle + (0)\,|11\rangle + (1)\,|10\rangle + (0)\,|01\rangle \Big) \\ &+ b\Big((0)\,|00\rangle + (0)\,|11\rangle + (0)\,|10\rangle + (1)|01\rangle \Big) \\ =& a\,|10\rangle\,| + b|01\rangle \\ =& |\psi\rangle \end{aligned} \tag{B.34}$$

Then it is clear that, when $|\psi\rangle$ *is a superposition of states unaffected by transformation* $\hat{Q}$*, then* $\hat{Q}\,|\psi\rangle = |\psi\rangle$*.*

This method generalises to systems with greater numbers of particles (qubits). If we briefly consider a 3 qubit system - and initialise all qubits in the standard basis state $|0\rangle$ - then the system is represented by $|000\rangle = |0\rangle \otimes |0\rangle \otimes |0\rangle = \begin{pmatrix} 0 \\ 1 \end{pmatrix} \otimes \begin{pmatrix} 0 \\ 1 \end{pmatrix} \otimes \begin{pmatrix} 0 \\ 1 \end{pmatrix}$. This quantity is an 8-row vector. To calculate the outer product $\langle 000|000\rangle$, we would be multiplying an 8-column bra $\langle 000|$ by an 8-row ket $|000\rangle$. Clearly then we will be working with 8×8 matrices, which will become quite difficult to maintain effectively and efficiently quite fast. As we move to systems of larger size, standard matrix multiplication becomes impractical for hand-written analysis, although of course remains tractable computationally up to $n \sim 10$ qubits. It is obvious that Dirac's bra/ket notation is a helpful, pathematically precise tool for QM.

C

EXAMPLE EXPLORATION STRATEGY RUN

Here we provide a complete example of how to run the Quantum Model Learning Agent (QMLA) framework, including how to implement a custom exploration strategy (ES), and generate/interpret analysis.

First, *fork* the QMLA codebase from [**?**] to a Github user account (referred to as username in Listing C.1). Now, we must download the code base and ensure it runs properly; these instructions are implemented via the command line[1].

The steps of preparing the codebase are (i) install redis; (ii) create a virtual Python environment for installing QMLA dependencies without damaging other parts of the user's environment; (iii) download the QMLA codebase from the forked Github repository; (iv) install packages upon which QMLA depends.

```
# Install redis (database broker)
sudo apt update
sudo apt install redis-server

# make directory for QMLA
cd
mkdir qmla_test
cd qmla_test

# make Python virtual environment for QMLA
# note: change Python3.6 to desired version
sudo apt-get install python3.6-venv
python3.6 -m venv qmla-env
source qmla-env/bin/activate

# Download QMLA
git clone --depth 1 https://github.com/username/QMLA.git #
   REPLACE username

# Install dependencies
cd QMLA
```

1 Note: these instructions are tested for Linux and presumed to work on Mac, but untested on Windows. It is likely some of the underlying software (redis servers) can not be installed on Windows, so running on *Windows Subsystem for Linux* is advised.

```
pip install -r requirements.txt
```

Listing C.1: QMLA codebase setup language

Note there may be a problem with some packages in the requirements.txt arising from the attempt to install them all through a single call to pip install. Ensure these are all installed before proceeding.

When all of the requirements are installed, test that the framework runs. QMLA uses redis databases to store intermittent data: we must manually initialise the database. Run the following (note: here we list redis-4.0.8, but this must be corrected to reflect the version installed on the user's machine in the above setup section):

```
~/redis-4.0.8/src/redis-server
```

Listing C.2: Launch redis database

which should give something like Fig. C.1.

Figure C.1: Terminal running redis-server.

In a text editor, open qmla_test/QMLA/launch/local_launch.sh; here we will ensure that we are running the QHL algorithm, with 5 experiments and 20 particles, on the ES named TestInstall. Ensure the first few lines of local_launch.sh read:

```
#!/bin/bash

##### ---------------------------------------------- #####
# QMLA run configuration
##### ---------------------------------------------- #####
num_instances=2 # number of instances in run
run_qhl=0 # perform QHL on known (true) model
run_qhl_multi_model=0 # perform QHL for defined list of models
```

```
experiments=2 # number of experiments
particles=10 # number of particles
plot_level=5


##### ---------------------------------------------- #####
# Choose an exploration strategy
# This will determine how QMLA proceeds.
##### ---------------------------------------------- #####
exploration_strategy="TestInstall"
```

Listing C.3: local_launch script

Now we can run Ensure the terminal running redis is kept active, and open a separate terminal window. We must activate the Python virtual environment configured for QMLA, which we set up in Listing C.1. Then, we navigate to the QMLA directory, and launch:

```
# activate the QMLA Python virtual environment
source qmla_test/qmla-env/bin/activate

# move to the QMLA directory
cd qmla_test/QMLA
# Run QMLA
cd launch
./local_launch.sh
```

Listing C.4: Launch QMLA

There may be numerous warnings, but they should not affect whether QMLA has succeeded; QMLA will raise any significant error. Assuming the run has completed successfully, QMLA stores the run's results in a subdirectory named by the date and time it was started. For example, if the run was initialised on January 1^{st} at 01:23, navigate to the corresponding directory by

```
cd results/Jan_01/01_23
```

Listing C.5: QMLA results directory

For now it is sufficient to notice that the code has run successfully: it should have generated (in results/Jan_01/01_23) files like storage_001.p and results_001.p.

C.1 CUSTOM EXPLORATION STRATEGY

Next, we design a basic ES, for the purpose of demonstrating how to run the algorithm. ESs are placed in the directory qmla/exploration_strategies. To make a new one, navigate to the exploration strategies directory, make a new subdirectory, and copy the template file.

```
cd ~/qmla_test/QMLA/exploration_strategies/
mkdir custom_es

# Copy template file into example
cp template.py custom_es/example.py
cd custom_es
```

Listing C.6: QMLA codebase setup

Ensure QMLA will know where to find the ES by importing everything from the custom ES directory into to the main exploration_strategy module. Then, in the custom_es directory, make a file called __init__.py which imports the new ES from the example.py file. To add any further ESs inside the directory custom_es, include them in the custom __init__.py, and they will automatically be available to QMLA.

```
# inside qmla/exploration_strategies/custom_es
#   __init__.py
from qmla.exploration_strategies.custom_es.example import *

# inside qmla/exploration_strategies , add to the existing
# __init__.py
from qmla.exploration_strategies.custom_es import *
```

Listing C.7: Providing custom exploration strategy to QMLA

Now, change the structure (and name) of the ES inside custom_es/example.py. Say we wish to target the true model

$$\begin{aligned} \vec{\alpha} &= (\alpha_{1,2} \quad \alpha_{2,3} \quad \alpha_{3,4}) \\ \vec{T} &= \begin{pmatrix} \hat{\sigma}_z^1 \otimes \hat{\sigma}_z^2 \\ \hat{\sigma}_z^2 \otimes \hat{\sigma}_z^3 \\ \hat{\sigma}_z^3 \otimes \hat{\sigma}_z^4 \end{pmatrix} \\ \implies \hat{H}_0 &= \hat{\sigma}_z^{(1,2)} \hat{\sigma}_z^{(2,3)} \hat{\sigma}_z^{(3,4)} \end{aligned} \tag{C.1}$$

QMLA interprets models as strings, where terms are separated by +, and parameters are implicit. So the target model in Eq. (C.1) will be given by

pauliSet_1J2_zJz_d4+pauliSet_2J3_zJz_d4+pauliSet_3J4_zJz_d4.

Adapting the template ES slightly, we can define a model generation strategy with a small number of hard coded candidate models introduced at the first branch of the exploration tree. We will also set the parameters of the terms which are present in $\hat{H}_0$, as well as the range in which to search parameters. Keeping the imports at the top of the example.py, rewrite the ES as:

```
class ExampleBasic(
    exploration_strategy.ExplorationStrategy
):

    def __init__(
        self,
        exploration_rules,
        true_model=None,
        **kwargs
    ):
        self.true_model = 'pauliSet_1J2_zJz_d4+
            pauliSet_2J3_zJz_d4+pauliSet_3J4_zJz_d4'
        super().__init__(
            exploration_rules=exploration_rules,
            true_model=self.true_model,
            **kwargs
        )

        self.initial_models = None
        self.true_model_terms_params = {
            'pauliSet_1J2_zJz_d4' : 2.5,
            'pauliSet_2J3_zJz_d4' : 7.5,
            'pauliSet_3J4_zJz_d4' : 3.5,
        }
        self.tree_completed_initially = True
        self.min_param = 0
        self.max_param = 10

    def generate_models(self, **kwargs):

        self.log_print(["Generating models; spawn step {}".format
            (self.spawn_step)])
```

```
        if self.spawn_step == 0:
            # chains up to 4 sites
            new_models = [
                'pauliSet_1J2_zJz_d4',
                'pauliSet_1J2_zJz_d4+pauliSet_2J3_zJz_d4',
                'pauliSet_1J2_zJz_d4+pauliSet_2J3_zJz_d4+
                    pauliSet_3J4_zJz_d4',
            ]
            self.spawn_stage.append('Complete')

        return new_models
```

Listing C.8: ExampleBasic exploration strategy.

To run[2] the example ES for a meaningful tests, return to the local_launch of Listing C.3, but change some of the settings:

```
prt=2000
exp=500
run_qhl=1
exploration_strategy=ExampleBasic
```

Listing C.9: local_launch configuration for QHL.

Run locally again as in Listing C.4; then move to the results directory as in Listing C.5.

C.2 ANALYSIS

QMLA stores results and generates plots over the entire range of the algorithm[3], i.e. the run, instance and models. The depth of analysis performed automatically is set by the user control plot_level in local_launch.sh; for plot_level=1, only the most crucial figures are generated, while plot_level=6 generates plots for every individual model considered. For model searches across large model spaces and/or considering many candidates, excessive plotting can cause considerable slow-down, so users should be careful to generate plots only to the degree they will be useful. Next we show some examples of the available plots.

2 Note this will take up to 15 minutes to run. This can be reduced by lowering the values of prt, exp, which is sufficient for testing but note that the outcomes will be less effective than those presented in the figures of this section.

3 Recall that a single implementation of QMLA is called an instance, while a series of instances – which share the same target model – is called the run.

C.2.1 *Model analysis*

We have just run quantum Hamiltonian learning (QHL) for the model in Eq. (C.1) for a single instance, using a reasonable number of particles and experiments, so we expect to have trained the model well. Instance-level results are stored (e.g. for the instance with qmla_id=1) in Jan_01/01_23/instances/qmla_1. Individual models' insights can be found in model_training, e.g. the model's learning_summary Fig. C.2a, and dynamics in Fig. C.2b.

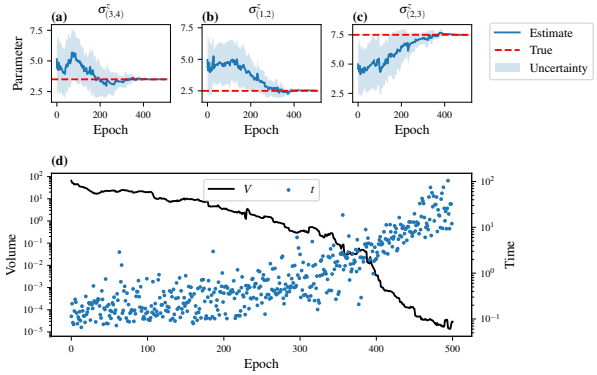

(a)

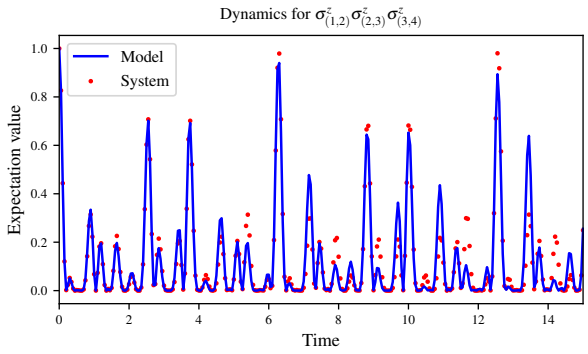

(b)

Figure C.2: Model analysis plots, stored in (for example) Jan_01/01_23/instances/qmla_1/model_training. **a** learning_summary_1. Displays the outcome of QHL for the given model: Subfigures (a)-(c) show the estimates of the parameters; (d) shows the total parameterisation volume against experiments trained upon, along with the evolution times used for those experiments. **(b)** dynamics_1 The model's attempt at reproducing dynamics from $\hat{H}_0$.

C.2.2 *Instance analysis*

Now we can run the full QMLA algorithm, i.e. train several models and determine the most suitable. QMLA will call the generate_models method of the ExampleBasic ES, set in Listing C.8, which tells QMLA to construct three models on the first branch, then terminate the search. Here we need to train and compare all models so it takes considerably longer to run: the purpose of testing, we reduce the resources so the entire algorithm runs in about 15 minutes. Some applications will require significantly more resources to learn effectively. In realistic cases, these processes are run in parallel, as we will cover in **??**.

Reconfigure a subset of the settings in the local_launch.sh script (Listing C.3) and run it again:

```
exp=250
prt=1000
run_qhl=0
```

```
exploration_strategy=ExampleBasic
```

Listing C.10: local_launch configuration for QMLA.

In the corresponding results directory, navigate to instances/qmla_1, where instance level analysis are available.

```
cd results/Jan_01/01_23/instances/qmla_1
```

Listing C.11: Navigating to instance results.

Figures of interest here show the composition of the models (Fig. C.3a), as well as the Bayes factors between candidates (Fig. C.3b). Individual model comparisons – i.e. Bayes factor (BF) – are shown in Fig. C.3c, with the dynamics of all candidates shown in Fig. C.4c. The probes used during the training of all candidates are also plotted (Fig. C.3e).

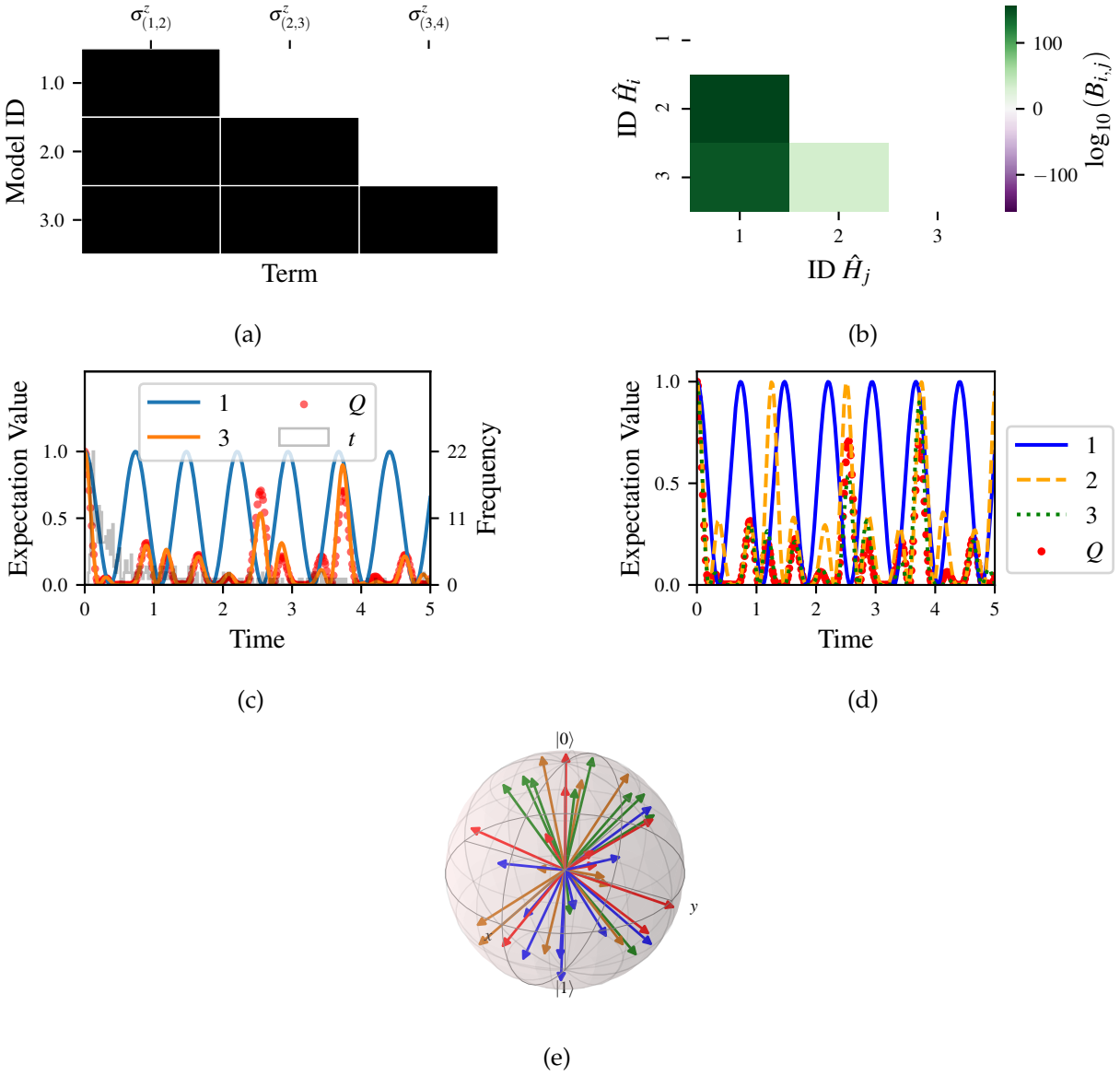

Figure C.3: QMLA plots; found within instance directory e.g. Jan_01/01_23/instances/qmla_1, and its subdirectories. **(a)** composition_of_models: constituent terms of all considered models, indexed by their model IDs. Here model 3 is $\hat{H}_0$. **(b)** bayes_factors: Bayes factor (BF) comparisons between all models. BFs are read as $B_{i,j}$ where i is the model with lower ID, e.g. $B_{1,2}$ rather than $B_{2,1}$. Thus $B_{ij} > 0$ (< 0) indicates $\hat{H}_i$ ($\hat{H}_j$), i.e. the model on the y-axis (x-axis) is the stronger model. **(c)** comparisons/BF_1_3: direct comparison between models with IDs 1 and 3, showing their reproduction of the system dynamics (red dots, Q), as well as the times (experiments) against which the BF was calculated. **(d)** branches/dynamics_branch_1: dynamics of all models considered on the branch compared with system dynamics (red dots, Q). **(e)** probes_bloch_sphere: probes used for training models in this instance (only showing 1-qubit versions).

C.2.3 *Run analysis*

Considering a number of instances together is a *run*. In general, this is the level of analysis of most interest: an individual instance is liable to errors due to the probabilistic nature of the model training and generation subroutines. On average, however, we expect those elements to perform well, so across a significant number of instances, we expect the average outcomes to be meaningful.

Each results directory has an analyse.sh script to generate plots at the run level.

```
cd results/Jan_01/01_23
./analyse.sh
```

Listing C.12: Analysing QMLA run.

Run level analysis are held in the main results directory and several sub-directories created by the analyse script. Here, we recommend running a number of instances with very few resources so that the test finishes quickly[4]. The results will therefore be meaningless, but allow fo elucidation of the resultant plots. First, reconfigure some settings of Listing C.3 and launch again.

```
num_instances=10
exp=20
prt=100
run_qhl=0
exploration_strategy=ExampleBasic
```

Listing C.13: local_launch configuration for QMLA run.

Some of the generated analysis are shown in Figs. C.4 to C.5. The number of instances for each model, i.e. their *win rates* are given in Fig. C.4a. The *top models*, i.e. those with highest win rates, analysed further: the average parameter estimation progression for $\hat{H}_0$ – including only the instances where $\hat{H}_0$ was deemed champion – are shown in Fig. C.4b. Irrespecitve of the champion models, the rate with which each term is found in the champion model ($\hat{t} \in \hat{H}'$) indicates thelikelihood that the term is really present; these rates – along with the parameter values learned – are shown in Fig. C.4c. The champion model from each instance can attempt to reproduce system dynamics: we group together these reproductions for each model in Fig. C.5.

4 This run will take about ten minutes

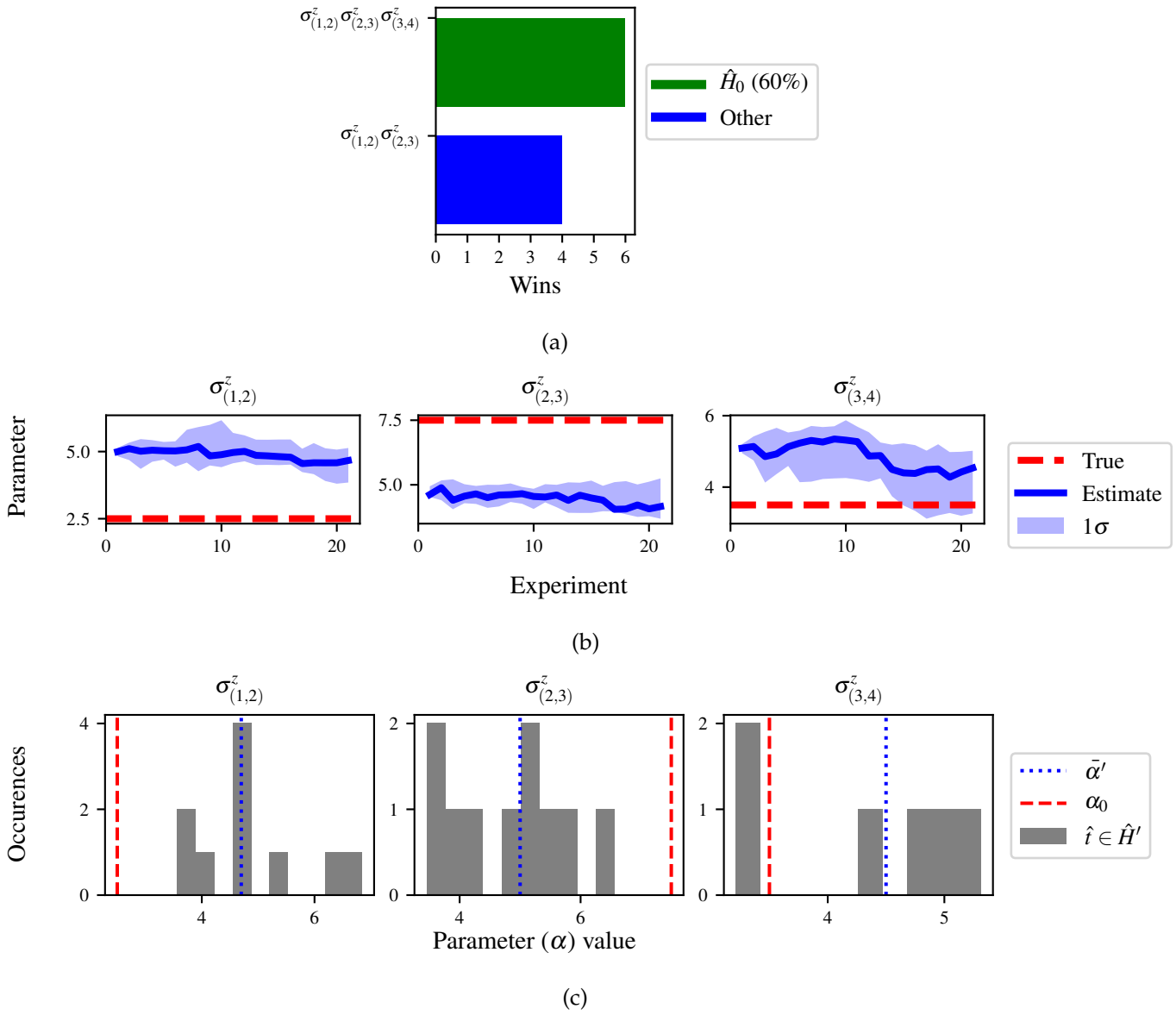

Figure C.4: QMLA run plots; found within run directory e.g. Jan_01/01_23/. **(a)** performace/model_wins: number of instance wins achieved by each model. **(b)** champion_models/params_params_pauliSet_1J2_zJz_d4+pauliSet_2J3_zJz_d4+pauliSet_3J4_zJz_d4: parameter estimation progression for the true model , only for the instances where it was deemed champion. **(c)** champion_models/terms_and_params: histogram of parameter values found for each term which appears in any champion model, with the true parameter (α_0) in red and the median learned parameter ($\bar{\alpha}'$) in blue.

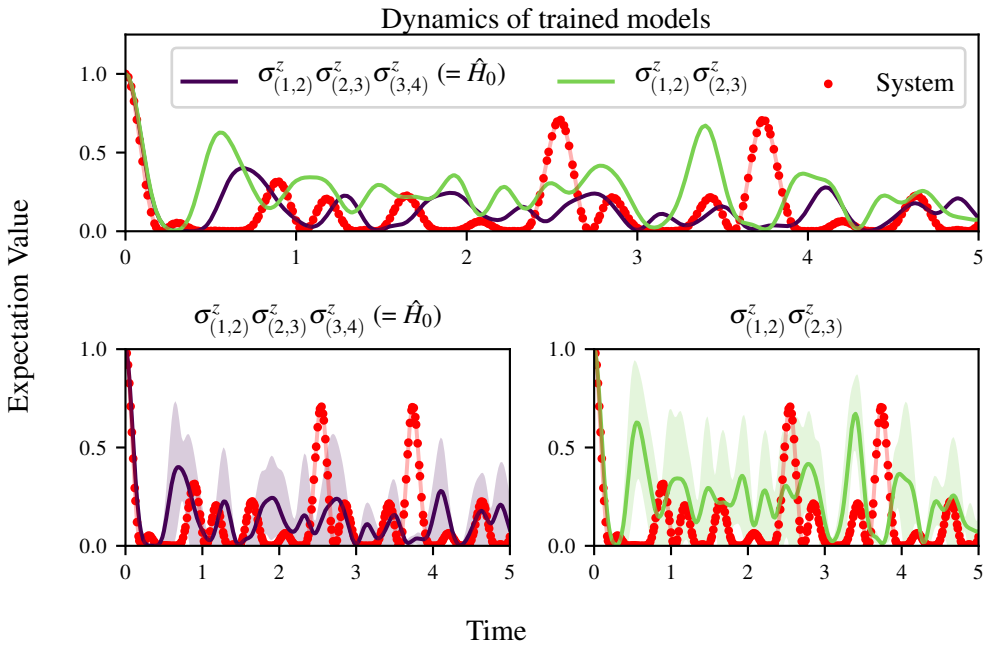

Figure C.5: Run plot performace/dynamics: median dynamics of the champion models. The models which won most instances are shown together in the top panel, and individually in the lower panels. The median dynamics from the models' learnings in its winning instances are shown, with the shaded region indicating the 66% confidence region.

C.3 PARALLEL IMPLEMENTATION

We provide utility to run QMLA on parallel processes. Individual models' training can run in parallel, as well as the calculation of BF between models. The provided script is designed for portable batch system (PBS) job scheduler running on a compute cluster. It will require a few adjustments to match the system being used. Overall, though, it has mostly a similar structure as the local_launch.sh script used above.

QMLA must be downloaded on the compute cluster as in Listing C.1; this can be a new fork of the repository, though it is sensible to test installation locally as described in this chapter so far, then *push* that version, including the new ES, to Github, and cloning the latest version. It is again advisable to create a Python virtual environment in order to isolate QMLA and its dependencies[5]. Open the parallel launch script, QMLA/launch/parallel_launch.sh, and prepare the first few lines as

```
#!/bin/bash
```

5 Indeed it is sensible to do this for any Python development project.

```
##### ---------------------------------------------- #####
# QMLA run configuration
##### ---------------------------------------------- #####
num_instances=10 # number of \glspl{instance} in run
run_qhl=0 # perform QHL on known (true) model
run_qhl_multi_model=0 # perform QHL for defined list of models
experiments=250
particles=1000
plot_level=5


##### ---------------------------------------------- #####
# Choose an exploration strategy
# This will determine how QMLA proceeds.
##### ---------------------------------------------- #####
exploration_strategy="ExampleBasic"
```

Listing C.14: parallel_launch script

When submitting jobs to schedulers like PBS, we must specify the time required, so that it can determine a fair distribution of resources among users. We must therefore *estimate* the time it will take for an instance to complete: clearly this is strongly dependent on the numbers of experiments (N_e) and particles (N_p), and the number of models which must be trained. QMLA attempts to determine a reasonable time to request based on the max_num_models_by_shape attribute of the ES, by calling QMLA/scripts/time_required_calculation.py. In practice, this can be difficult to set perfectly, so the timing_insurance_factor attribute of the ES can be used to correct for heavily over- or under-estimated time requests. Instances are run in parallel, and each instance trains/compares models in parallel. The number of processes to request, N_c for each instance is set as num_processes_to_parallelise_over in the ES. Then, if there are N_r instances in the run, we will be requesting the job scheduler to admit N_r distinct jobs, each requiring N_c processes, for the time specified.

The parallel_launch script works together with launch/run_single_qmla_instance.sh, though note a number of steps in the latter are configured to the cluster and may need to be adapted. In particular, the first command is used to load the redis utility, and later lines are used to initialise a redis server. These commands will probably not work with most machines, so must be configured to achieve those steps.

```
module load tools/redis-4.0.8

...
```

```
SERVER_HOST=$(head -1 "$PBS_NODEFILE")
let REDIS_PORT="6300 + $QMLA_ID"

cd $LIBRARY_DIR
redis-server RedisDatabaseConfig.conf --protected-mode no --port
    $REDIS_PORT &
redis-cli -p $REDIS_PORT flushall
```

Listing C.15: run_single_qmla_instance script

When the modifications are finished, QMLA can be launched in parallel similarly to the local version:

```
source qmla_test/qmla-env/bin/activate

cd qmla_test/QMLA/launch
./parallel_launch.sh
```

Listing C.16: run_single_qmla_instance script

Jobs are likely to queue for some time, depending on the demands on the job scheduler. When all jobs have finished, results are stored as in the local case, in QMLA/launch/results/-Jan_01/01_23, where analyse.sh can be used to generate a series of automatic analyses.

C.4 CUSTOMISING EXPLORATION STRATEGYS

User interaction with the QMLA codebase should be achieveable primarily through the exploration strategy (ES) framework. Throughout the algorithm(s) available, QMLA calls upon the ES before determining how to proceed. The usual mechanism through which the actions of QMLA are directed, is to set attributes of the ES class: the complete set of influential attributes are available at [**?**].

QMLA directly uses several methods of the ES class, all of which can be overwritten in the course of customising an ES. Most such methods need not be replaced, however, with the exception of generate_models, which is the most important aspect of any ES: it determines which models are built and tested by QMLA. This method allows the user to impose any logic desired in constructing models; it is called after the completion of every branch of the exploration tree on the ES.

C.4.1 *Greedy search*

A first non-trivial ES is to build models greedily from a set of *primitive* terms, $\mathcal{T} = \{\hat{t}\}$. New models are constructed by combining the previous branch champion with each of the remaining, unused terms. The process is repeated until no terms remain.

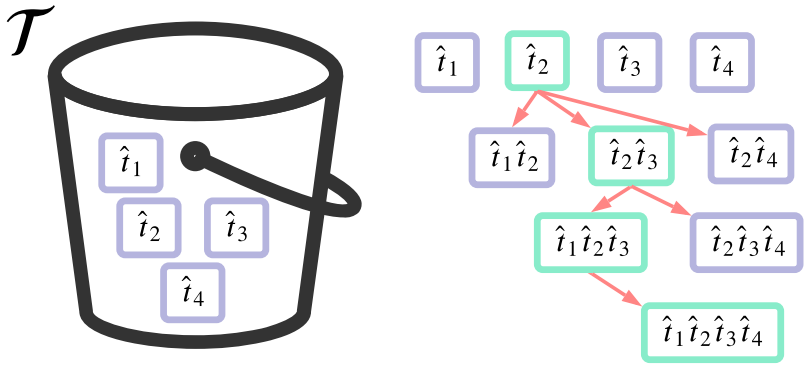

Figure C.6: Greedy search mechanism. **Left**, a set of primitive terms, $\mathcal{T}$, are defined in advance. **Right**, models are constructed from $\mathcal{T}$. On the first branch, the primitve terms alone constitute models. Thereafter, the strongest model (marked in green) from the previous branch is combined with all the unused terms.

We can compose an ES using these rules, say for

$$\mathcal{T} = \left\{\hat{\sigma}_x^1,\ \hat{\sigma}_y^1,\ \hat{\sigma}_x^1 \otimes \hat{\sigma}_x^2,\ \hat{\sigma}_y^1 \otimes \hat{\sigma}_y^2\right\}$$

as follows. Note the termination criteria must work in conjunction with the model generation routine. Users can overwrite the method check_tree_completed for custom logic, although a straightforward mechanism is to use the spawn_stage attribute of the ES class: when the final element of this list is Complete, QMLA will terminate the search by default. Also note that the default termination test checks whether the number of branches (spawn_step) exceeds the limit max_spawn_depth, which must be set artifically high to avoid ceasing the search too early, if relying solely on spawn_stage. Here we demonstrate how to impose custom logic to terminate the seach also.

```
class ExampleGreedySearch(
    exploration_strategy.ExplorationStrategy
):
    r"""
    From a fixed set of terms, construct models iteratively,
```

```
    greedily adding all unused terms to separate models at each
       call to the generate_models.

    """

    def __init__(
        self,
        exploration_rules,
        **kwargs
    ):

        super().__init__(
            exploration_rules=exploration_rules,
            **kwargs
        )
        self.true_model = 'pauliSet_1_x_d3+pauliSet_1J2_yJy_d3+
           pauliSet_1J2J3_zJzJz_d3'
        self.initial_models = None
        self.available_terms = [
            'pauliSet_1_x_d3', 'pauliSet_1_y_d3',
            'pauliSet_1J2_xJx_d3', 'pauliSet_1J2_yJy_d3'
        ]
        self.branch_champions = []
        self.prune_completed_initially = True
        self.check_champion_reducibility = False

    def generate_models(
        self,
        model_list,
        **kwargs
    ):
        self.log_print([
            "Generating models in tiered greedy search at spawn
               step {}.".format(
                 self.spawn_step,
            )
        ])
        try:
            previous_branch_champ = model_list[0]
            self.branch_champions.append(previous_branch_champ)
```

```
        except:
            previous_branch_champ = ""

        if self.spawn_step == 0 :
            new_models = self.available_terms
        else:
            new_models = greedy_add(
                current_model = previous_branch_champ,
                terms = self.available_terms
            )

        if len(new_models) == 0:
            # Greedy search has exhausted the available models;
            # send back the list of branch champions and
               terminate search.
            new_models = self.branch_champions
            self.spawn_stage.append('Complete')

        return new_models

def greedy_add(
    current_model,
    terms,
):
    r"""
    Combines given model with all terms from a set.

    Determines which terms are not yet present in the model,
    and adds them each separately to the current model.

    :param str current_model: base model
    :param list terms: list of strings of terms which are to be
       added greedily.
    """

    try:
        present_terms = current_model.split('+')
    except:
        present_terms = []
    nonpresent_terms = list(set(terms) - set(present_terms))
```

```
    term_sets = [
        present_terms+[t] for t in nonpresent_terms
    ]

    new_models = ["+".join(term_set) for term_set in term_sets]

    return new_models
```

Listing C.17: ExampleGreedySearch exploration stategy

This run can be implemented locally or in parallel as described above[6], and analysed as in Listing C.12, generating figures in accordance with the plot_level set by the user in the launch script. Outputs can again be found in the instances subdirectory, including a map of the models generated, as well as the branches they reside on, and the BFs between candidates, Fig. C.7.

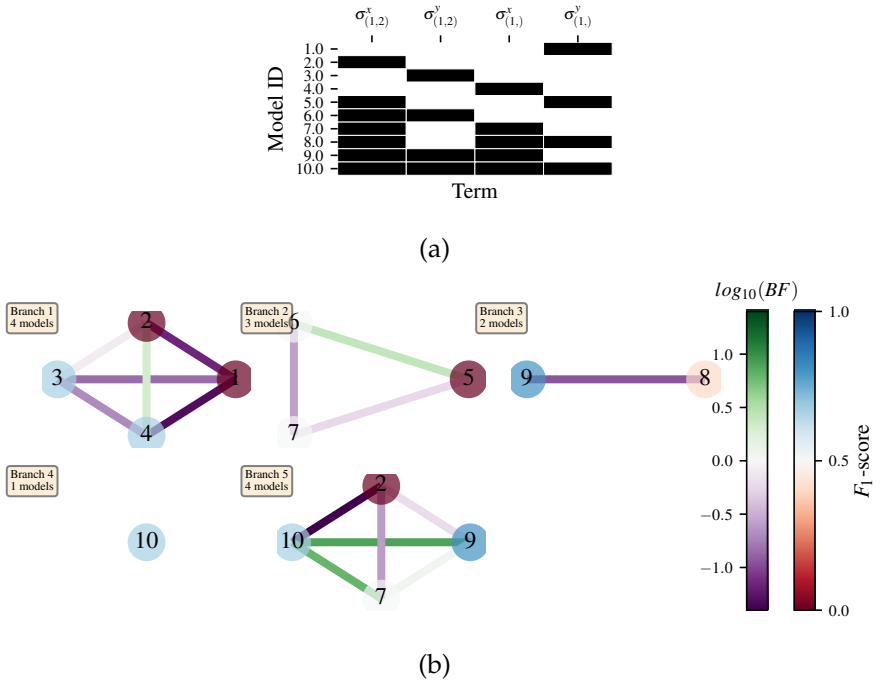

(a)

(b)

Figure C.7: Greedy exploration strategy. **(a)**, composition_of_models. **b**, graphs_of_branches_ExampleGreedySearch: shows which models reside on each branches of the exploration tree. Models are coloured by their F_1-score, and edges represent the BF between models. The first four branches are equivalent to those in Fig. C.6 , while the final branch considers the set of branch champions, in order to determine the overall champion.

6 We advise reducing plot_level to 3 to avoid excessive/slow figure generation.

C.4.2 *Tiered greedy search*

We provide one final example of a non-trivial ES: tiered greedy search. Similar to the idea of Appendix C.4.1, except terms are introduced hierarchically: sets of terms $\mathcal{T}_1, \mathcal{T}_2, \ldots \mathcal{T}_n$ are each examined greedily, where the overall strongest model of one tier forms the seed model for the subsequent tier. This is depicted in the main text in Fig. 9.4. A corresponding ES is given as follows.

```
class ExampleGreedySearchTiered(
    exploration_strategy.ExplorationStrategy
):
    r"""
    Greedy search in tiers.

    Terms are batched together in tiers;
    tiers are searched greedily;
    a single tier champion is elevated to the subsequent tier.

    """

    def __init__(
        self,
        exploration_rules,
        **kwargs
    ):
        super().__init__(
            exploration_rules=exploration_rules,
            **kwargs
        )
        self.true_model = 'pauliSet_1_x_d3+pauliSet_1J2_yJy_d3+
           pauliSet_1J2J3_zJzJz_d3'
        self.initial_models = None
        self.term_tiers = {
            1 : ['pauliSet_1_x_d3', 'pauliSet_1_y_d3', '
               pauliSet_1_z_d3' ],
            2 : ['pauliSet_1J2_xJx_d3', 'pauliSet_1J2_yJy_d3', '
               pauliSet_1J2_zJz_d3'],
```

```
            3 : ['pauliSet_1J2J3_xJxJx_d3', '
                pauliSet_1J2J3_yJyJy_d3', 'pauliSet_1J2J3_zJzJz_d3
                '],
        }
        self.tier = 1
        self.max_tier = max(self.term_tiers)
        self.tier_branch_champs = {k : [] for k in self.
            term_tiers}
        self.tier_champs = {}
        self.prune_completed_initially = True
        self.check_champion_reducibility = True

    def generate_models(
        self,
        model_list,
        **kwargs
    ):
        self.log_print([
            "Generating models in tiered greedy search at spawn
                step {}.".format(
                self.spawn_step,
            )
        ])

        if self.spawn_stage[-1] is None:
            try:
                previous_branch_champ = model_list[0]
                self.tier_branch_champs[self.tier].append(
                    previous_branch_champ)
            except:
                previous_branch_champ = None

        elif "getting_tier_champ" in self.spawn_stage[-1]:
            previous_branch_champ = model_list[0]
            self.log_print([
                "Tier champ for {} is {}".format(self.tier,
                    model_list[0])
            ])
            self.tier_champs[self.tier] = model_list[0]
            self.tier += 1
```

```
            self.log_print(["Tier now = ", self.tier])
            self.spawn_stage.append(None) # normal processing

            if self.tier > self.max_tier:
                self.log_print(["Completed tree for ES"])
                self.spawn_stage.append('Complete')
                return list(self.tier_champs.values())
        else:
            self.log_print([
                "Spawn stage:", self.spawn_stage
            ])

        new_models = greedy_add(
            current_model = previous_branch_champ,
            terms = self.term_tiers[self.tier]
        )
        self.log_print([
            "tiered search new_models=", new_models
        ])

        if len(new_models) == 0:
            # no models left to find - get champions of branches
               from this tier
            new_models = self.tier_branch_champs[self.tier]
            self.log_print([
                "tier champions: {}".format(new_models)
            ])
            self.spawn_stage.append("getting_tier_champ_{}".
               format(self.tier))
        return new_models

    def check_tree_completed(
        self,
        spawn_step,
        **kwargs
    ):
        r"""
        QMLA asks the exploration tree whether it has finished
           growing;
```

```
        the exploration tree queries the exploration strategy
           through this method
        """
        if self.tree_completed_initially:
            return True
        elif self.spawn_stage[-1] == "Complete":
            return True
        else:
            return False


def greedy_add(
    current_model,
    terms,
):
    r"""
    Combines given model with all terms from a set.

    Determines which terms are not yet present in the model,
    and adds them each separately to the current model.

    :param str current_model: base model
    :param list terms: list of strings of terms which are to be
       added greedily.
    """

    try:
        present_terms = current_model.split('+')
    except:
        present_terms = []
    nonpresent_terms = list(set(terms) - set(present_terms))

    term_sets = [
        present_terms+[t] for t in nonpresent_terms
    ]

    new_models = ["+".join(term_set) for term_set in term_sets]

    return new_models
```

Listing C.18: ExampleGreedySearchTiered exploration stategy

with corresponding results in Fig. C.8.

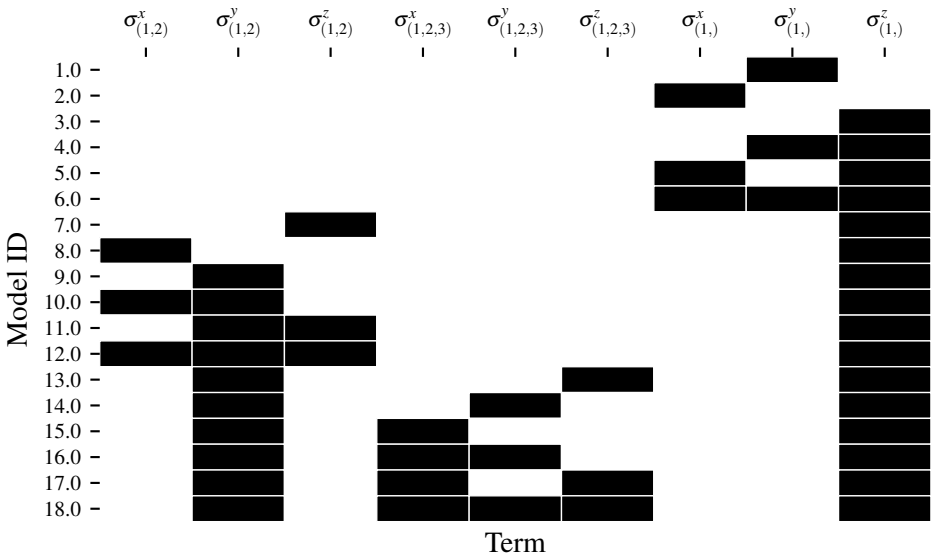

(a)

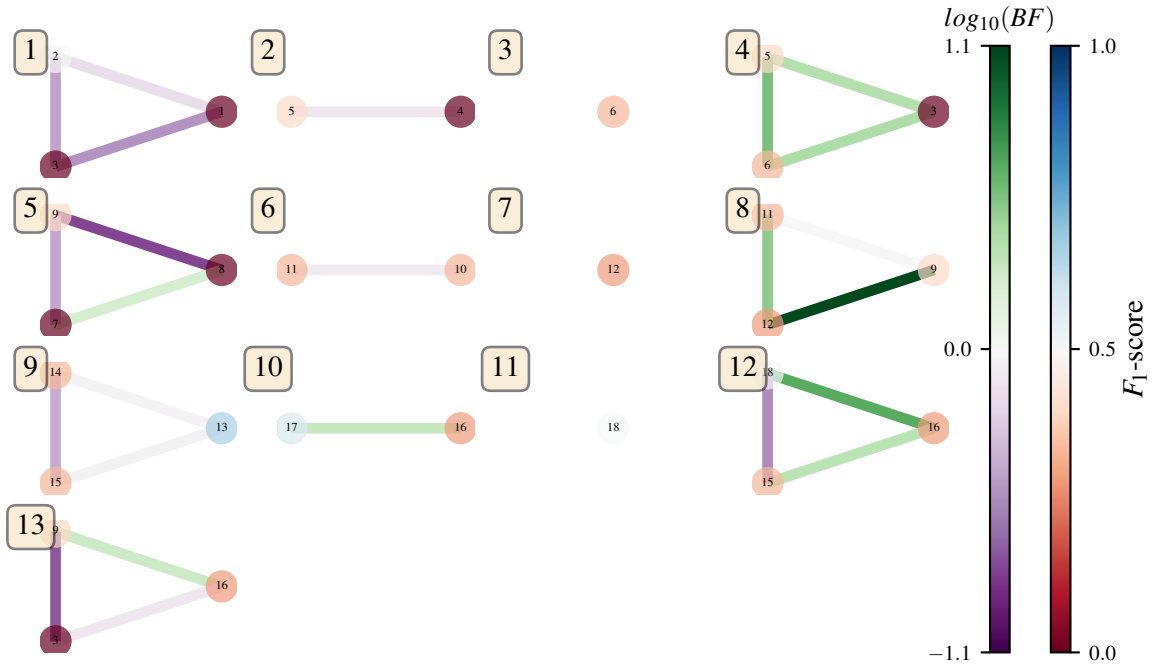

(b)

Figure C.8: Tiered greedy exploration strategy. **(a)**, composition_of_models. **b**, graphs_of_branches_ExampleGreedySearchTiered: shows which models reside on each branches of the exploration tree. Models are coloured by their F_1-score, and edges represent the BF between models. In each tier, three branches greedily add terms, and a fourth branch considers the champions of the first three branches in order to nominate a tier champion. The final branch consists only of the tier champions, to nominate the global champion, $\hat{H}'$.

BIBLIOGRAPHY

[1] Max Jammer et al. *The conceptual development of quantum mechanics*. McGraw-Hill New York, 1966.

[2] Albert Einstein. On a heuristic point of view concerning the production and transformation of light. *Annalen der Physik*, pages 1–18, 1905.

[3] Max Born. Quantenmechanik der stoßvorgänge. *Zeitschrift für Physik*, 38(11-12):803–827, 1926.

[4] Erwin Schrödinger. An undulatory theory of the mechanics of atoms and molecules. *Physical review*, 28(6):1049, 1926.

[5] Werner Heisenberg. Über quantentheoretische umdeutung kinematischer und mechanischer beziehungen. In *Original Scientific Papers Wissenschaftliche Originalarbeiten*, pages 382–396. Springer, 1985.

[6] John Von Neumann. *Mathematical foundations of quantum mechanics: New edition*. Princeton university press, 2018.

[7] Orazio Svelto and David C Hanna. *Principles of lasers*, volume 1. Springer, 2010.

[8] Bart Van Zeghbroeck. Principles of semiconductor devices. *Colarado University*, 34, 2004.

[9] David J Griffiths and Darrell F Schroeter. *Introduction to quantum mechanics*. Cambridge University Press, 2018.

[10] Leonard Susskind and Art Friedman. *Quantum mechanics: the theoretical minimum*. Basic Books, 2014.

[11] Eleanor G Rieffel and Wolfgang H Polak. *Quantum computing: A gentle introduction*. MIT Press, 2011.

[12] Michael A Nielsen and Isaac Chuang. Quantum computation and quantum information, 2002.

[13] Paul Adrien Maurice Dirac. *The principles of quantum mechanics*. Number 27. Oxford university press, 1981.

[14] T Mart. How do i introduce schr\" odinger equation during the quantum mechanics course? *arXiv preprint arXiv:2010.15589*, 2020.

[15] Edward Nelson. Derivation of the schrödinger equation from newtonian mechanics. *Physical review*, 150(4):1079, 1966.

[16] Leonard Susskind and George Hrabovsky. *Classical mechanics: the theoretical minimum*. Penguin Books, 2014.

[17] Heinz-Peter Breuer, Francesco Petruccione, et al. *The theory of open quantum systems*. Oxford University Press on Demand, 2002.

[18] Daniel Manzano. A short introduction to the lindblad master equation. *AIP Advances*, 10(2):025106, 2020.

[19] John Preskill. Lecture notes for physics 229: Quantum information and computation. *California Institute of Technology*, 16, 1998.

[20] Jonathan P Dowling and Gerard J Milburn. Quantum technology: the second quantum revolution. *Philosophical Transactions of the Royal Society of London. Series A: Mathematical, Physical and Engineering Sciences*, 361(1809):1655–1674, 2003.

[21] Vittorio Giovannetti, Seth Lloyd, and Lorenzo Maccone. Quantum-enhanced measurements: beating the standard quantum limit. *Science*, 306(5700):1330–1336, 2004.

[22] Vittorio Giovannetti, Seth Lloyd, and Lorenzo Maccone. Advances in quantum metrology. *Nature photonics*, 5(4):222, 2011.

[23] Charles H Bennett and Gilles Brassard. Quantum cryptography: Public key distribution and coin tossing. *arXiv preprint arXiv:2003.06557*, 2020.

[24] Artur K Ekert. Quantum cryptography based on bell's theorem. *Physical review letters*, 67(6):661, 1991.

[25] Nicolas Gisin, Grégoire Ribordy, Wolfgang Tittel, and Hugo Zbinden. Quantum cryptography. *Reviews of modern physics*, 74(1):145, 2002.

[26] Yu I Manin. Vychislimoe i nevychislimoe (computable and noncomputable), moscow: Sov, 1980.

[27] Paul Benioff. The computer as a physical system: A microscopic quantum mechanical hamiltonian model of computers as represented by turing machines. *Journal of statistical physics*, 22(5):563–591, 1980.

[28] Paul Benioff. Quantum mechanical hamiltonian models of turing machines. *Journal of Statistical Physics*, 29(3):515–546, 1982.

[29] Richard P Feynman. Simulating physics with computers. *Int. J. Theor. Phys*, 21(6/7), 1982.

[30] Seth Lloyd. Universal quantum simulators. *Science*, pages 1073–1078, 1996.

[31] J Ignacio Cirac and Peter Zoller. Goals and opportunities in quantum simulation. *Nature Physics*, 8(4):264–266, 2012.

[32] Benjamin P Lanyon, James D Whitfield, Geoff G Gillett, Michael E Goggin, Marcelo P Almeida, Ivan Kassal, Jacob D Biamonte, Masoud Mohseni, Ben J Powell, Marco Barbieri, et al. Towards quantum chemistry on a quantum computer. *Nature chemistry*, 2(2):106–111, 2010.

[33] Yudong Cao, Jonathan Romero, Jonathan P Olson, Matthias Degroote, Peter D Johnson, Mária Kieferová, Ian D Kivlichan, Tim Menke, Borja Peropadre, Nicolas PD Sawaya, et al. Quantum chemistry in the age of quantum computing. *Chemical reviews*, 119(19):10856–10915, 2019.

[34] Sam McArdle, Suguru Endo, Alan Aspuru-Guzik, Simon C Benjamin, and Xiao Yuan. Quantum computational chemistry. *Reviews of Modern Physics*, 92(1):015003, 2020.

[35] Alán Aspuru-Guzik, Anthony D Dutoi, Peter J Love, and Martin Head-Gordon. Simulated quantum computation of molecular energies. *Science*, 309(5741):1704–1707, 2005.

[36] Chris Sparrow, Enrique Martín-López, Nicola Maraviglia, Alex Neville, Christopher Harrold, Jacques Carolan, Yogesh N Joglekar, Toshikazu Hashimoto, Nobuyuki Matsuda, Jeremy L O'Brien, et al. Simulating the vibrational quantum dynamics of molecules using photonics. *Nature*, 557(7707):660–667, 2018.

[37] David Deutsch. Quantum theory, the church–turing principle and the universal quantum computer. *Proceedings of the Royal Society of London. A. Mathematical and Physical Sciences*, 400(1818):97–117, 1985.

[38] Daniel R Simon. On the power of quantum computation. *SIAM journal on computing*, 26(5):1474–1483, 1997.

[39] Charles H Bennett, Ethan Bernstein, Gilles Brassard, and Umesh Vazirani. Strengths and weaknesses of quantum computing. *SIAM journal on Computing*, 26(5):1510–1523, 1997.

[40] Ethan Bernstein and Umesh Vazirani. Quantum complexity theory. *SIAM Journal on computing*, 26(5):1411–1473, 1997.

[41] Lov K Grover. Quantum mechanics helps in searching for a needle in a haystack. *Physical review letters*, 79(2):325, 1997.

[42] Peter W Shor. Polynomial-time algorithms for prime factorization and discrete logarithms on a quantum computer. *SIAM review*, 41(2):303–332, 1999.

[43] John Watrous. Quantum computational complexity. *arXiv preprint arXiv:0804.3401*, 2008.

[44] Peter W Shor. Fault-tolerant quantum computation. In *Proceedings of 37th Conference on Foundations of Computer Science*, pages 56–65. IEEE, 1996.

[45] Dorit Aharonov and Michael Ben-Or. Fault-tolerant quantum computation with constant error rate. *SIAM Journal on Computing*, 2008.

[46] David P DiVincenzo. The physical implementation of quantum computation. *Fortschritte der Physik: Progress of Physics*, 48(9-11):771–783, 2000.

[47] Travis S Humble, Himanshu Thapliyal, Edgard Munoz-Coreas, Fahd A Mohiyaddin, and Ryan S Bennink. Quantum computing circuits and devices. *IEEE Design & Test*, 36(3):69–94, 2019.

[48] Pieter Kok, William J Munro, Kae Nemoto, Timothy C Ralph, Jonathan P Dowling, and Gerard J Milburn. Linear optical quantum computing with photonic qubits. *Reviews of Modern Physics*, 79(1):135, 2007.

[49] Jeremy C Adcock, Jueming Bao, Yulin Chi, Xiaojiong Chen, Davide Bacco, Qihuang Gong, Leif K Oxenløwe, Jianwei Wang, and Yunhong Ding. Advances in silicon quantum photonics. *IEEE Journal of Selected Topics in Quantum Electronics*, 27(2):1–24, 2020.

[50] John Michael Kovac, EM Leitch, C Pryke, JE Carlstrom, NW Halverson, and WL Holzapfel. Detection of polarization in the cosmic microwave background using dasi. *Nature*, 420(6917):772–787, 2002.

[51] Christopher Gerry, Peter Knight, and Peter L Knight. *Introductory quantum optics*. Cambridge university press, 2005.

[52] Robert Raussendorf, Daniel E Browne, and Hans J Briegel. Measurement-based quantum computation on cluster states. *Physical review A*, 68(2):022312, 2003.

[53] Caterina Vigliar, Stefano Paesani, Yunhong Ding, Jeremy C Adcock, Jianwei Wang, Sam Morley-Short, Davide Bacco, Leif K Oxenløwe, Mark G Thompson, John G Rarity, et al. Error protected qubits in a silicon photonic chip. *arXiv preprint arXiv:2009.08339*, 2020.

[54] Stefano Paesani, Massimo Borghi, Stefano Signorini, Alexandre Maïnos, Lorenzo Pavesi, and Anthony Laing. Near-ideal spontaneous photon sources in silicon quantum photonics. *Nature communications*, 11(1):1–6, 2020.

[55] Michel H Devoret, Andreas Wallraff, and John M Martinis. Superconducting qubits: A short review. *arXiv preprint cond-mat/0411174*, 2004.

[56] Morten Kjaergaard, Mollie E Schwartz, Jochen Braumüller, Philip Krantz, Joel I-J Wang, Simon Gustavsson, and William D Oliver. Superconducting qubits: Current state of play. *Annual Review of Condensed Matter Physics*, 11:369–395, 2020.

[57] M Kjaergaard, ME Schwartz, A Greene, GO Samach, A Bengtsson, M O'Keeffe, CM McNally, J Braumüller, DK Kim, P Krantz, et al. A quantum instruction set implemented on a superconducting quantum processor. *arXiv preprint arXiv:2001.08838*, 2020.

[58] John M Martinis and A Megrant. Ucsb final report for the csq program: Review of decoherence and materials physics for superconducting qubits. *arXiv preprint arXiv:1410.5793*, 2014.

[59] Göran Wendin. Quantum information processing with superconducting circuits: a review. *Reports on Progress in Physics*, 80(10):20, 2017.

[60] Ioan M Pop, Kurtis Geerlings, Gianluigi Catelani, Robert J Schoelkopf, Leonid I Glazman, and Michel H Devoret. Coherent suppression of electromagnetic dissipation due to superconducting quasiparticles. *Nature*, 508(7496):369–372, 2014.

[61] Jay M Gambetta, Jerry M Chow, and Matthias Steffen. Building logical qubits in a superconducting quantum computing system. *npj Quantum Information*, 3(1):1–7, 2017.

[62] David Kielpinski, Chris Monroe, and David J Wineland. Architecture for a large-scale ion-trap quantum computer. *Nature*, 417(6890):709–711, 2002.

[63] Christopher Monroe and Jungsang Kim. Scaling the ion trap quantum processor. *Science*, 339(6124):1164–1169, 2013.

[64] John P Gaebler, Ting Rei Tan, Y Lin, Y Wan, R Bowler, Adam C Keith, S Glancy, K Coakley, E Knill, D Leibfried, et al. High-fidelity universal gate set for be 9+ ion qubits. *Physical review letters*, 117(6):060505, 2016.

[65] Ye Wang, Mark Um, Junhua Zhang, Shuoming An, Ming Lyu, Jing-Ning Zhang, L-M Duan, Dahyun Yum, and Kihwan Kim. Single-qubit quantum memory exceeding ten-minute coherence time. *Nature Photonics*, 11(10):646–650, 2017.

[66] AH Myerson, DJ Szwer, SC Webster, DTC Allcock, MJ Curtis, G Imreh, JA Sherman, DN Stacey, AM Steane, and DM Lucas. High-fidelity readout of trapped-ion qubits. *Physical Review Letters*, 100(20):200502, 2008.

[67] VM Schäfer, CJ Ballance, K Thirumalai, LJ Stephenson, TG Ballance, AM Steane, and DM Lucas. Fast quantum logic gates with trapped-ion qubits. *Nature*, 555(7694):75–78, 2018.

[68] Colin D Bruzewicz, John Chiaverini, Robert McConnell, and Jeremy M Sage. Trapped-ion quantum computing: Progress and challenges. *Applied Physics Reviews*, 6(2):021314, 2019.

[69] Ryan LaRose. Overview and comparison of gate level quantum software platforms. *Quantum*, 3:130, 2019.

[70] John Preskill. Quantum computing in the nisq era and beyond. *Quantum*, 2:79, 2018.

[71] Aram W Harrow and Ashley Montanaro. Quantum computational supremacy. *Nature*, 549(7671):203–209, 2017.

[72] Frank Arute, Kunal Arya, Ryan Babbush, Dave Bacon, Joseph C Bardin, Rami Barends, Rupak Biswas, Sergio Boixo, Fernando GSL Brandao, David A Buell, et al. Quantum supremacy using a programmable superconducting processor. *Nature*, 574(7779):505–510, 2019.

[73] Han-Sen Zhong, Hui Wang, Yu-Hao Deng, Ming-Cheng Chen, Li-Chao Peng, Yi-Han Luo, Jian Qin, Dian Wu, Xing Ding, Yi Hu, et al. Quantum computational advantage using photons. *Science*, 370(6523):1460–1463, 2020.

[74] The Difference Between AI and Machine Learning, Jan 2021. [Online; accessed 7. Jan. 2021].

[75] Warren S McCulloch and Walter Pitts. A logical calculus of the ideas immanent in nervous activity. *The bulletin of mathematical biophysics*, 5(4):115–133, 1943.

[76] Alan M Turing. Computing machinery and intelligence. In *Parsing the turing test*, pages 23–65. Springer, 2009.

[77] Stuart Russell and Peter Norvig. Artificial intelligence: a modern approach. 2002.

[78] Fabian Pedregosa, Gaël Varoquaux, Alexandre Gramfort, Vincent Michel, Bertrand Thirion, Olivier Grisel, Mathieu Blondel, Peter Prettenhofer, Ron Weiss, Vincent Dubourg, et al. Scikit-learn: Machine learning in python. *the Journal of machine Learning research*, 12:2825–2830, 2011.

[79] Martín Abadi, Paul Barham, Jianmin Chen, Zhifeng Chen, Andy Davis, Jeffrey Dean, Matthieu Devin, Sanjay Ghemawat, Geoffrey Irving, Michael Isard, et al. Tensorflow: A system for large-scale machine learning. In *12th {USENIX} symposium on operating systems design and implementation ({OSDI} 16)*, pages 265–283, 2016.

[80] Adam Paszke, Sam Gross, Francisco Massa, Adam Lerer, James Bradbury, Gregory Chanan, Trevor Killeen, Zeming Lin, Natalia Gimelshein, Luca Antiga, et al. Pytorch: An imperative style, high-performance deep learning library. In *Advances in neural information processing systems*, pages 8026–8037, 2019.

[81] Trevor Hastie, Robert Tibshirani, and Jerome Friedman. *The elements of statistical learning: data mining, inference, and prediction*. Springer Science & Business Media, 2009.

[82] Rich Caruana and Alexandru Niculescu-Mizil. An empirical comparison of supervised learning algorithms. In *Proceedings of the 23rd international conference on Machine learning*, pages 161–168, 2006.

[83] Sotiris B Kotsiantis, I Zaharakis, and P Pintelas. Supervised machine learning: A review of classification techniques. *Emerging artificial intelligence applications in computer engineering*, 160(1):3–24, 2007.

[84] Geoffrey E Hinton, Simon Osindero, and Yee-Whye Teh. A fast learning algorithm for deep belief nets. *Neural computation*, 18(7):1527–1554, 2006.

[85] Bernhard E Boser, Isabelle M Guyon, and Vladimir N Vapnik. A training algorithm for optimal margin classifiers. In *Proceedings of the fifth annual workshop on Computational learning theory*, pages 144–152, 1992.

[86] Aurélien Géron. *Hands-on machine learning with Scikit-Learn, Keras, and TensorFlow: Concepts, tools, and techniques to build intelligent systems*. O'Reilly Media, 2019.

[87] Stan Franklin and Art Graesser. Is it an agent, or just a program?: A taxonomy for autonomous agents. In *International Workshop on Agent Theories, Architectures, and Languages*, pages 21–35. Springer, 1996.

[88] Michael Wooldridge. *An introduction to multiagent systems*. John Wiley & Sons, 2009.

[89] Jacob Biamonte, Peter Wittek, Nicola Pancotti, Patrick Rebentrost, Nathan Wiebe, and Seth Lloyd. Quantum machine learning. *Nature*, 549(7671):195–202, 2017.

[90] Jeremy Adcock, Euan Allen, Matthew Day, Stefan Frick, Janna Hinchliff, Mack Johnson, Sam Morley-Short, Sam Pallister, Alasdair Price, and Stasja Stanisic. Advances in quantum machine learning. *arXiv preprint arXiv:1512.02900*, 2015.

[91] Ewin Tang. A quantum-inspired classical algorithm for recommendation systems. In *Proceedings of the 51st Annual ACM SIGACT Symposium on Theory of Computing*, pages 217–228, 2019.

[92] Maria Schuld, Ilya Sinayskiy, and Francesco Petruccione. The quest for a quantum neural network. *Quantum Information Processing*, 13(11):2567–2586, 2014.

[93] Yudong Cao, Gian Giacomo Guerreschi, and Alán Aspuru-Guzik. Quantum neuron: an elementary building block for machine learning on quantum computers. *arXiv preprint arXiv:1711.11240*, 2017.

[94] Seth Lloyd, Masoud Mohseni, and Patrick Rebentrost. Quantum principal component analysis. *Nature Physics*, 10(9):631–633, 2014.

[95] Giuseppe Carleo and Matthias Troyer. Solving the quantum many-body problem with artificial neural networks. *Science*, 355(6325):602–606, 2017.

[96] Giacomo Torlai, Guglielmo Mazzola, Juan Carrasquilla, Matthias Troyer, Roger Melko, and Giuseppe Carleo. Neural-network quantum state tomography. *Nature Physics*, 14(5):447–450, 2018.

[97] Alberto Peruzzo, Jarrod McClean, Peter Shadbolt, Man-Hong Yung, Xiao-Qi Zhou, Peter J Love, Alán Aspuru-Guzik, and Jeremy L O'brien. A variational eigenvalue solver on a photonic quantum processor. *Nature communications*, 5:4213, 2014.

[98] Thomas Back. *Evolutionary algorithms in theory and practice: evolution strategies, evolutionary programming, genetic algorithms*. Oxford university press, 1996.

[99] Kenneth De Jong. Evolutionary computation: a unified approach. In *Proceedings of the 2020 Genetic and Evolutionary Computation Conference Companion*, pages 327–342, 2020.

[100] Sean Luke. 1 essentials of metaheuristicsl. 1.

[101] Lothar M Schmitt. Theory of genetic algorithms. *Theoretical Computer Science*, 259(1-2):1–61, 2001.

[102] Christopher E Granade, C Ferrie, N Wiebe, and D G Cory. Robust online Hamiltonian learning. *New Journal of Physics*, 14(10):103013, October 2012.

[103] Nathan Wiebe, Christopher Granade, Christopher Ferrie, and David Cory. Quantum hamiltonian learning using imperfect quantum resources. *Physical Review A*, 89(4):042314, 2014.

[104] N Wiebe, C Granade, C Ferrie, and D G Cory. Hamiltonian Learning and Certification Using Quantum Resources. *Physical Review Letters*, 112(19):190501–5, May 2014.

[105] Jianwei Wang, Stefano Paesani, Raffaele Santagati, Sebastian Knauer, Antonio A Gentile, Nathan Wiebe, Maurangelo Petruzzella, Jeremy L O'Brien, John G Rarity, Anthony Laing, et al. Experimental quantum hamiltonian learning. *Nature Physics*, 13(6):551–555, 2017.

[106] Antonio A. Gentile, Brian Flynn, Sebastian Knauer, Nathan Wiebe, Stefano Paesani, Christopher E. Granade, John G. Rarity, Raffaele Santagati, and Anthony Laing. Learning models of quantum systems from experiments, 2020.

[107] Jane Liu and Mike West. Combined parameter and state estimation in simulation-based filtering. In *Sequential Monte Carlo methods in practice*, pages 197–223. Springer, 2001.

[108] Christopher Granade, Christopher Ferrie, Steven Casagrande, Ian Hincks, Michal Kononenko, Thomas Alexander, and Yuval Sanders. QInfer: Library for statistical inference in quantum information, 2016.

[109] Rodolfo A Jalabert and Horacio M Pastawski. Environment-independent decoherence rate in classically chaotic systems. *Physical review letters*, 86(12):2490, 2001.

[110] Nathan Wiebe, Christopher Granade, and David G Cory. Quantum bootstrapping via compressed quantum hamiltonian learning. *New Journal of Physics*, 17(2):022005, 2015.

[111] Arseni Goussev, Rodolfo A Jalabert, Horacio M Pastawski, and Diego Wisniacki. Loschmidt echo. *arXiv preprint arXiv:1206.6348*, 2012.

[112] Bas Hensen, Hannes Bernien, Anaïs E Dréau, Andreas Reiserer, Norbert Kalb, Machiel S Blok, Just Ruitenberg, Raymond FL Vermeulen, Raymond N Schouten, Carlos Abellán, et al. Loophole-free bell inequality violation using electron spins separated by 1.3 kilometres. *Nature*, 526(7575):682–686, 2015.

[113] Alexandr Sergeevich, Anushya Chandran, Joshua Combes, Stephen D Bartlett, and Howard M Wiseman. Characterization of a qubit hamiltonian using adaptive measurements in a fixed basis. *Physical Review A*, 84(5):052315, 2011.

[114] Christopher Ferrie, Christopher E Granade, and David G Cory. How to best sample a periodic probability distribution, or on the accuracy of hamiltonian finding strategies. *Quantum Information Processing*, 12(1):611–623, 2013.

[115] Christopher E Granade. Characterization, verification and control for large quantum systems. page 92, 2015.

[116] Christopher Ferrie. High posterior density ellipsoids of quantum states. *New Journal of Physics*, 16(2):023006, 2014.

[117] Michael J Todd and E Alper Yıldırım. On khachiyan's algorithm for the computation of minimum-volume enclosing ellipsoids. *Discrete Applied Mathematics*, 155(13):1731–1744, 2007.

[118] Ian Hincks, Thomas Alexander, Michal Kononenko, Benjamin Soloway, and David G Cory. Hamiltonian learning with online bayesian experiment design in practice. *arXiv preprint arXiv:1806.02427*, 2018.

[119] Lukas J Fiderer, Jonas Schuff, and Daniel Braun. Neural-network heuristics for adaptive bayesian quantum estimation. *arXiv preprint arXiv:2003.02183*, 2020.

[120] Sheng-Tao Wang, Dong-Ling Deng, and Lu-Ming Duan. Hamiltonian tomography for quantum many-body systems with arbitrary couplings. *New Journal of Physics*, 17(9):093017, 2015.

[121] Stefan Krastanov, Sisi Zhou, Steven T Flammia, and Liang Jiang. Stochastic estimation of dynamical variables. *Quantum Science and Technology*, 4(3):035003, 2019.

[122] Emmanuel Flurin, Leigh S Martin, Shay Hacohen-Gourgy, and Irfan Siddiqi. Using a recurrent neural network to reconstruct quantum dynamics of a superconducting qubit from physical observations. *Physical Review X*, 10(1):011006, 2020.

[123] Murphy Yuezhen Niu, Vadim Smelyanskyi, Paul Klimov, Sergio Boixo, Rami Barends, Julian Kelly, Yu Chen, Kunal Arya, Brian Burkett, Dave Bacon, et al. Learning non-markovian quantum noise from moir\'{e}-enhanced swap spectroscopy with deep evolutionary algorithm. *arXiv preprint arXiv:1912.04368*, 2019.

[124] Eliska Greplova, Christian Kraglund Andersen, and Klaus Mølmer. Quantum parameter estimation with a neural network. *arXiv preprint arXiv:1711.05238*, 2017.

[125] Andrey Y Lokhov, Marc Vuffray, Sidhant Misra, and Michael Chertkov. Optimal structure and parameter learning of ising models. *Science advances*, 4(3):e1700791, 2018.

[126] Giovanni Acampora, Vittorio Cataudella, Pratibha R Hegde, Procolo Lucignano, Gianluca Passarelli, and Autilia Vitiello. An evolutionary strategy for finding effective quantum 2-body hamiltonians of p-body interacting systems. *Quantum Machine Intelligence*, 1(3):113–122, 2019.

[127] Daniel Burgarth and Ashok Ajoy. Evolution-free hamiltonian parameter estimation through zeeman markers. *Physical Review Letters*, 119(3):030402, 2017.

[128] Robert E Kass and Adrian E Raftery. Bayes factors. *Journal of the american statistical association*, 90(430):773–795, 1995.

[129] Ruhul A Sarker and Tapabrata Ray. Agent based evolutionary approach: An introduction. In *Agent-Based Evolutionary Search*, pages 1–11. Springer, 2010.

[130] Guido Van Rossum and Fred L. Drake. *Python 3 Reference Manual*. CreateSpace, Scotts Valley, CA, 2009.

[131] Roger W Hockney and Chris R Jesshope. *Parallel Computers 2: architecture, programming and algorithms*. CRC Press, 2019.

[132] Redis, Nov 2020. [Online; accessed 7. Nov. 2020].

[133] RQ: Simple job queues for Python, Nov 2020. [Online; accessed 7. Nov. 2020].

[134] Ernst Ising. Beitrag zur theorie des ferromagnetismus. *Zeitschrift für Physik*, 31(1):253–258, 1925.

[135] Lars Onsager. Crystal statistics. i. a two-dimensional model with an order-disorder transition. *Physical Review*, 65(3-4):117, 1944.

[136] Stephen G Brush. History of the lenz-ising model. *Reviews of modern physics*, 39(4):883, 1967.

[137] Francisco Barahona. On the computational complexity of ising spin glass models. *Journal of Physics A: Mathematical and General*, 15(10):3241, 1982.

[138] Michael R Garey and David S Johnson. *Computers and intractability*, volume 174. freeman San Francisco, 1979.

[139] Andrew Lucas. Ising formulations of many np problems. *Frontiers in Physics*, 2:5, 2014.

[140] Giuseppe E Santoro and Erio Tosatti. Optimization using quantum mechanics: quantum annealing through adiabatic evolution. *Journal of Physics A: Mathematical and General*, 39(36):R393, 2006.

[141] Victor Bapst, Laura Foini, Florent Krzakala, Guilhem Semerjian, and Francesco Zamponi. The quantum adiabatic algorithm applied to random optimization problems: The quantum spin glass perspective. *Physics Reports*, 523(3):127–205, 2013.

[142] Mark W Johnson, Mohammad HS Amin, Suzanne Gildert, Trevor Lanting, Firas Hamze, Neil Dickson, Richard Harris, Andrew J Berkley, Jan Johansson, Paul Bunyk, et al. Quantum annealing with manufactured spins. *Nature*, 473(7346):194–198, 2011.

[143] Walter Greiner, Ludwig Neise, and Horst Stöcker. *Thermodynamics and statistical mechanics*. Springer Science & Business Media, 2012.

[144] John Hubbard. Electron correlations in narrow energy bands. *Proceedings of the Royal Society of London. Series A. Mathematical and Physical Sciences*, 276(1365):238–257, 1963.

[145] Richard T Scalettar. An introduction to the hubbard hamiltonian. *Quantum Materials: Experiments and Theory*, 6, 2016.

[146] Editorial. The hubbard model at half a century. *Nature Physics*, 2013.

[147] Pascual Jordan and Eugene Paul Wigner. über das paulische äquivalenzverbot. In *The Collected Works of Eugene Paul Wigner*, pages 109–129. Springer, 1993.

[148] Mark Steudtner and Stephanie Wehner. Fermion-to-qubit mappings with varying resource requirements for quantum simulation. *New Journal of Physics*, 20(6):063010, 2018.

[149] Jarrod McClean, Nicholas Rubin, Kevin Sung, Ian David Kivlichan, Xavier Bonet-Monroig, Yudong Cao, Chengyu Dai, Eric Schuyler Fried, Craig Gidney, Brendan Gimby, et al. Openfermion: the electronic structure package for quantum computers. *Quantum Science and Technology*, 2020.

[150] John Henry Holland et al. *Adaptation in natural and artificial systems: an introductory analysis with applications to biology, control, and artificial intelligence*. MIT press, 1992.

[151] Eyal Bairey, Itai Arad, and Netanel H Lindner. Learning a local hamiltonian from local measurements. *Physical review letters*, 122(2):020504, 2019.

[152] Burnham KP Anderson DR. Model selection and multimodel inference: a practical information-theoretic approach, 2002.

[153] Jerome Friedman, Trevor Hastie, and Robert Tibshirani. *The elements of statistical learning*, volume 1. Springer series in statistics New York, 2001.

[154] Arpad E Elo. *The rating of chess players, past and present*. Arco Pub., 1978.

[155] FIFA.com. Who we are - news - 2026 fifa world cup™: Fifa council designates bids for final voting by the fifa congress, Jun 2018.

[156] Christof Neumann, Julie Duboscq, Constance Dubuc, Andri Ginting, Ade Maulana Irwan, Muhammad Agil, Anja Widdig, and Antje Engelhardt. Assessing dominance hierarchies: validation and advantages of progressive evaluation with elo-rating. *Animal Behaviour*, 82(4):911–921, 2011.

[157] Lars Magnus Hvattum and Halvard Arntzen. Using elo ratings for match result prediction in association football. *International Journal of forecasting*, 26(3):460–470, 2010.

[158] Marcus W Doherty, Neil B Manson, Paul Delaney, Fedor Jelezko, Jörg Wrachtrup, and Lloyd CL Hollenberg. The nitrogen-vacancy colour centre in diamond. *Physics Reports*, 528(1):1–45, 2013.

[159] Gordon Davies and MF Hamer. Optical studies of the 1.945 ev vibronic band in diamond. *Proceedings of the Royal Society of London. A. Mathematical and Physical Sciences*, 348(1653):285–298, 1976.

[160] J Meijer, B Burchard, M Domhan, C Wittmann, Torsten Gaebel, I Popa, F Jelezko, and J Wrachtrup. Generation of single color centers by focused nitrogen implantation. *Applied Physics Letters*, 87(26):261909, 2005.

[161] AM Edmonds, UFS D'Haenens-Johansson, RJ Cruddace, ME Newton, K-MC Fu, C Santori, RG Beausoleil, DJ Twitchen, and ML Markham. Production of oriented nitrogen-vacancy color centers in synthetic diamond. *Physical Review B*, 86(3):035201, 2012.

[162] A Lenef and SC Rand. Electronic structure of the n-v center in diamond: Theory. *Physical Review B*, 53(20):13441, 1996.

[163] Benjamin Smeltzer, Lilian Childress, and Adam Gali. 13c hyperfine interactions in the nitrogen-vacancy centre in diamond. *New Journal of Physics*, 13(2):025021, 2011.

[164] MS Blok, Cristian Bonato, ML Markham, DJ Twitchen, VV Dobrovitski, and R Hanson. Manipulating a qubit through the backaction of sequential partial measurements and real-time feedback. *Nature Physics*, 10(3):189–193, 2014.

[165] Adam Gali, Maria Fyta, and Efthimios Kaxiras. Ab initio supercell calculations on nitrogen-vacancy center in diamond: Electronic structure and hyperfine tensors. *Physical Review B*, 77(15):155206, 2008.

[166] MV Gurudev Dutt, L Childress, L Jiang, E Togan, J Maze, F Jelezko, AS Zibrov, PR Hemmer, and MD Lukin. Quantum register based on individual electronic and nuclear spin qubits in diamond. *Science*, 316(5829):1312–1316, 2007.

[167] P-Y Hou, L He, F Wang, X-Z Huang, W-G Zhang, X-L Ouyang, X Wang, W-Q Lian, X-Y Chang, and L-M Duan. Experimental hamiltonian learning of an 11-qubit solid-state quantum spin register. *Chinese Physics Letters*, 36(10):100303, 2019.

[168] L Childress, MV Gurudev Dutt, JM Taylor, AS Zibrov, F Jelezko, J Wrachtrup, PR Hemmer, and MD Lukin. Coherent dynamics of coupled electron and nuclear spin qubits in diamond. *Science*, 314(5797):281–285, 2006.

[169] L_G Rowan, EL Hahn, and WB Mims. Electron-spin-echo envelope modulation. *Physical Review*, 137(1A):A61, 1965.

[170] Forrest T Charnock and TA Kennedy. Combined optical and microwave approach for performing quantum spin operations on the nitrogen-vacancy center in diamond. *Physical Review B*, 64(4):041201, 2001.

[171] Antonio Andreas Gentile. *Operating practical quantum devices in the pre-threshold regime*. PhD thesis, University of Bristol, 2020.

[172] David A Broadway, Jean-Philippe Tetienne, Alastair Stacey, James DA Wood, David A Simpson, Liam T Hall, and Lloyd CL Hollenberg. Quantum probe hyperpolarisation of molecular nuclear spins. *Nature communications*, 9(1):1–8, 2018.

[173] Brian Flynn. Mathematical introduction to quantum computation, 2015. Undergraduate thesis.

[174] Brian Flynn. Quantum model learning agent. https://github.com/flynnbr11/QMLA, 2021.

[175] Quantum model learning agent documentation. https://quantum-model-learning-agent.readthedocs.io/en/latest/, Jan 2021. [Online; accessed 12. Jan. 2021].